Development of automated iMALDI assays for the robust quantitation of cell signalling proteins in the PI3K pathway to improve guided cancer treatment

by

Björn Fröhlich

Bachelor of Science, Hochschule Fresenius, 2013

Master of Science, Hochschule Fresenius, 2014

A Dissertation Submitted in Partial Fulfillment

of the Requirements for the Degree of

DOCTOR OF PHILOSOPHY

in the Department of Biochemistry and Microbiology

University of Victoria

Supervisory Committee

Development of automated iMALDI assays for the robust quantitation of cell signalling proteins in the PI3K pathway to improve guided cancer treatment

by

Björn Fröhlich

Bachelor of Science, Hochschule Fresenius, 2013

Master of Science, Hochschule Fresenius, 2014

Supervisory Committee

Christoph Borchers, Department of Biochemistry and Microbiology

Co-Supervisor

Caren Helbing, Department of Biochemistry and Microbiology

Co-Supervisor

Brad Nelson, Department of Biochemistry and Microbiology

Departmental Member

Fraser Hof, Department of Chemistry

Outside Member

Abstract

The PI3-kinase/AKT/mTOR pathway plays a central role in cancer signaling. While p110α is the catalytic α-subunit of PI3-kinase and a major drug target, PTEN is the main negative regulator of the PI3-kinase/AKT/mTOR pathway. PTEN and p110α protein expression in tumors is commonly analyzed by immunohistochemistry, which suffers from poor multiplexing capacity, poor standardization, and antibody cross-reactivity, and which provides only semi-quantitative data. Here, we present an automated, and standardized immuno-matrix-assisted laser desorption/ionization mass spectrometry (iMALDI) assay that allows precise and multiplexed quantitation of PTEN and p110α concentrations, without the limitations of immunohistochemistry. IMALDI, which combines immuno-enrichment with analysis using a benchtop MALDI-Time-of-Flight (TOF) mass spectrometer, is an especially well-suited method for translating mass-spectrometry based assays into the clinical lab.

We systematically optimized the iMALDI workflow regarding sensitivity, robustness, and throughput while developing highly flexible automation protocols using a Bravo 96LT liquid handling robot. We further developed custom R scripts to improve data visualization and analysis. One hour digestion using a protein to trypsin ratio of 1:2, followed by direct immuno-enrichment for 1 h yielded high and consistent peptide recoveries.

We demonstrated that the PTEN and p110α iMALDI assays can be multiplexed using both simultaneous and sequential enrichment, reducing the amount of required sample material as well as simplifying the workflow. The PTEN+p110α iMALDI assay was

validated and demonstrated high accuracy for both target proteins (90-112% recovery of known spiked-in concentrations) as well as high precision and 5-day reproducibility (overall CVs of 9%) across the linear range of the assay (0.6 to 20 fmol). Lower limits of quantitation below 1 fmol were achieved. Endogenous PTEN and p110α were quantified in cell lines as well as fresh-frozen tumor tissue samples.

A novel two-point internal calibration strategy (2-PIC) was developed, based on spiking two peptide isotopologues into the sample as internal standards, avoiding the need for an external calibration. We quantified endogenous PTEN in a Colo-205 cell line using the PTEN iMALDI assay, as well an orthogonal PTEN immuno-multiple reaction monitoring (immuno-MRM) method to demonstrate this technique. Excellent agreement was shown between both calibration approaches (residual standard deviation between 2-PIC and external calibration of 1.6-5.8%), as well as high correlation between PTEN iMALDI and PTEN immuno-MRM (R^2= 0.9966) and good agreement between quantified amounts (0.48±0.01 and 0.29±0.02 fmol/µg of total protein).

Finally, we analysed a set of patient samples from a AKT inhibitor AZD5363 drug trial using a multi-site workflow combining the developed PTEN+p110α assay with established AKT1+AKT2 iMALDI assays and untargeted proteomics. We demonstrated how the combination of targeted and untargeted proteomics approaches may be used to gain novel insights into the tumor biology of patient tissue samples. Further, we showed that the PTEN iMALDI assay has good correlation with a comparable immunohistochemistry method (R^2=0.86), and that our assays can be further multiplexed, reducing the required amount sample material. Thus, we showed that iMALDI is promising tool for biomarker quantitation.

Table of Contents

List of Tables

List of Figures

List of Abbreviations

Abbreviation	Definition
2-PIC	2-point internal calibration
ACN	Acetonitrile
AKT	Protein kinase B
AmBic	5 mM ammonium bicarbonate
AmCit	7 mM ammonium citrate dibasic
AUC	Area under the curve
BCA	Bicinchoninic acid assay
CEM	Chain ejection model
CID	Collision-induced fragmentation
CRM	Charged residue model
ctDNA	Cell-free circulating tumor DNA
dNTP	Deoxynucleotide
dSIS	Double isotope labeled standard
DTT	Dithiotreitol
DTT	Dithiothreitol
EC	External Calibration
EGFR	Epidermal growth factor receptor
EI	Electron impact ionization
eIF4A	Eukaryotic translation initiation factor 4
ELISA	Enzyme-linked immunosorbent assays
END	Endogenous peptide
ERK	Extracellular signal-regulated kinases
ESI	Electrospray ionization
FDA	Food and Drug Administration
FF	Fresh-frozen
FFPE	Formalin fixed paraffin embedded
FFPE	formalin fixation paraffin embedded
FISH	Fluorescence in-situ hybridisation
FWHM	Full width at half maximum
GSK3β	Glycogen synthase kinase 3 beta
HCCA	α-Hydroxy-Cyanocinnamic acid
HER2	Epidermal growth factor receptor 2
HIV	Human immunodeficiency virus
HPV	Human papillomavirus
IA	Immunoassays
IAA	Iodoacetamide
IAA	Iodoacemamide
IEM	Ion evaporation model
IHC	Immunohistochemistry

Abbreviation	Definition
iMALDI	immuno-matrix assisted laser desorption/ionization time of flight
iTRAQ	Isobaric tags for relative and absolute quantitation
LC	Liquid chromatography
LC-MS	Liquid chromatography coupled with mass spectrometry
LP	Linear positive ion mode
MAPK	Mitogen-activated protein kinase
MRM	Multiple reaction monitoring
MS	Mass spectrometry
mTOR	Mechanistic target of rapamycin
NAT	Synthetic peptide standard without any isotopic labelling
NGS	Next-generation sequencing
pAb	Polyclonal antibody
PAI	Protein abundance index
PAI	Protein abundance index
PBS	Phosphate-buffered saline
PBSC	PBS+0.015 % (w:w) CHAPS buffer
PBSC2	PBS+0.003% CHAPS
PCA	Principal component analysis
PD-1	Programmed cell death 1 protein
PDK1	Phosphoinositol-dependent kinase-1
PD-L1	Programmed cell-death ligand 1
PI3K	Phosphatidylinositol 3-kinase
PIP_2	Phosphatidylinositol-3,4-biphsphate
PIP_3	Phosphatidylinositol-3,4,5-biphosphate
PRAS40	Proline-rich AKT substrate of 40 kDa
PRM	Parallel reaction monitoring
PSA	Prostate-specific antigen
PTEN	Phosphatase and tensin homolog
RP	Reflectron positive ion mode
RTK	Receptor tyrosine kinases
S6K1	Ribosomal protein S6 kinase beta-1
SBL	Sequencing by ligation
SBS	Sequencing by synthesis
SILAC	Stable isotope labeling with amino acids in cell culture
SIM	Single-ion mode
SIS	Stable isotope-labelled standard
SMRT	Single-molecule real time sequencing
TCEP	mM tris(2-carboxyethyl)phosphine

Abbreviation	Definition
TFA	Trifluoroacetic acid
TMT	Tandem mass tags
TOF	Time-of-flight
TSC	Tuberous sclerosis complex
UMAP	Uniform Manifold Approximation and Projection

Acknowledgments

Firstly, I would like thank Dr. Christoph Borchers for accepting me as his student and for providing me with many opportunities to grow as a scientist. I am also very grateful to Dr. Caren Helbing for taking on the role as co-supervisor; whose tremendous commitment and support was instrumental in bringing this work to the finish line.

Naturally, I would also like to thank the members of my supervising committee Dr. Brad Nelson and Dr. Fraser Hof, for their continued support over the course of my studies.

Further, I would like to thank Dr. Andre LeBlanc and especially Dr. Rene Zahedi for providing supervision and input for my project. Additionally, I thank Dr. Carol Parker. Without her and Dr. Zahedi's writing expertise, none of my publications would have seen the light of day.

I am also very grateful for the help and support of the other people who worked with me on my research, especially Robert Popp, Constance Sobsey, and Sahar Ibrahim. Their positive impact cannot be overstated.

I am also extremely grateful to all staff members of the UVic-Genome BC Proteomics Centre, who provided me with an amazing workplace over the years. Further, I would like to thank Dr. Huiyan Li as well as and Dr. Michael Chen.

Finally, I would like to thank my friends within the department, especially Neda Savic, Nicholas Brody, Gillian Dornan, Kevin Yongblah, Teesha Baker, Anuj Joshi, and outside the department, especially Marianne, Thomas, Luc and Dan, as well as my family. I am very grateful for their presence in my life.

Dedication

I dedicate this thesis to my family and friends.

Chapter 1 Introduction

1.1 Cancer Diagnosis and Treatment

1.1.1 Carcinogenesis

Cancer is a collection of ~200 diseases characterized by the uncontrolled proliferation of aberrant cells.[1–3] Cancers are neoplastic diseases, forming malignant tumors which invade nearby tissue and as well as distant parts of the body (solid cancers).[1–3] It is one of the leading causes of death worldwide.[4] Cancer is an extremely heterogenous disease and can arise virtually anywhere in the body from many different contributing factors. For example, the most common cancer types in the USA for women are breast (30%), lung and bronchus (13%), colon and rectum (8%), uterine corpus (7%) and melanoma of the skin (5%). For men, prostate cancer (26%) lung and bronchus (12%), colon and rectum (8%), urinary and bladder (7%) and melanoma of the skin (6%) are the most common types.[4]

While having very heterogenous pathologies, all solid cancers have an underlying cause: dysregulated cell signalling pathways which leads the cells to become tumorigenic and malignant. The development of cancer is a multi-step process, during which cancer cells acquire what are commonly referred to as the 'hallmarks of cancer'.[3,5,6] These hallmarks are sustained proliferative signalling, resisting cell death, evasion of growth suppressors, replicative immortality, inducing angiogenesis, and tumor invasion and metastasis.[3,5,6] Acquisition of these hallmarks is enabled by genomic instability and resulting mutations as well as tumor-promoting inflammation,[5] which can have a variety

of causes such as genotoxic or non-genotoxic carcinogenic substances (e.g., asbestos or polycholinated biphenyls), ionizing radiation, oncogenic pathogens like the human papillomavirus (HPV), or hereditary genetic predisposition. For example, women with germline BRCA 1/2 mutations have a significantly higher chance of developing breast cancer later in life.[6–12]

1.1.2 Treatment Approaches for Cancer

Cancer is a complex disease, which is reflected in the various treatment approaches which include tumor resection, chemotherapy, radiotherapy, and targeted therapies such as hormone therapy or therapy using antibodies and small-molecule inhibitors with the aim of disrupting aberrant cell signalling in tumors. [13–17] A key component in guiding treatment is the proper characterization and staging of the cancer to determine the severity of the disease. The most common staging system for tumors is the TNM system, which classifies cancers based on the size of the primary tumor (T), invasion of regional lymph nodes (N) and presence of distant metastases (M). These parameters are assessed and re-assessed at different times throughout the progression of the disease.[18]

TMN classifications are grouped into prognostic stage groups, ranging from stage I to stage IV. Patients in each stage group have similar prognoses. Stage I represents smaller cancers, which are not deeply invasive into the surrounding tissue and have not yet spread to nearby lymph nodes. Stage II and stage III represent cancers with increasing tumor size and invasiveness into surrounding tissues and lymph nodes. Stage IV represents metastatic cancers.[18]

Surgery, with the aim of resecting as much of the tumor as possible, is the cornerstone of many treatment regimens. Apart from, ideally, removing all of the tumor, it also aides

in tumor staging and allows performance of histopathological and genomic analyses.[19,20] This helps to further guide treatment. Treatment is often classified whether it is performed before (neoadjuvant) or after (adjuvant) surgery. Neoadjuvant treatment often serves to shrink the tumor prior to surgery or transform it from a non-operable to an operable stage, while adjuvant therapy aims to prevent recurrence or slow down further spread in the case of advanced cancers.[14,15]

Chemotherapy is a systemic therapy based on destroying cancer cells using cytotoxic chemotherapeutic agents, which interfere with processes that are commonly upregulated in cancer cells, such as DNA synthesis and maintenance, and mitosis. Inhibiting these processes harms rapidly proliferating cancer cells much more than normal cells. Examples of such drugs are anthracyclines and taxanes, which are effective in a wide variety of cancers. [13,15,20,21]

Radiation therapy is based on exposing tumors to high energy radiation with the aim to cause enough damage to the cells to destroy them. It can be either used as monotreatment, for example in early-stage skin cancers, or as neoadjuvant or adjuvant treatment, for example after a mastectomy.[14,16,22]

Targeted therapy refers to drugs which target specific molecules involved in the development of cancer, such as signalling proteins in cancer cells which promote proliferation and survival. This class of therapeutic agents consists of antibodies and small molecule inhibitors.

Hormone therapy, or endocrine therapy, is used in tumors which are hormone-receptor positive, for example in estrogen-receptor positive breast cancer. Drugs used for hormone therapy either inhibit the synthesis of growth hormones, or act as antagonists to growth

factor receptors to prevent cancer cells from utilizing them for proliferation. In breast cancer, a common hormone therapy dug is tamoxifen, which acts as an estrogen receptor antagonist.[14,15,23]

Targeted therapy using antibodies typically focuses on receptors on the surface of cancer cells such as receptor tyrosine kinases (RTKs). A prominent example are antibodies which target the epidermal growth factor receptor 2 (HER2) in HER positive breast cancers, such as trastuzumab.[13,20]

The other type of targeted agents are small molecule inhibitors which are membrane-permeable and thus can target cell signalling molecules within the cancer cell. This strategy is successfully used for example in treating melanoma using vemurafenib, an inhibitor targeting the BRAF protein with a V600E mutation, or in treating breast cancers using the PIK3CA inhibitor alpelisib.[13,24–26] These inhibitors are often used as second- or third-line treatment in advanced or metastatic cancer, and often in combination with other anti-cancer drugs. The mTOR inhibitor everolimus for example is used concomitantly with endocrine therapy.[14,23]

Another form of targeted therapy which aims not to directly damage cancer cells, but instead aims to utilize the body's own immune system to destroy cancer cells, is immunotherapy. The two main branches of immunotherapy are immune checkpoint therapy and adoptive T cell transfer therapy.

Immune checkpoints are cell signalling mechanisms which regulate immune cell activity. An example of such a mechanism is the programmed cell death 1 (PD-1) protein, expressed on the surface of activated T cells, and programmed cell-death ligand 1 (PD-L1), which is expressed at the surface of antigen-presenting cells of tumor cells. Binding

of PD-1 to PD-L1 inactivates an activated T cell. Many cancers evolve to use immune checkpoints to evade T-cell attacks, for example by overexpressing PD-L1. Immune checkpoint therapy aims to block this inactivation by blocking, for example, either PD-1 or PD-L1 using antibodies. An example is pembrolizumab, an anti-PD-1 antibody used in treating melanoma.[13–15,27]

Adoptive T-cell transfer therapy on the other hand is based on infusing cancer patients with T cells. For example, tumor-infiltrating lymphocytes are extracted from a tumor sample, isolated, and expanded using interleukin-2. These cells are then injected back into the patient. This approach has been used for example in the treatment of metastatic melanoma.[13,27]

1.1.3 The Role of the PI3K Pathway in Cancer and Drug Development

The PI3K pathway is one of the most commonly altered pathways in many cancers such as breast cancer and colorectal cancer. [28–41] It is involved in cell proliferation, cell growth, survival, and apoptosis. This pathway is activated by receptor tyrosine kinases (RTKs), a class of G-protein coupled receptors. Among the ligands for RTKs are growth factors such as epidermal growth factor and hormones, such as estrogen. Upon ligand binding, RTKs dimerize, which activates their cytosolic tyrosine kinase domain, resulting in autophosphorylation.[28] This recruits phosphatidylinositol 3-kinase (PI3K) to the receptor, either directly or via an adaptor protein.[29,31,37] PI3Ks are a diverse class of kinases, however the most common class of PI3Ks involved in carcinogenesis are class IA PI3Ks, specifically PI3Kα. These consist of a heterodimer of the regulatory subunit p85α and the catalytic subunit p110α. Following the binding of the p85α subunit to the intracellular domain of dimerized RTKs, it facilitates the generation of

phosphatidylinositol-3,4-biphsphate (PIP_2) to phosphatidylinositol-3,4,5-biphosphate (PIP_3). PIP_3 then recruits phosphoinositol-dependent kinase-1 (PDK1) and protein kinase B (AKT) to the membrane, where PDK1, together with the mechanistic target of rapamycin (mTOR) complex 2 (C2), phosphorylates and activates AKT.[36,39,40]

AKT is a central node of the PI3K pathway (Figure 1). One of its main functions is the activation of the mTOR complex 1 (C1), both directly by phosphorylating mTORC1 via a proline-rich AKT substrate of 40 kDa (PRAS40), or indirectly via phosphorylation and subsequent inactivation of the tuberous sclerosis (TSC) 1 and TSC 2 complex, an inhibitor of mTORC1. mTORC1 in turn activates proteins involved in mRNA translation, such as eukaryotic translation initiation factor 4 (eIF4A), as well as ribosomal protein S6 kinase beta-1 (S6K1), a protein involved in protein synthesis and suppression of apoptosis. Further, AKT phosphorylates forkhead box protein O3, BAD and p27, suppressing autophagy and apoptosis (Figure 1). [36,37,39,40]

Several feedback loops exist within the PI3K pathway. For example, phosphatase and tensin homolog (PTEN) acts as the corresponding phosphatase to PI3K, converting PIP3 back to PIP2, thereby down-regulating AKT activity.[40,42] The mTORC1/S6K1 axis is also an important node for various feedback loops within the pathway. For example, it promotes the inactivation and degradation of RTK adaptor proteins, as well as the inactivation of mTORC2, thereby downregulating pathway activity.[37,43] Additionally, the PI3K pathway is connected to other pathways vital for tumorigenesis. For example, AKT and mTORC1 crosstalk with the Wnt/ β-catenin pathway via the phosphorylation of glycogen synthase kinase 3 beta (GSK3β), a central

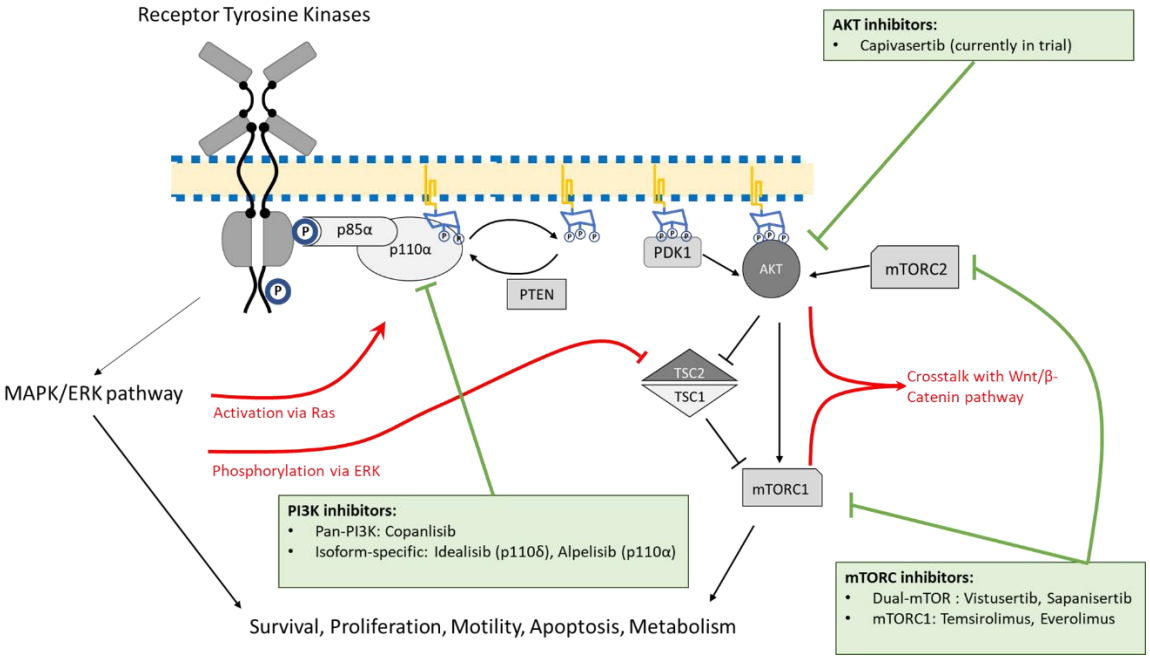

Figure 1. Overview of the PI3K pathway showing the main signalling cascade (grey), crosstalk between to the Wnt/β-Catenin and the MAPK/ERK pathway (red), as well as drug classes targeting this pathway (green).

protein in the β-catenin destruction complex, as well as by affecting the expression of the Wnt receptor FZD (Figure 1).[34,41]

Further, extensive crosstalk exists between the PI3K pathway and mitogen-activated protein kinase (MAPK) pathway, which is also activated by RTKs. For example, the GTPase Ras binds to PI3K recruited to activated RTKs, increasing PI3K's activity.[31] Also, the extracellular signal-regulated kinases (ERK) 1/2 can activate mTORC1 signalling via phosphorylation and inhibition of the TSC1/2 complex (Figure 1).[31,33,43]

Common alterations in the PI3K pathway are activating gene mutations, amplifications as well as loss-of-function mutations.[29,30,32,35,36,41] PIK3CA, the gene encoding the catalytic subunit of PI3K, and its corresponding phosphatase PTEN are among the most highly mutated genes in various cancers. [29,35,44,45]The most common

activating PI3K pathway alterations are gain-of-function mutations or amplifications of PI3K (for example, PIK3CA is mutated in up to 40% of breast cancers), loss of function mutations or deletions of PTEN (25% of $HER2^+$ breast cancers), and AKT gain-of-function mutations and amplifications.[29,32,35,44]

As such, this pathway has become a focus for drug development, with dozens of different inhibitors in various clinical trials. The most common inhibitor classes are PI3K inhibitors (Pan-inhibitors or isoform-specific), mTOR inhibitors, and AKT inhibitors.[33,35] However, only few drugs have been approved by the Food and Drug Administration (FDA), such as the mTOR inhibitors everolimus and temsirolimus and the PI3K inhibitors copanlisib, idealisib, and alpelisib, with AKT inhibitors still in clinical trials (Figure 1).[26,33,35] There are many reasons for drug candidates failing during clinical trials, the most common being intolerable toxicities and insufficient efficacy. A significant challenge is the lack of biomarkers and biomarker technology to effectively stratify patients for PI3K treatment.[33,35]

1.2 Disease Biomarkers

Due to the complex nature of cancer, many different biomarkers are necessary to diagnose the disease and guide the various treatment approaches. The nature of available biomarkers evolves with the analytical technology to detect and quantify them. For example, genome sequencing has had major impact in clinical diagnostics. With the increasing role of targeted therapies, the need for personalized medicine i.e., tailoring treatment to each patient's individual tumor biology, has become apparent. There is a need to find new biomarkers and biomarker technologies.

1.2.1 Definition of Disease Biomarkers

Biomarkers are biological characteristics that can be objectively measured and evaluated as an indicator of normal biological processes, pathogenic processes, or pharmacological responses to a therapeutic intervention.[46] They have been used extensively in the clinic for many decades to improve patient care. For example, the autoantibody rheumatoid factor has been used for the diagnosis of rheumatism since the 1940s.[47,48] Similarly, the presence of antibodies against the human immunodeficiency virus (HIV) has been used for diagnosing HIV since the 1980s.[49]

At different disease stages, biomarkers provide different insights (Figure 2). They indicate the development, progression, treatment response and outlook for a disease and thus are powerful tools for its management and prevention.[46,50–52]

Antecedent biomarkers are useful for exploring the etiology of a disease and the likelihood of developing a certain disease or condition.[51] These biomarkers include risk factors such as environmental, genetic, microbial, and behavioural risks. For example, pathogenic germline mutations of the BRCA1 and BRCA2 genes are genetic risk factors that are strongly associated with a highly elevated risk for breast cancer.[53] Screening for these mutations can be extremely beneficial for preventative care.

Diagnostic biomarkers are used to detect a disease or condition. An example of such markers are blood pressure readings to diagnose hypertension[50]. Ideally, diagnostic biomarkers should identify the intended disease early and with high sensitivity (accurate detection of individuals with the disease) and high specificity (accurate detection of individuals without the disease).

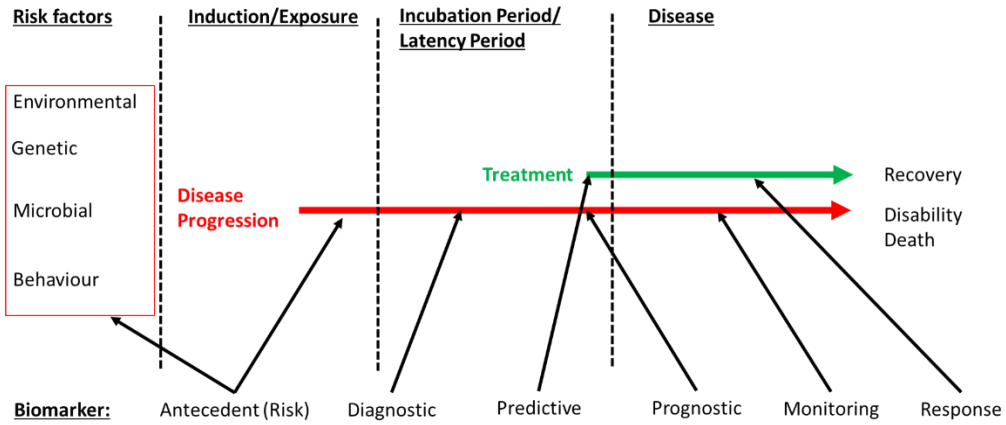

Figure 2. Biomarkers at different stages of the natural history of disease.

Prognostic biomarkers are used to assess the likelihood of certain outcomes or progression of diseases in patients such as death or disease reoccurrence.[46,50,51] In oncology, such biomarkers may include tumor size, metastasis, or molecular signatures which are associated with the five-year survival rate.[50,52] Notably, while prognostic biomarkers are used to establish the likelihood of medical events associated with the disease, they do not predict the effectiveness of a particular treatment. Biomarkers that are used to stratify patients based on their likely response to a particular treatment are called predictive biomarkers.[46,50,51]

Predictive biomarkers can have different clinical utilities. Biomarker guided treatment strategies (treatment-by-biomarker interaction) can be either of quantitative nature, where treatment is *more effective* in biomarker positive patients, or of qualitative nature, where a treatment is *only* effective in biomarker positive patients.[50] For example, the mutation status of epidermal growth factor receptor (EGFR) for the EGFR inhibitor erlotinib is a quantitative interaction. While effective in patients both with and without activating EGFR mutations, erlotinib has been shown to be more effective in mutation-positive patients .[54] An example of a qualitative treatment-by-biomarker interaction is the BRAF

inhibitor vemurafenib, a kinase inhibitor used to treat melanoma. It is only effective in tumors harboring the BRAF V600K mutation and does not act on wild-type BRAF.[55] However, it is important to note that a biomarker can be both prognostic and predictive. Thus, it is important to evaluate potential biomarkers for both characteristics, and to re-evaluate existing biomarkers if considerable technological advances in the quantitation of this biomarker are made. For example, an existing prognostic biomarker measured by a qualitative assay may also prove to be predictive for certain treatments when analysed by a sensitive quantitative assay.

To monitor the progression of a disease and to gain feedback on whether a selected treatment has a positive effect, monitoring and response biomarkers are used. Monitoring biomarkers are regularly measured to provide an update on the status of a medical condition. For example, prostate-specific antigen (PSA) is routinely measured in prostate cancer patients both during active surveillance of the cancer as well as for post-treatment follow-up[50,56]. Response biomarkers are used to assess the patient's response to a treatment. For example, blood pressure is used to evaluate treatment against hypertension.

1.2.2 Biomarker Validation

Before a new biomarker can enter use in a clinical laboratory as a laboratory test, it must undergo extensive validation. The potential clinical benefits and the role of the biomarker in the respective clinical pathway, the algorithm guiding the management of a specific condition in a specific group of patients, must be defined.[57,58]

The biomarker's purpose, target condition, use case, target population as well as sample type, target analyte and data interpretation (qualitative or quantitative) need to be considered prior to evaluation.[59] However, these parameters may also change during the validation of a biomarker.

Generally, a new biomarker should provide a new benefit such as better treatment outcomes in the case of a predictive biomarker, earlier diagnosis of a condition using a diagnostic biomarker, or reducing costs. For an *in vitro* laboratory assay for quantifying a specific biomarker, the evaluation encompasses three key aspects: analytical performance, clinical performance and clinical utility.[57,59]

Analytical performance describes an assay's ability to reliably quantify the target biomarker within the clinically relevant range. To demonstrate this, an assay needs to be validated for linearity (the range in which the assay is directly proportional to the analyte concentration), accuracy (trueness of the assay compared to a reference) and precision and reproducibility (distribution of replicate measurements), the limit of detection and quantitation (the lowest amount that the assay can detect and accurately quantify), as well as specificity (e.g., no interference from sample matrix).[57,60]

Clinical performance assesses whether the measurements of the biomarker assay have a meaningful association with the clinical condition the test was designed for. For example, a diagnostic biomarker needs to demonstrate adequate sensitivity and specificity in discriminating populations with and without the targeted disease.[46,57]

The clinical utility describes the ability of the biomarker to improve health and treatment outcomes for a patient. It is ideally assessed using a randomized clinical trial.

Lastly, cost-effectiveness should also be taken into consideration, since the cost of a test has broad implications for its clinical adaptation and feasibility. [46,57]

These evaluation steps are however not strictly linear. Analytical improvements may open up new avenues for clinical performance, or insights gained during the assessment of clinical performance and utility may inform additional method development for the test, prompting new validation.[57]

1.2.3 Technologies Currently Used in the Clinic for Biomarker Quantitation in Cancer

Biomarkers evolve rapidly with analytical technology. For cancer diagnostics, classification, and treatment, histopathology is one of the oldest tools available. Histopathology relies on the examination of a tissue section of a tumor resection. Tumors are preserved for analysis either 'fresh-frozen' (FF) or using formalin fixation coupled with paraffin embedding (FFPE)(Figure 3).

Fresh-frozen refers to snap-freezing a biological specimen, for example in liquid nitrogen. This rapid freezing prevents the formation of ice crystals which would otherwise damage the tissue.[61]

Tissue preservation using FFPE requires several steps. First, the tissue section is immersed in formalin, a formaldehyde formulation, which leads to the formation of protein-protein crosslinks throughout the tissue. The tissue is dehydrated, followed by paraffin infiltration by placing the tissue in a paraffin solution and then embedding it in a paraffin block. This preservation method allows specimens to be stored at room temperature for years.[62,63]

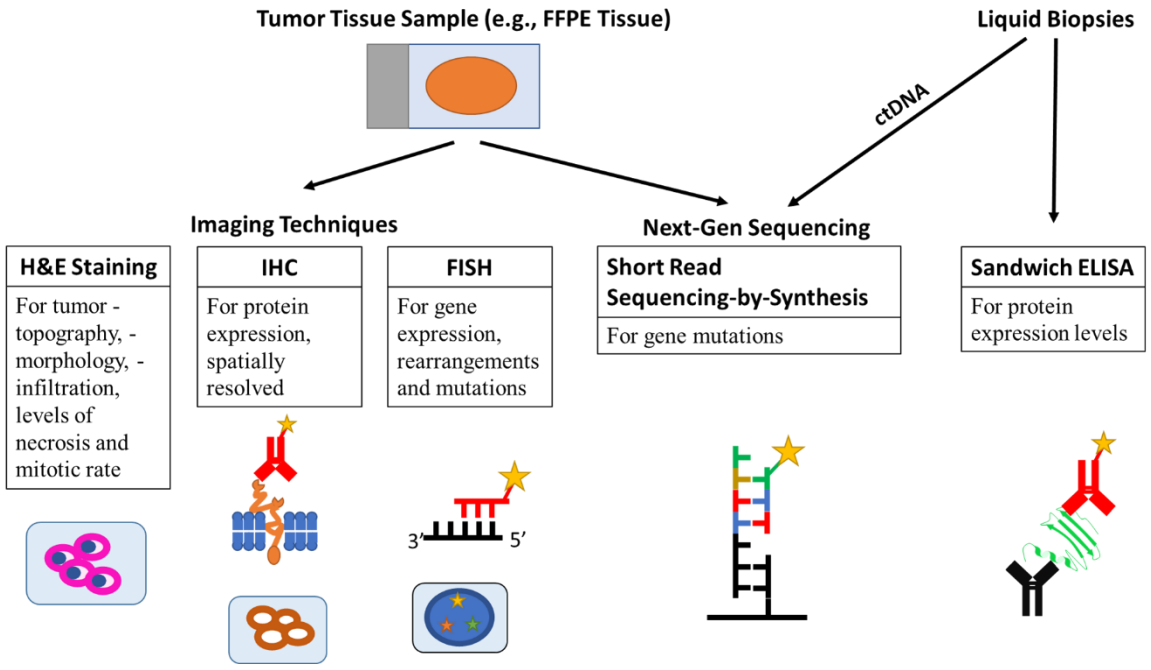

Figure 3. Overview of commonly used technologies for assessing biomarkers for guiding cancer treatment.

Such tumor tissue samples are then sectioned and stained using hematoxylin and eosin (H&E staining).[64] Hematoxylin stains nucleic acids blue and is thus particularly useful for staining cell nuclei.[64] Eosin is the most used counterstain and non-specifically colors proteins red.[64] This staining method reveals a great level of cellular detail in tissue sections. Examples for its uses in analyzing cancer biomarkers are assessing tumor topography, morphology, and infiltration, as well as levels of necrosis and mitotic rate.[65] For example, histomorphologic assessment of non-small cell lung cancer makes it possible to differentiate between squamous cell carcinoma and adenocarcinoma.[66]. This technology is well established, cheap, and versatile.

However, it is insufficient by itself since tumor morphology often is not predictive of response to therapy nor does it provide enough information to guide current treatment approaches.[65] Hence, complementary diagnostic tools for molecular profiling of tumors

are necessary that assess protein expression levels as well as gene expression and mutations status (Figure 3).

One of the most common tools for assessing protein expression is immunohistochemistry (IHC). IHC is an immunostaining method based on applying antibodies against target biomarkers to a tissue sample. Generally, IHC consists of an antigen retrieval step, for example heating, to remove methylene protein crosslinks which may interfere with the antibody binding. Then, anti-biomarker antibodies are added to the tissue section. After the binding is complete, the antibody-antigen complex is visualized either directly, using an enzyme linked to the primary antibody which produces a chromogenic or fluorogenic reaction, or indirectly using a secondary antibody coupled to such an enzyme.[67] Using IHC, protein expression profiles for various tumors can be generated, providing more detailed insight into tumor biology. This allows further subclassification of cancers.[65,66] Not only does IHC improve cancer classification, protein biomarkers assessed using this technique have prognostic and predictive value, and are used to guide treatment. It has since become a standard in cancer diagnostics and an essential part of clinical treatment algorithms. For example, IHC is used to assess the expression of HER2 in breast cancer. Overexpression of HER2 is associated with poor prognosis and is predictive for resistance to endocrine therapies. HER2 status is also used to guide treatment decisions for therapy with trastuzumab, an anti-HER2 antibody, and lapatinib, a small molecule inhibitor for HER2.[68,69]

Other technologies often used to quantify proteins are immunoassays such as enzyme-linked immunosorbent assays (ELISA) as well as electrochemical, chemiluminescent and fluorescence immunoassays. [70–72] ELISA is based on capturing a target using an antibody,

followed by visualization of the antibody-antigen complex by an antibody-coupled enzyme which produces a colorimetric reaction. Direct ELISAs use enzyme-coupled primary antibodies which bind to their target analyte. Upon addition of suitable substrate, the enzyme, for example horseradish peroxidase, produces a colored product. In indirect ELISA, the enzyme is not coupled to the primary antibody, but to a secondary antibody which binds to the primary antibody. A similar method is sandwich ELISA, in which a primary antibody binds the antigen, followed by addition of a second, enzyme-coupled primary antibody.[73] Chemiluminescent and fluorescent immunoassays work similarly to ELISAs, however the antibody-antigen complex is not visualized using an antibody-coupled enzyme. Instead, the antibodies are coupled to a fluorophore, which emits light upon excitations using an external light source, or to a molecule which is chemiluminescent such as luminol, which emits blue light upon oxidation.[74] Immunoassays are primarily used for protein quantitation in liquid biopsies such as blood or urine samples. For example, prostate specific antigen, a biomarker for prostate cancer, and alpha-fetoprotein, a biomarker associated with primary liver cancer, are quantified using various immunoassays.[70,72]

Apart from protein expression, gene expression and gene mutation status are also routinely assessed. Two commonly used technologies are fluorescence in-situ hybridisation (FISH) and next-generation sequencing (NGS). FISH is an imaging technique based on the binding of fluorescence-labeled DNA or RNA probes with complementary strands in a cell or tissue sample. The sample is denatured, followed by adding the DNA/RNA probes which anneal with the complementary part of the endogenous DNA/RNA. This is visualized either directly using probes labeled with a

fluorophore, or indirectly using anti-probe antibodies labeled with a fluorophore. This makes it possible to visualize specific genes in a cell or tissue sample using an imaging system or fluorescence microscope.[75] FISH is used to detect genetic biomarkers such as ALK gene rearrangements in non-small lung cancer.[66]

NGS is collective term for high-throughput genome sequencing technologies which have dramatically decreased the cost and turn-around time of genome sequencing and made sequencing a viable tool for clinical diagnostics in the past 15 years. It is divided into two sequencing approaches: short-read NGS and long-read NGS.[76] In short-read NGS, DNA is first amplified, followed by fragmentation of larger DNA strands into smaller templates (up to 3000 base pairs), which are then sequenced. This is done either using sequencing by ligation (SBL) or sequencing by synthesis (SBS), with SBS being the most commonly used technique.[76–78]

SBS relies on the synthesis of complementary DNA strands using an immobilized template, polymerases, and fluorescence-labeled deoxynucleotides (dNTPs). After each incorporation of a dNTP, the fragments are imaged, successively revealing the nucleotide sequence. This step can be performed in two ways: (a) either by repeating a cycle of adding one labeled dNTP at a time, for example adenine, imagining the template then adding the next dNTP, or (b) by using a cycle of adding all four dNTPs at once, which requires four different fluorophore labels as well as using dNTPs with the 3’-binding group blocked to prevent the incorporation of more than one dNTP, followed by an unblocking step. [76–78]

Long-read NGS encompasses two main technological approaches: Single-molecule real time sequencing (SMRT) and synthetic long reads. SMRT functions similar to SBS;

sequencing is achieved by synthesising a DNA strand based on a template using polymerases and fluorescence-labeled dNTPs.[79] Synthetic long read is based on fragmenting larger DNA strands and uses SBS technology to sequence them. These fragments are then assembled into long reads using bioinformatics.[76,79]

Currently, short-read NGS is often the method of choice for assessing the gene mutation status in various cancers. This is often done using gene hotspot panels, which focus on specific genome regions harbouring known mutation sites for various known oncogenes. Using DNA samples from a cancer tumor, these specific regions are amplified using PCR and sequenced using short-read NGS. This approach is widely used for cancer diagnostics, for example in determining EGFR, KRAS and BRAF mutation status in non-small cell lung cancer, or PIK3CA and AKT1 mutation status in breast cancer. [66,76,80]

Additionally, NGS is also used for quantifying and sequencing cell-free circulating tumor DNA (ctDNA). ctDNA are DNA fragments circulating in the bloodstream, released from circulating tumor cells or tumor sites via both passive mechanisms (e.g., cell death) or active mechanisms (e.g., released from tumor cells through extracellular vesicles). Since ctDNA can be assessed from liquid biopsies, which are far less invasive than solid tumor biopsies , NGS assays for ctDNA are emerging tools for cancer diagnosis and monitoring, detection of residual disease after definitive therapy, and for detecting cancer recurrence or metastasis.[81–83]

These molecular technologies have drastically changed cancer diagnosis and treatment. Current diagnosis and treatment algorithms typically include all of the above methods. ELISA is used for quantifying diagnostic biomarkers for example in liquid

biopsies. Imaging techniques such as H&E staining, IHC and FISH provide insight into tumor topography, morphology and infiltration, as well as spatially resolved expression of protein biomarkers or gene rearrangements, and NGS detects relevant gene mutations in the tumor tissue.[66]

1.3 Mass Spectrometry-based Proteomics

Currently, biomarkers used for patient stratification in cancer treatment are either protein based, such as HER2 expression levels in breast cancer, or DNA based, such as BRAF mutation status in melanoma.

However, there are technological and biological challenges with these approaches. Gene mutation biomarkers are surrogate biomarkers for the protein they encode i.e., an activating mutation in PIK3CA is assumed to lead to an overactive PI3K enzyme on the protein level. However, gene mutation status alone may not be enough to fully assess the activity of the actual oncogene, as each stage of DNA→RNA→Protein pathway is subject to dysregulation in cancer. Indeed, omics analysis of cancer cell lines and tumor tissues revealed low correlation between DNA→RNA→Protein translation.[84–86] Hence, the use of gene-mutation based biomarkers for patient stratification for targeted treatment may leave some patients over-or under-treated. A patient may show activating mutations which would indicate that they would benefit from the treatment, but the implied pathway activation may not actually manifest at the protein level (false positive, leading to overtreatment). Alternatively, a patient may be mutation-negative, but the relevant cell signalling pathway may be elevated through other forms of dysregulation such as proteosomal degradation (false negative, leading to under-treatment). Additionally, it

cannot always be predicted how gene mutations drive tumor biology[85,87], hence it is necessary to incorporate protein-based biomarkers for patient stratification, since it is at the protein level where the tumor phenotype manifests.

Protein-quantitation technologies currently for clinical diagnostics in cancer are immunoassays such as ELISA and IHC. While powerful, these assays often suffer from a lack of standardization, varying degrees of specificity, vulnerability to interferences and artefacts, cross-reactivity and limited multiplexity [73,88–91]. Mass spectrometry-based proteomics has emerged as a powerful tool to mitigate the issues with current protein quantitation methods and has the potential to give a much greater insight into tumor biology.

1.3.1 Principles of Mass Spectrometry

Mass spectrometry (MS) is an analytical technique based on the separation of gas-phase ions using electrical or magnetic fields.[92] It was first developed at the beginning of the 20th century, with the first mass spectrometer being reported in 1914.[92,93] A mass spectrometer consists of three major parts: the ion source, the mass analyser, and the detector (Figure 4).

Molecules are ionized in the ion source using either hard or soft ionization techniques. Hard ionization like electron impact ionization (EI) leads to strong fragmentation of the analyte, making it less useful for larger, complex molecules. Soft ionization techniques such as electrospray ionization (ESI) and matrix-assisted laser desorption/ionization (MALDI) allow the ionisation of large intact molecules, which is why they have become widely adapted in biochemistry.[94] Specifically, the ability of ESI to be coupled with liquid chromatography (LC) was a major breakthrough.[95]

The ions are then guided through the mass analyser, which separates ions based on their mass-to-charge ratio, and into the detector. The most common mass analysers used today are quadrupoles, time-of-flight mass analysers (TOF), and various ion traps such as linear ion traps or orbitraps.

1.3.2 Ion Sources

Electrospray ionization

Electrospray ionization occurs at atmospheric pressure. The sample, consisting of the target analyte suspended in a solution, is injected into the ion source via a capillary. A high potential is applied to the capillary, leading to the formation of positively or negatively charged droplets at the end of the capillary, depending on the applied potential. These charged droplets are then dried in a stream of nitrogen gas (Figure 4). As the droplets shrink (from μm to nm diameter), the repulsive forces between the charged molecules in the sample increase.[92,94]

Depending on the size of the analyte suspended in this droplet, the gas-phase ion is generated in one of three ways. Ions of low molecular weight are ejected from the surface of the shrinking droplet following the ion evaporation model (IEM). Larger, globular molecules, such as folded proteins, are not ejected from the shrinking droplet. Rather, the droplet evaporates to dryness around it, leaving the highly charged ion in the gas phase. This mechanism is referred to as the charged residue model (CRM). Finally, large disordered molecules, such as unfolded or intrinsically unstructured proteins, follow the chain ejection model (CEM): starting from one terminus, they are sequentially ejected from the droplet. [94,96] Following the ionization, the ions are then accelerated into the mass

spectrometer using ion optics with a potential opposite of the injection needle. This ionization mechanism has the major advantage that it can be coupled with liquid chromatography. Thus, it is possible to perform large-scale proteomic analyses on complex biological samples.

Matrix-assisted laser desorption/ionization

Unlike ESI, MALDI ions are not generated from a continuously injected stream of sample, but from a solid surface. In MALDI, the analyte, suspended in a buffer solution, is spotted onto a metal plate (MALDI target or MALDI plate). A solution of small organic molecules capable of absorbing UV-light (the matrix) is added to this spot. Typical MALDI matrices for proteomics are α-Hydroxy-Cyanocinnamic acid (HCCA) or sinapinic acid. As the spot dries, the analyte co-crystallizes with the matrix molecules. A laser beam is then fired at the MALDI spot containing the analyte-matrix crystals. The matrix absorbs the laser, leading to desorption of both the matrix and the analyte into the gas phase (Figure 4).[92]

Ionization occurs following two different mechanisms, both of which happen to varying degrees at the same time, depending on the sample/matrix composition as well as laser intensity. According to the ”Lucky Survivor“ model, analytes retain the charge they had in solution. The charged analytes, together with their counterions, co-crystallize with the matrix and are liberated by the laser beam in a cluster. Charge separation in this cluster, together with the buffering of counterions by protonated or deprotonated matrix ions, leaves the lucky survivor ions.[92,97]

The other ionization mechanism is the ’Gas Phase Protonation’ model. The analytes are present as neutral species. Upon laser ablation, they are ionized by colliding with protonated (or deprotonated) matrix ions, leading to a proton transfer with analyte.[92,97] Compared to ESI, MALDI typically generates ion species with far fewer charge states. Unlike ESI, MALDI is typically performed under vacuum, though atmospheric pressure applications exist.[98,99] Also, since MALDI uses samples in a solid state, combination with liquid chromatography is not easily possible.

1.3.3 Mass analysers

Quadrupole

A quadrupole consists of four metal rods arranged in parallel (Figure 4). Direct and alternating current voltages are applied to each opposing pair of rods. When an ion enters the quadrupole, it will be attracted toward the rods with opposite charge. However, due to the alternating current voltage, the rods switch polarity, thus repulsing the ion. This leads to the ion entering an oscillating trajectory through the quadrupole. Depending on the applied currents, only ions of a specific mass to charge ratio will have a trajectory which will lead to the exit of the mass analyzer.[92,100]

Additionally, quadrupoles can also be switched to only use direct current potential. This allows all ions to pass through it, making it useful as ion lenses, focussing ion beams and passing them between different parts of an instrument.

Quadrupoles are the most used mass analyser. They have fast scan rates and allow continuous sample injection, making it easy to be combined with liquid chromatography. They are also often used as collision cells, which are used to induce fragmentation in a target ion (MS/MS). An example of a collision cell is a quadrupole filled with an inert

gas, through which an ion beam is directed. The ions collide with the gas, fragmenting in the process (collision-induced fragmentation or CID).

However, quadrupoles have a limited mass range of only 2000-3000 Da and a low resolution (~1000-2000 full width at half-maximum (FWHM)) compared to other mass analysers.[92,100,101]

Time-of-flight

Time-of-flight mass analyser work on the principle of accelerating ions through a field-free path in a vacuum. The flight time of the ion is dependent on its mass-to-charge ratio. In a TOF analyser, packets of ions are accelerated into the flight tube from a pulsed ion source. The ions then travel down a linear flight path and hit a detector.[92,100] This configuration is called 'linear mode' (Figure 4).

Many TOF analysers additionally use a reflectron, an electrostatic ion mirror which repels the ions and sets them onto a new trajectory to a different detector. This serves two purposes: First, it equalizes the kinetic energy of ions. Between ions of the same m/z ratio, there are generally small differences between their kinetic energy because of their acceleration into the flight tube. The reflectron compensates for that, as ions with higher kinetic energy penetrate deeper into it, equalizing these differences. Secondly, using a reflectron extends the flight path of the ions considerably. Through the combination of these two effects, the resolution in reflectron mode is considerably higher than in linear mode. For example, the benchtop TOF instrument Microflex (Bruker) achieves resolutions of <1000 FWHM in linear mode and up to 15000 in reflectron mode.[102,103]

TOF analysers have a very large mass range, extending to several hundred thousand Da, making them extremely useful in protein analysis.[92,100] Additionally, since TOF allows to detect many ions of different m/z ratios at once in a single mass spectrum, TOF is used extensively for fingerprinting, for example for peptide mass fingerprinting or lipid analysis for identifying microorganisms.[104–107]

Ion traps

Ion trap mass analysers trap ions in an electronic or magnetic field for an extended period, rather than having them pass through. Many different architectures for ion traps exist. Two designs commonly used in proteomics are linear ion traps and orbitraps.

Linear ion traps function like quadrupoles, with ions being confined within alternating and direct current electric fields. In fact, quadrupoles are commonly used as linear ion traps in many instruments. Instead of letting only certain m/z ratios pass through the quadrupole, the ions are trapped inside and selectively ejected according to their m/z ratio. Linear ion traps allow ion enrichment, leading to higher sensitivity, or to perform MS3 fragmentation. However, their mass resolution is lower than that of TOF analysers.[100,108]

Orbitraps are high-resolution ion traps. They contain a central electrode, flanked by two outer electrodes (Figure 4). Ions enter the trap and assume stable trajectories around the central electrode which ramps its voltage. The frequency of their oscillation is dependent on their m/z ratio and it is measured as an image current induced in the outer electrodes of the ion trap. Orbitraps achieve very high resolution and allow for the analysis of intact, large molecules in the hundreds of kDa.[108,109]

Hybrid and Tandem Mass Spectrometers

Most mass spectrometers do not only use one mass analyser, but a combination of several analysers that enable more complex applications such as ion fragmentation. In proteomics, commonly used hybrid mass spectrometers are usually a combination of three mass analysers, for example three quadrupoles (QQQ), quadrupoles and TOF analyser (Q-TOF), quadrupoles and linear ion traps (Q-TRAP) or ion trap and orbitrap (IT-Orbitrap).[92,109–111]

In proteomics experiments, the first mass analyser (MS1) is used to select a precursor ion from the incoming ionized sample. Only the selected precursor can pass through to the second mass analyser (MS2), which is used to induce fragmentation of the selected ion. There are several fragmentation mechanisms, the most used one being CID. Using CID, the second mass analyser is filled with an inert collision gas that causes the precursor ion to fragment into several product ions, which are detected in the third mass analyser. Depending on the setting of the final mass analyser (MS3), either only one product ion (selected ion monitoring, SIM), multiple product ions (multiple reaction monitoring, MRM), or all product ions (parallel reaction monitoring, PRM) may be observed.[92,109] The combination of several mass analysers thus makes it possible to detect analytes with higher sensitivity and specificity.

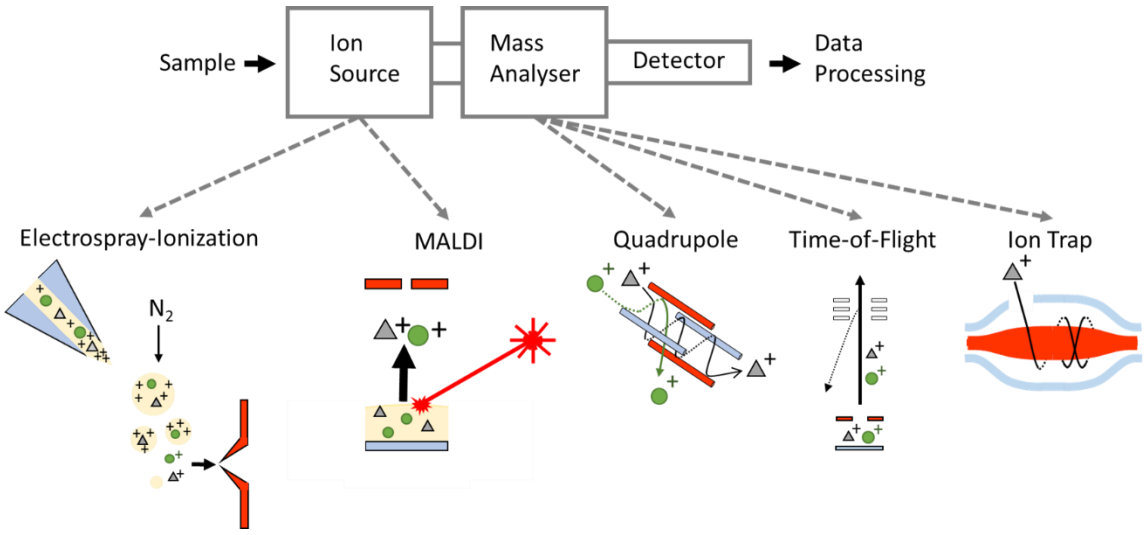

Figure 4. Overview of the architecture of a mass spectrometer, showing ion sources and mass analysers commonly used in mass spectrometry-based proteomics. Red and blue represents electrodes of opposing polarity.

1.3.4 Mass Spectrometry-Based Quantitative Proteomics Approaches

Untargeted proteomics

Untargeted proteomics aims not to quantify specific proteins but aims for maximum proteome coverage.[112] It is often used for discovery studies, for example to investigate differential protein expression in cancers to elucidate cell signalling pathway activation and to identify potential drug targets. Several strategies are used to achieve protein quantitation using untargeted approaches.

Isobaric Labeling is an approach based on covalently coupling heavy isotope labeled molecular tags to peptides prior to MS analysis using reagents such as tandem mass tags (TMT) and isobaric tags for relative and absolute quantitation (iTRAQ). Typically, a sample (for example a tumor tissue sample) is enzymatically digested and then coupled to the isobaric tags. The tags consist of a reporter group and a balancing group. They have

the same molecular weight, but a different distribution of heavy isotopes between the reporter and balancing group. Samples from different experiments can thus be labeled with different tags that all have the same mass and analysed simultaneously using MS. During MS analysis, all tagged peptides with the same sequence are selected in the first mass analyser, and then fragmented. Upon fragmentation the different isobaric tags release reporter ions of different mass, thus allowing to simultaneously compare peptide expression between the different experiments.[113–116]

Stable isotope labeling with amino acids in cell culture (SILAC) is a labeling technique based on growing cell cultures in media enriched with amino acids that are labeled with heavy isotopes. These labeled amino acids are incorporated into the cell's proteins, leading to an isotope labeled proteome. Cells grown using SILAC and cells grown in regular growth media can then be compared in a single MS run, allowing relative protein quantitation between different testing conditions.[113,115,116]

Label-free quantitation does not rely on any kind of labeling prior to analysis. It instead relies on spectral counting or intensities of chromatographic peaks. One approach is to calculate the ratio of identified peptides of a protein to the number of theoretically observable peptides for that protein, called protein abundance index (PAI).[113,115–119] Another approach is to calculate the area under the curve (AUC) for a given peptide peak in the ion chromatogram, and then compare this to AUCs of the same peptide observed in other experiments, allowing relative quantitation. However, label-free quantitation has worse precision, accuracy and reproducibility compared to labeled or targeted approaches.

Targeted proteomics

In contrast to untargeted proteomics, targeted proteomics aims to only quantify specific proteins or peptides. This is achieved both by pre-selecting proteins prior to analysis by mass spectrometry, for example by using antibody-enrichment, and by using synthetic peptide standards, analogous to the targeted peptide, for relative and absolute protein quantitation. Generally, targeted methods have better reproducibility and precision than untargeted methods.[112,120]

MRM-based Quantitation

Multiple-reaction monitoring coupled with liquid chromatography (MRM-MS) is frequently used for protein quantitation. In a typical MRM-MS workflow, a panel of target proteins is chosen. For each target protein, a proteotypic peptide (a peptide with a unique amino acid sequence that is released from the protein after digestion by a proteolytic enzyme) is selected and analogous synthetic peptide standards are made. These standards typically consist of a stable isotope-labelled standard (SIS), with a mass several Da higher than the endogenous peptide (END), as well as a synthetic peptide standard without any isotopic labelling (NAT).

To each unknown sample, SIS is added as an internal standard, co-eluting with the targeted END peptide. Additionally, an external calibration curve with varying amounts of NAT and constant SIS is also run using the same method. Using this calibration, the END:SIS ratio can then be used to determine absolute protein concentrations in the unknown samples. MRM-MS can be coupled with immuno-enrichment on both the protein and the peptide level (pre-or post-digest). [112,120]

iMALDI

Immuno-MALDI-TOF MS (iMALDI) combines antibody enrichment of proteotypic peptides with MALDI-TOF MS analysis. A protein sample, for example a tumor tissue sample, is first digested using trypsin. SIS peptides, analogous to the targeted endogenous END peptide, are added to the digested sample. The peptides are then enriched using anti-peptide antibodies coupled to magnetic beads. The peptide-antibody-bead complex is then magnetically separated, washed, and spotted onto a MALDI target plate. After drying, matrix is added on top of the dried beads, eluting the bound peptides. The sample is then analysed using a MALDI-TOF MS. The ratio of END to SIS peptides allows absolute protein quantitation using an external calibration curve. [121]

1.4 Project Outline and Approach

Personalized medicine has become the focus of the development of new cancer treatments. With standard chemotherapy having reached an efficacy plateau, the focus of drug development lies with targeted therapy such as monoclonal antibodies or protein inhibitors.[122] This approach has seen great success. Targeted therapy, often in combination with classic chemotherapy, has become the standard of care, for example in breast cancer and melanoma treatment. [14,20,123]

However, targeted therapy requires potent predictive and prognostic biomarkers for patient stratification to be effective, since treatment efficacy is highly dependent on the individual patient's tumor biology. Gene mutation-based biomarkers alone may be insufficient since they provide an incomplete picture of pathway activity at the protein level where the drugs act.

Protein-based biomarkers are necessary to provide complementary information. Protein-quantitation technologies currently used for clinical diagnostics in cancer are immunoassays such as ELISA and IHC. While powerful, these assays often suffer from a lack of standardization, varying degrees of specificity, vulnerability to interferences and artifacts, cross-reactivity and limited multiplexicity.[73,88–91]

Liquid chromatography mass spectrometry (LC-MS)-based proteomics has emerged as a powerful tool for protein quantitation. However, it has drawbacks such as expensive instrumentation, long run times (10-60 min) and the need for specialized operators. A solution for this problem is iMALDI, which combines immune-enrichment with MALDI-TOF mass spectrometry. Immunoenrichment allows high sensitivity, and MALDI-TOF MS readout alleviates problems such as antibody cross-reactivity of which ELISAs frequently suffer. All liquid handling steps can be automated using a benchtop liquid handling robot, and MALDI-TOF MS analysis is done using a Microflex (Bruker, Germany), an FDA-approved MS which is already present in many clinics as a biotyper (Figure 6).[124,125] Additionally, sample analysis times are seconds per run, compared to minutes per run for LC-MS. iMALDI is a targeted proteomics approach, which allows absolute protein quantitation, and thus the establishment of clinical reference ranges for protein biomarkers, better reproducibility and easier translation of biomarkers between systems.[87]

This may further help to address another major issue with proteomics-based biomarkers. Indeed, while many candidate biomarkers are identified in the discovery stage, very few proteomics-based tests, as little as 10%, make progress towards clinical application. [126] This highlights the need to develop technologies to facilitate biomarker

translation. iMALDI is an optimal method for translating mass spectrometry-based assays into the clinical environment, since it uses instruments and workflows which are already established, while allowing a high degree of automation.

This project aims to develop automated iMALDI assays for the use of quantifying cell signalling proteins in the PI3K pathway for improving patient stratification for targeted cancer treatment. Specifically, the aim is to develop iMALDI assays for PI3K catalytic subunit p110α and PTEN, evaluate their analytical performance, and combine them with an already developed AKT assay.[121] AKT and p110α are central upstream nodes in the PI3K pathway and thus are common drug targets for targeted therapy, with inhibitors either currently in clinical trials or having already received FDA approval.[26,35,127,128] PTEN is a tumor suppressor immediately downstream of p110α and upstream of AKT. It is commonly dysregulated in many cancers, and loss of PTEN is associated with PI3K pathway activation and resistance to p110α inhibition.[129]

All three proteins are dysregulated not only via gene mutations, but also via aberrant expression levels.[86,128,130–132] Thus, this project may help establish mass-spectrometry-based proteomics as a tool for clinical oncology, specifically for improving patient stratification for targeted cancer treatment.

As described in chapter 2, the development of the PTEN+p110α iMALDI assays began with selecting suitable proteotypic peptides for both target proteins and generating anti-peptide antibodies, followed by optimizing assay parameters such as digestion conditions and incubations times (Figure 5). The assay was automated using a liquid handling robot, and R scripts were developed to improve data analysis. In chapter 3, different multiplexing strategies were explored to integrate the iMALDI assay to with the existing

AKT assay. After development, the assay was validated for linearity, accuracy, precision, and reproducibility to demonstrate that they are fit-for-purpose. As described in chapter 4, a novel two-point internal calibration strategy using two internal standards was developed and demonstrated with the developed PTEN iMALDI assay as well as an orthogonal PTEN immuno-MRM assay, increasing assay throughput, and eliminating the need for surrogate calibration matrices. Here, it is also shown that the developed iMALDI assay performs comparable to the 'gold-standard' LC-MS method.

Finally, in chapter 5, the assays, combined with the existing iMALDI assay for AKT1+2, were applied to patient tumor samples from a clinical trial of the AKT inhibitor capivasertib (AZD5363) in order to demonstrate that the assays allow automated, robust absolute protein quantitation using instrumentation already present in many clinics, thus making clinical translation of these assays easier and demonstrating the analytical performance of the assay.

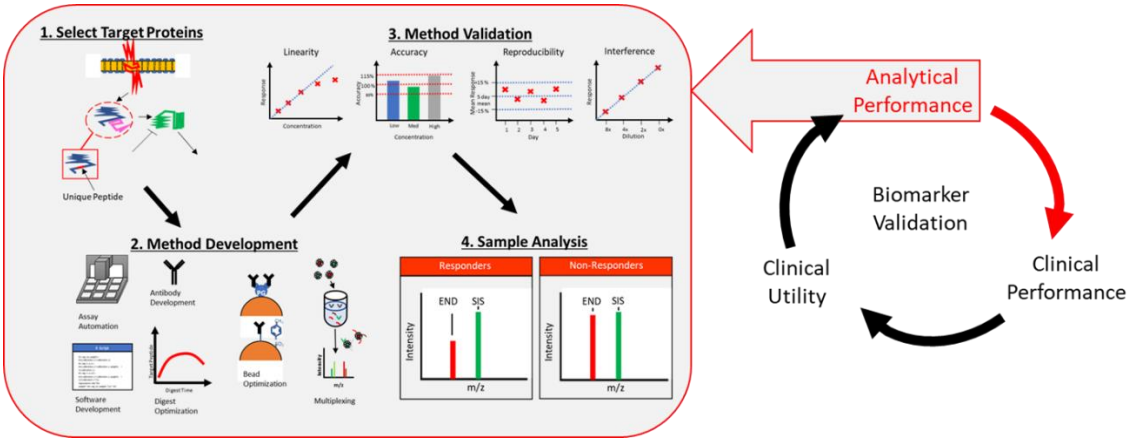

Figure 5 Thesis project outline and its role in the biomarker validation framework. The project aims to develop iMALDI assay for p110α and PTEN. Step 1: Selection of suitable proteotypic peptides for antibody development. Step 2: Method development, consisting of antibody evaluation, assay optimization and multiplexing, as well as assay automation. Step 3: Method validation of the PTEN+p110α assay for linearity, precision and accuracy, reproducibility and interferences. Step 4: Analysis of a set of patients samples from the phase II drug trial of the AKT inhibitor Capivasertib to demonstrate that the assays are fit-for-purpose.

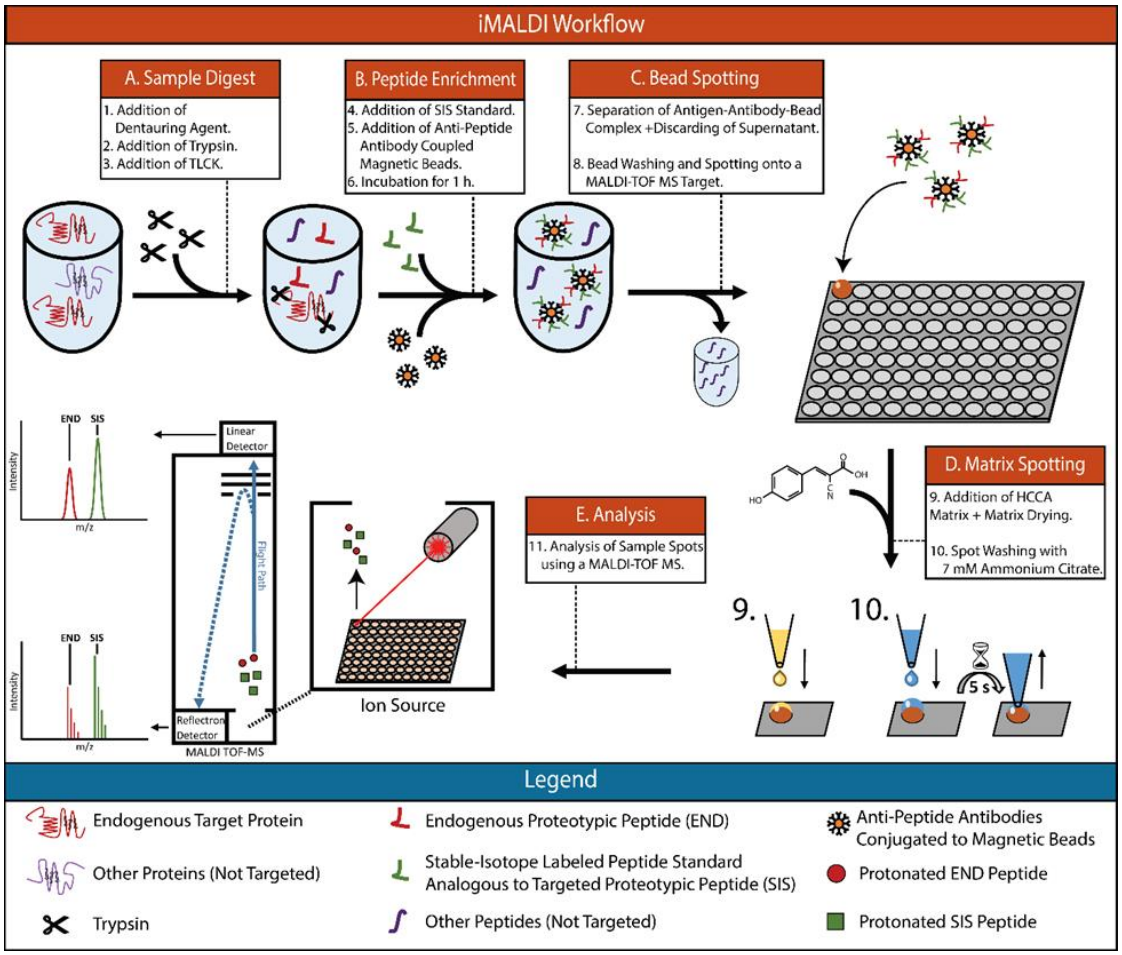

Figure 6. Automated iMALDI workflow for quantifying cell signalling proteins. Following proteolytic digestion (A), SIS standards are added and both the END and SIS peptides are enriched using antibodies coupled to magnetic beads (B). The antibody-antigen bead complex is magnetically separated, washed and spotted onto a MALDI plate (C). After drying, the spots washed and matrix is added (D), followed by analysis using a Microflex in either linear or reflectron mode. Differential expression levels of the targeted proteins may give insight into tumor biology which can be used to guide treatment. All liquid handling steps (A-D) can be automated using a liquid handling robot. END= Endogenous Peptide. SIS= Stable-isotope labelled standard. HCCA= hydroxy-Cyanocinammic acid. Nα-Tosyl-L-lysine chloromethyl ketone hydrochloride

Chapter 2 Systematic optimization of the iMALDI workflow for the robust and straightforward quantification of signalling proteins in cancer cells

Work in this chapter was performed at the UVic Genome BC Proteomics Centre (PC) and at the Jewish General Hospital in Montreal (JGH). MDA-MB 231 cell lysates were prepared by Adriana Aguilar-Mahecha (JGH). All experiments herein, and the data analysis thereof, were performed by Bjoern Froehlich. Experimental design was performed by Bjoern Froehlich, Andre LeBlanc, Rene Zahedi, and Christoph Borchers. Christoph Borchers oversaw the project. The contents of this chapter were adapted from the following publication:

Bjoern C. Froehlich, Constance A. Sobsey, Sahar Ibrahim, Andre LeBlanc, Yassene Mohammed, Adriana Aguilar-Mahecha, Oliver Pötz, Alan Spatz, Mark Basik, Gerald Batist, René Zahedi, and Christoph Borchers,

"Systematic optimization of the iMALDI workflow for the robust and straightforward quantification of signalling proteins in cancer cells". PROTEOMICS – Clin. Appl., 2020, 2000034. 10.1002/prca.202000034.

2.1 Introduction

The most commonly used methods in clinical diagnostics for quantifying protein levels are immunoassays (IA) such as ELISA and IHC.[133–135] The general advantages of IAs are a simple workflow and high sensitivity, while IHC additionally provides spatial information about protein concentrations within tissue samples. Despite their widespread use, these assays can suffer from antibody cross-reactivity and matrix effects. Moreover, IHC is only semi-quantitative and has limited multiplexing capability.[135–137]

Mass spectrometry has emerged as a technology that allows these issues to be addressed. Recent advances in untargeted mass spectrometry using liquid chromatography coupled with mass spectrometry (LC-MS) has enabled the large-scale detection and quantification of low-abundance proteins and peptides in complex matrices.[138–141] These methods offer high reproducibility and selectivity but have comparatively long analysis times, and require relatively expensive instrumentation and well-trained operators. Additionally, these methods often lead to only "relative" results (i.e. up or down regulation), whereas, in a clinical context, the precise determination of protein/peptide levels is often required.[112]

A more appropriate technique for clinical analysis using mass spectrometry is *absolute* quantification using targeted proteomics.[87,112] Combining anti-peptide antibody-based immuno-enrichment of peptides with mass spectrometry as quantitative readout has been shown to be a simple approach for improving selectivity and for achieving high sensitivity and throughput in complex biological samples.[142]

iMALDI in particular useful for targeted proteomics.[121] The low complexity of the immuno-enriched samples circumvents the need for elaborate and expensive LC-MS

instrumentation, and the presence of MALDI-MS instruments in many clinical laboratories for microbial identification makes this technology especially well-suited to clinical translation.[143,144]

One iMALDI application of particular interest is the quantification of cell signalling proteins in patient tumor samples, which should be helpful for stratifying patients for targeted cancer treatment.[84,86,134,145]

In this study, we focus on the PI3K pathway which controls cell proliferation, survival, and apoptosis. It is commonly altered in many cancers, including breast cancer and colorectal cancer, and is a major drug target. PI3K p110α, and PTEN are commonly dysregulated on both the genetic and protein levels, and are a indicators of PI3K pathway activity. [35,36,131,132] Quantifying these proteins in cancer tumors might, therefore, improve patient stratification for treatments targeting the PI3K pathway. Since iMALDI is typically conducted using anti-peptide antibodies specific to proteotypic peptides of the target protein, the use of synthetic SIS peptides allows the precise determination of protein concentrations.

An iMALDI assay comprises a number of sample preparation steps that can affect the overall outcome: (i) digestion of protein lysates (both digestion time and relative trypsin amount used) to release endogenous target peptides (Figure 6), (ii) coupling of the antibodies to magnetic beads, (iii) peptide enrichment using anti-peptide antibodies (Figure 6, B), (iv) separation of the antibody-antigen-bead complex from the sample, (v) transfer of the beads to a MALDI target plate (Figure 6, C), (vi) matrix addition and target spot washing (Figure 6, D), (vii) and data acquisition and analysis (Figure 6, E). Optimization and automation of these steps in order to improve handling time,

robustness, and sensitivity is essential for translation of the developed assay into the clinic. For instance, digestion conditions need to be optimized to achieve reproducible release of the target peptide(s) as quickly as possible.[146] Similarly, antibody enrichment conditions need to be optimized, which can be challenging since various antibodies can exhibit very different binding kinetics.[147,148] The surface chemistry of magnetic beads used to bind anti-peptide antibodies plays a crucial role as well, as it is important to minimize non-specific binding of background peptides to the antibody-coupled magnetic beads. This is of major importance for iMALDI, as it does not include liquid chromatography to reduce sample complexity and is therefore more susceptible to interferences from the sample and dynamic range issues than other MS-based assays. While this lack of liquid chromatography is a major advantage for the ease of translation, it requires a higher level of specificity of the actual enrichment in order to minimize and avoid interferences from the matrix.

Another challenge is to find suitable calibration matrices. Calibration using standard addition, i.e., by using the sample itself as the matrix, is often impractical since large amounts of sample would be required for the complete workflow. Since, after successful and efficient immuno-enrichment, both the complexity and the dynamic range of the matrix are limited, the use of surrogate matrices for generating calibration curves and determining the parameters of the assay is a valid strategy.[149]

In this chapter, we systematically evaluated and optimized critical steps of the iMALDI workflow to streamline the procedure and further improve the robustness and sensitivity of iMALDI for quantifying cell signalling proteins. This chapter provides a template that can be followed to optimize future iMALDI assays.

2.2 Materials and Methods

2.2.1 Materials

Reagents were purchased from Sigma Aldrich (St. Louis, MO) unless otherwise specified. LC-MS grade water and LC-MS grade acetonitrile were purchased from Thermo Fisher (Waltham, MA). Unlabelled (NAT) and stable-isotope labelled peptides (SIS) analogues of the PTEN peptide ^{148}AQEALDFYGEVR^{159}, as well as a double-isotope labeled standard (dSIS) analog of the AKT2 peptide ^{468}THFPQFSYSASIRE^{481}, were synthesized, purified, and quantified in-house at the UVic- Genome BC Proteomics Centre (Victoria, Canada).[150] PTEN dSIS, as well as unlabelled, mono-and-double isotope labelled standards analogues of the p110α peptide ^{503}EAGFSYSHAGLSNR^{516} were obtained from SynPeptide (Shanghai, China). Peptide concentration and purity were determined by amino-acid analysis and capillary zone electrophoresis at the UVic-Genome BC Proteomics Centre.[150] Polyclonal rabbit anti-peptide antibodies (pAbs) were ordered from Signatope (Reutlingen, Germany). Antibodies were generated and purified as described previously, but using the peptides AQEALDFYGEVR for PTEN and EAGFSYSHAGLSNR for p110α. as antigens.[151]

Protein G Dynabeads and M280 Tosylactivated Dynabeads were obtained from Invitrogen (Carlsbad, CA). MagReSyn Protein G beads were purchased from Resyn Biosciences (Gauteng, South Africa). Trypsin (TLCK treated) was purchased from Worthington (Lakewood, USA). Bravo 96 LT liquid handling robot (Agilent Technologies), equipped with a tip wash station and a plate shaker, was used for assay automation. Samples were analysed using a Microflex LRT MALDI-TOF MS (Bruker

Daltonics, Bremen, Germany). µFocus MALDI target plates were purchased from Hudson Surface Technologies (Suwon, S. Korea).

2.2.2 General iMALDI Method

Preparation of Cell Lysates

E. coli BL21 DE3 cells were grown overnight in lysogeny broth (10 g/L Tryptone, 10 g/L NaCl, 5 g/L yeast extract) at 37 °C. Cells were pelleted and resuspended in PBS (pH 7.4). Protein extraction was performed using T-PER buffer (Thermo Fisher). Protein concentration was determined using a Bicinchoninic acid assay (BCA) assay (Thermo Fisher). *MDA-MB 231* cell lysates were prepared as described previously.[121]

Antibody-bead Coupling

Protein G Dynabeads were washed 7x with 25:75 acetonitrile:(PBS+0.015 % (w:w) CHAPS (PBSC)) and 3x PBSC buffer, using 1:10 bead-slurry: buffer (v:v). This step was automated using Bravo 96 LT liquid handling robot (Supporting Figure S 2 A). Rabbit polyclonal anti-peptide antibodies (1 µg/µL in PBS+0.05 % sodium azide) were added (0.2 µg antibody per 30 µg beads) and incubated while being rotated at room temperature for 1 h. Prior to use, the antibody-coupled beads were washed 3x with PBSC and reconstituted in PBSC to give a final concentration of 1.5 µg beads/µL (0.01 µg antibody/µL).

Tryptic Digest

E.coli and *MDA-MB 231* lysates were diluted to a concentration of 0.1 µg protein/µL using cold (4° C) 20 mM TRIS HCl at pH 8 supplemented with 0.015 % CHAPS (TRIS+C). Each sample was aliquoted in 100-µL aliquots (10 µg total protein, each). Using a Bravo 96LT liquid handling robot (Supporting Figure S 2 B), 10 µL of 10 % sodium deoxycholate (final concentration = 0.9 %) were added to each aliquot, and samples were incubated for 30 min at 60 °C. 10 µL of trypsin solution (0.2 µg trypsin/µL in 1 mM HCl, 20 µg total trypsin per replicate) were added and samples were incubated at 37 °C for 1 h. Ten µL of 170 µM Nα-Tosyl-L-lysine chloromethyl ketone hydrochloride (TLCK) solution were added to stop the digestion (Figure 6 A).

Peptide Enrichment

The following liquid handling steps were performed using a Bravo 96 LT liquid handling robot (Supporting Figure S 2**,** Supporting Figure S 3). Internal standard (SIS or dSIS) and, where applicable, NAT were added to the digested samples prior to enrichment, the precise amounts are specified in the according sections below. Twenty µL of antibody-bead slurry (1.5 µg beads/µL, 10 ng antibody/µL) was added to the sample and incubated for 1 h at room temperature, while shaking at 1000 RPM (Microplate Vortex 120V ADV, Thermo Fisher). The antigen-antibody-bead complex was separated, washed 1x using 70 µL of PBSC, 3x using 80 µL of 5 mM ammonium bicarbonate (AmBic). After resuspension in 10 µL of AmBic, the beads were subsequently spotted onto a 2600 µm µFocus MALDI target plate. After the spots were dried, 1.5 µL of matrix (3 mg/mL α-cyano-4-hydroxycinnamic acid, 7 mM ammonium

citrate (dibasic) in 70% acetonitrile (ACN), 0.1% trifluoroacetic acid (TFA, Thermo Fisher) were added. After drying, spots were washed three times as follows: 5 µL of 7 mM ammonium citrate dibasic (AmCit, pH≈5) were added on top of each spot, and removed after 5 s (Figure 6 B-E).

Data Acquisition and Analysis

The MALDI plates were analysed on a Bruker Microflex LRT in both linear positive (LP) and reflectron positive (RP) mode. One thousand shots were accumulated per spot in 25-shot intervals using a 'random walk' pattern. The data was analysed using FlexAnalysis (Bruker, v3.4, Build 70). Linear mode spectra were smoothed using the Savitzky Golay algorithm (10 cycles with a 1-Da width and TopHat baseline subtraction). Peaks were detected using Centroid (Peak width= 1 Da, height= 80 %). Reflectron mode mass spectra were smoothed using Savitzky Golay (1 cycle, Peak width= 0.2 Da and TopHat baseline subtraction). Peaks were detected using SNAP (SNAP average composition= Averagine[152]). Mass lists were exported and analysed using R (Supporting Figure S 1).[153]

2.2.3 Selection of Proteotypic Peptides for Antibody Development

Recombinant PTEN protein was purchased from Abcam (85 % purity). Recombinant PI3K p85α p110α was gifted by Dr. John Burke. Candidate proteotypic peptides for antibody development were identified using *Peptide Picker*[154]. Candidate peptides were experimentally confirmed using tryptic digests of the respective recombinant proteins analysed by MALDI-TOF MS.

One microgram of recombinant protein was denatured in 15 µL of 2 M urea, reduced with 2 µL 20 mM dithiothreitol (DTT) for 30 min at 37 °C, and alkylated with 2 µL of 80 mM iodoacetamide (IAA) for 30 min at 37 °C. Alkylation was quenched using 1 µL 80 mM of DTT, followed by digestion using 1 µL trypsin solution (0.1 µg/µL in 1 mM HCl) for 1 h at 37 °C. The digests were desalted using C18 ZipTips (Millipore, Burlington, MA) and eluted in 20 µL of 50% ACN, 0.1% TFA, 2 µL (0.05 µg digested protein) of which were used for analysis. Matrix addition and spot washing were done as described above. The samples were analysed using an Ultraflex III *(*Bruker).

pAbs were raised against the most intense proteotypic peptides identified in the respective protein digests (PTEN: ^{148}AQEALDFYGEVR^{159}, p110α: ^{503}EAGFSYSHAGLSNR^{516}). Two pAbs were generated for each target peptide. Corresponding synthetic peptide standards with and without isotopic labeling were generated as described in above.

To compare the pAb performance, the *E.coli* lysate digest (10 µg total protein per replicate) was spiked with 2.5 fmol per replicate of PTEN and p110α NAT peptides. Using the spiked *E.coli* digest as the sample, PTEN and p110α NAT peptides were enriched using the different pAbs coupled to Protein G Dynabeads, as described above (N=4 per and pAb). Additionally, the MALDI matrix was spiked with AKT2 dSIS peptide as external standard to a concentration of 0.67 fmol/µL, resulting in 1 fmol peptide per sample spot using 1.5 µL of matrix. Antibody-enrichment efficiencies between the antibodies were compared between pAbs using the NAT:AKT2 dSIS ratios and two-sided t-tests with a confidence level of 0.99.

2.2.4 Comparison of Manual versus Automated Washing

Ten 10-µg aliquots of *E. coli cell lysate* were each spiked with 2.5 fmol PTEN ($AQEAL_{(+7)}DFYGEVR_{(+10)}$) and p110α ($EAGFSYSHAGL_{(+7)}SNR_{(+10)}$) double-SIS (dSIS) peptide. iMALDI assays were done according to the procedure described above. For 5 samples, the antigen-antibody-magnetic bead complexes were washed and spotted manually after incubation with the sample; the other 5 were washed and spotted using the automated bead washing+spotting protocol (Supporting Figure S 3). AKT2 dSIS ($THF_{(+10)}PQFSYSASIR_{(+10)}E$) peptide was added to the matrix to a concentration of 0.67 fmol/µL as an external standard, resulting in 1 fmol AKT dSIS peptide per sample spot. Automated and manual bead washing were compared based on the ratio between PTEN and p110α dSIS to the AKT2 dSIS intensities, respectively by two-sided t-tests with a confidence level of 0.99.

2.2.5 Optimization of Tryptic Digestion

Protein:trypsin ratios of 10:1 and 1:2 as well as digestion times of 0.5, 1, 2, and 4 h were compared. Using *MDA-MB 231* cell lysate (0.1 µg total protein/µL), thirty-two 100-µL aliquots were prepared (10 µg of total protein each). Sixteen aliquots each were digested using a protein:trypsin ratio of 10:1 (w:w) and 1:2 (w:w), respectively. For both tested ratios, four replicates each were digested for 0.5, 1, 2 h, and 4 h at 37 °C. Afterwards, 2.5 fmol PTEN and p110α SIS and dSIS peptides were added as internal standards. iMALDI assays, with AKT2 dSIS peptide added as internal standard to the matrix, were done as described above. Peptide recoveries were calculated using the ratio of the peak intensities of the released endogenous peptide to the spiked-in dSIS peptide.

The release of endogenous proteotypic peptides was compared for the different incubation times and for both protein:trypsin ratios. The results were evaluated using a two-sided t-tests with a confidence level of 0.99.

2.2.6 Optimization of Calibration Strategies

PBSC, BSA digest (0.1 µg/µL in TRIS+C buffer), and *E.coli* digest (0.1 µg/µL in TRIS+C buffer) were tested as possible calibration matrices. PTEN (AQEALDFYGEVR) and p110α (EAGFSYSHAGLSNR) NAT peptide standards (c= 1.000, 0.500, 0.250, 0.125, 0.062, 0.030, 0.000 fmol/µL) were prepared manually.

Calibration curves were prepared by adding 20 µL of the respective standards to either PBSC, BSA digest (10 µg total protein per replicate) or *E.coli* digest (10 µg total protein per replicate), yielding amounts from 0 to 20 fmol per replicate. Additionally, four replicates of *MDA-MB 231* digest (100 µL of 0.1 µg total protein/µL) were prepared to quantify endogenous PTEN and p110α using the different calibration strategies. A solution containing 2.5 fmol PTEN and p110α SIS and dSIS peptides were added as internal standards to each sample. iMALDI assays were conducted as described above iMALDI assays were conducted as described above using automated wash protocols.

To determine whether the peak parameters used for generating the calibration curve would affect the quantification, calibration curves were generated using NAT:dSIS ratios based on either the peak intensities, the S/N ratios of the respective NAT and dSIS ratios, or the peak areas, generating a total of 3 calibration curves per matrix.. For the *MDA-MB 231* samples, the NAT:dSIS ratios were determined the same way: PTEN and p110α

were quantified using the three different calibration curve strategies for each matrix. The results were compared using two-sided t-tests with a confidence level of 0.99.

2.2.7 Optimization of Immuno-enrichment

E.coli cell lysate digest was used as sample matrix for the experiments described below. Prior to digestion as described above, the lysate was reduced and alkylated as described previously. [121]

Optimization of Bead Types and MALDI Plate Spot Sizes

Three different types of magnetic beads were tested for antibody coupling: Protein G Dynabeads, M280 Tosylactivated Dynabeads, and Protein G MagReSyn microspheres. Additionally, two types of MALDI plates were tested for each bead type: 2600 µm µFocus MALDI plates and 700 µm MFX µFocus MALDI plates (Hudson).

Bead Preparation

Protein G Dynabeads were prepared as described above (bead suspension 'PG #1'). The bead suspension was diluted 10-fold using PBSC (3 µg beads (0.02 µg antibody)/10 µL, bead suspension 'PG #1_1/10').

M280 Tosylactivated Dynabeads were prepared by washing 0.625 mg of beads with 200 µL of 0.1 M sodium phosphate buffer (pH 7.5), resuspending them in 6.25 µL of PTEN and 6.25 µL p110α antibody (c=1 mg/mL each) in 1 M ammonium sulfate and incubating them for 20 h at 37 °C with rotation. The supernatant was removed, 0.2 mL of 20 mM TRIS+0.015 % CHAPS buffer (buffer C) were added for quenching, and samples

were incsubated for 1 h at 37 °C with rotation. The beads were washed twice with 0.2 mL of buffer C and resuspended in 20.6 µL of buffer C (30 µg beads (0.6 µg antibody/µL)). From this stock suspension, two dilutions were prepared using PBSC: 'C #1' (30 µg beads, 0.6 µg total antibody per 20 µL), and 'C #1_1/10' (3 µg beads, 0.06 µg total antibody per 20 µL).

Protein G MagReSyn beads (bead suspension 'PG #2') were prepared by resuspending 40.8 µg beads in 600 µL PBSC and sonicating them with a sonication probe (Sonic Dismembrator Model 100, Thermo Fisher) using short bursts (1 s using intensity level 1) until the suspension was homogenous and free of clumps. The beads were then placed on a magnet to remove the supernatant and the beads were resuspended in 20 µL PBSC. The beads were washed 7x with 25:75 ACN:PBSC and 3x with PBSC, as described for the in Antibody-bead Coupling. After washing, the beads were resuspended in 50 µL of PBSC and split into two aliquots. A solution of 4.3 µL of PTEN and p110α antibody solution were added, respectively, and incubated for 1 h with rotation. The conjugated beads were stored at 4 °C with rotation, until used. Prior to use, PTEN and p110α aliquots were combined, the supernatant was removed, and the beads were washed 3 times using 300 µL of PBSC. Finally, the beads were resuspended in 263 µL of PBSC (final concentration= 0.155 µg beads, 0.025 µg antibody per 1 µL).

Assay Preparation

E.coli digest (0.083 µg total protein/µL) was used as sample matrix, from which thirty two 120-µL aliquots were prepared. Additionally, eight 100-µL PBSC aliquots were prepared. PTEN+p110α NAT+SIS+dSIS peptides (1.25 fmol) were added to each

sample. To 4 replicates of *E.coli* digest and 1 replicate of PBS+CHAPS, 20 µL of bead suspensions 'PG #1', 'PG 1_1/10', 'PG #2', or 'C' #1' and 'C #1_1_1/10' were added, respectively. To 8 replicates of *E.coli* digest and 2 replicates of PBSC, 20 µL of bead suspension 'PG #2' were added.

The assays were done as described above. The antigen-antibody-bead complexes were spotted onto two different MALDI Plates: 'PG #1', 'C #1', and 'PG #2' (half of the prepared replicates) were spotted onto a 2600 µm µFocus MALDI plate; 'PG #1_1/10', 'C #1_1/10', and 'PG #2' (second half of the prepared replicates) were spotted onto a 700 µm MFX µFocus MALDI plate. Matrix spotting for the 700 µm MFX µFocus MALDI plate was performed by manually adding 0.2 µL of matrix solution.

Direct vs. Indirect Immuno-enrichment

Twelve aliquots of *E. coli* digest (150 µL, 10 µg of total protein), spiked with 1 fmol PTEN NAT and dSIS standards, were prepared in a 1.1-mL Deep Well plate. Six samples were enriched using direct immuno-enrichment; the other six were enriched using indirect immuno-enrichment, as described below.

Direct immuno-enrichment was performed as described above.

Indirect enrichment was performed as follows. Ten µL of 0.02 µg/µL PTEN anti-peptide antibody solution were added to each of the 6 aliquots and incubating for 1 h at 1000 RPM at room temperature. A 30-µg aliquot of Protein G Dynabeads was added to the sample solution to bind the peptide-antibody complex. Bead washing, spotting, and analysis were done as described before. After immuno-enrichment, the matrix (1.5 µL) was spiked to 0.67 fmol/µL AKT2 dSIS peptide, resulting in 1 fmol of external standard

per sample spot. Two-sided t-tests with a confidence level of 0.99 were performed for comparing the NAT: AKT2 dSIS peptide ratios between the two conditions tested.

Incubation Times

Three PCR plates were prepared containing 10 aliquots of *E.coli* digest (150 µL, 10 µg of total protein) spiked with 1.25 fmol (20 µL 0.0625 fmol peptide/µL) of PTEN and p110α NAT standard (Plates A, B, C). Additionally, 6 more aliquots were prepared in the same way in a 1.1-mL U-bottom deep well plate (Plate D). Plates A, B, and C were incubated rotating (8 RPM), Plate D was incubated shaking at 1000 RPM. Plates A, B, and D were incubated at room temperature, while Plate C was incubated at 4 °C. Plates A and D were incubated for 1 h, while plates B and C were incubated for 22 h overnight. Plate incubation was timed so that all plates would finish the incubation step at the same time. iMALDI assays were conducted as described above, but the matrix was spiked with AKT2 dSIS peptide as external standard to a concentration of 0.67 fmol/µL, resulting in 1 fmol peptide per sample spot using 1.5 µL matrix. Two-sided t-tests with a confidence level of 0.99 were performed to compare the NAT:AKT2 dSIS peptide ratios of plate A to plates B, C, and D, as well as plate B to plate C.

2.3 Results and Discussion

2.3.1 Antibody Generation

Potential proteotypic peptide targets for PTEN and p110α were identified *in-silico* using our Peptide Picker software.[154] Peptides with a length of 7 to 20 amino acids

following Keil rules, present in all isoforms and without Tryptophan or strings of Proline and Serine were considered. Candidate peptides were experimentally confirmed by analyzing tryptic digests of recombinant PTEN and p110α using MALDI-TOF MS (Figure 7**,** Supporting Table S 1). The most intense proteotypic peptides were selected for antibody generation, namely the PTEN peptide ^{148}AQEALDFYGEVR^{159} (Figure 7 A) and the p110α peptide ^{503}EAGFSYSHAGLSNR^{516} (Figure 7 B, Supporting Figure S 4). Having identified the proteotypic peptide with the highest sensitivity using MALDI-TOF MS, rabbit polyclonal antibodies were generated against these target peptides and used for the experiments described below.

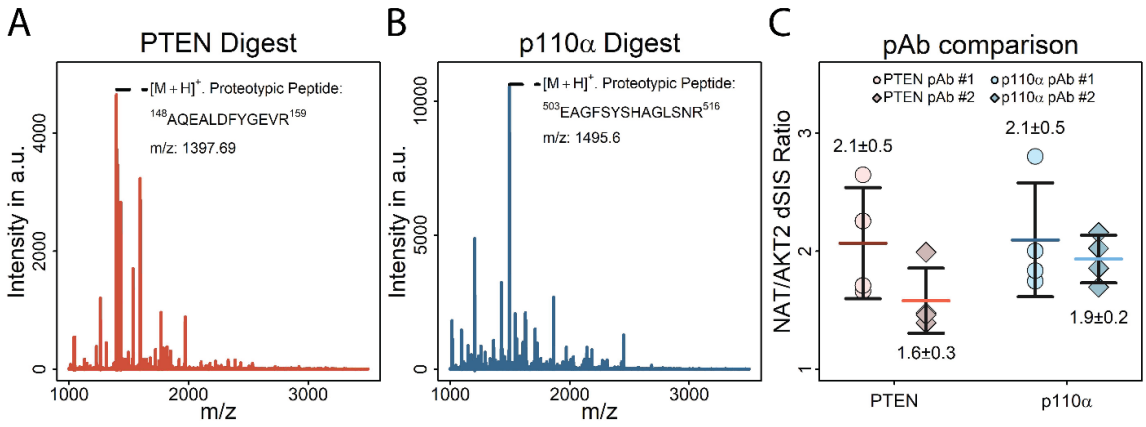

Figure 7. Selection of proteotypic peptides for antibody development and comparison of developed antibodies. Candidate proteotypic peptides for PTEN and p85α/p110α were selected using Peptide Picker and experimentally confirmed by analyzing tryptic digests of recombinant PTEN (A) and p85α/p110α (B) using MALDI-TOF-MS. The most intense proteotypic peptides were selected for antibody development. (C) Comparison of the polyclonal antibodies (pAb). E.coli lysate was spiked with 2.5 fmol PTEN and p110α NAT peptide, which were enriched by iMALDI using each antibody. The signal of isotope-labeled AKT2 peptide ($THF_{(+10)}PQFSYSASIR_{(+10)}E$) spiked into the MALDI matrix (1 fmol per spot) was used for normalization. Error bars represent standard deviation, horizontal bars indicate means. Values above and below the data points represent the mean and absolute standard deviations. No significant difference ($p<0.01$) was detected between the antibodies, showing that different antibodies provided from the same manufacturer (Signatope) provide the same results.

2.3.2 Comparison of Automated and Manual Wash

All liquid handling steps were automated using a Bravo liquid handling robot (Agilent Technologies). The automated separation of the antigen-antibody-bead complex from the sample solution, and the washing and spotting onto a MALDI plate can lead to losses of target peptide at various stages. Loss of antigen-antibody-bead complex may occur during liquid transfer and bead washing steps, and bead washing steps may be less effective due to less efficient removal of supernatants, leading to higher non-specific background levels. Due to the complexity of the procedure and the potential for numerous pitfalls during automation, automated bead washing, and spotting were also compared to the manual procedure (Figure 8**,** Supporting Table S 2).

A comparison of manual and automated washing and spotting revealed no significant difference ($p>0.01$) in enrichment efficiency, as measured by the ratio of PTEN and p110α dSIS to AKT2 dSIS ($PTEN_{automated/manual}= 0.98$; $p110\alpha_{automated/manual}= 0.80$), but particularly for p110α automation improved the CV considerably from 15% to 9%. (Figure 8 **A**). Additionally, mass spectra of iMALDI assays with automated and manual bead washing and spotting show similar backgrounds, demonstrating that both are equally effective (Figure 8 B+C). However, hands-on time is reduced by approximately a factor of six using automation -- manual bead washing and spotting using a full 96-well plate took approximately 90 min, compared to 15 min using the liquid handling system. Manual matrix spotting and spot washing of 96 spots took approximately 60-80 min, whereas the automated protocols required 30 min with little hands-on time. Thus, automation allows the preparation of hundreds of samples per day, without compromising precision ($PTEN_{Manual/Automated\ CV}= 11/10$ %, $p110\alpha_{Manual/Automated\ CV}= 15/9$ %).

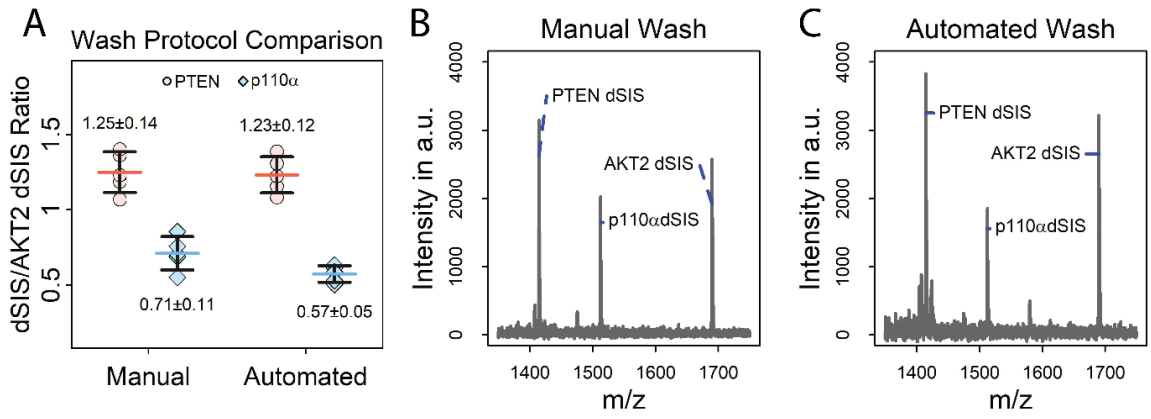

Figure 8. Comparison of automated versus manual washing of antigen-antibody-bead complex. (A) Comparison of the efficiency of manual versus automated bead washing for enriching PTEN and p110α dSIS peptide (2.5 fmol) spiked into E.coli digest. The signal of the stable isotope labelled AKT2 peptide ($THF_{(+10)}PQFSYSASIR_{(+10)}E$) spiked into the MALDI matrix (1 fmol per spot) was used for normalization. Error bars represent standard deviation, horizontal bars indicate means. Values above and below the data points represent the mean and absolute standard deviation. N=5. (B+C) Mass spectra of antigen-antibody-bead complex using manual (B) and automated (C) bead washes, data recorded in the reflectron mode, showing similar non-specific backgrounds between both bead-washing methods.

2.3.3 Optimization of Tryptic Digestion

One of the characteristics of our previously reported protein iMALDI assays is the use of protease inhibitors during lysis and consequently the use of a relatively high amount of trypsin, compared to standard proteomics workflows.[146,155] In this chapter, we report the optimization of the iMALDI digestion conditions for the PTEN and p110α assays in which different protein:trypsin ratios were tested. Specifically, we compared the results of using a 1:2 protein:trypsin ratio, which had previously been used for an AKT iMALDI assay, to a 10:1 protein:trypsin ratio which is more commonly used in typical proteomics experiments, to reduce the occurrence of potential none-tryptic cleavages derived from residual contamination with chymotrypsin and to reduce the abundance of tryptic autoproteolysis products.[121] In addition, different incubation times (from 0.5 to 4 h) were

tested (Figure 9). Ten µg of MDA MB 231 lysate was used as sample, 2.5 fmol of PTEN and p110α dSIS were spiked in.

For both target peptides and the two protein:trypsin ratios tested, the release of the endogenous target peptide as determined by the END:dSIS ratio, did not significantly improve with incubation times greater than 1 h. For example, no significant difference ($p>0.01$) between END:dSIS ratios was observed between a 1-h and 4-h incubation using 10:1 protein:trypsin, for either target peptide ($PTEN_{1h:4h}=0.91$, $p110\alpha_{1h:4h}=0.97$). Peptides are readily released, and the END:SIS ratios observed indicate that chymotryptic side-activity is unlikely, even when very high amounts of trypsin are used, as chymotryptic side-activity would have been more pronounced in the samples with higher trypsin concentration, leading to reduced END levels that would have been reflected by lower END:SIS ratios. Overall, peptide recoveries were approximately 30% higher when using a 1:2 protein:trypsin ratio (Figure 9A,B**,** Error! Reference source not found.).

For both PTEN and p110α, at both protein:trypsin ratios tested and digestion times, no change in the non-specific background of the mass spectra was observed. No background peaks interfered with either PTEN or p110α END peptides, or their respective SIS and dSIS standards at either digestion ratio (Figure 9 C, D). CVs were consistently below 10 % for both peptides, with the exception of 0.5 h incubation using 1:2 protein:trypsin (PTEN/p110α CV= 15/14 %).

For further experiments, we chose to use a 1-h incubation time using a 1:2 protein:trypsin ratio, since incubation times of greater than 1 h did not improve the release of endogenous target peptide and it was desirable to keep turnaround times short. Using a high amount of trypsin ensures high digestion efficiency, and after

immunoenrichment, we found no background peaks which interfere with the peaks of the enriched peptides.

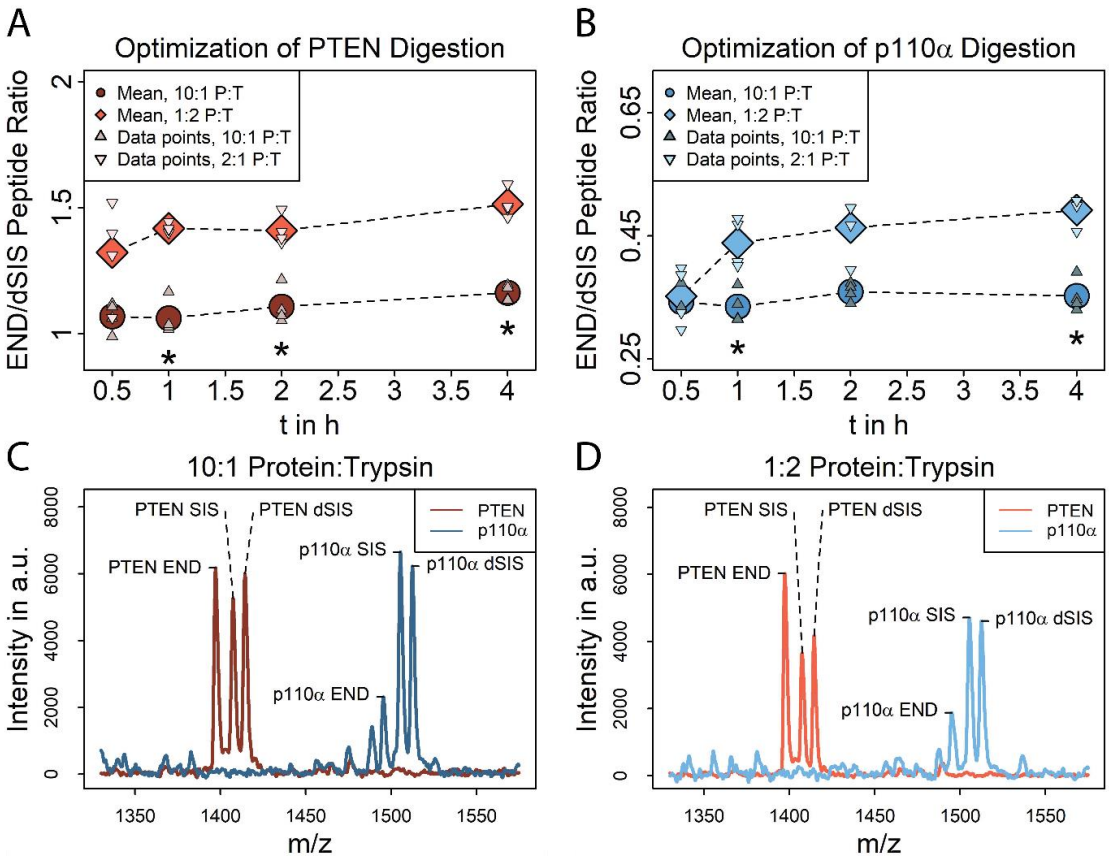

Figure 9. Optimization of tryptic digestion using MDA-MB 231 lysate spiked with 2.5 fmol of both SIS and dSIS peptide. (A) PTEN (^{148}AQEALDFYGEVR^{159}) peptide recoveries at different incubation times (0.5-4 h) and at protein:trypsin (P:T) ratios of 1:10 (dark red) and 2:1 (light red). (*) indicates a significant difference ($p<0.01$) between two protein:trypsin ratios at the same incubation time. N=4 per tested incubation time. (B) p110α (^{503}EAGFSYSHAGLSNR^{516}) recoveries at different incubation times (0.5-4 h) at protein:trypsin ratios of 1:10 (light blue) and 2:1 (dark blue). (*) indicates significant difference ($p<0.01$) between two protein:trypsin ratios at the same incubation time. N=4 per tested incubation time. (C+D) Overlaid mass spectra of sequentially enriched PTEN and p110α peptides after 1 h digest using (C) 10:1 and (D) 1:2 protein:trypsin, recorded in the linear mode. Spectra show similar background for both tested protein:trypsin ratios and no peaks are interfering with the target peptide peaks.

2.3.4 Optimization of Calibration Strategies

Different methods of creating a calibration curve were evaluated by quantifying endogenous PTEN and p110α in MDA-MB 231 cell lysate. This was done to test the influence of the calibration matrix and the peak parameters used for quantification. Three

external calibration curves were generated using matrices of increasing complexity: PBS+CHAPS buffer, BSA digest (10 µg total protein/replicate), and *E.coli* digest (10 µg total protein/replicate). The target peptides were measured using both the linear and reflectron modes to determine if whether the difference in resolution and signal intensity would affect the quantitation.

NAT:dSIS ratios of samples and calibrators were calculated using either (i) peak intensity, (ii) S/N ratios, or (iii) peak areas of the respective peaks, in both linear and reflectron modes, resulting in six calibration curves for each matrix. The amounts of PTEN and p110α in the individual samples were calculated independently using the different calibration matrices and NAT:dSIS readouts (intensity, S/N ratio, peak area) (Figure 10A-D, Supporting Table S 4-6).

Comparing the amount of quantified PTEN peptide in the samples using the different peak properties for generating the calibration curve showed no significant difference using either S/N, peak intensities, or peak areas in the linear and reflectron modes. For example, using PBS+CHAPS as calibrator matrix, the mean quantified peptide amounts in the linear mode were 4.1 fmol using S/N (CV= 7 %), 4.1 fmol using intensities (CV= 7 %), and 4.3 fmol using peak areas (CV= 5 %). No significant difference was found between using S/N and intensities (p=1.00), S/N and peak areas (p= 0.38), or Intensities and peak areas (p= 0.38). Furthermore, no significant differences were observed between using S/N ratio, peak area or intensity when using BSA or *E.coli* digests as the matrix. (Figure 10 A+B).

Notably, a significant difference *was* observed when quantifying p110α in the reflectron mode based on peak areas. For example, when PBS+CHAPS was used as the

calibrator matrix, mean p110α amounts of 1.1 fmol (CV= 9 %) were found using both S/N and peak intensities, compared to 2.6 fmol (CV= 6 %, $p<0.01$) calculated using peak areas ((Figure 10 C+D). This is likely due to inaccurate peak fitting during the reflectron-mode peak analysis. Particularly for low-intensity peaks, such as the endogenous p110α peaks observed here, the peak modelling using SNAP may be less accurate for projected isotope patterns, which affects peak areas more than S/N ratios.
A comparison between the calibrator matrices showed no significant differences for the quantification of p110α ((Figure 10 C+D).

For PTEN, no significant differences between calibration matrices were observed in the reflectron mode. Using the linear mode, the quantified amounts were higher using an *E.coli* digest as the matrix. This can be explained by an interference of a background peak with the internal standard peak in the linear mode, which was avoided in the reflectron mode because of the increased resolution (Figure 10A, Supporting Figure S 5). These results indicate that evaluating different matrices in both linear and reflectron modes is recommended when developing a new iMALDI assay.

In conclusion, we found that the calibration matrix has little impact on the quantification, other than potential interferences from background peaks in the mass spectrum. This, however, can be a major concern, especially in MALDI-TOF MS, since - without LC separation - there are fewer options for resolving such interferences compared to LC-MS. Thus, the use of a BSA digest (10 µg/replicate) seems the most appropriate compromise. Peak intensity is the preferred quantification strategy, as we

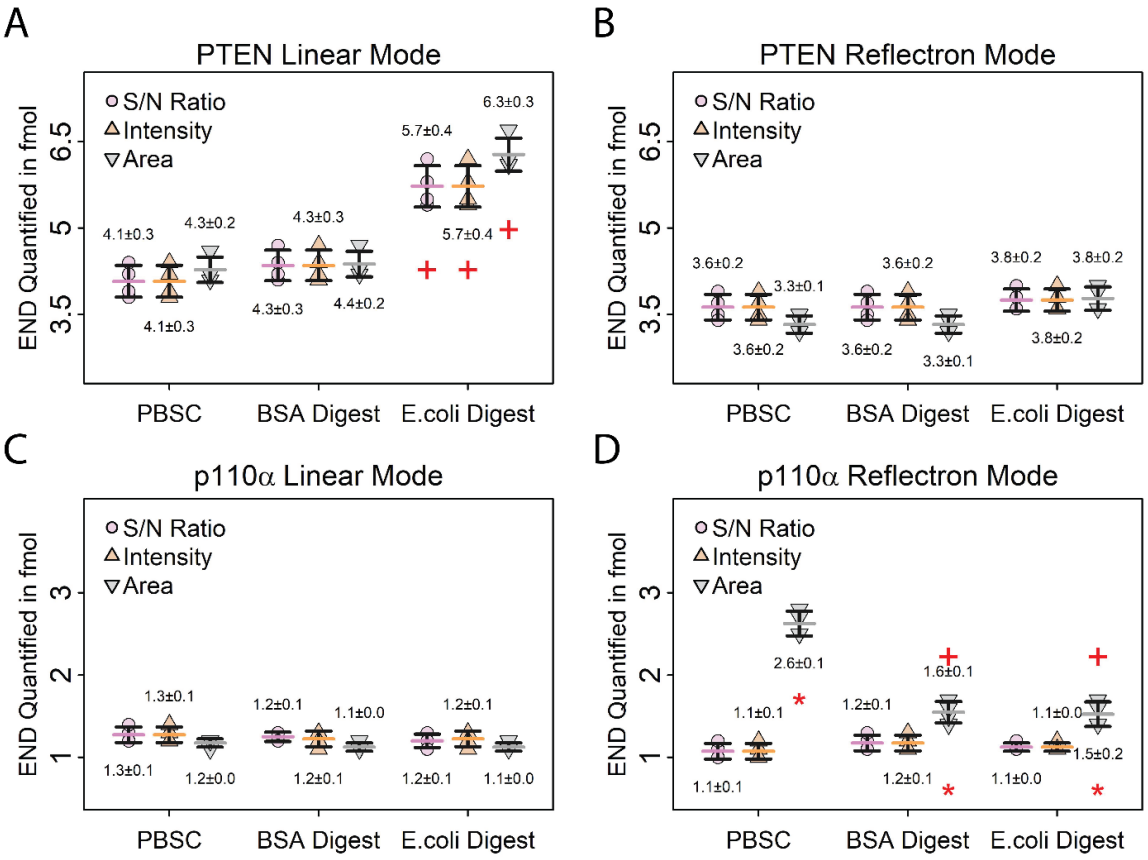

Figure 10. Evaluation of different calibration strategies by quantifying PTEN and p110α in the same sample using different calibration matrices and peak parameters. Error bars represent standard deviation, horizontal bars indicate means. Values above and below the data points represent the mean and absolute standard deviation (A+B) Quantification of endogenous PTEN in 10 µg MDA-MB 231 digest using different calibration matrices and peak parameters. Data recorded in the linear mode (A) shows differences in PTEN quantification using E.coli digest as matrix, whereas data recorded in the reflectron mode (B) shows no difference between the matrices. (+) indicates a significant difference ($p<0.01$) between E.coli digest and PBS+CHAPS matrices for PTEN quantification using the same peak parameters for calculating the calibration. This difference is due to an interference with the internal standard for PTEN from the calibration matrix. (C+D) Quantification of endogenous p110α in 10 µg MDA-MB 231 digest using different calibration matrices and peak parameters. Data recorded in the linear mode (C) shows no difference in p110α quantification using different matrices and peak parameters, while the reflectron mode (D) data shows differences when peak area is used for quantification, likely due to less accurate SNAP peak modelling for low-intensity peaks. (+) indicates a significant difference ($p<0.01$) between E.coli digest and BSA to PBS+CHAPS matrices using the same peak parameter for calculating the calibration. (*) indicates a significant difference ($p<0.01$) between peak area and S/N ratio for p110α quantification. N= 4 per calibration matrix.

have found that peak area is more dependent on the particular peak fitting method used and therefore is more prone to errors, for example, in the case of p110α in the reflectron

mode. In our hands, S/N ratios were slightly more prone to errors when calculated by the FlexAnalysis software, so again peak intensity appears to be the parameter that is the least influenced by spectrum processing. The lower limit of quantitation was 0.7 fmol on the MALDI target spot for both peptides in the linear mode, or 0.9 fmol for p110α and 1.4 fmol for PTEN in the reflectron mode. Notably, both the linear and reflectron modes were found to be suitable for peptide quantification, and it is feasible to measure all samples in *both* modes as an internal quality control measure.

2.3.5 Optimization of Immuno-enrichment

2.3.5.1 Optimization of Bead Types and MALDI Plate Spot Sizes

Different types of magnetic beads were compared for antibody coupling (Figure 11 A+B**,** Supporting Table S 7): two types of protein G coupled beads (one a solid bead (PG #1) and the other a porous microsphere (PG #2)), as well as tosyl-activated magnetic beads (solid spheres) which covalently bind antibodies (C #1). In addition to different bead types, different MALDI plates with different spot sizes were tested: 2600 µm µFocus and 700 µm µFocus plates. Concentrating the same amount of analyte on a much smaller surface area could potentially lead to higher sensitivities.[156]

A comparison of different types and amounts of beads showed that the covalently coupled antibody-beads, in general, did not perform as well as antibodies non-covalently bound to protein G beads. This was indicated by a mean p110α dSIS S/N of 3 for the covalently coupled beads, compared to 17 for the protein G-coupled beads (PG #1). Both protein-G beads performed similarly, giving mean p110α S/N ratios of 17 for PG #1 compared to 19 for PG #2, and mean PTEN S/N ratios of 20 versus 10 for PG #1 and #2. The porous microspheric PG #2 beads have an approximately 20x higher binding

capacity than PG #1, which is why only 3 µg of PG #2 beads were used per replicate, compared to 30 µg for PG #1 (note that using less than 3 µg of PG #2 proved impractical). Still, using 3 µg PG #2 resulted in 0.5 µg of antibody available per replicate, twice as much as the 0.2 µg of antibody using 30 µg PG #1. However, neither the lower amount of beads nor the higher amount of available antibody using PG #2 seemed to improve enrichment. CVs of S/N ratios between PG #1 and PG #2 were comparable for PTEN, while CVs for p110α peptides were slightly lower using PG #2 ($PTEN_{PG\#1/PG\#2\ CV}$=0.8, $p110\alpha_{PG\#1/PG\#2\ CV}$= 3).

For evaluating the 700 µm µFocus plates, PG #1 and C #1 bead amounts had to be reduced by a factor of 10 in order to avoid overloading the MALDI plate (PG #1_1/10 and C #1_1/10). PG #2 already required a very small amount of beads for the 2600 µm µFocus plates (3 µg) and did not need downscaling.

Using a 700 µm µFocus plate, very low S/N ratios (S/N=2) were observed for both PTEN and p110a using PG #1_1/10. Using C #1_1/10, no analytes were detected. In contrast, S/N ratios of 14 for PTEN and 8 for p110a were observed using PG #2, which are closer to the observed S/N ratios of 10 for PTEN and 19 for p110a on a 2600 µm µFocus plate. Thus, using PG #2 beads yielded comparable results on both MALDI target spot sizes tested. However, no increase in sensitivity was achieved. Handling the extremely small volumes (as low as 0.2 µL) and bead amounts (3 µg and lower) necessary for using small anchor plates also posed major challenges to the liquid handling system used in this study.

In conclusion, both types of protein G beads were found to be suitable for iMALDI. However, in our experience, bead performance may vary substantially depending on the

antibody and sample matrix used. We found no improvement using smaller MALDI target spots for iMALDI, which may be related to the additional challenges posed by the automation of a miniaturized system.

2.3.5.2 Direct versus Indirect Immuno-enrichment

Both direct immuno-enrichment (i.e. adding antibodies immobilized to magnetic beads to the sample) and indirect immuno-enrichment (i.e. adding unbound antibody to the sample, then enriching the antigen-antibody complex using magnetic beads) of the target peptides were compared using *E.coli* digest spiked with PTEN NAT and dSIS peptides as the sample (Figure 11C**,** Supporting Table S 8). Samples were immuno-enriched on antibody-immobilized beads for 1 h (direct) or by using free antibody for 1 h, followed by a 1-h incubation with magnetic protein G coupled beads (indirect). AKT2 dSIS peptide was added to the MALDI matrix as an internal standard to allow comparison of the two methods.

Our data demonstrate that the direct approach increases the recovery of the target peptide ($NAT_{Direct/Indirect}$= 1.4, $p<0.01$). Low CVs were achieved using either approach (CV_{Direct}= 7 %, $CV_{Indirect}$= 10 %). Although direct enrichment performed slightly better, indirect enrichment is still feasible with iMALDI.

2.3.5.3 Optimization of Incubation Times

To optimize incubation conditions, the influence of (i) incubation time of the sample with the antibody-coupled beads, (ii) sample mixing during enrichment, and (iii) enrichment temperature were evaluated (Figure 11 D**,** Error! Reference source not f

ound.). An *E.coli* digest spiked with PTEN and p110α NAT and dSIS peptides was used as the sample. AKT2 dSIS peptide was added to the MALDI matrix as internal standard, and enrichment efficiencies were compared based on the ratios of PTEN NAT/AKT2 dSIS, and p110α NAT/ AKT2 dSIS.

(i)To test the impact of incubation time on peptide yield, samples were incubated at room temperature either overnight or for 1 h, while rotating. Longer incubation time slightly improved the enrichment ($PTEN_{1h\_rotating/Overnight\_RT\_rotating}$= 0.67, $p110\alpha_{1h\_rotating/Overnight\_RT\_rotating}$= 0.66).

(ii) Immuno-enrichment for 1 h at room temperature either using end-over-end rotation or shaking at 1000 RPM, yielded comparable results for PTEN ($PTEN_{1h\_rotating/1h\_shaking}$= 0.98) and slightly better enrichment for p110α ($p<0.01$, though the observed increase was small, with $p110\alpha_{1h\_rotating/1h\_shaking}$= 0.83).

(iii) The effect of incubation temperature (RT vs 4 °C) was tested by incubating samples overnight while rotating. Both incubation temperatures showed comparable enrichment ($PTEN_{Overnight\_4°C\_rotating/Overnight\_RT\_rotating}$= 0.86, $p110\alpha_{Overnight\_4°C\_rotating/Overnight\_RT\_rotating}$= 1.04). Low CVs between 5-12 % were achieved regardless of incubation time or sample mixing approaches.

In conclusion, increasing incubation times clearly improved enrichment efficiency, while neither the incubation temperature nor the mixing method led to significant changes in assay performance. Indeed, this is an important finding for clinical translation: the general iMALDI workflow yielded reproducible results even when conducted under slightly varying conditions, a situation which cannot be avoided even *within* a given hospital setting and even more so across different sites.

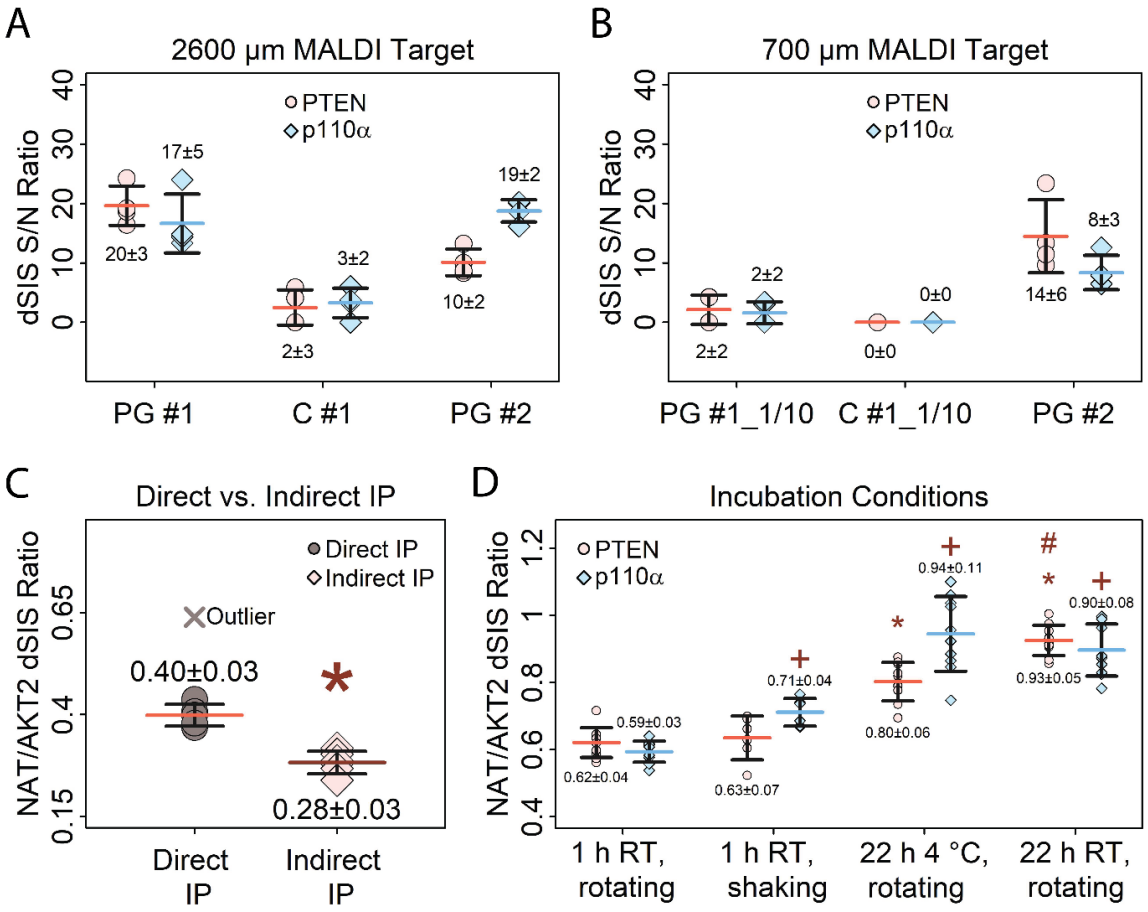

Figure 11. Optimization of immuno-enrichment. Error bars represent standard deviation, horizontal bars indicate means. Values above and below the data points represent the mean and absolute standard deviation (A) Comparison of different bead types for enriching 2.5 fmol PTEN and p110a dSIS peptides spiked into 10 µg *E.coli* digest, using a 2600 µm MALDI target plate. Protein G Dynabeads (PG #1), Protein G MagReSyn beads (PG #2) and M280 tosylactivated Dynabeads (C #1) were tested. Peak S/N ratios of the enriched dSIS peptides are used for comparison. (B) Comparison of different beads for enriching 2.5 fmol PTEN and p110α dSIS peptides spiked into 10 µg *E.coli* digest, using a 700 µm MALDI target plate. Peak S/N ratios of the enriched dSIS peptides are used for comparison. The same antibody-coupled beads as in (A) were tested, using 1/10 of the bead amount (PG #1_1/10, C #1_1/10), except for PG #2 (same as in (A)). N=4 per bead type and MALDI target plate. Data for A+B recorded in the reflectron mode. (C) Comparison of direct and indirect immuno-enrichment for PTEN NAT peptide (1 fmol) spiked into 10 µg *E.coli* digest, showing better recovery using direct IP. Outlier (> Q3+3x Interquartile Range) was excluded due to poor quality of the mass spectrum. $\text{Mean}_{\text{Direct IP}}$ (outlier included) = 0.44 ± 0.1. The signal of AKT2 dSIS standard spiked into the MALDI matrix (1 fmol per spot) was used for normalization. (*) indicates significant difference ($p<0.01$) to direct IP. Data recorded in linear mode. (D) Testing different incubation times, temperatures and mixing conditions for enriching PTEN and p110α NAT peptide (1.25 fmol) spiked into 10 µg of *E.coli* digest. The signal of the double-stable-isotope-labelled AKT2 peptide (THF(+10)PQFSYSASIR(+10)E) spiked into the MALDI matrix (1 fmol per spot) was used for

normalization. (*) indicates significant difference ($p<0.01$) of PTEN enrichment after 22 h incubation compared to 1 h incubation, (+) significant difference ($p<0.01$) between p110α enrichment compared to 1 h incubation, and (#) indicates significant difference between PTEN enrichment after 22 h at room temperature (RT) and 22 h at 4 °C. N=10 for each condition, except 1 h shaking (N=6). Data was recorded in the linear mode.

2.4 Conclusions

The iMALDI workflow was optimized for the efficient and automated quantification of cell signalling proteins from cell lysates. The essential steps inherent in every iMALDI procedure, including assay automation, tryptic digest, calibration, antibody-sample incubation times, temperatures as well as using different enrichment strategies and different types of antibody-coupled magnetic beads, were systematically evaluated (Table 1).

The liquid handling steps were successfully automated. In particular, the labour-intensive and comparatively complicated washing and spotting of the antibody-antigen bead complex were automated without compromising sensitivity, while the turnaround time for 96 samples was reduced from approximately 90 min using manual preparation to 15 min using automation.

Regarding the sample preparation, it was found that digestion using 1:2 protein:trypsin was the ratio-of-choice, as it combined high digestion efficiency with short incubation times. In contrast to conventional proteomics experiments, most potential interferences are removed during anti-peptide immuno-enrichment after the proteolytic digestion. For the enrichment step, direct enrichment using protein G coupled beads was found to be the most sensitive method for cell lysate digests. Importantly, we found that different pAbs from the same manufacturer (Signatope) provided the same results. Given that only minimal amounts of antibody are required to conduct iMALDI assays with high

sensitivity - even for proteins of low abundance - this is an important result, as 10,000s of assays can be conducted using a single pAb preparation, theoretically reducing the need for the generation of monoclonal antibodies.

In addition, different matrices were evaluated, as well as alternative peak parameters (S/N, intensity, area) for quantifying peptides in cell digests. For generating an external calibration, the complexity of the matrix was found to have little influence on the amount of target peptide measured in the sample and a BSA digest was found to be completely acceptable as a generic sample matrix.

In summary, this chapter provides a comprehensive template on how to set up, optimize, and evaluate future iMALDI assays. This will facilitate the transfer of this technology into the clinic, where protein-based assays are becoming increasingly important for patient stratification.[112,157]

Table 1. Summary of optimized iMALDI method parameters.

Parameter	Optimal condition
Peptide Length for Antibody Development and MALDI-TOF MS analysis	7 to 20 Amino acids
Tryptic Digest	1:2 protein:trypsin (w:w) for 1 h at 37° C
Bead Type	Protein G Dynabeads (MagReSyn Protein G beads perform similarly but with different background peaks overserved in the mass spectrum)
Enrichment	Direct enrichment (antibodies coupled to beads prior to enrichment).
Incubation condition	1 h to overnight, shaking (1000 RPM, too rapid shaking may cause loss of antigen) or rotating.
Incubation temperature	Room temperature (1 h incubation) or 4 dC (overnight incubation)
Wash Protocol	1x 70 µL PBS +0.015 % (w:w) CHAPS, 3x 80 µL 5 mM Ammonium Bicarbonate (Automated)
MALDI Matrix	3 mg/mL HCCA+ 7 mM AmCit in 70:29.9:0.1 ACN:H2O:TFA (1.5 µL matrix used per spot)
Spot Wash Procedure	3x 7 mM Ammonium Citrate Dibasic (pH=5, 10 µL wash buffer with 5 s incubation time on spot)
Calibration surrogate matrix	BSA Digest (0.1 µg/µL in TRIS+C buffer)
Peak parameter used for peak calculations	Peak Intensity

Chapter 3 A Multiplexed, Automated Immuno-Matrix Assisted Laser Desorption/Ionization Mass Spectrometry Assay for Simultaneous and Precise Quantitation of PTEN and p110α in Cell Lines and Tumor Tissues

Work in this chapter was performed at the UVic Genome BC Proteomics Centre (PC) and at the Jewish General Hospital in Montreal (JGH). MDA-MB 231 cell lysates were prepared by Adriana Aguilar-Mahecha (JGH). All experiments herein, and the data analysis thereof, were performed by Bjoern Froehlich. Experimental design was performed by Bjoern Froehlich, Andre LeBlanc, Rene Zahedi, and Christoph Borchers. Christoph Borchers oversaw the project. The contents of this chapter were adapted from the following publication:

Bjoern C. Froehlich, Robert Popp, Constance A. Sobsey, Sahar Ibrahim, Andre LeBlanc, Yassene Mohammed, Marguerite Buchanan, Adriana Aguilar-Mahecha, Oliver Pötz, Michael X. Chen, Alan Spatz, Mark Basik, Gerald Batist, René P. Zahedi, and Christoph H. Borchers,

"A Multiplexed, Automated Immuno-Matrix Assisted Laser Desorption/Ionization Mass Spectrometry Assay for Simultaneous and Precise Quantitation of PTEN and p110α in Cell Lines and Tumor Tissues", **submitted**

3.1 Introduction

Targeted therapies that selectively inhibit key proteins in oncogenic signaling networks have emerged as new and promising method to treat cancer patients[158]. It has been shown for different combinations of drugs and cancers, that this type of targeted treatment is more effective in tumors that have specific molecular signatures, and that the availability of specific biomarkers can greatly enhance patients' overall survival[25,159]. Cancer biomarkers that are currently being used in the clinic for patient stratification include specific genomic markers, such as BRAF mutations in melanoma or KRAS mutational status in colorectal cancer, as well as protein markers whose expression levels are typically assessed by immunohistochemistry, such as PD-L1 in lung cancer.[24,160,161]

For certain cancers and drugs, however, it has become evident that the current practice of patient stratification can still lead to unexpectedly low response rates. One reason for these low response-rates is that changes on the genome and transcriptome level do not necessarily correlate with the proteome and *vice versa*.[84,86] Thus, *genomic biomarkers* do not readily reflect the activity and/or expression of a drug's target protein or pathway[42,162–164]. Moreover, the expression of *protein biomarkers* is typically assessed by immunohistochemistry (IHC)[134,135,165], which is poorly standardized, strongly depends on antibody-specificity, suffers from interference from post-translational modifications, and provides only subjective and semi-quantitative data (e.g., "amplified" vs. "normal") [135,137,166]. There is therefore an urgent need for improved and standardized methods that enable the precise measurement of protein biomarkers as surrogates of oncogenic pathway activity which can either complement genomic biomarkers or assist in IHC-based patient stratification.

The PI3K/AKT/mTOR pathway controls cell proliferation, survival, and apoptosis, and is one of the most frequently altered pathways in cancer, including breast and colorectal cancer. The PI3K/AKT/mTOR pathway is, therefore, a major drug target. Up to 40 different inhibitors are currently being investigated in pre-clinical and clinical trials, and several inhibitors have already received FDA approval[35,167–170]. Some of these, however, show unexpectedly low response rates. [25,35,127]

The PI3K catalytic subunit p110α and the phosphatase and tensin homolog (PTEN), which is the main negative regulator of the PI3K/AKT/mTOR pathway, are frequently mutated and dysregulated in many cancers, and are considered as strong indicators of PI3K pathway activity[36,86,131,132,171–174]. The precise and standardized quantitation of these proteins in individual tumors should, therefore, help to improve patient stratification for treatments that target the PI3K/AKT/mTOR pathway, and thus help to overcome the problem of low response rates.

Targeted mass spectrometry (MS) using stable isotope labeled standard (SIS) peptides is a robust technology that enables the precise and standardized measurement of protein concentrations without facing the limitations of IHC. The measurement of actual protein concentrations in tumors using a standardized platform enables the comparison of results that were obtained in different laboratories and at different times, thus allowing the generation of reference ranges and facilitating the correlation of biomarker concentrations with clinical outcomes, which is virtually impossible for IHC. Targeted MS is usually performed using liquid chromatography coupled with multiple or parallel reaction monitoring (LC-MRM or LC-PRM) to achieve high sensitivity, reproducibility, and selectivity. LC-based approaches, however, suffer from comparatively long analysis

times (commonly 15-60 minutes per sample) and require relatively expensive and sophisticated instrumentation.

In contrast, protein quantitation using immuno-matrix-assisted laser-desorption ionization (iMALDI) time-of flight (TOF) mass spectrometry is a powerful alternative methodology that combines antibody-based peptide enrichment with quantitation by MALDI-TOF MS to achieve high selectivity, sensitivity, and precision. Moreover, MALDI requires only a few seconds of analysis-time on bench-top MALDI-TOF instruments such as the Bruker Microflex, which is an FDA-approved instrument that is already present in many clinical laboratories for microbial identification. In iMALDI, endogenous proteins are first enzymatically digested to release the endogenous proteotypic peptide (END) that is specifically targeted by the anti-peptide antibody. Then, a defined amount of the SIS analogue of this peptide is spiked into the sample, and both the END and SIS peptides are simultaneously enriched using the anti-peptide antibody coupled to magnetic beads, followed by direct analysis using MALDI-TOF MS. We have previously demonstrated that quantifying cancer signaling pathway proteins by iMALDI requires as little as 10 µg of total protein per measurement, which is in-line with the severely limited amounts of tissue that can be obtained for many clinical samples.[121]

Following the development of anti-PTEN and anti-p110α antibodies, as well as optimizing key assay parameters such as tryptic digestion, automation and immuno-enrichment in the previous chapter, this chapter describes the validation of the developed assay to demonstrate that it is fit-for-purpose.

3.2 Materials and Methods

All major iMALDI liquid handling steps were conducted using a BRAVO liquid handling system (Agilent Technologies), as described in the previous chapter.[175] Refer to section 2.2.1 for the materials used.

3.2.1 iMALDI Workflow

Preparation of Antibody-coupled Beads. Protein G Dynabeads were washed 7x 25:75 acetonitrile:(PBS+0.015 % (w:w) CHAPS (PBSC)) and 3x PBSC buffer, using 1:10 bead-slurry: buffer (v:v), followed by addition of 0.2 µg anti-peptide antibodies per 30 µg beads.

Peptide Enrichment. Ten µg of total lysate protein in 100 µL were used for each experiment. The sample was digested for 1 h at 37 °C using 1:2 (w:w) protein:trypsin, followed by quenching using Nα-Tosyl-L-lysine chloromethyl ketone hydrochloride (TLCK). The target peptides were enriched using 0.2 µg antibody coupled to 30 µg Protein G Dynabeads per replicate and 1 h incubation at room temperature. Then, the antigen-antibody-bead complexes were washed 1x with PBS+0.015% CHAPS (PBSC) and 3x with 5 mM ammonium bicarbonate. The beads were then spotted onto a MALDI target plate. After the spots were dry, HCCA matrix (3 mg/mL α-cyano-4-hydroxycinnamic acid, 7 mM ammonium citrate (dibasic) in 70% acetonitrile (ACN), 0.1% trifluoroacetic acid (Thermo Fisher)) was spotted on top. After drying, the spots were washed 3x with 7 mM ammonium citrate and analyzed using a Bruker Microflex

LRT in both linear positive (LP) and reflectron positive (RP) ion mode. Liquid handling steps were automated using an Agilent Bravo 96LT.

3.2.2 Preparation of cell and tissue samples

E. coli BL21 DE3 cells were grown overnight in lysogeny broth (10 g/L Tryptone, 10 g/L NaCl, 5 g/L yeast extract) at 37 °C. Cells were pelleted and resuspended in PBS (pH 7.4). Protein extraction was performed using T-PER buffer (Thermo Fisher).

MDA-MB 231 cell lysates were prepared as previously described.[121] Briefly, cells were grown overnight at 37 °C and 5% CO_2, followed by overnight starvation in 0.25% fetal bovine serum and harvesting at 80% confluency.

Cells were pelleted, and protein extraction was performed using T-PER buffer (4 °C, Thermo Fisher) containing 1x halt protease and 1x halt phosphatase inhibitor (Thermo Fisher), supported by sonication. Protein concentration was determined using a BCA assay (Thermo Fisher).

E.coli, *MDA-MB 231*, and tissue lysates were diluted to a concentration of 0.1 µg protein/µL using cold TRIS supplemented with 0.015 % CHAPS (TRIS+C). Each sample was divided into 100-µL aliquots (with 10 µg total protein, each).

All patients provided informed consent, breast cancer tissues were collected as part of the Jewish General Hospital (JGH) breast biobank (protocol 05-06), and gastric tumor and colorectal cancer liver metastasis samples were collected as part of the JGH central biobank (protocol #10–153). Protocols were reviewed and approved by the local JGH REB committee. PDXs from the gastric cancer tumor were generated as previously

reported (38), all experiments were performed in accordance with the protocol approved by the Lady Davis Institute/McGill University animal care committee.

3.2.3 Evaluation of the impact of reduction and alkylation on PTEN and p110α iMALDI assays

MDA-MB 231 lysate (10 µg of total protein per replicate in 100 µL) was digested using trypsin (1:10 protein:trypsin) either with (+RA) or without prior reduction of disulfide bonds and alkylation of free Cys residues (-RA), using five replicates per condition. Reduction and alkylation were performed by adding 10 µL 0.74 mM tris(2-carboxyethyl)phosphine (TCEP), followed by 10 µL 0.74 mM iodoacetamide (IAA), followed by incubation for 30 min at 37 °C in the dark, and quenching using 10 µL 1.48 mM dithiothreitol (DTT). Tryptic digestion was performed the same way for both conditions, as described above. To each replicate, 2.5 fmol PTEN SIS and p110α SIS were added as internal standards. iMALDI assays were conducted as described above. Two-sided t-tests with a confidence level of 0.99 were performed to compare the END:dSIS ratios and SIS:dSIS ratios for PTEN and p110α between samples digested with and without reduction and alkylation.

3.2.4 Evaluation of iMALDI multiplexing strategies

Sequential enrichment was performed by coupling Protein G Dynabeads to either anti-AQEALDFYGEVR (PTEN) or anti-EAGFSYSHAGLSNR (p110α) antibodies, and then using these antibody-bead complexes to separately enrich the target peptides from

different sample aliquots. For each sample, 30 µg of coupled beads were used, and the samples were incubated while shaking at 1000 RPM for 1 h at room temperature. Beads were washed as described above. Before the first wash step, the supernatant was transferred to a fresh 1.1 mL U-bottom deep well plate, and 30 µg of beads coupled to the second antibody were added (i.e. if anti-PTEN antibodies were used in the first enrichment, anti-p110α antibodies were added during the second enrichment), for the second immuno-enrichment. The antigen-antibody-bead complexes were washed and spotted on a MALDI plate.

For simultaneous enrichment (PTEN/p110α), anti-PTEN and anti-p110α coupled beads were mixed in a 1:1 ratio prior to enrichment. Thirty µg of the bead mixture (containing 15 µg anti-PTEN and anti -p110α antibody coupled beads each) were added to each sample. After a 1-h incubation at room temperature while shaking at 1000 RPM, the antigen-antibody-bead complexes (containing both target peptides) were washed and spotted on a MALDI plate as described above.

3.2.5 iMALDI method validation – linearity

MDA-MB 231 lysate was used as matrix and 10 µg total protein per replicate was digested as described above. Mixed calibration stock solutions of PTEN+p110α dSIS (2.5, 1.75, 1, 0.75, 0.5, 0.375, 0.25, 0.125, 0.06, 0.03, 0.016, 0 fmol/µL, each) were prepared in PBSC using an automated calibration curve-preparation protocol.

Calibrations standards were prepared by adding 20 µL of calibration stock solution to 10 µg MDA-MB 231 digest, resulting in 50, 35, 20, 15, 10, 7.5, 5, 2.5, 1.25, 0.6, 0.3, 0 fmol dSIS per standard. Three replicates were prepared for each standard. 2.5 fmol

PTEN SIS and p110α SIS (PTEN+p110α SIS) were added to each replicate as internal standards. Peptides were analysed using the developed iMALDI assay as described above.

The peak intensities ratios of PTEN dSIS and p110α dSIS (PTEN+p110α dSIS) to the respective SIS peptides were calculated and calibration curves were generated. 1/x^2 weighted regressions were calculated for each both target peptides in linear mode and 1/x weighted regressions in reflectron mode. To assess the linearity, the ratios of the residuals divided by the calculated fitted values (in percent) were calculated.

3.2.6 iMALDI method validation – accuracy

MDA-MB 231 digest was used as matrix. Ten µg of total protein per replicate was digested as described above, and three accuracy test solutions were prepared. Acc #1: MDA-MB 231 digest was spiked with PTEN dSIS and p110α dSIS, both to a final concentration of 1.8 fmol/µg total protein (18 fmol total PTEN/ p110α dSIS per replicate). Acc #2: Acc #1 was diluted with MDA-MB 231 digest to a final concentration of 1.0 fmol/µg total protein for both dSIS (10 fmol total PTEN/ p110α dSIS per replicate). Acc #3: Acc #1 was diluted as above to a final concentration of 0.2 fmol/µg total protein (2 fmol total PTEN/ p110α dSIS per replicate). Four replicates were prepared for each accuracy test solution.

For external calibration, BSA digest (10 µg total protein per replicate) was spiked with increasing amounts of PTEN+p110α dSIS ranging from 0 to 20 fmol. Peptide enrichment, bead washing and spotting, matrix spotting, and spot washing was performed as above. To each accuracy sample and calibration standard, 2.5 fmol PTEN+p110α SIS

were added as internal standard (normalizer). To assess accuracy, PTEN+p110α dSIS concentrations in the Acc 1-3 samples were determined using the calibration generated in above.

3.2.7 iMALDI method validation – interference

Recombinant PTEN and p110α/p85α protein were each spiked into MDA-MB 231 lysate to a concentration of 1.5 fmol recombinant protein/1 µg total lysate protein (15 fmol protein per protein and 10-µg replicate). The sample was then diluted either 2-, 4-, or 8-fold using PBSC and digested as described above. To each digest, 2.5 fmol PTEN+p110α dSIS were spiked in as internal standards. Four replicates were prepared per dilution. Assay preparation, bead washing and spotting, matrix spotting and spot washing were performed as described above. For external calibration, constant PTEN+p110α dSIS (2.5 fmol per replicate) were spiked in with variable amounts of PTEN and p110α NAT (ranging from 0 to 20 fmol) and 10 µg total protein BSA digest as surrogate matrix. Three replicates were prepared for each calibration standard. Concentrations of recombinant PTEN and p110α were determined based on the external calibration.

3.2.8 iMALDI method validation – precision

To assess the five-day precision across the working range of the multiplexed PTEN+p110α assay, three different pools of MDA-MB 231 cell lysate (labeled ‘low’, ‘medium’, ‘high’) were prepared by adding PTEN+p110α dSIS to achieve concentrations of 2, 10, and 18 fmol /10 µg total lysate protein, respectively. The pools were then

diluted to a total protein concentration of 0.1 µg/µL, and each pool was split into 5 aliquots and stored at -80 °C until used.

For five consecutive days, one aliquot of the 'low', 'medium' and 'high' pool was analyzed in three technical replicates each. Ten µg total protein was analyzed per replicate, resulting in PTEN+p110α dSIS amounts of 2, 10, and 18 fmol. An external calibration curve with varying concentrations of PTEN+p110α dSIS (0-20 fmol per replicate) in BSA digest (10 µg total protein per replicate) was generated fresh, daily. Constant amounts of 2.5 fmol PTEN+p110α SIS were added as internal standards to each sample and calibration standard. Antibody-coupled magnetic beads were prepared fresh daily and stored while rotating at 4 °C until use. Assay preparation, bead washing and spotting, matrix spotting and spot washing was performed as above. Spiked-in PTEN+p110α dSIS concentrations were determined using the calibration curve prepared on the same day.

Overall CVs were calculated based on the average Intra-day CVs and the inter-day CVs (Equation 1).[176]

$$CV_{Total} = \sqrt{mean(Intra - Day\ CV)^2 + Inter - Day\ CV^2}$$

Equation 1. Calculation of overall 5-Day CVs

3.3 Results

3.3.1 Multiplexed analysis of PTEN and p110α using iMALDI is feasible

The multiplexing of iMALDI assays allows the precise quantification of different protein targets in a single sample without the need for additional sample material. This is particularly relevant for clinical samples, including needle biopsy samples or formalin-fixed paraffin-embedded (FFPE) tissue cores and slides, where the available sample amounts are often severely limited, while the demand for measuring biomarker panels for patient stratification is high.

We, therefore, evaluated two different strategies of multiplexing iMALDI assays and compared these to the classical singleplex enrichment with regard to efficacy and robustness: *simultaneous enrichment* and *sequential enrichment* of both target peptides (Figure 12 A). While simultaneous enrichment is a faster and more straightforward workflow, sequential enrichment is preferred in cases where either the antibodies used interfere with each other or the different END and SIS peptides have very similar molecular masses and may result in overlapping peaks in MALDI-TOF MS.

The two multiplexing methods were compared using *E. coli digest* (10 µg total protein per replicate) that was spiked with 1 fmol NAT and 2.5 fmol SIS peptides for PTEN and p110α, respectively (n=4 for each concentration and multiplexing strategy). For both PTEN and p110α, the NAT/SIS ratios showed good agreement between the multiplexed and singleplex assays, with mean $NAT/SIS_{Multiplex}$ and $NAT/SIS_{Singleplex}$ ratios of 1.03 (PTEN) and 0.97 (p110α) for both tested concentrations. High precision was also achieved using the multiplexed assays (CV_{Mean_PTEN}= 4%, $CV_{Mean\_p110\alpha}$= 5%), which was

comparable to the singleplexed assays (CV_{Mean_PTEN}= 10%, $CV_{Mean\_p110\alpha}$= 8%) (Figure 12 D, E; Supporting Table S 10).

Peptide recoveries of the 1 fmol NAT spike-in, as determined from the peak-intensity ratios of enriched NAT and AKT2 dSIS peptides, were 25-30 % lower using simultaneous enrichment compared to sequential enrichment (with the target peptide being enriched first), though this difference was not significant ($p>0.01$) (Supporting Figure S 6; Supporting Table S 11). Using sequential enrichment, the order of enrichment did not lead to significant differences, for either PTEN (Figure 12B) or p110α (Figure 12C).

These results indicate that multiplexed PTEN/p110α iMALDI is feasible without compromising assay accuracy or precision. All of the subsequent steps in the validation and application of the multiplexed PTEN/p110α iMALDI assay were performed using simultaneous enrichment because of its more straightforward and simpler workflow, compared to sequential enrichment.

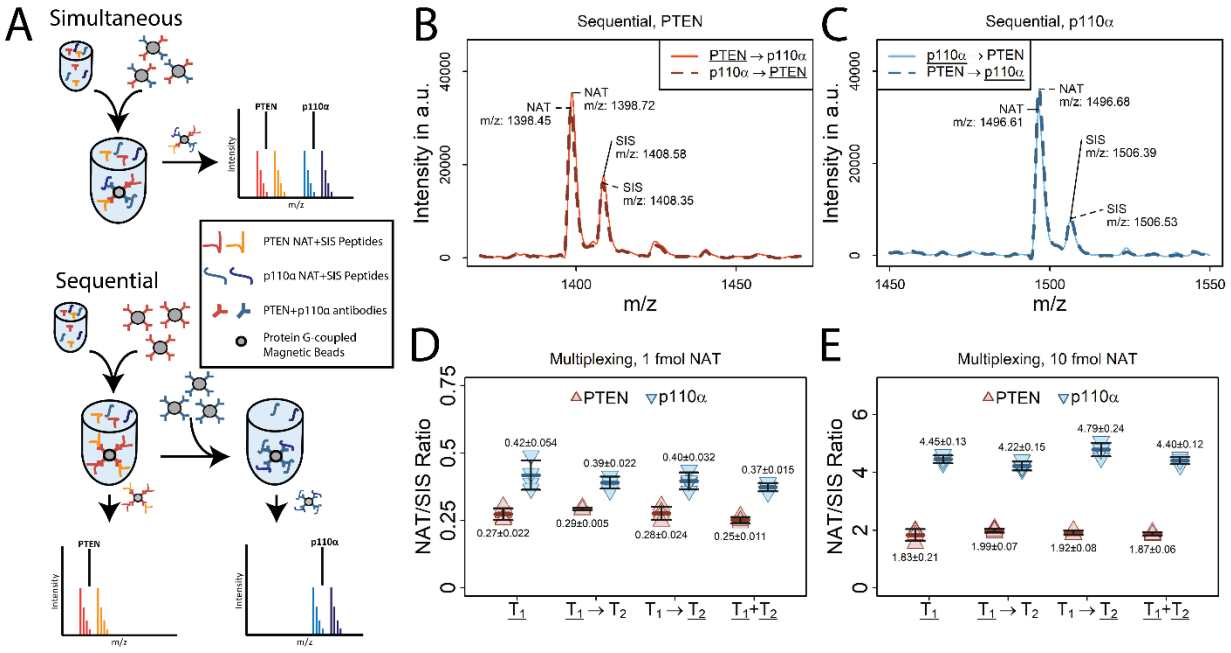

Figure 12 Multiplexed PTEN/p110α iMALDI assay. (A) E.coli digest was spiked with either 1 fmol or 10 fmol PTEN and p110α NAT peptides and 2.5 fmol corresponding SIS peptides, followed by PTEN and p110α enrichment, either sequentially or simultaneously. Both sequential multiplexing strategies were compared to the PTEN and p110α singleplex iMALDI assays. AKT2 dSIS peptide ($THF_{+10}PQFSYSASIR_{+10}E$) was spiked into the MALDI matrix (1 fmol per spot) as an external standard (n=4 per condition). (B+C) Representative MALDI TOF MS spectra of 10 fmol PTEN NAT and p110α NAT after sequential enrichment as either first (T_1) or second target (T_2) (D+E) Comparison of PTEN and p110α peptide enrichment performed as singleplex ($\underline{T_1}$), sequential enrichment with PTEN/p110α enriched either as first ($\underline{T_1}$ before T_2) or second (T_1 before $\underline{T_2}$) target, or simultaneous enrichment of both peptides ($\underline{T_1}$+$\underline{T_2}$). NAT/SIS ratios were calculated for both the (D) 1 fmol and (D) 10 fmol NAT spike-in samples, showing no significant differences in accuracy and precision between all strategies.

3.3.2 Validation of our multiplexed PTEN and p110α iMALDI assay

After confirming that reduction and alkylation of Cys residues, a central part of our AKT1 and AKT2 iMALDI assays, could be omitted for PTEN and p110α (Supporting Figure S 7,Supporting Table S 12), we validated our simultaneous multiplexed PTEN/p110α iMALDI assay's precision and accuracy (referring to the surrogate peptide).[60,121]

To assess linearity of our assay, we prepared a calibration curve using MDA-MB-231 digest (10 µg total protein/replicate), which was spiked with constant amounts of PTEN and p110α SIS (2.5 fmol/replicate) and varying amounts of PTEN dSIS and p110α dSIS (PTEN+p110α dSIS) (ranging from 0-50 fmol/replicate). The samples were analysed in both linear positive (LP) and reflectron positive (RP) ion modes (Figure 13 1A, Figure 13 1B; Figure 13 2A; Figure 13 2B; Supporting Table S 13, Supporting Table S 14). Because of the heteroscedasticity of the calibration data, weighted linear regression (WLS) is preferred over ordinary least squares regression (OLS) in mass-spectrometry based assays[177].

In the LP mode, the linear range of the assay was from 0.6 to 20 fmol on-spot, with R^2 values of 0.99 and CVs consistently below 15% for both PTEN and p110α (Figure 13 1A, Figure 13 1B). The lower-limit of quantitation (LLOQ) was 0.7 fmol of peptide on-spot for both targets, as previously determined, with CVs of <20%, thus meeting the FDA requirements for bioanalytical method validation (Supporting Figure S 8 A).[60,175] The sensitivity of our iMALDI assay is comparable to immuno-enrichment based LC-MS assays. For example, our recently developed immuno-MRM assay for PTEN quantitation in cancer cells achieved LLOQs of 1 fmol on-column.[178] In the RP mode, the linear range of the assay was from 1.25 to 50 fmol on-spot with R^2 values of 0.98 (PTEN) and 0.99 (p110α), and CVs of <20% (for >0.6 fmol peptide on-spot) (Figure 13 2A; Figure 13 2B, Supporting Figure S 8 B). Based on our previous experience, we did not expect any target protein concentrations above 20 fmol/10 µg total lysate protein, so we used the linear range of the assay in LP mode as the working range for our assay.[178] This is also

advantageous for further adoption of this technology by clinical laboratories, since not all MALDI-MS instruments used in clinics have a reflectron mode.

To evaluate the accuracy of our multiplexed PTEN/p110α iMALDI assay, we used 10 µg of a MDA-MB-231 cell lysate that had been spiked with (i) 2, 10, or 18 fmol of PTEN dSIS plus p110α dSIS, corresponding to 10%, 50%, and 90% of the linear range in LP (designated as low, medium, and high levels, respectively), and (ii) 2.5 fmol of PTEN SIS and p110α SIS. PTEN and p110α dSIS amounts were determined based on dSIS/SIS ratios and were compared to the theoretical spike-in amounts (Figure 13 1C; Figure 13 2C; Supporting Table S 15, Supporting Table S 16). Calibration curves were prepared in BSA digest as the surrogate matrix. In the LP mode, high accuracies were achieved for both PTEN (102%, 100%, and high 90% for low, medium, and high levels, respectively) and p110α (112%, 105%, 97% for low, medium, and high levels, respectively), all of which were well within FDA's cut-off of ±20% for immunoassays, with CVs of 2 to 6%.[60] Comparably high accuracies were achieved in the RP mode for both target peptides (PTEN: 99%, 109%, and 112%; and p110α: 105%, 107%, and 108%, for low, medium, and high levels, respectively), with CVs ranging from 2 to 7%. These results demonstrate that our multiplexed PTEN/p110α iMALDI assay provides high accuracy and precision across its entire working range.

To test dilutional linearity, recombinant PTEN and p110α/p85α protein were spiked into MDA-MB-231 cell lysate to give a final concentration of 1.5 fmol recombinant protein per µg of total lysate protein. The sample was diluted 2-, 4-, and 8-fold with PBSC, followed by tryptic digestion and mutliplexed iMALDI analysis. Additionally, to evaluate the potential impact of using high amounts of trypsin (specifically potential

chymotrypsin-like digestions), we kept the total amount of trypsin constant, thus successively decreasing the protein:trypsin ratio (w:w) from 1:2 to 1:16, and performed a linear regression analysis on the serially diluted samples (Figure 13 1D; Figure 13 2D*;* Supporting Table S 17*;* Supporting Table S 18). For both PTEN and p110α, high linear coefficients of determination were found across the dilution series (R^2 of 0.996 and 0.995 for PTEN and p110α, respectively), demonstrating dilutional linearity.

These results demonstrate that our multiplexed PTEN/p110α iMALDI assay is free from interferences caused by trypsin and confirm that it is robust even when different protein:trypsin ratios are used. Importantly, our data also demonstrate dilutional linearity: samples can still be reliably analysed even after an 8-fold dilution, with CVs ranging from 2 to 7%. Thus, even though the linear range of the assay is comparatively narrow (0.6-20 fmol), it is still applicable to samples with higher PTEN and/or p110α concentrations or higher amounts of starting material.

To test the intra- and inter-day precision of our multiplexed PTEN/p110α iMALDI assay, three pools of MDA-MB-231 cell lysate were prepared. The pools were then spiked with 2, 10, or 18 fmol of PTEN+p110α dSIS per 10 µg of total protein, respectively, corresponding to the low, medium, and high levels, of the assay's linear range. Each pool (low, medium, high) was divided into 5 aliquots à 10 µg, which were stored at -80 °C. For five consecutive days, one fresh aliquot of each pool was analysed using our multiplexed iMALDI assay. To assess precision, intra- and inter-day CVs and total CVs were calculated according to Equation 1 (Figure 14 1, Figure 14 2, Supporting Table S 19-22).

For PTEN average the intra-day CVs were 3%, 5%, and 5%, while the inter-day CVs were 6%, 10%, and 9% for low, medium, and high levels, respectively (Figure 14 1A,1B). For p110α, the average intra-day CVs were 4%, 6%, and 4%, while the inter-day CVs were 4%, 10%, and 7% for low, medium, and high levels, respectively (Figure 14 1C,1D).

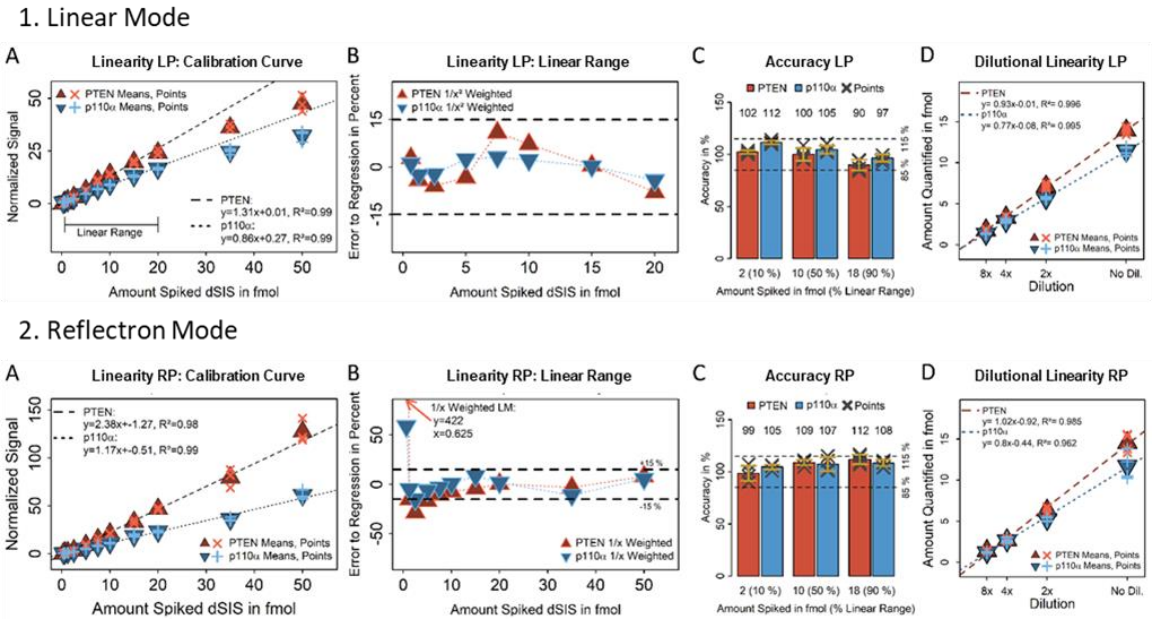

Figure 13 Method validation of the multiplexed PTEN+p110α iMALDI assay. Data shown was recorded in the linear positive ion mode (1) or reflectron mode (2). 10 µg of MDA-MB-231 digest were spiked with varying amounts of PTEN+p110α dSIS peptides and 2.5 fmol PTEN and p110α SIS as normalizer. (1A) Calibration curve (n=3): The linear range is from 0.6-20 fmol and (1B) all means within that range were within a ±15% error margin of the regression for . In reflectron mode, the linear range extends from 1- fmol (2A, 2B). (C1+C2) To determine accuracy, PTEN+p110α dSIS amounts were determined based on dSIS/SIS ratios and compared to the theoretical spike-ins. (n=4). (D1+D2) For interference testing, 10 µg MDA-MB-231 lysate (total protein) was spiked with 15 fmol of recombinant PTEN and p110α/p85α, respectively, and diluted 2-, 4-, and 8-fold prior to tryptic digestion

These data indicate that our multiplexed PTEN/p110α iMALDI assay is highly reproducible throughout its linear range, with mean total CVs over all experiments and

days of 9.5% for PTEN and 8.4% for p110α in the LP mode, and similarly low CVs (14.7% and 12.4%) in the RP mode (Figure 14 2).

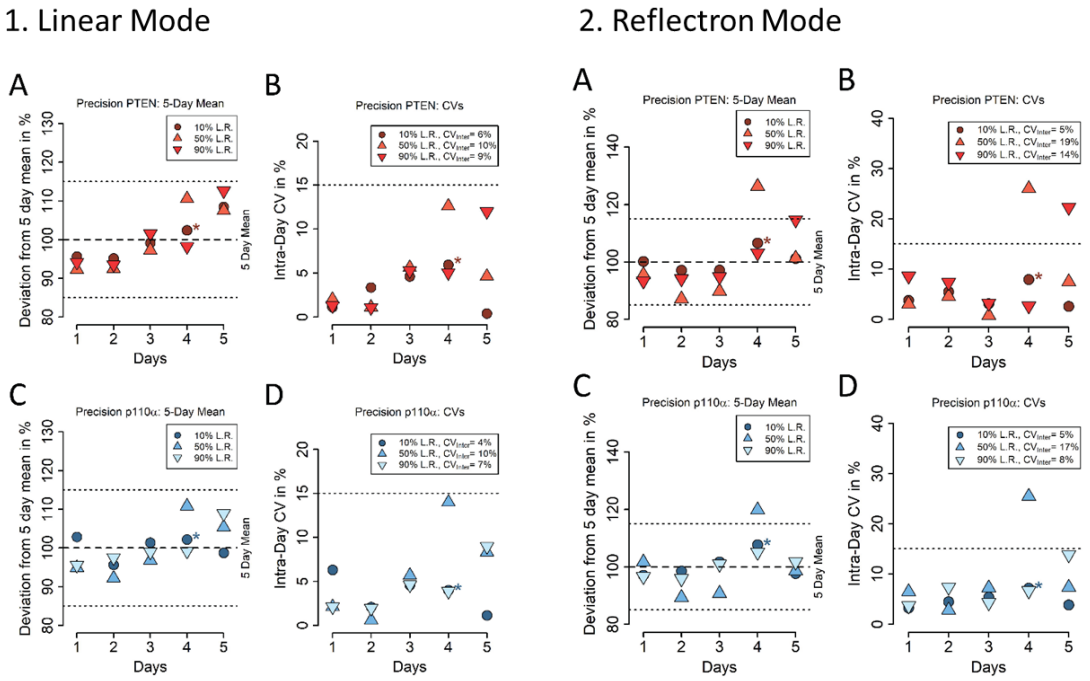

Figure 14 Inter- and intra-day precision of the multiplexed PTEN/p110α iMALDI assay. Three pools of MDA-MB-231 lysate were spiked with 2, 10, or 18 fmol of PTEN+p110α dSIS, corresponding to 10%, 50%, and 90% of the assay's linear range in linear mode (low, medium, and high levels, respectively). One fresh aliquot from each pool was analyzed each day for five consecutive days in triplicate. Data was recorded in the linear positive ion mode (1) and reflectron mode (2). (A+C) The deviation from the 5-day mean for low, medium, and high samples is given for (A) PTEN and (C) p110α. (B+D) Intra-day CVs and 5-day inter-day CVs for low, medium, and high-level samples. An outlier (amount quantified > 3rd quartile$_{\text{5-day 'low' results}}$+3x Interquartile Range$_{\text{5-day 'low' results}}$) was excluded from the 'low' sample on Day 4.

3.3.3 Multiplexed quantitation of PTEN and p110α in tissue samples

Having validated our multiplexed iMALDI assay, we then evaluated the performance of the assay for the quantitation of endogenous PTEN and p110α in tumor tissue samples. The assay was used to analyze fresh-frozen (FF) tissue samples from a mouse patient-derived xenograft (PDX) model, which underwent three consecutive drug trials, two of

which were reported previously.[179] The samples used in this study originated from the third drug trial, where trastuzumab-resistant gastric tumors were transplanted into 12 mice, which were either treated with trastuzumab (Tra) at 5mg/kg intraperitoneal once a week, everolimus (Ev) at 5mg/kg daily gavage, both trastuzumab and everolimus (Tra-Ev) at the same concentrations and schedule, or served as untreated controls (Ctrl). The tumors showed PIK3CA mutations (c317G>T), but no PTEN deletions.

Trastuzumab is a monoclonal antibody that targets the HER2 receptor, while everolimus is an mTOR inhibitor that can be used in locally advanced or metastasized gastrointestinal cancers. The combination of trastuzumab and everolimus is a potential combinatorial treatment for patients who are HER2-positive but have aberrant PI3K/AKT/mTOR-pathway activation, which is associated with resistance to trastuzumab therapy.[180] The Tra-Ev group showed a partial response to the treatment, with two animals showing stable disease and one animal showing a partial response based on RECIST guidelines[181]. The other groups showed progressive disease. In all samples (except for one out of three animals in the control group), we were able to quantify both proteins from only 10 µg of total protein extract with high reproducibility (the median CV across duplicates was <6%) (Figure 15 A, Figure 15 B; Supporting Table S 23). While PI3K expression levels were stable across the different samples, showing no significant differences (Ctrl: 0.4±0.5 fmol/10 µg; Tra: 0.8±0.2 fmol/10 µg; Ev: 0.9±0.2 fmol/10 µg; Tra-Ev: 0.9±0.2 fmol/10 µg), the PTEN expression levels appeared to be up-regulated upon treatment in 2 out of the 3 treatment groups (Ctrl: 2.0±2.0 fmol/10 µg; Tra: 3.6±0.5 fmol/10 µg; Ev: 4.6±1.0 fmol/10 µg; Tra-Ev: 4.2±0.5 fmol/10 µg), although these differences were not statistically significant due to high variability in

the control group. This dose-dependant upregulation of PTEN expression upon treatment with everolimus has previously been reported for A549 cells, while PI3K levels have been reported as being reduced upon everolimus treatment. [182,183]

We further analyzed fresh-frozen tissue samples of four colorectal cancer liver metastases and five breast cancer tumors using exactly the same workflow, and we again were able to quantify both proteins in all samples with high reproducibility (the median CV across 3 technical replicates was ≤10 %), using only 10 µg of total protein extract (Figure 15 C, Figure 15 D). While PI3K shows a surprisingly stable protein expression level across the two tumor tissues -- from 0.6 to 1.2 fmol per 10 µg of total protein in both colorectal cancer liver metastases (mCRC, 0.9±0.3 fmol/10 µg) and breast tumors (0.8±0.4 fmol/10 µg) -- the protein expression levels of PTEN showed a higher variability (mCRC: 2.0±1.2 fmol/10 µg; breast tissue: 2.0±1.0 fmol/10 µg).

We compared our 'absolute' PTEN and PI3K protein levels to the ProteinAtlas database, which shows higher RNA expression levels for PTEN than for PI3K in both breast cancer (9.4 vs. 3.9 Fragments Per Kilobase Million (FKPM) in >1000 breast cancer samples) and colorectal cancer (6.1 vs. 1.9 FKPM in >590 colorectal cancer samples).[184–186] Notably, although the number of analyzed samples in the ProteinAtlas database is much higher than in this study, the difference between colorectal cancer and breast cancer RNA and protein expression levels may reflect the known low correlation between the transcriptome and the proteome, and thus may underscore the need for

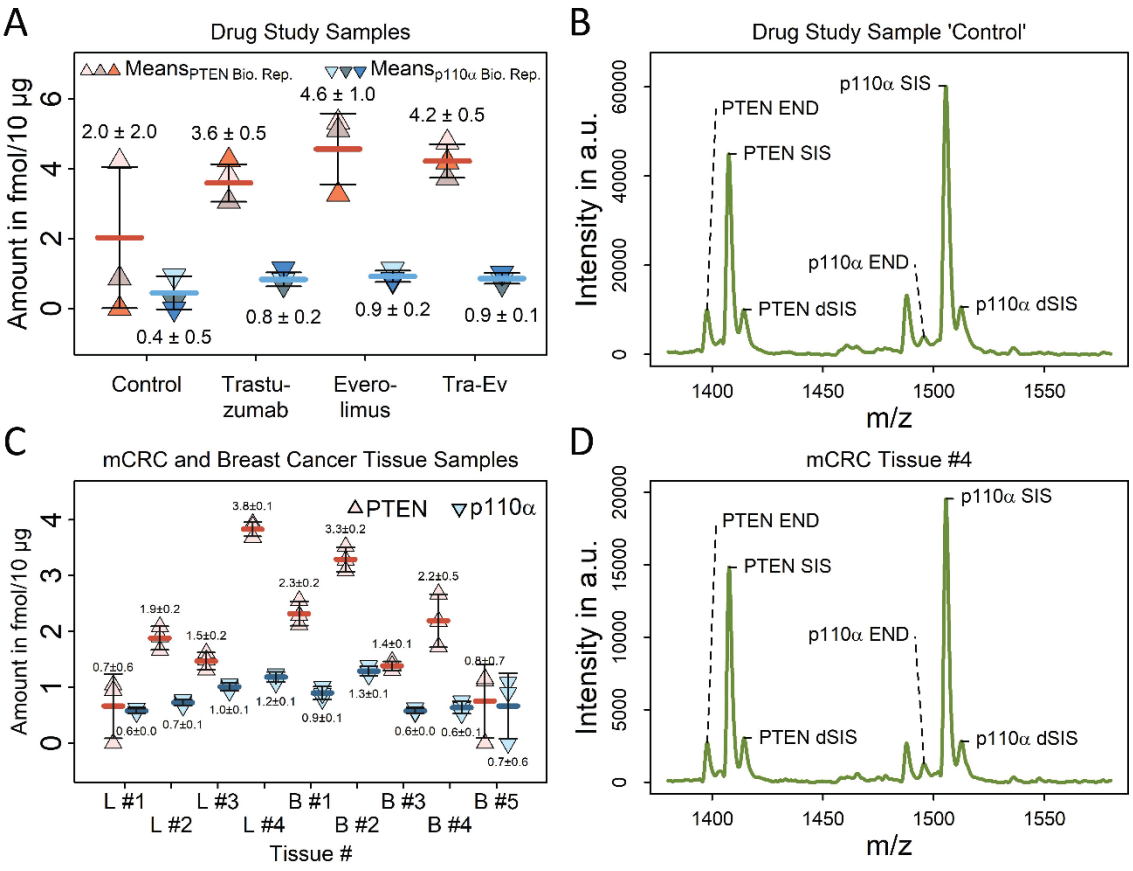

Figure 15 Multiplexed quantitation of PTEN and p110α in human tissue samples. (A) Endogenous PTEN and p110α were quantified in fresh-frozen (FF) tissue samples which were part of a mouse-PDX drug study. Trastuzumab resistant gastric tumors were transplanted into 12 mice and were either treated with Trastuzumab, Everolimus, or Trastuzumab+Everolimus (Tra-Ev), or not treated (control). (B) Mass spectrum of a control group sample showing PTEN and p110α END peaks as well as SIS+dSIS standard. (C) Endogenous PTEN and p110α concentrations in various FF breast tumor (B) and colorectal cancer liver metastasis (L) tissue samples (10 µg total protein/replicate). (D) MALDI TOF spectrum of sample L #4 showing the endogenous PTEN and p110α target peptides as well as the SIS and dSIS standards with low non-specific background.

precise protein assays to quantify relevant cancer genes on the *protein* level, where cancer drugs act.[84,86]

In summary, our results show that our validated multiplexed PTEN/ p110α iMALDI assay is fit-for-purpose for high-throughput analysis of tumor samples. In addition, our

data show surprisingly robust expression levels of PTEN from fresh-frozen PDX samples and from breast tumors and colorectal cancer liver metastases.

3.3.4 Conclusions

We developed and validated an automated, rapid (same-day results), and multiplexed iMALDI assay for quantifying PTEN and p110α. Our assay requires as little as 0.2 µg of antibody per sample and the MS readout requires only a low-cost benchtop MALDI-TOF MS which is already present in many clinical laboratories. We validated the linearity of our assay and found it to be linear from 0.6 fmol to 20 fmol on-spot, with an LLOQ of 0.7 fmol for both protein targets). The accuracy was 90-102% for PTEN and 97-112% for p110α, and the intra- and inter-day precision was below 15%. [60]

Using this assay, we were able to quantify endogenous PTEN and p110α in cancer cell lines as well fresh-frozen tumor tissue samples, including a PDX model of trastuzumab-resistant gastric tumor. We were able to detect small changes in the expression levels of PTEN upon treatment with everolimus and everolimus+trastuzumab, which agree with data in the literature, and the differences between PI3K and PTEN protein expression levels were in good agreement with transcriptomic data for breast cancer and colorectal cancer, while concurrently underlining the discrepancy between transcriptome readouts and absolute protein expression levels.

Chapter 4 Using two peptide isotopologues as internal standards for the streamlined quantification of low-abundance proteins by immuno-MRM and immuno-MALDI

Work in this chapter was performed at the UVic Genome BC Proteomics Centre (PC) and at the Jewish General Hospital in Montreal (JGH). *Colo-205* cell lysates were prepared by Adriana Aguilar-Mahecha (JGH) and Sahar Ibrahim (JGH). iMALDI experiments were performed by Bjoern Froehlich, iMRM experiments were performed by Sahar Ibrahim. Data analysis was performed by Bjoern Froehlich and Sahar Ibrahim. Experimental design was performed by Bjoern Froehlich, Sahar Ibrahim, Rene Zahedi, and Christoph Borchers. Christoph Borchers oversaw the project. The contents of this chapter were adapted from the following publication:

Sahar Ibrahim, Bjoern C. Froehlich, Adriana Aguilar-Mahecha, Raquel Aloyz, Oliver Poetz, Mark Basik, Gerald Batist, René P. Zahedi, and Christoph H. Borchers,
"Using Two Peptide Isotopologues as Internal Standards for the Streamlined Quantification of Low-Abundance Proteins by Immuno-MRM and Immuno-MALDI", *Anal. Chem.* 2020, 92, 18, 12407–12414

4.1 Introduction

Major advances in instrumentation and methods for MS-based proteomics have enabled the relative quantification of 1000s of proteins across different samples and conditions.[138,187,188] In many cases, however, relative quantification showing only up/down-regulation of a protein compared to a control may not be sufficient, and a more precise determination of the actual protein concentration, i.e. the expression level is required.[112,157,189] This is of particular importance in precision oncology. Since not all patients' tumors have pharmacologically tractable alterations in their DNA, a deeper understanding of cancer biology - at the level of proteins and their post-translational modifications - may help to determine whether these proteins might either be drug targets, or serve as diagnostic, prognostic or predictive biomarkers.[112,190]

PTEN, a tumour suppressor which negatively regulates the PI3K/mTOR pathway, is an important example: Despite the low incidence of PTEN mutations and deletions in breast, prostate, and colon cancer, PTEN expression is commonly found to be downregulated in these tumors.[191] Importantly, PTEN downregulation correlates with the severity of these cancers in a dose-dependent manner.[192] These findings make PTEN a good biomarker candidate for prognosis, as well as for predicting the response to therapeutics that target the PI3K/mTOR pathway. Typically, IHC is used to evaluate PTEN expression in patient clinical samples, but it lacks the sensitivity, specificity, and precision to distinguish subtle differences in protein expression levels between tumors. These shortcomings of IHC have hindered the accurate correlation of PTEN expression with disease severity, and thus have prevented PTEN's approval as a biomarker.

Whether a target protein can be quantified or even detected by MS strongly depends on the dynamic range that can be covered in a given type of analysis. Great advances have been made to expand the dynamic range of MS -- and thus enable and improve the quantification of low abundance proteins -- however, this often requires pre-fractionation, or state-of-the-art instrumentation and technology which may not always be available.[138,193,1942,10,11] In particular, the robustness of a specific workflow and of the required instrumentation are important determinants for clinical MS, which is in stark contrast to fundamental research, that is constantly pushing technological boundaries.[195–197]

Immuno-MS approaches using SIS peptides as internal standards, as described in chapter 1.3.4, are well suited for this task. SIS peptides not only enable quantifying endogenous protein concentrations but can also be used as internal standards to control, e.g., immuno-enrichment recovery. Controlling immuno-enrichment recovery is a crucial control-step that is virtually impossible for anti-protein immuno-enrichment.[198,199] Furthermore, using SIS peptides allows the generic normalization of the END signal and therefore compensates for issues that are often hard to control, such as sample-specific ion suppression, or spray instabilities in ESI.[200] Typically, the most precise and robust quantification using SIS peptides involves targeted MS, i.e. multiple reaction monitoring (MRM) or parallel reaction monitoring (PRM), where mass spectrometers specifically monitor and quantify specific peptides-of-interest.

The choice of calibration strategy can greatly affect the precision (and accuracy) of protein quantification assays. While some proteomics studies use only the END/SIS ratio measured in the sample to directly determine protein concentrations, proper

quantification requires a careful characterization of the assay-at-hand, ideally including the assessment of the linear range, the lower limit of quantification, etc., as well as the generation of a calibration curve in order to deduce the actual END concentration from that END/SIS ratio. The calibration curve directly examines the relationship between the measured signal and the actual peptide quantity, which can demonstrate that the measured concentration is precise, and that the signal is above the lower limit of quantification (LLOQ), and within the linear range of the assay. When measuring an unknown sample, all these requirements have to be met to guarantee that the measured signal really reflects a certain quantity of the analyte.[201]

External calibration is a "gold standard" for quantitative MS assays: a synthetic version of the END peptide (often referred to as NAT, for "native") and its SIS are used to generate the calibration curve. While the SIS is kept constant, different levels of NAT are spiked into the individual standards of the calibration curve (Figure 17 A). The same amount of SIS is then also added to all "real" samples with unknown END concentrations. This approach enables the signal to be normalized and corrected for variations in analyte response: once added during sample processing, the SIS peptide reflects all losses from that point forward, including fluctuations in LC-MS response, and consequently corrects the final quantification. External calibration requires the use of a representative sample matrix that, ideally, does not contain endogenous analyte which would interfere with the measurements, particularly at the lower end of the calibration curve. Surrogate matrices are often used for external calibration, based on the assumption that an analyte's LC-MS response is the same in different types of samples[202], thus ignoring a major source of error in external calibration, i.e., matrix effects.[203,204]

Because the complete elimination of matrix effects is often either impossible or not feasible in trace analysis, external calibration should be used only when matrix effects can be expected to be low.[202]

Recently, we have reported a strategy to compensate for matrix effects in plasma, by using two different SIS isotopologues that differ in mass, in order to prepare an external calibration curve in the exact same matrix without interference from potential END signals.[205] Chiva et al. presented an extension of our approach, where five different isotopically labeled peptide standards were incorporated for internal calibration, and demonstrated its applicability for high precision MRM-based quantification of HER2 FFPE samples.[206]

Herein, we present a strategy for the internal calibration of immuno-MRM and immuno-MALDI assays. Mimicking the matrix of iMRM and iMALDI assays in order to generate a representative external calibration curve proved to be challenging, as the background obtained after immuno-enrichment depends strongly on both the antibody used and the sample. Even when external calibration curves were generated from the same sample type after immuno-enrichment, endogenous signals may still interfere.[205] Using surrogate matrices to generate external calibration curves, such as BSA or *E.coli* digests, has previously been shown to be feasible, as described above in chapter 2.2.6 ,[175] but may not sufficiently represent interference and suppression events occurring in clinical samples, including FFPE specimens, where considerable unanticipated off-target binding of antibodies may occur. Proving that a particular external calibration works for a given combination of immuno-MS assay and patient tissue sample on a case-by-case basis is virtually impossible. As recently argued by Hoofnagle et al, external calibration

of each sample batch substantially increases the cost[207] and turnaround time[208], so that the concept of running full calibration curves in each sample batch as "ideal" has been challenged.[209] This practice might be even more questionable for precision-medicine assays which often demand timely analysis and thus are likely to be analyzed individually rather than in large batches. Since iMRM and iMALDI have the great advantage of co-enriching SIS and END peptides with the same efficiency, we evaluated the merit of using two SIS isotopologues at different concentrations in order to quantify the protein of interest using internal calibration (Figure 17 B). Our rationale for the use of only two SIS isotopologues for immuno-MS was to keep the costs for clinical assays low without compromising precision, as (i) generation, purification and quantification of SIS peptides is costly and (ii) spiked-in SIS will compete with endogenous peptides for antibody-occupancy, thus either reducing peptide recovery or requiring the use of more antibody. We therefore compared our two-point internal calibration (2-PIC) strategy with the gold-standard, external calibration.

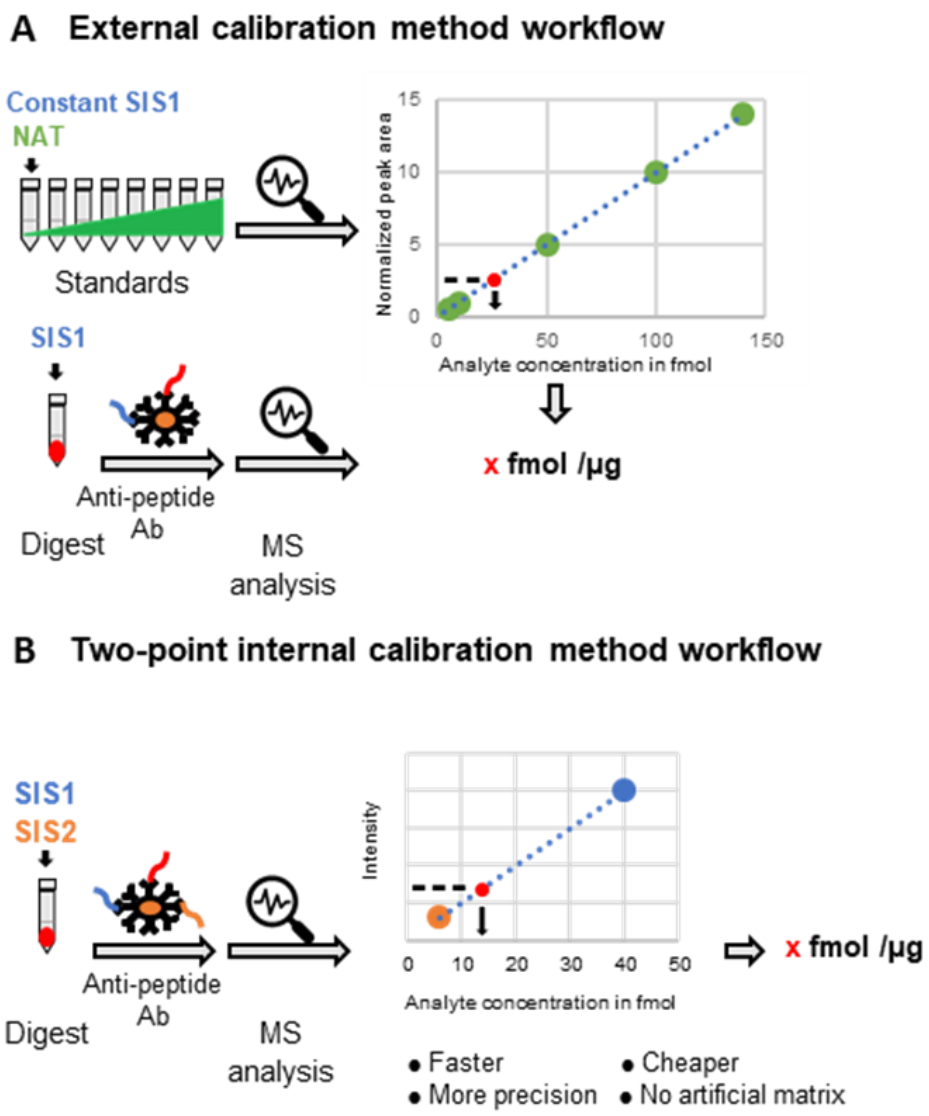

Figure 17. Comparing external calibration to two-point internal calibration (2-PIC). Schematic workflows for immuno-MS based protein quantification. A: External calibration: multiple standards have different concentrations of NAT in a constant concentration of SIS. Calibration standards are prepared in a surrogate matrix without immuno-enrichment and analyzed together with the sample to determine a calibration curve that is used to calculate the analyte's concentration in real samples. B: Two-point internal calibration where two different SIS isotopologues that differ in mass are spiked into the real sample at different concentrations, prior to immuno-enrichment, and the two-point internal calibration curve is used to calculate the concentration of the analyte.

4.2 Materials and Methods

4.2.1 Reagents

Reagents were obtained from Sigma Aldrich (Oakville, Canada), if not stated otherwise. The Bicinchoninic acid assay (BCA) kit was obtained from Thermo Scientific (Ottawa, Canada). Trypsin/Lys-C Mix, MS Grade was from Promega (Madison, USA), while TPCK treated trypsin, was purchased from Worthington (Lakewood, USA). Microcon-30 kDa Centrifugal Filters were purchased from Millipore-Sigma (Oakville, Canada). LC-MS grade acetonitrile (ACN) and water were purchased from VWR International (Montreal, Canada) and Honeywell B&J Brand (Muskegon, USA), respectively. Acetic acid was purchased from Honeywell Fluka (Montreal, Canada).

The iMRM SIS2 (NNIDDVVR+10 Da; bold letters indicate stable-isotope labeled amino acids; the total mass shift in Da is given) peptide, as well as the iMALDI NAT (AQEALDFYGEVR) and SIS1 (AQEALDFYGEVR+10 Da) peptides were synthesized at the University of Victoria Genome BC Proteomics Centre (Victoria, BC, Canada), and their purities and concentrations were determined by capillary zone electrophoresis and amino acid analysis, respectively.[210,211]1,2 The iMRM NAT (NNIDDVVR, , Supporting Figure S 4) and SIS1 (NNIDDVVR+6 Da) and the iMALDI SIS2 (AQEALDFYGEVR+17 Da) peptides were purchased from Synpeptides (Shanghai, China). Anti-NNIDDVVR and anti-AQEALDFYGEVR rabbit polyclonal antibodies were obtained from Signatope (Reutlingen, Germany). Protein A Dynabeads and Protein G Dynabeads were purchased from Invitrogen (Ottawa, Canada).

4.2.2 Cell lines samples and sample digestion

Colon adenocarcinoma Colo-205 cells were second-passage cells obtained from ATCC. Cells were mycoplasma-free and 6.66 x 10^6 cells were seeded in 10 cm dishes and cultured in RPMI-1640 medium (ATCC 30-2001) with 10% FBS at 37°C in 5% CO_2. Cells were collected at 80% confluence within 24 h of seeding, washed with D-PBS, trypsinized (0.25% trypsin), centrifuged at 12,000 x g for 5 min, and the pellet was collected.

The Colo-205 cell pellet was washed 3 times with 1 mL of 50 mM Tris buffer (pH 8.5) and spun down at 15,000 x g for 1 min at 4 °C. Then the pellet was re-suspended in 400 µL of 2% sodium deoxycholate in 50 mM Tris, vortexed for 30 s before being centrifuged at 18,000 x g for 30 min at 4 °C. The supernatant was transferred into an Eppendorf LoBind microcentrifuge tube, and a 10 µL aliquot was used to determine total protein concentration by BCA, following the manufacturer's protocol. Twenty-µL aliquots were then prepared.

For iMRM, 7 µL of lysate (equivalent to 60 µg of total protein) were reduced with 10 mM Dithiothreitol (DTT) for 30 minutes at 56 °C, with shaking. After cooling on ice, free Cys residues were alkylated with 25 mM of iodoacetamide (IAA), incubated at 22 °C for 30 min in the dark, followed by quenching with 5 mM of DTT. Prior to proteolytic digestion, sodium deoxycholate[146] was diluted to a final concentration of below 0.3% with freshly[212] prepared 8 M urea, 100 mM TRIS-HCl, pH 7.8. The sample was then transferred to a molecular weight cutoff spin filter (Microcon-30 kDa Centrifugal Filter Unit, Millipore) for filter-aided sample preparation.[213,214] After centrifugation at 13,500 x g for 15 minutes, the sample was washed 3 times with 200 µL of 8 M urea, 100 mM

TRIS-HCl, followed by another 3 washes with 200 µL of 50 mM ammonium bicarbonate (AmBic). The filter device was transferred into a fresh LoBind microcentrifuge tube and 100 µL of 30 ng/µL Trypsin/LysC in 50 mM AmBic were added (1:20 protein:enzyme, w:w). The sample was incubated overnight at 37 °C, under gentle shaking. The generated peptides were collected by centrifugation at 13,500 x g for 15 minutes, followed by a wash with 50 µL of 50 mM AmBic, and another wash with 50 µL of dH_2O. The sample was dried in a Speedvac and reconstituted in 60 µL of 1x PBS supplemented with 0.003% CHAPS (PBSC2), followed by vortexing for 1 min.

For iMALDI, the Colo-205 lysate was diluted using 20 mM TRIS+0.015% CHAPS (TRIS+C) to a final concentration of 0.5 µg/µL in a 1.5 mL Axygen MaxRecovery tube. For proteolytic digestion, aliquots of 105 µL were prepared in triplicate. The samples were denatured by adding 10.5 µL 10% DOC in 200 mM TRIS, pH 8.1 (DOC2), to a final DOC2 concentration of 0.91%, followed by incubation at 60 °C for 30 min. Then, 10.5 µL of 10 µg/µL trypsin in 1 mM HCl (1:2, w:w protein:trypsin) were added, followed by incubation at 37 °C for 1 h. The digestion was quenched by adding 10.5 µL of 850 µM Nα-tosyl-L-lysine chloromethyl ketone hydrochloride (TLCK).

In addition, bovine serum albumin (BSA) digest was prepared as surrogate matrix for the experiments described below by first preparing a 10 mL BSA solution at a concentration of 0.1 µg/µL in TRIS+C in a Falcon® 15 mL conical centrifuge tube. The sample was digested as described above, using 1 mL 10% DOC2 for denaturation, 1 mL 2 µg/µL trypsin solution (1:2 protein:trypsin) for digestion and 1 mL 170 µM TLCK for quenching.

4.2.3 LC-MRM analysis

Samples were analyzed on an Agilent 6495 triple-quadrupole MS, coupled online to an Agilent 1290 Infinity UHPLC system. Peptides were separated using an Agilent 1290 Infinity UHPLC system equipped with an Agilent RRHD Eclipse Plus C18 column (2.1 mm inner diameter × 150 mm length, 1.8 μm particle size). The column was maintained at 50 °C. The following 11-min multistep gradient was used at a flow rate of 0.4 mL/min, using 0.1% formic acid (FA) as mobile phase B, and 0.1% FA in ACN as mobile phase B: 0 min: 2 % B, 1 min: 3 % B, 8 min: 35 % B, 9.5 min: 85 % B, 10 min: 85 % B, 10.5 min, 2 % B, 11 min: 2 % B. The UHPLC system was interfaced to an Agilent 6495 triple quadrupole mass spectrometer via an ESI source with Agilent Jet Stream technology, in the positive ion mode. The capillary and nozzle voltages were set to 3500 V and 300 V, respectively. In the MRM method, the NNIDDVVR NAT and SIS peptide ions y6, y5, y4 were targeted using collisional energies of 19, 17, 19, and 13, respectively.

The MRM data was quantified with Skyline-Daily 19.1.[215] Peak picking was manually checked, and the data was exported to Excel.

4.2.4 iMALDI analysis

The automated iMALDI assays, including antibody-bead conjugation, assay preparation and bead washing+spotting were conducted following the workflow described in chapter 2.2.2 and 3.2.1.

A mixture of iMALDI SIS1 (AQEALDFYGEV**R**+10 Da) and SIS2 (AQEA**L**DFYGEV**R**+17 Da) peptides was prepared and spiked into each sample as the internal standards. Next, 30 μg of antibody-coupled beads (0.2 μg antibody per replicate)

were added to each sample, followed by a 1-h incubation at room temperature while shaking at 1000 RPM on a Microplate Vortex 120V ADV (Thermo Fisher, Ottawa, Canada).

After incubation, the antigen-antibody-bead complex was magnetically separated from the sample and washed and spotted on a MALDI plate. After the spots dried, they were washed as described above in section 2.2.2.

The MALDI plates were analyzed in reflectron positive ion mode (RP). One thousand laser shots per spot, were accumulated in 25-shot intervals using a 'random walk' pattern. The data was analyzed using FlexAnalysis (v3.4, Build 70). Mass spectra were smoothed using Savitzky Golay (1 cycle, Peak width= 0.2 Da and TopHat baseline subtraction). Peaks were detected using Snap (SNAP average composition set to Averagine). Mass lists were exported and analyzed using R (Supporting Figure S 1).[153,216]

4.2.5 External calibration

To generate an external calibration curve for iMRM, eight different standard samples were created by mixing different concentrations of iMRM SIS2 (NNIDDVVR+10 Da) peptide to a constant concentration of 2 fmol/µL of SIS1 (NNIDDVVR+6 Da) in 0.1% FA, resulting in SIS2 concentrations of 0.025, 0.05, 0.125, 0.25, 0.42, 1.67, 3.33, 6.67 fmol/µL. Then, 20 µL of each standard sample were injected and analyzed by LC-MRM in triplicate, as described above.

To generate an external calibration curve for iMALDI, six standards were created with varying amounts of AQEALDFYGEVR NAT peptide in PBSC2: 0.03, 0.063, 0.125,

0.25, 0.5, and 1.0 fmol/µL. A SIS2 (AQEALDFYGEVR+17 Da) peptide standard, with a concentration of 0.088 fmol/µL, was prepared similarly.

Aliquots of 130 µL BSA digest, prepared as described above, were used as the surrogate sample matrix yielding 10 µg total protein per aliquot. These samples were spiked with 20 µL iMALDI NAT standard and 20 µL SIS2 standard, resulting in constant SIS2 amounts of 1.75 fmol per replicate and varying NAT amounts of 0.6, 1.25, 2.5, 5, 10, and 20 fmol per replicate. Three technical replicates were prepared for each standard. The samples were analyzed using iMALDI as described above.

4.2.6 Internal Calibration

In LC-MS, instrument response is proportional to the concentration (x), and larger deviations at higher analyte concentrations tend to disproportionately influence regression curves (heteroscedasticity). Weighting regression curves using weighted least squares (WLS) significantly reduces the impact of the variance at the upper end of the calibration curve[217], so that $1/x^2$ is the appropriate weighting factor.[177] Thus, SIS peptide peak areas were used for internal and for external calibration with $1/x^2$ weighted linear regression. The 2-PIC calibration curve was generated using WLS through the origin.

For iMALDI, PTEN NAT peptide amounts were determined using either external calibration, or 2-PIC and ordinary least squares regression (OLS).[218]

Sample preparation for the use of 2-PIC for quantifying (i) a constant NAT at different SIS1 and SIS2 levels and (ii) different NAT levels at constant SIS1 and SIS2 levels, using both MRM and iMALDI, are described in the Supporting Information, and outlined in Figures 2 and 3, respectively.

4.2.7 2-point internal calibration for quantifying a constant NAT at different SIS1 and SIS2 levels

Sample preparation and analysis using MRM. The following samples were generated with varying amounts of NNIDDVVR NAT:SIS1:SIS2 (fmol:fmol:fmol): (A1) 10:5:1, (A2) 10:20:4, and (A3) 10:40:4. Next, to determine whether internal calibration can provide precise quantification over an extended dynamic range, a second set of samples were generated: (B1) 10:40:2, (B2) 10:60:2, and (B3) 10:100:2. Finally, to determine whether our strategy allows precise quantification of NAT levels if SIS1 and SIS2 span a dynamic range of up to 2 orders of magnitude and, importantly, even in the hypothetical case that both standards are at a higher concentrated than the NAT, a third set of samples were generated: (C1) 10:100:1, (C2) 10:500:5, and (C3) 10:2000:20. Samples were measured as described above. For each sample, the NAT concentration was calculated using the NAT and SIS intensities determined by Skyline. The 2-PIC curves using iMRM SIS1 (NNIDDVV**R**+6 Da), SIS2 (NNIDDVV**R**+10 Da), were generated with 1/x2 WLS linear regression (see Figure 2A) through the origin. Thus, the calculated NAT amounts were compared to the actual 10 fmol NAT spike-in. Mean values and relative standard deviations (RSD) were calculated from triplicates.

Sample preparation and analysis using iMALDI. Aliquots of 130 µL BSA digest were used as the surrogate sample matrix. The following samples, with varying amounts AQEALDFYGEVR NAT:SIS1:SIS2 (fmol:fmol:fmol), were generated by adding 20 µL NAT and 20 µL SIS1+SIS2 standard to the sample: 10:5:1 (M1), 10:12.5:2.5 (M2), 10:17.5:1.75 (M3), 10:20:1 (M4), and 10:15:5 (M5). Four technical replicates were prepared each, and the samples were analyzed using iMALDI. NAT concentrations were calculated using the NAT and SIS peak intensities as determined by FlexAnalysis.

Theoretical NAT amounts were calculated using ordinary least squares regression (OLS) 2-PIC, with SIS1 (AQEALDFYGEV**R**+10 Da) and SIS2 (AQEA**L**DFYGEV**R**+17 Da), and compared to the actual amount of NAT spike-in. The mean values and the RSDs were calculated.

4.2.8 2-point calibration for quantifying different NAT levels at constant SIS1 and SIS 2 levels

Sample preparation and analysis using MRM. Nine samples were generated by mixing different iMRM NNIDDVVR NAT concentrations with a constant 2 fmol/µL of SIS1 (NNIDDVV**R**+6 Da) and 0.1 fmol/ µL of SIS2 (NNIDDVV**R**+10 Da) in 0.1% FA, resulting in NAT concentrations of 0.05, 0.1, 0.25, 0.5, 1.0, 1.5, 2.0, and 2.5 fmol/µL. Twenty µL of each sample were injected and increasing amounts of NAT (1, 2, 5, 10, 20, 30, 40, and 50 fmol; see Figure 3A) were analyzed, with constant amounts of SIS1 (40 fmol) and SIS2 (2 fmol). Samples were measured by LC-MRM.

Sample preparation and analysis using iMALDI. Aliquots of 130 µL BSA digest, were used as surrogate sample matrix. Five samples were generated in quadruplicate by adding 20 µL AQEALDFYGEVR iMALDI NAT standards of varying concentrations (0.05, 0.125, 0.25, 0.5, and 1.0 fmol/µL) in PBSC2. Then, 20 µL of a mixture of 0.875 fmol/µL iMALDI SIS1 (AQEALDFYGEV**R**+10 Da) and 0.0875 fmol/µL SIS2 (AQEA**L**DFYGEV**R**+17 Da) were added. The resulting samples contained five different NAT amounts (1.0, 2.5, 5.0, 10, and 20 fmol) with constant amounts of SIS1 (17.5 fmol) and SIS2 (1.75 fmol) and were analysed using iMALDI (see Figure 3D).

4.2.9 Comparison of 2-point internal calibration with external calibration for quantifying endogenous PTEN levels in the Colo-205 colon cancer cell line

The utility of 2-PIC was evaluated for clinical samples, and the precision of quantifying endogenous PTEN was compared to external calibration. The 2-point calibration curve was evaluated for clinical samples, and the precision of quantifying endogenous PTEN was compared to external calibration.

Sample preparation and analysis using MRM. A mixture of iMRM SIS1 (NNIDDV**V**R+6 Da) and SIS2 (NNIDDVV**R**+10 Da) peptides was added to Colo-205 digests to obtain final concentrations of 2 fmol SIS2 and 40 fmol SIS 1 per 10 µg/15 µg/30 µg of total protein. Each sample was diluted to a final volume of 100 µL using PBSC, prior to immuno-enrichment.

One day before the immuno-enrichment, 8 µL of Magnetic Protein A Dynabeads slurry (Invitrogen, 2.8 µm, 30 µg/µL) were transferred to a fresh reaction tube, and the beads were washed 3 times with PBSC, followed by reconstitution in 72 µL of PBSC. Eight µL of anti-NNIDDVVR antibody (0.5 mg/mL) were added and the samples were incubated overnight at 4 °C, shaking.

The following steps were conducted in a cold room, using a pre-cooled magnetic rack and pre-cooled PBSC. The antibody-coupled beads were washed 3 times with 80 µL of PBSC and reconstituted in 80 µL of PBSC. Twenty µL of the reconstituted antibody-bead complex were spiked into each of the three Colo205 digests, and the samples were incubated overnight at 4 °C, shaking. The beads were washed with 200 µL of PBSC, 200 µL of 0.1x PBSC, and finally with 200 µL of H_2O. Bound peptides were eluted with 20 µL of 3% ACN, 5% acetic acid, 50 mM citrate for 2 min. The eluate was analyzed by LC-MRM.

Sample preparation and analysis using iMALDI. Colo-205 lysate was prepared as described above. From the 0.5 µg total protein/µL stock solution, three dilutions with concentrations of 0.1, 0.15, and 0.3 µg total protein/µL were prepared in duplicate using TRIS+C as diluent. A mixture of iMALDI standards -- SIS1 (AQEALDFYGEV**R**+10 Da; 0.875 fmol/µL) and SIS2 (AQEA**L**DFYGEV**R**+17 Da; 0.0875 fmol/µL) -- was prepared in PSBC.

iMALDI was performed as described above, using 130 µL Colo-205 digest and 20 µL of iMALDI standard mix as internal standard, yielding constant total amounts of 17.5 fmol SIS1 and 1.75 fmol SIS2 across all samples, and varying Colo-205 amounts of 10, 15, and 30 µg per sample. Additionally, an external calibration curve was prepared as described above. The endogenous PTEN amounts were quantified using both 2-PIC and external calibration.

4.3 Results and Discussion

This study was designed to determine whether 2-point internal calibration using two different SIS peptides can be used to quantify NAT (or respectively endogenous) peptide/protein levels precisely by immuno-MRM and immuno-MALDI. For this purpose, it is important to address the following questions: (i) does the method generally work with good precision and accuracy, (ii) does a SIS1/SIS2 internal calibration mixture enable the quantification of different NAT (or endogenous) levels over a biologically relevant dynamic range, and (iii) how the quantification would be affected if some real-life samples fall outside the pre-defined calibration curve. The minimum amounts of NAT and SIS peptides used were 1 fmol either on-column (MRM) or on-spot (MALDI),

which agrees with the lower limits of quantification (LLOQ) that we determined by external calibrations using the same setups (1.0 fmol for MRM and 0.9 fmol for MALDI). Thus, different standard samples were generated in order to determine whether a constant NAT level could be correctly quantified using different amounts of SIS1 and SIS2, spanning up to two orders of magnitude, even if both SIS standards were either below or above the concentration of the NAT (Figure 18). Next, standards with fixed amounts of SIS1 and SIS2 were prepared, and we evaluated whether those would allow the precise quantification of different levels of NAT, again, even if both standards are below/above the NAT concentration (Figure 19). The second setup better reflects the real-life situation where a specific assay would be developed using a predefined amount of calibrant in order to quantify unknown samples. Finally, we used our 2-PIC method to quantify levels of the tumor suppressor protein PTEN in the Colo-205 cells (Figure 20). To evaluate the general applicability of 2-PIC, we conducted all experiments for two independent immuno-MS workflows, immuno-MRM and immuno-MALDI. Importantly, these two workflows (i) have completely different sample preparation protocols, (ii) target different PTEN peptides (^{48}NNIDDVVR^{55} for iMRM, ^{148}AQEALDFYGEVR^{159} for iMALDI) both of which were selected to be proteotypic and devoid of known mutations or post-translational modifications (see SI), (iii) utilize two different ionization methods (ESI and MALDI), and (iv) use two different MS techniques (LC-MRM and MALDI-TOF). These methods can therefore be orthogonal and, importantly, they have been carried out by two different individuals in two different laboratories (an inter-laboratory comparison).

4.3.1 2-PIC for quantifying a constant NAT at different SIS1 and SIS2 levels

MRM. 2-PIC was used to determine the precision of quantifying a constant 10 fmol NAT spike-in, when different amounts of iMRM SIS1 (NNIDDVV**R**+6 Da) and SIS2 (NNIDDVV**R**+10 Da) were used as standards. For this purpose, three sample sets, A-C, were generated (Figure 18A, C).

Sample set A included 3 samples with the following NNIDDVVR SIS1:SIS2 (fmol:fmol) ratios and a constant amount of 10 fmol of NNIDDVVR NAT: (A1) 5:1, (A2) 20:4, and (A3) 40:4. Samples were prepared and measured in triplicate. The amounts of NAT determined based on the internal calibration curves were 9.4±2.1 fmol (A1), 10.6±0.7 fmol (A2), 10.2±1.0 fmol (A3), with relative standard deviations (RSD) of 21.7% (A1), 6.2% (A2), 9.3% (A3). Thus, except for A1, where both standards SIS1 (5 fmol) and SIS2 (1 fmol) were below the 10 fmol NAT, the error was $\leq$10%, and recoveries for all samples were between 94% and 106%.

Sample set B was used to evaluate how well 2-PIC performs when the internal standards span different levels in dynamic range, reflecting changes that might occur in biological samples. Thus, NNIDDVVR NAT and SIS2 were kept constant at 10 fmol and 2 fmol, respectively, while SIS1 was 40 fmol (B1; dynamic range of 20), 60 fmol (B2; dynamic range of 30), and 100 fmol (B3; dynamic range of 50). Samples were prepared and measured in triplicate. The 10 fmol NAT spike-in was quantified as 9.8±0.3 fmol (B1), 9.3±0.2 fmol (B2), 10.4±0.6 fmol (B3), with RSDs of 2.6%, 2.6%, and 5.9%, respectively. Recoveries were 98±3% (B1), 93±2% (B2), and 104±6% (B3).

In sample set C, the dynamic range of the internal standards was extended to 100. Three samples were prepared in triplicate with the following NNIDDVVR SIS1:SIS2

(fmol:fmol) ratios and a constant amount of 10 fmol of NNIDDVVR NAT: (C1) 100:1, (C2) 500:5, and (C3) 2000:20. The 10 fmol NAT spike-in was quantified as 8.8±0.4 fmol (C1), 8.6±0.1 fmol (C2), 11.2±1.1 fmol (C3), with RSDs of 5.0%, 0.6%, and 9.9%, respectively. Recoveries were 88±4% (C1), 86±1% (C2), and 112±11% (C3).

iMALDI. To determine if the 2-PIC concept is also applicable to iMALDI assays, which involve a completely different sample preparation protocol and type of MS analysis, five samples, M1-5, were prepared with constant AQEALDFYGEVR NAT (10 fmol) and varying amounts of internal standards (Figure 18B). Because MALDI generally has a smaller linear range than MRM, we adjusted the amounts of iMALDI SIS1 (AQEALDFYGEV**R**+10 Da) and SIS2 (AQEA**L**DFYGEV**R**+17 Da) accordingly, reflecting the PTEN amounts we would expect to find in 10 µg of total protein cell lysate, based on in-house data. Samples M1-M5 had the following AQEALDFYGEVR SIS1:SIS2 ratios (fmol:fmol): (M1) 5:1, (M2) 12.5:2.5, (M3) 17.5:1.75, (M4) 20:1, and (M5) 15:5. The samples were prepared in quadruplicate, using BSA digest as the surrogate sample matrix, followed by analysis using iMALDI (Figure 18D).

The amounts of NAT (10 fmol spike-in) determined based on 2-PIC were 8.5±0.2 fmol (M1), 9.1±0.1 fmol (M2), 9.1±0.1 fmol (M3), 9.0±0.1 fmol (M4), 9.3±0.1 fmol (M5). In all five samples, the NAT levels could be determined with high precision using 2-PIC, with RSDs of 1.8, 1.3, 0.9, 1.6, and 1.5% (Figure 18D) as well as with high accuracy, with the quantified NAT amounts being well within ±20% of the spiked-in concentration. High recoveries were achieved even in cases where (i) SIS1 and SIS2 were both below the NAT amount (M1) with 85±2%, (ii) SIS2 was 20-fold higher than SIS1 (M4) with a 90±1%, and (iii) when SIS1 was only 3-times higher than SIS2 (M5) with 93±1%.

Collectively, these results demonstrate that 2-PIC provides high accuracy and precision for iMALDI-based protein quantification, and is a good alternative to the use of external calibration.

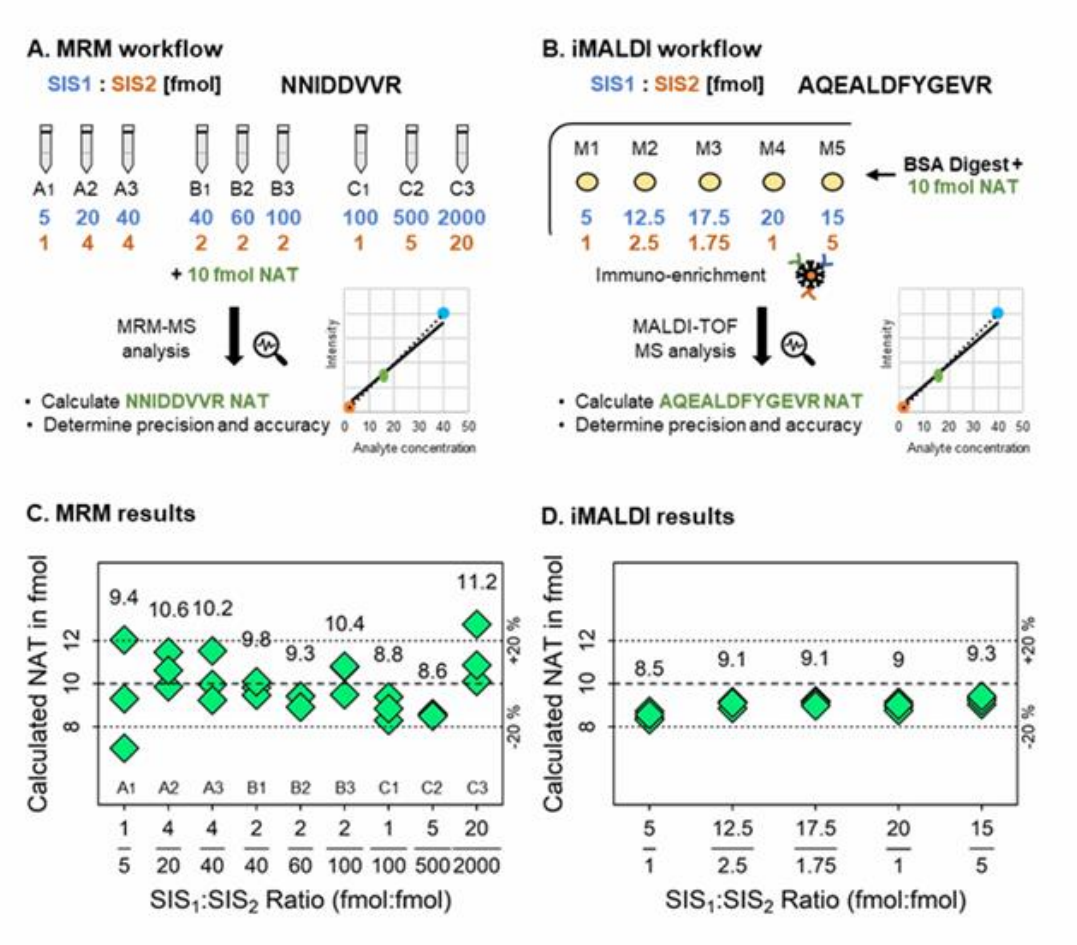

Figure 18. Testing 2-PIC for quantifying a constant NAT level using different SIS1 and SIS2 levels. A: MRM workflow targeting the PTEN peptide 48NNDDVVR55. B: iMALDI workflow targeting the PTEN peptide 148AQEAKDFYGEVR159. C: MRM results of samples A1-A3, B1-B3, C1-C3. NAT levels calculated using 2-PIC are shown as light green rhombuses (N=3). D: iMALDI results of samples M1-M5. NAT levels calculated using 2-PIC are shown as light green rhombuses (N=3).

4.3.2 2-PIC for quantifying different NAT levels at constant SIS1 and SIS2 levels

MRM. We next evaluated the precision and accuracy when different levels of NAT were quantified using a fixed SIS1:SIS2 ratio, as would be the case for a fully optimized assay.

Eight different levels of NNIDDVVR NAT spikes (D1: 1 fmol, D2: 2 fmol, D3: 5 fmol, D4: 10 fmol, D5: 20 fmol, D6: 30 fmol, D7: 40 fmol, and D8: 50 fmol) were used to mimic a 50-fold change in PTEN amount, using fixed amounts of 40 fmol SIS1 and 2 fmol SIS2 as 2-PIC standards (Figure 19A). Samples were prepared in triplicate and measured by LC-MRM. In sample D1, the NAT level (1 fmol) was below both internal standards, and in sample D8, the NAT level (50 fmol) was above both internal standards. For all eight samples highly reproducible results were obtained, with the RSD from the triplicate analyses between 1% and 13%, and with a correlation between determined and known NAT levels of r^2= 0.9791 (y= 1.05x–0.23). For D2-D8, PTEN quantification was clearly within a 20% cut-off, with recoveries between 83% and 110% (average 103%), while for D1, recovery was 77±2%. Notably, for the D8 sample where 50 fmol NAT was above both SIS standards, the recovery was 97±3% (Figure 19C).

These results clearly show that -- given a defined set of SIS1 and SIS2 levels in an optimized assay -- 2-PIC yields accurate and precise results, over a reasonable range of fold-changes that might be expected in a given biological sample.

iMALDI. We prepared another set of 5 samples (N1-N5) with different AQEALDFYGEVR NAT levels (1, 2.5, 5, 10, and 20 fmol) in quadruplicate, using BSA digest as surrogate matrix and 17.5 fmol iMALDI SIS1 and 1.75 fmol SIS2 as the 2-PIC standards (Figure 19B). Again, the NAT level of one sample (N1; 1 fmol NAT) was

below the levels of both internal standards, while in the sample N5 (20 fmol NAT) the NAT level was above both internal standards. In all samples, the NAT levels could be quantified with high precision, with RSDs between 0.6% and 3.1%, and with a good correlation between the experimentally determined and known NAT levels (r^2= 0.9912, y=0.86x+0.31).

For N2-N5 all measurements were within the 20% cutoff, with recoveries between 89% and 93% (average 91%), while for sample N1 (1 fmol NAT), the recovery was 121±3% (Figure 19D).

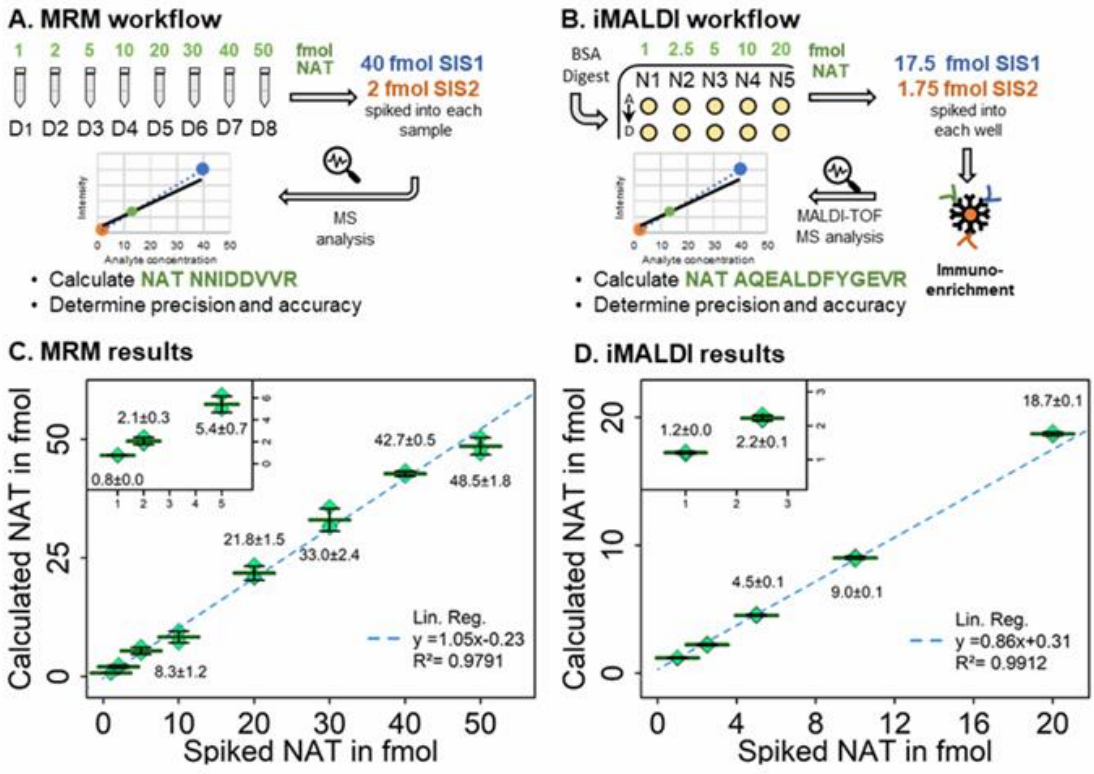

Figure 19. Quantifying different NAT levels using 2-PIC with fixed SIS levels. A: MRM workflow targeting the PTEN peptide ^{48}NNDDVVR^{55}. B: iMALDI workflow targeting the PTEN peptide ^{148}AQEALDFYGEVR^{159}. C: MRM results of the samples D1-D8. Dashed blue line: 1/x2 WLS regression curve. D: iMALDI results of the samples N1-N5. Dashed blue line: 1/x2 WLS regression curve**.**

These results agree with the results from our MRM experiments, and demonstrate the applicability of the 2-PIC strategy for the quantification of low-abundance proteins.

4.3.3 Comparison of 2-PIC with external calibration for quantifying endogenous PTEN levels in Colo-205 cells

In clinical laboratories, the concept of internal calibration in LC-MS was first introduced for drug monitoring of immunosuppressants.[219] In fact, the Clinical Laboratory Improvement Amendments guidelines do not require a calibration curve for every batch of runs.[220] For targeted proteomics MS methods, internal calibration can increase the throughput, thus reduce expenses while avoiding the dependence on potentially misleading surrogate matrices.[207] Moreover, as clinical laboratories need to analyze small numbers of patient samples when they are received, reducing the workload required for preparing and running the calibrators can be very important. This means that applying internal calibration strategies for targeted proteomics will facilitate its clinical translation.

We therefore compared our 2-PIC strategy to conventional external calibration for their abilities to precisely determine endogenous PTEN expression levels in Colo-205 cells, a cell line that is commonly used to study metastatic colorectal cancer and which shows a down-regulation of PTEN expression compared to other colorectal cell lines.[221,222] Colo-205 cells have wildtype *PTEN*, showing neither copy-number variations nor single nucleotide variations. Notably, they have a $BRAF^{V600E}$ mutation and show increased activity of the PI3K/AKT/mTOR pathway and lower PTEN protein expression levels than $BRAF^{V600E}$-positive melanomas.

Thus, Colo-205 are a good model to test our immuno-MS PTEN assays, because the typically low endogenous PTEN expression level in normal tissue is further reduced in many cancers. We used both orthogonal workflows, immuno-MRM targeting the peptide ^{48}NNIDDVVR^{55} and immuno-MALDI targeting the peptide ^{148}AQEALDFYGEVR^{159}. To evaluate the robustness of both methods three different amounts of starting material were used: 10, 15, and 30 µg of total Colo-205 lysate protein, rather than just using the same amount three times.

Although one of the advantages of immuno-MS is that the amount of starting material can be scaled-up to improve the detection of low-abundance proteins, relatively low amounts of starting material are often all that can be obtained from clinical samples. Thus, each Colo-205 cell lysate was divided into two aliquots, one each for iMRM and iMALDI. Sample preparation, immuno-enrichment, data acquisition, and data analysis for iMRM and iMALDI, respectively, were performed by two different individuals in two different laboratories as described above.

For all three amounts of cell lysate (10, 15, and 30 µg of total Colo-205 protein) and both methods (iMRM and iMALDI), the two calibration methods (2-PIC and conventional external calibration) showed good agreement on the determined amounts of endogenous PTEN. For iMRM, the RSDs between 2-PIC and external calibration were 6.4%, 4.6%, and 3.7% using 10 µg, 15 µg, and 30 µg of Colo-205 lysate, respectively, and the iMALDI RSDs were 1.6%, 0.2%, and 1.6%, respectively (Figure 20A). These results demonstrate that both setups are extremely robust and very precise, and that 2-PIC yields results that are fully comparable to those from external calibration, while requiring much less effort, time, antibody, and standards - and fewer samples analyzed.

Moreover, although the two methods were orthogonal - being based on two different peptides, using different anti-peptide antibodies, and being performed by two different individuals in two different laboratories – they showed good agreement on the determined amounts of endogenous PTEN when 2-PIC was used, with an average of 0.48±0.01 fmol/µg of total Colo-205 protein for iMRM (RSD of 1.6%) and 0.29±0.02 fmol/µg of total Colo-205 protein for iMALDI (RSD of 5.6%). Using 2-PIC, the endogenous PTEN concentrations determined by iMALDI and iMRM had an average inter-assay RSD of 25% and these results reflect the good correlation between iMALDI and iMRM for quantifying endogenous PTEN (r^2=0.9966, y=0.64x; (Figure 20B).

For many years, MS researchers have been studying inter-laboratory assay performance and how to manage the resulting imprecision.[223–226] For example, Kuhn et al. demonstrated using a SISCAPA workflow that the overall inter-laboratory %CV, (including protein digestion, desalting, peptide antibody enrichment, and scheduled LC-MRM-MS analysis) was below 25% at or near the LOQ and below 20% at or near the midpoint of the linear range. While Abbatiello et al. studied the reproducibility of MRM assays across 11 laboratories and using 14 LC-MS systems, demonstrating that the median inter-laboratory CV% was <20% across the concentration range tested.

To our knowledge, there are no inter-laboratory precision studies that involved the quantification of a protein using two completely different MS techniques using two different ionization methods, such as shown here for iMRM and iMALDI. The agreement between the two methods on quantifying endogenous PTEN in Colo-205 cells (RSD=25%; r^2=0.9966; y=0.64x) is comparable to values that have been reported for

inter-laboratory variation when using a single method and standardized sample preparation protocols.

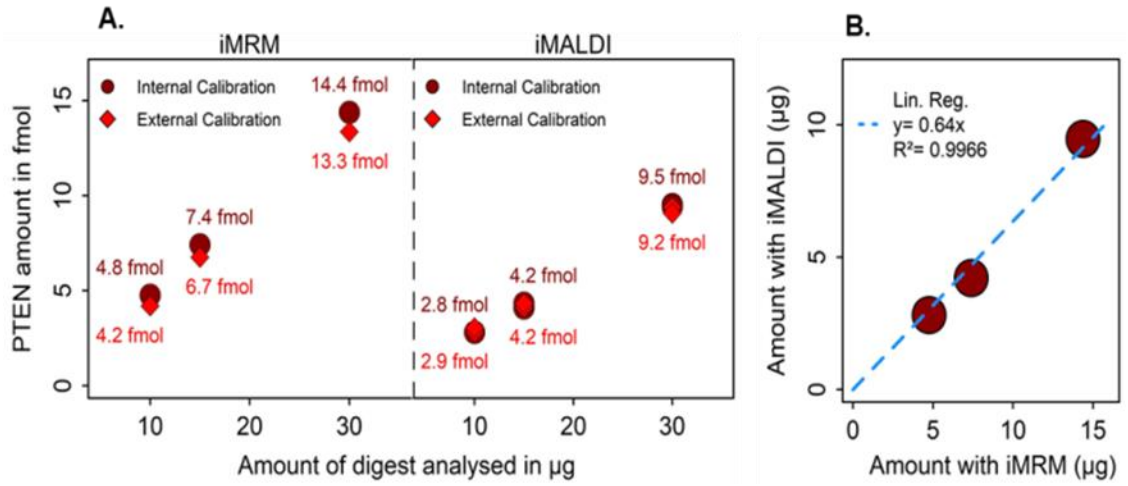

Figure 20. Quantifying endogenous PTEN levels from 10, 15, and 30 µg of Colo205 cell lysate total protein. A: iMRM and iMALDI measurements. Left: iMRM results. The PTEN peptide NNIDDVVR was immuno-enriched from lysate, followed by MRM analysis. Right: iMALDI results. The PTEN peptide AQEALDFYGEVR was immuno-enriched from lysate, followed by MALDI analysis. B: Correlation between iMRM and iMALDI results. iMRM and iMALDI show a good correlation (r^2=0.9966; y=0.64x), even though they are orthogonal methods targeting different PTEN peptides and being conducted by two different individuals in two different laboratories.

4.4 Conclusions

Using two orthogonal workflows, namely iMRM and iMALDI, targeting two different PTEN peptides, the utility of our 2-PIC strategy for immuno-MS assays was compared with a conventional, multipoint external calibration approach. We found that both the cost and burden of preparing multiple calibration standards with every batch of samples can be reduced, while analytical quality was maintained. Importantly, we demonstrated that even if the difference between the internal standards levels was 100-fold, precise quantification of the analyte is possible, as long as the standards are in the linear range. Furthermore, 2-PIC allowed quantification of the analyte in samples with levels below

that of the lower internal standard, as well as in samples with levels above the higher internal standard. We also demonstrated that the endogenous PTEN concentrations determined from the cell line Colo-205 using the 2-PIC method were in good agreement with the results obtained using external calibration. Although quantification of endogenous PTEN in Colo-205 was conducted in two different laboratories by two different individuals, using completely different workflows targeting two different peptides with two different MS techniques and ionization methods, the results obtained strongly agreed with an RSD of only 25%.

This demonstrates that the developed PTEN iMALDI assay delivers results comparable to an orthogonal LC-MRM-MS method, the gold standard for quantitative proteomics. At the same time, iMALDI uses simpler, less expensive instrumentation (Bruker Microflex (~USD200,000) compared to Agilent 6495 triple-quadrupole (~USD600000)) and achieving faster analysis times (10 s per sample using MALDI-TOF MS compared to 11 min using LC-MS).

Chapter 5 Quantitation of AKT1, AKT2, PTEN and p110α in FFPE tissue samples from patients enrolled in an AKT inhibitor AZD5363 clinical trial using an integrated, multi-site workflow

Work in this chapter was performed at the UVic Genome BC Proteomics Centre (PC) and at the Jewish General Hospital in Montreal (JGH). Samples were provided by AstraZeneca UK. Tissue extraction of FFPE tissues belonging to patients from the AZD5363 trial (Study #D3610C00001) was performed in Montreal by Constance Sobsey and Sahar Ibrahim. AKT1+2 iMALDI analysis was performed by Constance Sobsey and Robert Popp. Untargeted proteomics data collection was performed by Constance Sobsey, Georgia Mitsa, and Rene Zahedi at JGH. Analysis of PTEN and p110α was done by Bjoern Froehlich. Data analysis for this data set presented in this chapter was performed by Bjoern Froehlich and Constance Sobsey. The methods section describing sample extraction, AKT1+2 iMALDI analysis and global proteomics data collection was provided by Constance Sobsey and Rene Zahedi. Experiments relating to multiplexing the AKT1+2 and PTEN+p110α iMALDI assays were performed at PC by Bjoern Froehlich. MDA-MB 231 cell lysates were prepared by Adriana Aguilar-Mahecha (JGH).

Experimental design was performed by Constance Sobsey, Bjoern Froehlich, Andre LeBlanc, Rene Zahedi, Gerald Batist, and Christoph Borchers. Christoph Borchers oversaw the project.

5.1 Introduction

The PI3K pathway is frequently activated in many cancers and thus an important target for drug development.[35] Overexpression of AKT isoforms specifically have been investigated and targeted for their role in cancer progression.[227] The AKT inhibitor AZD5363 (capivasertib) is a competitive inhibitor drug candidate with high potency and selectivity and has promise for patients with advanced solid cancers for whom other lines of treatment failed.[228] In clinical trials, patient stratification for this drug was performed using gene mutation status, specifically activating PI3KCA or AKT mutations or PTEN deletions. However, this approach has met with limited success. In a recent trial (Study #D3610C00001), only 30% of patients tested for anti-tumor activity of the drug showed a response (stable disease or partial response).[127] This could potentially be due to insufficiencies in the current patient stratification strategy. Since activation of the PI3K pathway may occur independent of mutations in pathway components, patients who present with activating mutations do not necessarily have an overactive PI3K pathway, and some tumors without activating mutations may nonetheless an activated PI3K pathway.

This clinical trial represents a demonstration and analytical performance evaluation for the application of our developed iMALDI assays . Patient FFPE tissue samples from the AZD5363 clinical trial# D3610C00001 were analysed at two sites (the Jewish General Hospital in Montreal and the UVic-Genome BC Proteomics Centre in Victoria) in an integrated workflow combining several iMALDI assays as well as label-free protein quantitation using untargeted proteomics. AKT1 and AKT2 were assessed using a previously published iMALDI assay (Figure 21 Step 1-3)[121,229], followed by quantifying PTEN and p110α using the multiplexed PTEN+p110α iMALDI assay using both 2-PIC

as well as external calibration approaches (Figure 21 Step 4). Additionally, a fraction of the remaining supernatant was used to perform global proteomics by LC-MS/MS (Figure 21 Step 5).

Herein, we demonstrate that the multiplexed PTEN+p110α iMALDI assay can be integrated not only with other iMALDI assays, but also with untargeted proteomics approaches, and that this combination may provide further insights into tumor biology. Further, we show that the PTEN assay has good correlation with established IHC methods, that the 2-PIC calibration approach developed in chapter 3 works in these complex patient samples, and that the iMALDI assays can be further multiplexed, thus reducing the required amount of sample material.

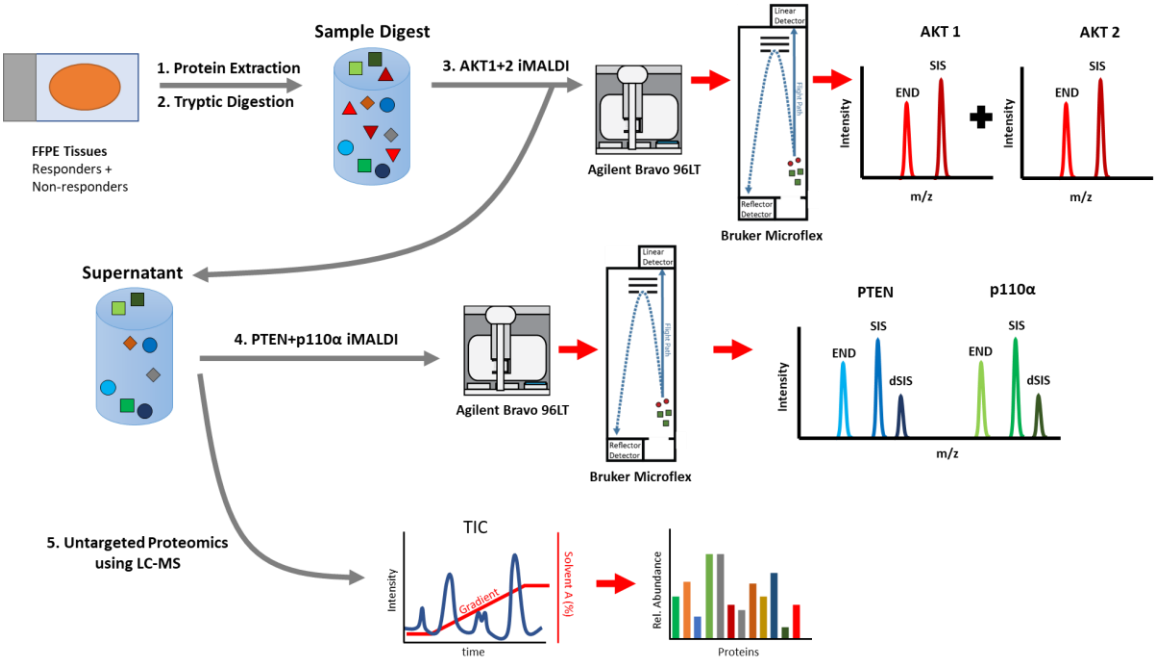

Figure 21. Workflow for analyzing patient samples from phase II trial of the AKT inhibitor AZD 5363. Sample extraction, digestion, AKT quantitation using iMALDI and global proteomics by LC-MS (steps 1-3+5) was performed at the Jewish General Hospital in Montreal, Canada. Quantitation of PTEN and p110α was performed at the UVic-Genome BC Proteomics Centre in Victoria, Canada.

5.2 Materials and Methods

5.2.1 Analysis of Patient Samples from AZD5363 trial # D3610C00001

Patient samples. A set of 24 mutation-positive samples from AstraZeneca's clinical trial of AZD5363 (Study #D3610C00001), consisting of adult patients with breast cancers, gynecological cancers, and other advanced solid tumors, was analysed (Supporting Table S 26). FFPE tumour tissue were selected for analysis based on the following criteria: minimum 50% tumour content, tissue volume ≥75mm^3, screened for mutations in AKT, PI3K and/or PTEN (by PCR or NGS), and accompanied by a pathology report indicating hormone-receptor status in breast cancer cases. Two slide-mounted slices of 4 µm FFPE were provided per patient in an anonymized format. These samples are from Part C of the trial which includes ER positive (ER+) or progesterone positive (PR+) breast or gynecologic (ovarian, cervical, or endometrial) tumours with activating PIK3CA mutations. All patients in this subset received the study drug and have detailed treatment response data available. Samples were stored at room temperature until extraction.

Sample Extraction. Slide-mounted 4 µm FFPE slices were deparaffinized using xylene followed by ethanol rehydration, 20 minute high-temperature incubation in sample extraction buffer (99^{o}C) to break formalin crosslinks, sonication, and an additional 2 hour incubation at 80^{o}C. The total protein in each sample was then quantified using a BCA assay (Thermo Fisher), or BCA-reducing agent compatible assay kits.

Targeted protein quantitation using iMALDI. AKT1 and AKT2 were analysed using a previously published method.[121,229] In brief, samples were diluted to 0.1 µg/µL and denatured using 5% sodium deoxycholate, followed by reduction with 0.74 mM tris(2-

carboxyethyl)phosphine (TCEP) and alkylation using 0.74 mM IAA. Alkylkation was quenched using 0.74 mM DTT. The samples were then digested for 1 hour at 37^{o}C with trypsin with a 2:1 protein:trypsin ratio, after which the digest was quenched with TLCK and treated with phosphatase (1U/µg) for 2 hours at 37^{o}C. SIS peptide was added prior to immunoenrichment overnight at 4^{o}C with antibodies coupled to Protein G Dynabeads. Beads were washed and spotted onto a MALDI target. HCCA matrix added, dried, and each spot was washed with ammonium citrate. Liquid handling steps were automated using a Bravo 96LT (Agilent) liquid handling robot.

Sample analysis was done using a Bruker MicroflexTM LRF benchtop MALDI-TOF-MS. Calibration curves were generated using $1/x^2$ weighted linear regressions as described in chapter 4. Supernatant from the immunoenrichment step was retained for further analysis. A portion of the supernatant was used for global proteome analysis, with the remainder being used for PTEN and p110α quantitation using the iMALDI method described in chapters 3 and 4. In brief, the supernatants were spiked with 17.5 fmol PTEN and p110α SIS and 1.75 fmol PTEN and p110α dSIS, respectively. An external calibration was prepared as described in chapters 3 and 4. Both the spiked supernatant samples and were then analysed simultaneously as described above in chapter 3. The workflow of sample analysis is depicted in Figure 21.

Global proteomics by LC-MS/MS analysis of supernatants. A 2 µL aliquot of supernatant from the iMALDI workflow, corresponding to 117.5 ng total protein, was reserved for global proteome analysis. Samples were desalted using pipette tips packed

with C18 and R3 substrate (prepared in-house), dried, and resuspended in 6 µL 0.1% formic acid.

Mass spectrometry data was acquired on a Thermo Scientific UltiMate 3000 RSLC nano system coupled to a ThermoFisher Scientific Q-Exactive Hybrid Quadrupole-Orbitrap MS. Five µL sample were injected resulting in 107 ng total protein digest on-column. LC was performed using a 78-minute method which incorporates a 50 minute gradient with 250 nL/minute flow rate. The 15 most abundant precursor ions (charge states: 2+ to 4+) are selected for MS/MS fragmentation.

The resulting raw MS spectra were processed, and consensus peptide-protein IDs were generated using Proteome Discoverer 2.4 (PD, Thermo Scientific). Database searches were performed using SequestHT and a human Swissprot database (January 2019; 20,414 target entries), with trypsin as the enzyme and a maximum of one missed cleavage. Carbamidomethylation of cysteine (+57.021 Da) was set as fixed modification and oxidation of methionine (+15.995 Da) as variable modifications. Mass tolerances were set to 10 ppm for precursor ions and 0.02 Da for product ions. Percolator was used to calculate posterior error probabilities and the data was filtered to a false discovery rate (FDR) <1% on the peptide and protein levels. Label free quantitation (LFQ) was performed using the Minora feature detector node and applying low abundance resampling imputation which replaces missing values randomly with values from the lower 5% of detected values. Samples were normalized based on the total summed protein intensities to correct for differences in sample loading. Per protein, all obtained quantitative values were scaled, such that for a total of 20 quantified samples, the scaled abundance of a protein would amount to 20 x 100 = 2000, with the value 2000 being

distributed among the individual samples in such a way that it reflects the normalized abundances. Only proteins that were quantified with at least one protein unique peptide were considered for the quantitative comparison. For samples with multiple technical replicates, scaled abundances of the two technical replicate measurements were averaged. Scaled abundances for the proteins quantified in datasets SN1 and SN2 were combined. The scaled, normalized abundances were then exported to Microsoft Excel for further analysis.

Data analysis: Data exported from Proteome Discoverer was filtered and cleaned by selecting protein IDs with "high" confidence (FDR<1%) and at least two protein-unique peptides. Multivariate statistical analysis was performed using MetaboAnalyst. PCA, UMAP and sPLSDA analysis was performed using.[230–232] The final UMAP analysis was performed using the metric 'manhattan' with the following settings: init='spectral', pca= 10, n_neighbors= 3, min_dist= 0.1.[233] UMAP cluster analysis was performed using hierarchical DBSCAN.[234]

5.2.2 Multiplexing AKT1+2, PTEN and p110α iMALDI Assays

Simultaneous enrichment of AKT1, AKT2, PTEN and p110α in spiked E.coli lysate.

Ten µg E.coli cell lysate per replicate was prepared as described in chapter 2. A calibration curve was prepared, ranging from 0.6 to 20 fmol, AKT1, AKT2, PTEN and p110α each. Samples were enriched either using a singleplex approach, using 0.2 µg of either AKT1, AKT2, PTEN or p110α pAb, or simultaneously using 0.05 µg of each pAb (0.2 µg total antibody) per replicate. Four replicates were prepared for each condition. One fmol AKT2 dSIS peptide was spiked into the MALDI matrix as described in chapter

3. Assay preparation, bead washing and spotting, and data analysis was performed as described in chapter 2.2.2 and 3.2.1.

Sequential enrichment of AKT1 and AKT2. Assay preparation, bead washing and spotting, and data analysis was performed as described in in chapter 2.2.2 and 3.2.1. Ten µg E.coli lysate were spiked with 2.5 fmol AKT1 and AKT2 NAT peptides. Analogous to the experiment described in chapter 3.2.5, AKT1 and AKT2 were enriched sequentially, either ATK1→AKT2 or AKT2→AKT1. One fmol AKT2 dSIS peptide was spiked into the MALDI matrix as described in chapter 3. Six replicates were prepared per enrichment sequence.

Quantitation of endogenous AKT1, PTEN and p110α in MDA-MB 231 lysate. Ten µg MDA-MB 231 lysate were digested and dephosphorylated as described in chapter 2.2.2 and 3.2.1 in triplicate, though no reduction+alkylation step was performed. An external calibration curve was prepared in BSA digest as described in chapter 2.2. Each sample was spiked with 1.75 and 17.5 fmol AKT1+PTEN+p110α SIS and dSIS peptides, respectively. Analytes were enriched using 0.2 µg total antibody per replicate (0.067 µg AKT1, PTEN and p110α pAb each). Bead washing, spotting and data analysis was performed as described in chapter 4.

5.3 Results and Discussion

5.3.1 Quantitation of endogenous AKT1+2, PTEN and p110α from FFPE patient tissue samples

Using the developed PTEN+p110α assay, as well as the already developed AKT1+2 iMALDI assay[121], the four target analytes were quantified in the FFPE tissues of the AZD5363 patient samples (N= 19). As demonstrated in chapter 3, it is possible to use the supernatant of one iMALDI assay as the sample for a subsequent assay without compromising the ensuing analysis. This sequential enrichment using iMALDI was used to successfully combine the multiplexed PTEN+p110α assay with the singleplexed AKT1 and AKT2 assays.

Analysed sample amounts ranged from 6.8 to 10 µg per replicate, depending on the availability of sample material. Not all patient samples were sufficient to conduct both untargeted LC-MS proteomic analyses. AKT, PTEN and p110α were quantified in the remaining samples (Figure 22). AKT1 and AKT2 concentrations ranged from 0.09 to 0.41 fmol/µg and from not detected to 0.21 fmol, respectively. PTEN amounts ranged between not detectable to 0.45 fmol/µg, and p110α amounts ranged between not detected and 0.11 fmol/µg. Notably, p110α amounts were generally low, with p110α being detectable, but frequently below the assay's LLOQ (Supporting Table S 27).

While the target proteins were quantified in the patient samples, no direct correlation between protein expression and the patient's response to the treatment could be found (Figure 23).

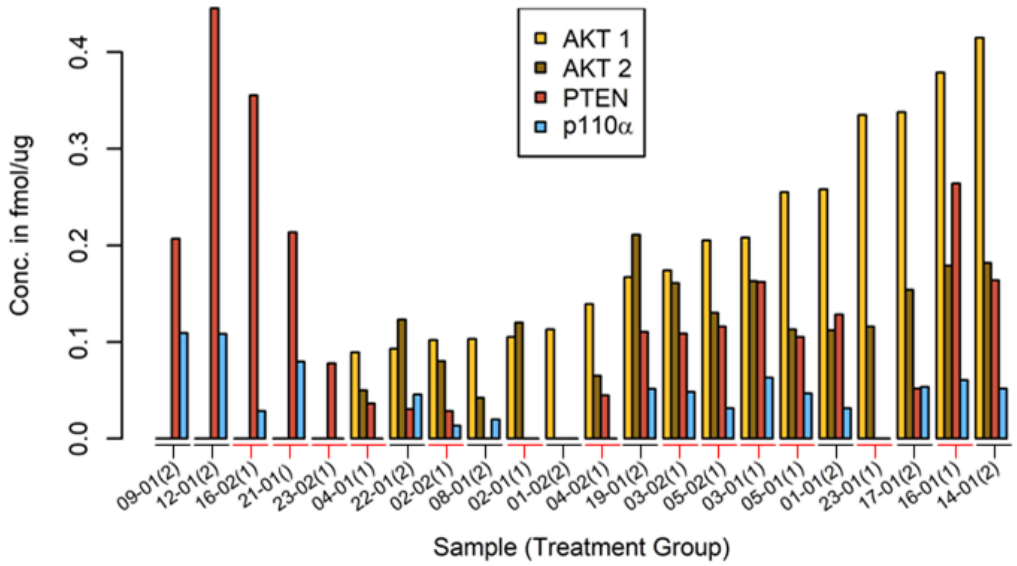

Figure 22. AKT1+2, PTEN and p110α concentrations in AZD5363 patient samples quantified using the developed, multiplexed iMALDI assays. Sample IDs with their corresponding treatment group (in parenthesis) are displayed**.** Treatment group 1= no treatment response, treatment group 2= treatment response (either stable disease or partial response)

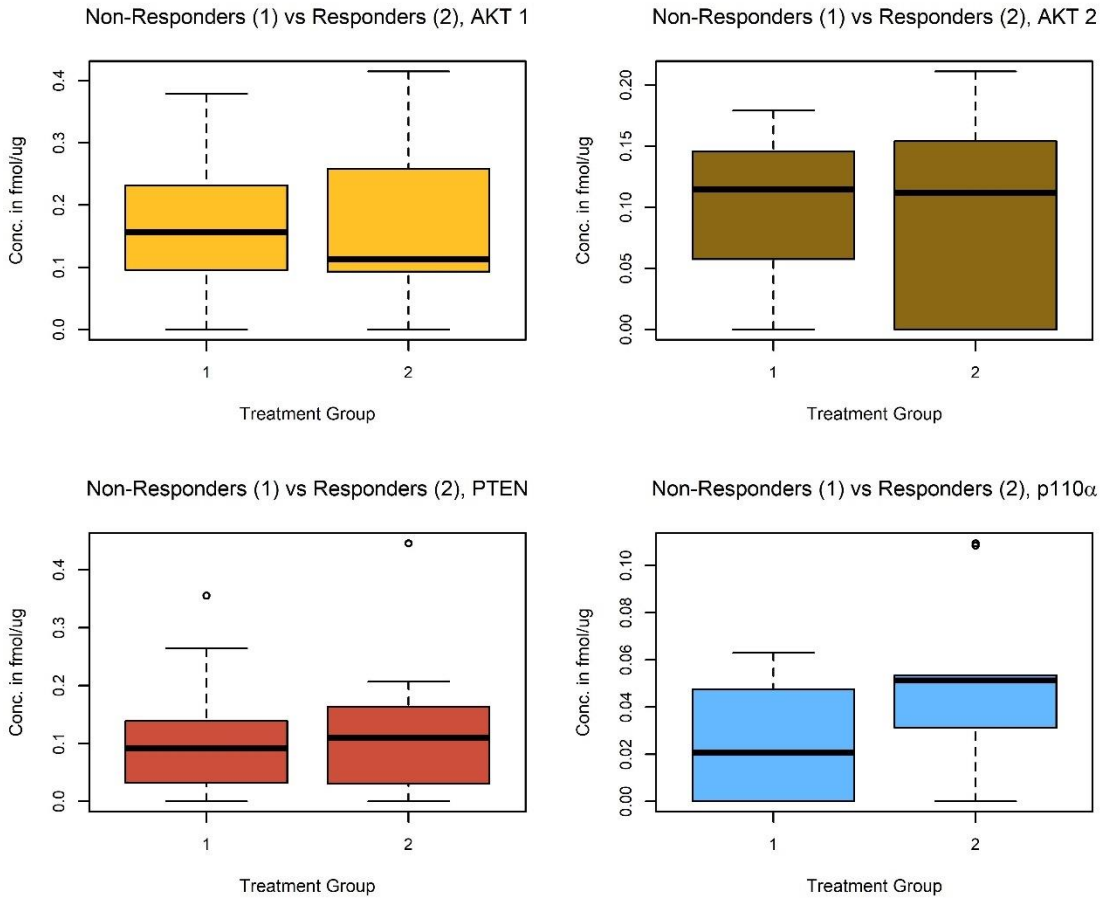

Figure 23. AKT1+2, PTEN and p110α concentrations, sorted by patient's treatment response to AZD5363 inhibitor treatment. Treatment group 1= no treatment response, treatment group 2= treatment response (either stable disease or partial response)

5.3.2 Analysis of FFPE patient tissue samples using an untargeted, label-free proteomics approach.

In addition to analysis by iMALDI, untargeted proteomics analysis was performed on the patient samples. The samples were analysed in two batches (Supporting Table S 27). Significant batch effects were observed; the number of proteins quantified by label-free proteomics varied between approximately 600 proteins in batch #1 and approximately 1460 proteins in batch #2. This poses a significant challenge for downstream analysis. For the analysis of this data set, only complete features i.e., proteins identified in all samples, were considered. Protein amounts were normalized by sum and scaled by range (Supporting Figure S 9) prior to further analysis.

First, principal component analysis (PCA) was performed on the data set (Figure 24 A, Supporting Figure S 10). No clear trends were observed. While samples from adjacent slides of the same tissue cluster together (for example samples 02-01 and 02-02), PCA did not readily discriminate between responders/non-responders, tissue type, or by AKT1/AKT2/PTEN/p110α concentration. However, the sample set is very heterogenous and has likely significant covariance, making it very difficult to reliably identify trends in the data. In addition to PCA, a non-linear dimension reduction technique, uniform manifold approximation and projection (UMAP) was applied to the data set. UMAP parameters such as minimum distance and nearest neighbours were optimized, and hierarchical density-based spatial clustering of applications with noise (HDBSCAN) was applied to the optimized UMAP (Figure 24 B, Supporting Figure S 11, Supporting Figure S 12), which revealed two clusters. When comparing the samples in both clusters with their corresponding results from the targeted iMALDI assays (where available), cluster 2 encompasses samples with elevated AKT1 and AKT2 levels cluster

(mean$_{AKT1}$/median$_{AKT1}$=0.16 fmol/µg/ 0.17 fmol/µg, mean$_{AKT2}$/median$_{AKT2}$=0.10 / 0.11 fmol/µg) compared to cluster 1 (mean$_{AKT1}$/median$_{AKT1}$=0.12 fmol/µg/ 0.096 fmol/µg, mean$_{AKT2}$/median$_{AKT2}$=0. 05 / 0 (n.d.)). While the greatest care needs to be taken to not overinterpret these results, especially since UMAP projections are not directly interpretable the way PCA is, they still provide a useful avenue for further exploring the data set.

Using the clusters identified by UMAP, sparse partial least squares-discriminant analysis (sPLSDA) was performed on the data (Figure 24 D, Supporting Figure S 14).

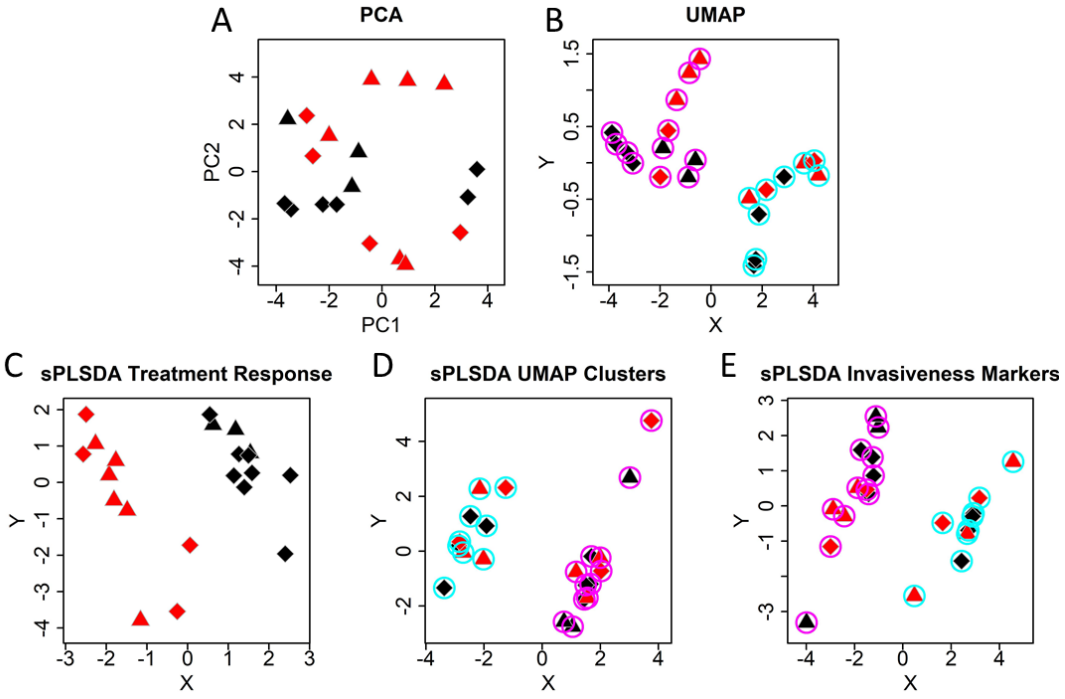

Figure 24. Untargeted proteomics analysis of FFPE tissue samples from patients treated with AZD5363. Samples are represented as colored shapes representing their tissue type. Triangles represent breast cancer tissue, rhombuses represent gynecological cancer tissue. Red filling represents responders, black filling represents non-responders**.** Pink circles around the points represent samples associated with UMAP cluster #2, turquoise circles represent UMAP cluster #1. A. PCA of the label-free protein quantitation data. B. UMAP projection of the label-free protein quantitation data, clusters were identified by HDBSCAN. C. sPLSDA discriminating the samples by treatment response. D. sPLSDA discriminating the samples by the clusters identified using UMAP (B). E. sPLSDA discriminating the samples by the clusters identified using UMAP (B), using only proteins associated with tumor invasiveness.

sPLSDA readily discriminates the samples based on their association with their respective clusters identified by UMAP. Interestingly, β-catenin was found to be a strong VIP feature in the sPLSDA loadings. β-Catenin is a major component of the Wnt signalling pathway, which is linked to AKT, as described in chapter 1. As the clusters identified by UMAP seem to correspond to 'high' and 'low' AKT concentration as identified by iMALDI, the significant contribution of β-catenin to the pLSDA discrimination may point towards a difference in AKT pathway activation. Another significant contributor is peroxiredoxin-1, a known biomarker for tumor invasiveness. Indeed, a sPLSDA analysis using the UMAP cluster and using only proteins with a known association with tumor invasiveness[235], two clear clusters overlapping with the UMAP cluster form (Figure 24 E). This association may be an interesting avenue for future exploration of these results, potentially linking AKT pathway activation and tumor invasiveness.

Additionally, sPLSDA was performed to test if the patient samples can be stratified based on the patient's response to treatment with AZD5363 (Figure 24 C, Supporting Figure S 13). While AKT, PTEN and p110α did not correlate directly with treatment response, responders and non-responders were well stratified using the untargeted proteomics data. This suggests that there may indeed be a difference between the protein expression profiles based on treatment response. This investigation however is ongoing and is outside the scope of this thesis.

However, we demonstrated that by combining targeted and untargeted proteomics, together with various dimension reduction techniques, a very challenging set of patient samples could be explored. While one has to be cautious to not overinterpret these

findings due to the challenges associated with this data set (such as low N and a heterogeneous patient population), they provide a promising avenue for future research.

5.3.3 Comparison of PTEN quantitation by iMALDI and Immunohistochemistry

IHC is currently the standard method for assessing protein concentrations in tissue samples in clinical oncology. Indeed, PTEN concentrations for patients enrolled in this study had been assessed using IHC. Hence, comparing our developed iMALDI assay to IHC is useful for assessing its utility as a tool for clinical protein quantitation.

Here, we compared the Hscores obtained from IHC with the average PTEN concentration per patient, as determined by iMALDI (Figure 25). Hscores were calculated by multiplying the PTEN expression levels (0-3, lowest to highest) with the corresponding percentage of expressing cells, giving an Hscore range of 0-300 (PTEN deficient to fully PTEN proficient). For the PTEN iMALDI results, the PTEN concentrations were averaged per patient in cases where multiple tissue slices were analysed.

The absolute PTEN concentrations determined by iMALDI show a good correlation with the IHC Hscores. Specifically, iMALDI results for patients #01, 03, 09, 14, 21, 22, and 23 are closely correlated with their corresponding Hscores (R^2=0.86). However, there are notable cases in which both do not correlate. For example, samples #14 and #16 have almost identical Hscores (135 compared to 140), however, the PTEN amounts calculated by iMALDI differ by a factor of two (0.16 fmol/µg *vs* 0.36 fmol/µg). This difference could be clinically relevant but may not be detected in some cases using IHC.

Another example is sample #04, where IHC shows the maximum Hscore of 300, suggesting full PTEN proficiency, while PTEN iMALDI shows very low PTEN amounts

(0.05 fmol/µg, very close the assay LOQ). By iMALDI, this sample would likely be classified as PTEN deficient, but IHC classifies it as proficient. Sample #22 has a similarly low PTEN concentration, which is matched by a low Hscore. For both samples #22 and #4, label-free protein quantitation was performed. UMAP analysis of this data showed that samples #4 and #22 frequently cluster together, suggesting similar protein expression profiles (Supporting Figure S 11). While certainly not a definitive answer to whether the IHC or iMALDI results are correct, it suggests that sample #4 is not as PTEN proficient as IHC might suggest.

Overall, these results show that the developed iMALDI assay has a good correlation with the established IHC method, but there may be some edge cases in which the targeted proteomics approach used by iMALDI may provide insights into the sample which may be lost using IHC.

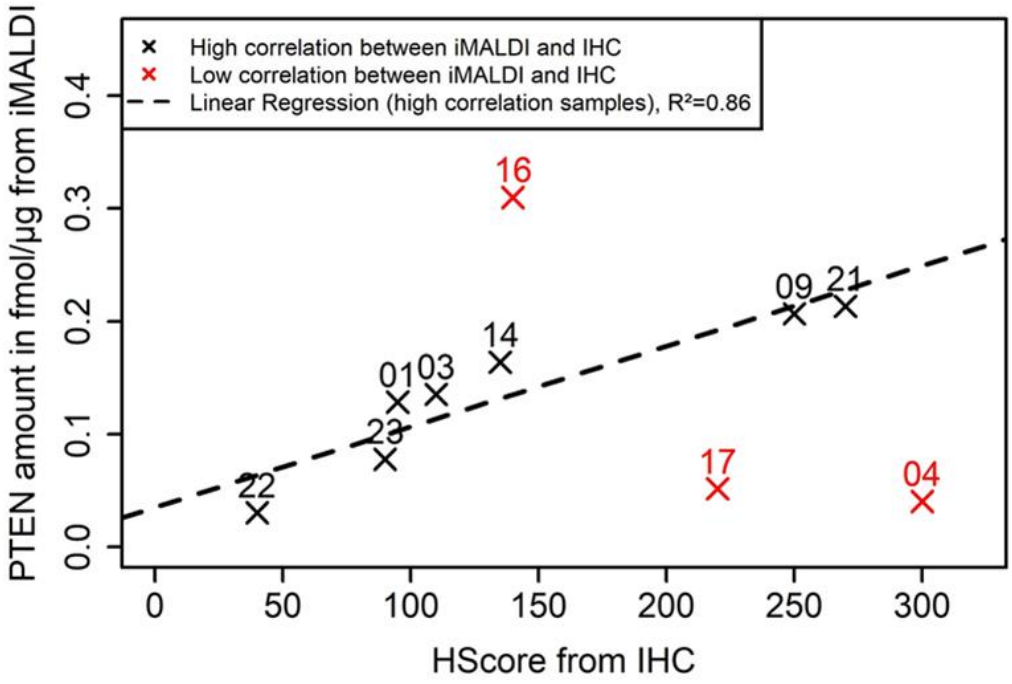

Figure 25. Comparison of PTEN iMALDI with PTEN IHC. PTEN amounts measured by iMALDI were compared to the corresponding HScore of the same sample, obtained from IHC.

5.3.4 Evaluation of the 2-point internal calibration strategy for quantifying PTEN in FFPE patient tissue samples

As demonstrated in chapter 4, a 2-point calibration curve generated from two different isotopologues, which are spiked into the sample and enriched together with the endogenous target peptide, allows accurate peptide quantitation comparable with the standard approach of using an external calibration (EC). However, the experiments comparing EC and 2-PIC were done using a cell line, not tissue samples which are a considerably more complex matrix. Here, we compared the performance of 2-PIC in the FFPE patient tissue samples of the AZD5363 trial, a very heterogenous set of samples.

PTEN amounts for all replicates were quantified using both EC and 2-PIC (Figure 26). Plotting the quantified PTEN amounts, obtained using both calibration strategies, against each other reveals an excellent correlation between both methods ($y=0.93+0.2$, $R^2= 0.97$). This demonstrates the robustness of our 2-PIC quantitation approach and confirms our conclusion from chapter 4: even in a very heterogenous set of FFPE tissue samples, 2-PIC delivers results comparable to the established calibration method without the need for preparing and measuring an external calibration, reducing instrument run time and, ostensibly, costs.

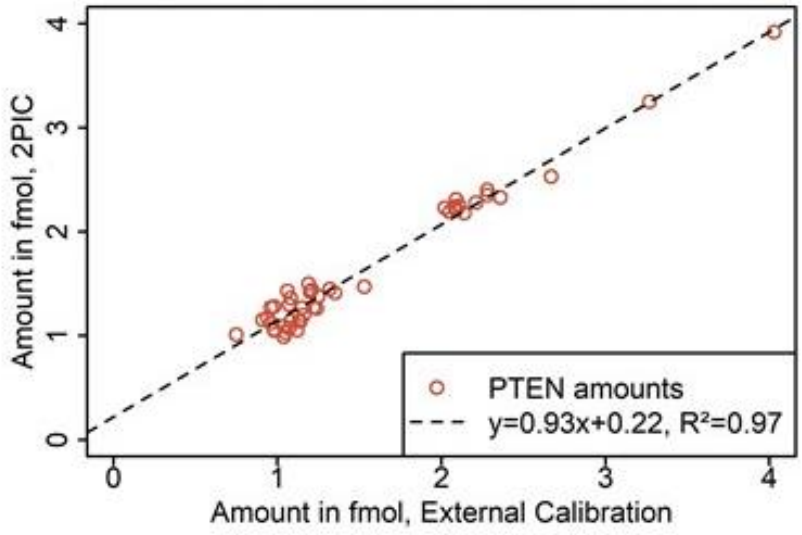

Figure 26. Comparison of using internal and external calibration for PTEN quantitation in AZD5363 patient samples. PTEN amounts for the samples from the AZD5363 study were quantified by iMALDI using both external calibration and 2-point internal calibration (2-PIC). The results of both calibration strategies were plotted against each other, and a linear regression was calculated to determine their correlation.

5.3.5 Improving multiplexing strategies for the AKT1+2, PTEN and p110α assay

While the AKT1 and AKT2 assay were combined with the PTEN+p110α assay using sequential enrichment, all targets should ideally be enriched in a single workflow. As we experienced with the analysis of the AZD5363 study samples, sample material is often very limited, making further multiplexing of the assays desirable.

First, the simultaneous enrichment of all four targets was tested by preparing a calibration from 0.6 to 20 fmol AKT1+2/PTEN/p110α NAT per replicate. These samples were analysed using simultaneous enrichment of AKT1+2, PTEN and p110α, as well as using the respective singleplex assays. Both approaches where compared in a similar way as described in chapter 3: a double-SIS-labeled peptide analogous to the target AKT2 peptide was spiked into the MALDI matrix. The peak intensity of the enriched NAT peptides was then normalized against the intensity of the AKT2 dSIS peptide in the matrix, making it easier to compare enrichment efficiencies between the multiplexed and the singleplexed assays by plotting the resulting NAT/AKT2 dSIS ratios against each other (Figure 27 A).

The results show similar performance of AKT1, PTEN and p110α using simultaneous enrichment, with high correlation between the singleplex and multiplexed approaches (R^2>0.99) and slopes of ~0.6, suggesting a slight loss in sensitivity which is comparable to the multiplexed PTEN+p110α assay as described previously (chapter 3, Supporting Figure S 6). However, AKT2 enrichment is far worse using the multiplexed approach, with a slope of only 0.26. This is in line with our previous experience with trying to enrich AKT1+2 simultaneous and might be due to the AKT2 antibody having some cross-reactivity with AKT1.

Hence, in order to combine all analytes into a single workflow, a combination of simultaneous enrichment of AKT1, PTEN and p110α and sequential enrichment of AKT2 is necessary. To determine the optimal order of AKT enrichment, *E. coli* cell lysate was spiked with 2.5 fmol of both AKT1 and AKT2 NAT peptides, which were enriched sequentially, either AKT1→AKT2 or vice versa (Figure 27 B). Enriching AKT1 first, then AKT2 was shown to be optimal, with AKT1 enrichment being significantly better when enriched first (NAT/AKT2 dSIS of 0.7 vs 0.6, $p<0.95$), and AKT2 enrichment being more efficient if performed after AKT1 (NAT/AKT2 dSIS of 0.3 vs 0.2).

Finally, with the correct enrichment order established, we tested if endogenous AKT1, PTEN and p110α could be enriched simultaneously from 10 µg MDA-MB 231 lysate (Figure 28) using both EC and 2-PIC. Endogenous peptides were quantified using both EC and 2-PIC, with good agreement between both approaches, each falling within 20% of the mean quantified amount using both approaches (1.35+-0.27 fmol/10 µg for AKT1, 2.05+-0.41 fmol/10µg for PTEN and 0.75+-0.15 fmol/10µg for p110α). CVs were consistently below 20%.

This demonstrates that the 2-PIC approach is feasible for AKT1, and that simultaneous enrichment of AKT1, PTEN and p110α is possible. Further development of this assay will include validating the workflow consisting of enriching AKT1+PTEN+p110α followed by sequential AKT2 enrichment, simplifying the assay and reducing the required amount of sample.

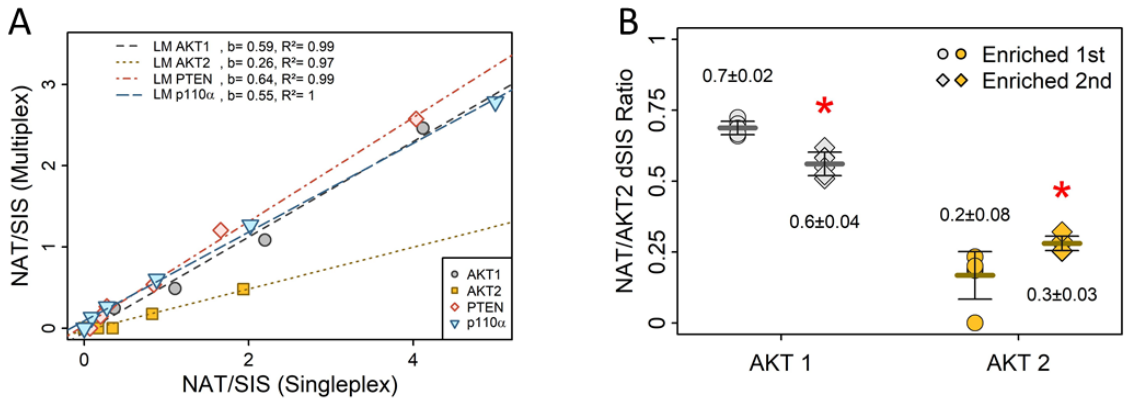

Figure 27. Multiplexing of PTEN, p110α and AKT1+2 assays. A. Six standards ranging from 0.6 to 20 fmol AKT1/AKT2/PTEN/p110α NAT peptides were prepared and analysed using singleplex approaches as well as simultaneous enrichment of AKT1+AKT2+PTEN+p110α. NAT peak intensities were normalized against the peak intensity of 1 fmol AKT2 dSIS peptide spiked into the matrix (NAT/SIS ratios).**B.** E.coli lysate was spiked with 2.5 fmol AKT1 and AKT2 NAT, and enriched sequentially either AKT1→AKT2 or AKT2→AKT1. (*) indicates significant difference ($p<0.01$) between enrichment order.

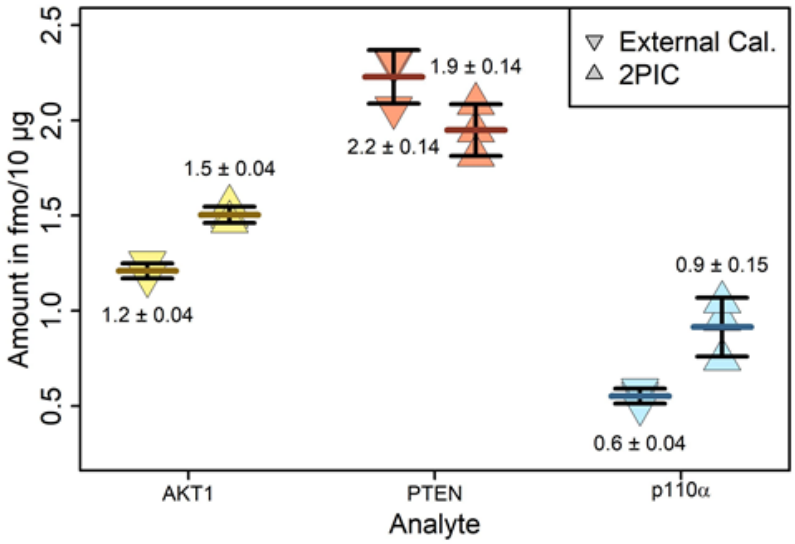

Figure 28. Simultaneous quantification of endogenous AKT1, PTEN and p110α in MDA-MB 231 cell lysate using both intern and external calibration.

5.4 Conclusions

We demonstrated that the PTEN+p110α assay can be integrated with existing AKT iMALDI assays, and further that targeted proteomics by iMALDI can be combined with an untargeted proteomics approach using the same sample. By applying various dimension reduction techniques to the label-free quantitation data, and combining in it with the results from our iMALDI assays, we were able to show potential avenues for future research to improve patient stratification for AZD5363 and further elucidate the tumor biology in this data set. However, our experience with untargeted proteomics also highlights the need for targeted proteomics approaches, especially for validating biomarkers, as the analysis of the untargeted data was very challenging, while the analysis of the iMALDI results was extremely robust and straightforward.

We also demonstrated that our 2-PIC approach is works well not only in cell lines, but in complex FFPE tissue samples. Additionally, we showed a good correlation between PTEN iMALDI and PTEN IHC, proving that the assays are fit-for-purpose for analyzing complex samples while delivering results comparable to established methods. Further, we showed how our iMALDI assays may be further multiplexed, reducing the amount of sample material needed even further while simplifying the workflow.

Chapter 6 Conclusions and Future Perspectives

The aim of this thesis was to develop automated, multiplexed iMALDI assays for quantifying PTEN and p110α in tumor tissues and cell lines, integrating them with established AKT1 and AKT2 assays, and applying them to tissue samples from a clinical trial for the AKT inhibitor AZD5363 to prove their analytical performance and their potential for biomarker validation.

We successfully developed iMALDI assay for PTEN and p110α, while systematically optimizing the iMALDI workflow for these proteins and providing a template for developing and optimizing other iMALDI assays for cell signaling proteins. We developed robust automation protocols, which not only work for these specific assays but are highly flexible and can be applied to other iMALDI assays with minimal effort.[236] We also significantly improved data analysis and visualization using custom R scripts which made data analysis faster and more reproducible.[237]

The assay was successfully multiplexed using both simultaneous and sequential enrichment strategies, proving that the supernatant of one iMALDI assay may serve as the sample for another without compromising the following assay. We validated the multiplexed PTEN+p110α assay in both linear and reflectron positive ion mode, demonstrating high reproducibility and accuracy. Linear ranges (0.6-20 fmol on the MALDI target), as well as sensitivity (LLOW below 1 fmol) were comparable to previously published assays.

Using the PTEN iMALDI assays as well as an orthogonal PTEN immuno-MRM method, we developed a novel calibration strategy using an internal calibration generated by two differently isotopically labeled peptide standards spike into the sample, which

alleviates issues faced with finding suitable surrogate matrices for external calibration, as well as dramatically reducing instrument run time. Additionally, by comparing the PTEN iMALDI assay with an orthogonal immuno-MRM assay and finding excellent agreement between both methods (RSD 25% in an inter-lab study), we showed that iMALDI can have comparable performance to LC-MS assays, the current 'gold standard' for mass-spectrometry based proteomics.

Having demonstrated that sequential enrichment using iMALDI is possible, we combined the PTEN+p110α assay with the established AKT1 and AKT2 assays, as well as with untargeted proteomics using LC-MS, in a multi-site integrated workflow and applied it to a challenging set of FFPE samples from a clinical trial of the AKT inhibitor AZD5363. Using iMALDI, we were able to reliably quantify the target proteins in these samples. We further showed that our developed 2-PIC quantitation approach works in these complex samples, and that the PTEN amounts quantified by iMALDI have good correlation with PTEN IHC results. Thus, not only does iMALDI perform well when compared with the 'gold standard' LC-MS approach used for proteomics, it also performs well when compared to the 'gold standard' for assessing protein concentrations in tumor tissue currently used in the clinical lab.

Combining both targeted and untargeted proteomics approaches, as well as various dimension reduction techniques, provided potential insights into differences in pathway activation between the different patient samples, which opens avenues for continued future work for improving patient stratification for targeted treatment. At the same time, this showed the advantages of targeted proteomics approaches: absolute protein quantitation allows straightforward data analysis which can be used to establish reference

ranges for protein biomarker which are reproducible between different sites. Analysis of untargeted proteomics data proved much more challenging, with batch effects significantly affecting data analysis, while this problem does not present itself the same way using targeted approaches. Thus, we demonstrated the potential of iMALDI as a tool for protein quantitation and biomarker validation.

Finally, we showed ways in which the developed iMALDI assays may be further improved by combining the enrichment of AKT1, AKT2, PTEN and p110α into a single workflow. The next steps of assay development should include validating the iMALDI workflow of simultaneous enrichment of AKT1, PTEN and p110α, followed by sequential enrichment of AKT2, in a similar way as described in chapter 3. Additionally, 2-PIC calibration strategies should be included in this validation from the outset.

The selected biomarkers (PTEN, p110α, AKT1+2) did not appear to have a significant correlation with treatment outcome. A reason for this might be the quality of the FFPE tissue samples. Since it is not feasible to collect fresh tissue samples (e.g., through a tumor biopsy) from patients at the time of enrollment for an early trial for of an experimental drug, archived tissue samples were used. While, pragmatically, these constitute the best available samples, the tissues have been collected years prior to enrollment in the trial. Also, many enrolled patients underwent several lines of treatment since the tissue samples were collected. Thus, the tumor samples we analysed may not actually be representative of the tumor at the time of treatment. Additionally, the patients were selected for treatment based on perceived PI3K pathway activation. However, it may be necessary to also screen potential recipients for possible escape mechanisms to

AKT inhibition (e.g., potential pathway activation in connected pathways such as the Wnt pathway).

Still, we found potential differences in protein expression profiles between responders and non-responders based on global proteome analysis, as well as potential differences in protein expression profiles in patients between high and low AKT expression. While outside of the scope of this thesis, this opens potential new avenues for future biomarker assessment. For example, eukaryotic initiation factor 4A-I (EIF4A-I) was found to be differentially expressed between responders and non-responders, pointing to potential evasion of AKT inhibition. Analysis of this data set is still ongoing, and a list of potential biomarkers for further evaluation by targeted MS is currently compiled. At this stage, no statement can be made how many, if any, promising biomarker candidates may be found.

In conclusion. we developed a powerful workflow combining targeted and untargeted proteomics, which may help to establish proteomics as tool for clinical oncology.

Bibliography

(1) Types of Cancer https://www.cancer.net/cancer-types (accessed 2021 -06 -02).

(2) What is cancer? - Canadian Cancer Society https://www.cancer.ca:443/en/cancer-information/cancer-101/what-is-cancer/?region=on (accessed 2021 -06 -02).

(3) Hanahan, D.; Weinberg, R. A. The Hallmarks of Cancer. *Cell* **2000**, *100* (1), 57–70. https://doi.org/10.1016/S0092-8674(00)81683-9.

(4) Siegel, R. L.; Miller, K. D.; Fuchs, H. E.; Jemal, A. Cancer Statistics, 2021. *CA. Cancer J. Clin.* **2021**, *71* (1), 7–33. https://doi.org/10.3322/caac.21654.

(5) Hanahan, D.; Weinberg, R. A. Hallmarks of Cancer: The Next Generation. *Cell* **2011**, *144* (5), 646–674. https://doi.org/10.1016/j.cell.2011.02.013.

(6) Baan, R. A.; Stewart, B. W.; Straif, K. *Tumor Site Concordance and Mechanisms of Carcinogenesis.Pdf*; IARC Scientific Publication; International Agency for Research on Cancer: 150 cours Albert Thomas, 69372 Lyon Cedex 08, France, 2019.

(7) Lee, S. J.; Yum, Y. N.; Kim, S. C.; Kim, Y.; Lim, J.; Lee, W. J.; Koo, K. H.; Kim, J. H.; Kim, J. E.; Lee, W. S.; Sohn, S.; Park, S. N.; Park, J. H.; Lee, J.; Kwon, S. W. Distinguishing between Genotoxic and Non-Genotoxic Hepatocarcinogens by Gene Expression Profiling and Bioinformatic Pathway Analysis. *Sci. Rep.* **2013**, *3* (1), 2783. https://doi.org/10.1038/srep02783.

(8) Hernández, L. G.; van Steeg, H.; Luijten, M.; van Benthem, J. Mechanisms of Non-Genotoxic Carcinogens and Importance of a Weight of Evidence Approach. *Mutat. Res. Mutat. Res.* **2009**, *682* (2–3), 94–109. https://doi.org/10.1016/j.mrrev.2009.07.002.

(9) Münger, K.; Baldwin, A.; Edwards, K. M.; Hayakawa, H.; Nguyen, C. L.; Owens, M.; Grace, M.; Huh, K. Mechanisms of Human Papillomavirus-Induced Oncogenesis. *J. Virol.* **2004**, *78* (21), 11451–11460. https://doi.org/10.1128/JVI.78.21.11451-11460.2004.

(10) Munger, K.; Jones, D. L. Human Papillomavirus Carcinogenesis: An Identity Crisis in the Retinoblastoma Tumor Suppressor Pathway. *J. Virol.* **2015**, *89* (9), 4708–4711. https://doi.org/10.1128/JVI.03486-14.

(11) Pira, E.; Donato, F.; Maida, L.; Discalzi, G. Exposure to Asbestos: Past, Present and Future. *J. Thorac. Dis.* **2018**, *10* (S2), S237–S245. https://doi.org/10.21037/jtd.2017.10.126.

(12) Inagaki-Kawata, Y.; Yoshida, K.; Kawaguchi-Sakita, N.; Kawashima, M.; Nishimura, T.; Senda, N.; Shiozawa, Y.; Takeuchi, Y.; Inoue, Y.; Sato-Otsubo, A.; Fujii, Y.; Nannya, Y.; Suzuki, E.; Takada, M.; Tanaka, H.; Shiraishi, Y.; Chiba, K.; Kataoka, Y.; Torii, M.; Yoshibayashi, H.; Yamagami, K.; Okamura, R.; Moriguchi, Y.; Kato, H.; Tsuyuki, S.; Yamauchi, A.; Suwa, H.; Inamoto, T.; Miyano, S.; Ogawa, S.; Toi, M. Genetic and Clinical Landscape of Breast Cancers with Germline BRCA1/2 Variants. *Commun. Biol.* **2020**, *3* (1), 578. https://doi.org/10.1038/s42003-020-01301-9.

(13) Seebacher, N. A.; Stacy, A. E.; Porter, G. M.; Merlot, A. M. Clinical Development of Targeted and Immune Based Anti-Cancer Therapies. *J. Exp. Clin. Cancer Res.* **2019**, *38* (1), 156. https://doi.org/10.1186/s13046-019-1094-2.

(14) Cardoso, F.; Paluch-Shimon, S.; Senkus, E.; Curigliano, G.; Aapro, M. S.; André, F.; Barrios, C. H.; Bergh, J.; Bhattacharyya, G. S.; Biganzoli, L.; Boyle, F.; Cardoso, M.-J.; Carey, L. A.; Cortés, J.; El Saghir, N. S.; Elzayat, M.; Eniu, A.; Fallowfield, L.; Francis, P. A.; Gelmon, K.; Gligorov, J.; Haidinger, R.; Harbeck, N.; Hu, X.; Kaufman, B.; Kaur, R.; Kiely, B. E.; Kim, S.-B.; Lin, N. U.; Mertz, S. A.; Neciosup, S.; Offersen, B. V.; Ohno, S.; Pagani, O.; Prat, A.; Penault-Llorca, F.; Rugo, H. S.; Sledge, G. W.; Thomssen, C.; Vorobiof, D. A.; Wiseman, T.; Xu, B.; Norton, L.; Costa, A.; Winer, E. P. 5th ESO-ESMO International Consensus Guidelines for Advanced Breast Cancer (ABC 5). *Ann. Oncol.* **2020**, *31* (12), 1623–1649. https://doi.org/10.1016/j.annonc.2020.09.010.

(15) Korde, L. A.; Somerfield, M. R.; Carey, L. A.; Crews, J. R.; Denduluri, N.; Hwang, E. S.; Khan, S. A.; Loibl, S.; Morris, E. A.; Perez, A.; Regan, M. M.; Spears, P. A.; Sudheendra, P. K.; Symmans, W. F.; Yung, R. L.; Harvey, B. E.; Hershman, D. L. Neoadjuvant Chemotherapy, Endocrine Therapy, and Targeted Therapy for Breast Cancer: ASCO Guideline. *J. Clin. Oncol.* **2021**, *39* (13), 1485–1505. https://doi.org/10.1200/JCO.20.03399.

(16) Baskar, R.; Lee, K. A.; Yeo, R.; Yeoh, K.-W. Cancer and Radiation Therapy: Current Advances and Future Directions. *Int. J. Med. Sci.* **2012**, *9* (3), 193–199. https://doi.org/10.7150/ijms.3635.

(17) Hassett, M. J.; Somerfield, M. R.; Baker, E. R.; Cardoso, F.; Kansal, K. J.; Kwait, D. C.; Plichta, J. K.; Ricker, C.; Roshal, A.; Ruddy, K. J.; Safer, J. D.; Van Poznak, C.; Yung, R. L.; Giordano, S. H. Management of Male Breast Cancer: ASCO Guideline. *J. Clin. Oncol.* **2020**, *38* (16), 1849–1863. https://doi.org/10.1200/JCO.19.03120.

(18) Gress, D. M.; Edge, S. B.; Greene, F. L.; Washington, M. K.; Asare, E. A.; Brierley, J. D.; Byrd, D. R.; Compton, C. C.; Jessup, J. M.; Winchester, D. P.; Amin, M. B.; Gershenwald, J. E. Principles of Cancer Staging. In *AJCC Cancer Staging Manual*; Amin, M. B., Edge, S. B., Greene, F. L., Byrd, D. R., Brookland, R. K., Washington, M. K., Gershenwald, J. E., Compton, C. C., Hess, K. R., Sullivan, D. C., Jessup, J. M., Brierley, J. D., Gaspar, L. E., Schilsky, R. L., Balch, C. M., Winchester, D. P., Asare, E. A., Madera, M., Gress, D. M., Meyer, L. R., Eds.; Springer International Publishing: Cham, 2017; pp 3–30. https://doi.org/10.1007/978-3-319-40618-3_1.

(19) Ho, C.; Argáez, C. *Sentinel Lymph Node Biopsy for the Management of Breast Cancer: A Review of Guidelines*; CADTH Rapid Response Reports; Canadian Agency for Drugs and Technologies in Health: Ottawa (ON), 2019.

(20) Cardoso, F.; Kyriakides, S.; Ohno, S.; Penault-Llorca, F.; Poortmans, P.; Rubio, I. T.; Zackrisson, S.; Senkus, E. Early Breast Cancer: ESMO Clinical Practice Guidelines for Diagnosis, Treatment and Follow-Up. *Ann. Oncol.* **2019**, *30* (8), 1194–1220. https://doi.org/10.1093/annonc/mdz173.

(21) Giovannetti, E.; Rodriguez, J. A. Targeted Therapies in Cancer: Where Are We Going? *Cancer Drug Resist.* **2018**, *1*. https://doi.org/10.20517/cdr.2018.05.

(22) Recht, A.; Comen, E. A.; Fine, R. E.; Fleming, G. F.; Hardenbergh, P. H.; Ho, A. Y.; Hudis, C. A.; Hwang, E. S.; Kirshner, J. J.; Morrow, M.; Salerno, K. E.; Sledge, G. W.; Solin, L. J.; Spears, P. A.; Whelan, T. J.; Somerfield, M. R.; Edge, S. B. Postmastectomy Radiotherapy: An American Society of Clinical Oncology, American Society for Radiation Oncology, and Society of Surgical Oncology Focused Guideline Update. *J. Clin. Oncol.* **2016**, *34* (36), 4431–4442. https://doi.org/10.1200/JCO.2016.69.1188.

(23) Rugo, H. S.; Rumble, R. B.; Macrae, E.; Barton, D. L.; Connolly, H. K.; Dickler, M. N.; Fallowfield, L.; Fowble, B.; Ingle, J. N.; Jahanzeb, M.; Johnston, S. R. D.; Korde, L. A.; Khatcheressian, J. L.; Mehta, R. S.; Muss, H. B.; Burstein, H. J. Endocrine Therapy for Hormone Receptor–Positive Metastatic Breast Cancer: American Society of Clinical Oncology Guideline. *J. Clin. Oncol.* **2016**, *34* (25), 3069–3103. https://doi.org/10.1200/JCO.2016.67.1487.

(24) Cheng, L.; Lopez-Beltran, A.; Massari, F.; MacLennan, G. T.; Montironi, R. Molecular Testing for BRAF Mutations to Inform Melanoma Treatment Decisions: A Move toward Precision Medicine. *Mod. Pathol.* **2018**, *31* (1), 24–38. https://doi.org/10.1038/modpathol.2017.104.

(25) Chapman, P. B.; Hauschild, A.; Robert, C.; Haanen, J. B.; Ascierto, P.; Larkin, J.; Dummer, R.; Garbe, C.; Testori, A.; Maio, M.; Hogg, D.; Lorigan, P.; Lebbe, C.; Jouary, T.; Schadendorf, D.; Ribas, A.; O'Day, S. J.; Sosman, J. A.; Kirkwood, J. M.; Eggermont, A. M. M.; Dreno, B.; Nolop, K.; Li, J.; Nelson, B.; Hou, J.; Lee, R. J.; Flaherty, K. T.; McArthur, G. A. Improved Survival with Vemurafenib in Melanoma with BRAF V600E Mutation. *N. Engl. J. Med.* **2011**, *364* (26), 2507–2516. https://doi.org/10.1056/NEJMoa1103782.

(26) André, F.; Ciruelos, E.; Rubovszky, G.; Campone, M.; Loibl, S.; Rugo, H. S.; Iwata, H.; Conte, P.; Mayer, I. A.; Kaufman, B.; Yamashita, T.; Lu, Y.-S.; Inoue, K.; Takahashi, M.; Pápai, Z.; Longin, A.-S.; Mills, D.; Wilke, C.; Hirawat, S.; Juric, D. Alpelisib for *PIK3CA* -Mutated, Hormone Receptor–Positive Advanced Breast Cancer. *N. Engl. J. Med.* **2019**, *380* (20), 1929–1940. https://doi.org/10.1056/NEJMoa1813904.

(27) Waldman, A. D.; Fritz, J. M.; Lenardo, M. J. A Guide to Cancer Immunotherapy: From T Cell Basic Science to Clinical Practice. *Nat. Rev. Immunol.* **2020**, *20* (11), 651–668. https://doi.org/10.1038/s41577-020-0306-5.

(28) Jiang, W.; Ji, M. Receptor Tyrosine Kinases in PI3K Signaling: The Therapeutic Targets in Cancer. *Semin. Cancer Biol.* **2019**, *59*, 3–22. https://doi.org/10.1016/j.semcancer.2019.03.006.

(29) Zhang, M.; Jang, H.; Nussinov, R. The Mechanism of PI3Kα Activation at the Atomic Level. *Chem. Sci.* **2019**, *10* (12), 3671–3680. https://doi.org/10.1039/C8SC04498H.

(30) Sathe, A.; Chalaud, G.; Oppolzer, I.; Wong, K. Y.; von Busch, M.; Schmid, S. C.; Tong, Z.; Retz, M.; Gschwend, J. E.; Schulz, W. A.; Nawroth, R. Parallel PI3K, AKT and MTOR Inhibition Is Required to Control Feedback Loops That Limit Tumor Therapy. *PLOS ONE* **2018**, *13* (1), e0190854. https://doi.org/10.1371/journal.pone.0190854.

(31) Nussinov, R.; Tsai, C.-J.; Jang, H. Does Ras Activate Raf and PI3K Allosterically? *Front. Oncol.* **2019**, *9*, 1231. https://doi.org/10.3389/fonc.2019.01231.

(32) Vasan, N.; Toska, E.; Scaltriti, M. Overview of the Relevance of PI3K Pathway in HR-Positive Breast Cancer. *Ann. Oncol.* **2019**, *30*, x3–x11. https://doi.org/10.1093/annonc/mdz281.
(33) Cao, Z.; Liao, Q.; Su, M.; Huang, K.; Jin, J.; Cao, D. AKT and ERK Dual Inhibitors: The Way Forward? *Cancer Lett.* **2019**, *459*, 30–40. https://doi.org/10.1016/j.canlet.2019.05.025.
(34) Prossomariti, A.; Piazzi, G.; Alquati, C.; Ricciardiello, L. Are Wnt/β-Catenin and PI3K/AKT/MTORC1 Distinct Pathways in Colorectal Cancer? *Cell. Mol. Gastroenterol. Hepatol.* **2020**, *10* (3), 491–506. https://doi.org/10.1016/j.jcmgh.2020.04.007.
(35) Janku, F.; Yap, T. A.; Meric-Bernstam, F. Targeting the PI3K Pathway in Cancer: Are We Making Headway? *Nat. Rev. Clin. Oncol.* **2018**, *15* (5), 273–291. https://doi.org/10.1038/nrclinonc.2018.28.
(36) Danielsen, S. A.; Eide, P. W.; Nesbakken, A.; Guren, T.; Leithe, E.; Lothe, R. A. Portrait of the PI3K/AKT Pathway in Colorectal Cancer. *Biochim. Biophys. Acta BBA - Rev. Cancer* **2015**, *1855* (1), 104–121. https://doi.org/10.1016/j.bbcan.2014.09.008.
(37) Saxton, R. A.; Sabatini, D. M. MTOR Signaling in Growth, Metabolism, and Disease. *Cell* **2017**, *168* (6), 960–976. https://doi.org/10.1016/j.cell.2017.02.004.
(38) Bosch, A.; Li, Z.; Bergamaschi, A.; Ellis, H.; Toska, E.; Prat, A.; Tao, J. J.; Spratt, D. E.; Viola-Villegas, N. T.; Castel, P.; Minuesa, G.; Morse, N.; Rodón, J.; Ibrahim, Y.; Cortes, J.; Perez-Garcia, J.; Galvan, P.; Grueso, J.; Guzman, M.; Katzenellenbogen, J. A.; Kharas, M.; Lewis, J. S.; Dickler, M.; Serra, V.; Rosen, N.; Chandarlapaty, S.; Scaltriti, M.; Baselga, J. PI3K Inhibition Results in Enhanced Estrogen Receptor Function and Dependence in Hormone Receptor–Positive Breast Cancer. *Sci. Transl. Med.* **2015**, *7* (283), 283ra51-283ra51. https://doi.org/10.1126/scitranslmed.aaa4442.
(39) Fruman, D. A.; Chiu, H.; Hopkins, B. D.; Bagrodia, S.; Cantley, L. C.; Abraham, R. T. The PI3K Pathway in Human Disease. *Cell* **2017**, *170* (4), 605–635. https://doi.org/10.1016/j.cell.2017.07.029.
(40) Hoxhaj, G.; Manning, B. D. The PI3K–AKT Network at the Interface of Oncogenic Signalling and Cancer Metabolism. *Nat. Rev. Cancer* **2020**, *20* (2), 74–88. https://doi.org/10.1038/s41568-019-0216-7.
(41) Solzak, J. P.; Atale, R. V.; Hancock, B. A.; Sinn, A. L.; Pollok, K. E.; Jones, D. R.; Radovich, M. Dual PI3K and Wnt Pathway Inhibition Is a Synergistic Combination against Triple Negative Breast Cancer. *Npj Breast Cancer* **2017**, *3* (1), 17. https://doi.org/10.1038/s41523-017-0016-8.
(42) Correia, N. C.; Gírio, A.; Antunes, I.; Martins, L. R.; Barata, J. T. The Multiple Layers of Non-Genetic Regulation of PTEN Tumour Suppressor Activity. *Eur. J. Cancer* **2014**, *50* (1), 216–225. https://doi.org/10.1016/j.ejca.2013.08.017.
(43) Rozengurt, E.; Soares, H. P.; Sinnet-Smith, J. Suppression of Feedback Loops Mediated by PI3K/MTOR Induces Multiple Overactivation of Compensatory Pathways: An Unintended Consequence Leading to Drug Resistance. *Mol. Cancer Ther.* **2014**, *13* (11), 2477–2488. https://doi.org/10.1158/1535-7163.MCT-14-0330.

(44) Zubair, M.; Wang, S.; Ali, N. Advanced Approaches to Breast Cancer Classification and Diagnosis. *Front. Pharmacol.* **2021**, *11*, 632079. https://doi.org/10.3389/fphar.2020.632079.
(45) Lawrence, M. S.; Stojanov, P.; Mermel, C. H.; Robinson, J. T.; Garraway, L. A.; Golub, T. R.; Meyerson, M.; Gabriel, S. B.; Lander, E. S.; Getz, G. Discovery and Saturation Analysis of Cancer Genes across 21 Tumour Types. *Nature* **2014**, *505* (7484), 495–501. https://doi.org/10.1038/nature12912.
(46) Naylor, S. Biomarkers: Current Perspectives and Future Prospects. *Expert Rev. Mol. Diagn.* **2003**, *3* (5), 525–529. https://doi.org/10.1586/14737159.3.5.525.
(47) ROSE, H. M.; RAGAN, C. Differential Agglutination of Normal and Sensitized Sheep Erythrocytes by Sera of Patients with Rheumatoid Arthritis. *Proc. Soc. Exp. Biol. Med. Soc. Exp. Biol. Med. N. Y. N* **1948**, *68* (1), 1–6. https://doi.org/10.3181/00379727-68-16375.
(48) On The Occurrence Of A Factor In Human Serum Activating The Specific Agglutintion of Sheep Blood Corpuscles. *APMIS* **2007**, *115* (5), 422–438. https://doi.org/10.1111/j.1600-0463.2007.apm_682a.x.
(49) Alexander, T. S. Human Immunodeficiency Virus Diagnostic Testing: 30 Years of Evolution. *Clin. Vaccine Immunol.* **2016**, *23* (4), 249–253. https://doi.org/10.1128/CVI.00053-16.
(50) Cagney, D. N.; Sul, J.; Huang, R. Y.; Ligon, K. L.; Wen, P. Y.; Alexander, B. M. The FDA NIH Biomarkers, EndpointS, and Other Tools (BEST) Resource in Neuro-Oncology. *Neuro-Oncol.* **2018**, *20* (9), 1162—1172. https://doi.org/10.1093/neuonc/nox242.
(51) Mayeux, R. Biomarkers: Potential Uses and Limitations. **2004**, *1* (2), 7.
(52) Duffy, M. J.; Harbeck, N.; Nap, M.; Molina, R.; Nicolini, A.; Senkus, E.; Cardoso, F. Clinical Use of Biomarkers in Breast Cancer: Updated Guidelines from the European Group on Tumor Markers (EGTM). *Eur. J. Cancer* **2017**, *75*, 284–298. https://doi.org/10.1016/j.ejca.2017.01.017.
(53) Petrucelli, N.; Daly, M. B.; Pal, T. BRCA1- and BRCA2-Associated Hereditary Breast and Ovarian Cancer. 36.
(54) Ballman, K. V. Biomarker: Predictive or Prognostic? *J. Clin. Oncol.* **2015**, *33* (33), 3968–3971. https://doi.org/10.1200/JCO.2015.63.3651.
(55) Roskoski, R. Targeting ERK1/2 Protein-Serine/Threonine Kinases in Human Cancers. *Pharmacol. Res.* **2019**, *142*, 151–168. https://doi.org/10.1016/j.phrs.2019.01.039.
(56) Sanda, M. G.; Chen, R. C.; Crispino, T.; Freedland, S.; Greene, K.; Klotz, L. H.; Makarov, D. V.; Reston, J.; Rodrigues, G.; Sandler, H. M.; Taplin, M. E.; Cadeddu, J. A. CLINICALLY LOCALIZED PROSTATE CANCER: AUA/ASTRO/SUO GUIDELINE. *Prostate Cancer* **2017**, 56.
(57) Horvath, A. R.; Lord, S. J.; StJohn, A.; Sandberg, S.; Cobbaert, C. M.; Lorenz, S.; Monaghan, P. J.; Verhagen-Kamerbeek, W. D. J.; Ebert, C.; Bossuyt, P. M. M. From Biomarkers to Medical Tests: The Changing Landscape of Test Evaluation. *Clin. Chim. Acta* **2014**, *427*, 49–57. https://doi.org/10.1016/j.cca.2013.09.018.
(58) OECD; World Health Organization. *Improving Healthcare Quality in Europe: Characteristics, Effectiveness and Implementation of Different Strategies*; OECD, 2019. https://doi.org/10.1787/b11a6e8f-en.

(59) Pennello, G. A. Analytical and Clinical Evaluation of Biomarkers Assays: When Are Biomarkers Ready for Prime Time? *Clin. Trials J. Soc. Clin. Trials* **2013**, *10* (5), 666–676. https://doi.org/10.1177/1740774513497541.
(60) Food and Drug Administration. Bioanalytical Method Validation Guidance for Industry. **2018**, 44.
(61) NIH. National Cancer Institute Best Practices for Biospecimen Resources - Fresh Frozen Tissues.Pdf.
(62) Kokkat, T. J.; Patel, M. S.; McGarvey, D.; LiVolsi, V. A.; Baloch, Z. W. Archived Formalin-Fixed Paraffin-Embedded (FFPE) Blocks: A Valuable Underexploited Resource for Extraction of DNA, RNA, and Protein. *Biopreservation Biobanking* **2013**, *11* (2), 101–106. https://doi.org/10.1089/bio.2012.0052.
(63) Hermann, J.; Noels, H.; Theelen, W.; Lellig, M.; Orth-Alampour, S.; Boor, P.; Jankowski, V.; Jankowski, J. Sample Preparation of Formalin-Fixed Paraffin-Embedded Tissue Sections for MALDI-Mass Spectrometry Imaging. *Anal. Bioanal. Chem.* **2020**, *412* (6), 1263–1275. https://doi.org/10.1007/s00216-019-02296-x.
(64) Feldman, A. T.; Wolfe, D. Tissue Processing and Hematoxylin and Eosin Staining. In *Histopathology: Methods and Protocols*; Day, C. E., Ed.; Springer New York: New York, NY, 2014; pp 31–43. https://doi.org/10.1007/978-1-4939-1050-2_3.
(65) Ahmed, A. A.; Abedalthagafi, M. Cancer Diagnostics: The Journey from Histomorphology to Molecular Profiling. *Oncotarget* **2016**, *7* (36), 58696–58708. https://doi.org/10.18632/oncotarget.11061.
(66) Brainard, J.; Farver, C. The Diagnosis of Non-Small Cell Lung Cancer in the Molecular Era. *Mod. Pathol.* **2019**, *32* (S1), 16–26. https://doi.org/10.1038/s41379-018-0156-x.
(67) Crowe, A.; Yue, W. Semi-Quantitative Determination of Protein Expression Using Immunohistochemistry Staining and Analysis: An Integrated Protocol. *BIO-Protoc.* **2019**, *9* (24). https://doi.org/10.21769/BioProtoc.3465.
(68) Wolff, A. C.; Hammond, M. E. H.; Schwartz, J. N.; Hagerty, K. L.; Allred, D. C.; Cote, R. J.; Dowsett, M.; Fitzgibbons, P. L.; Hanna, W. M.; Langer, A.; McShane, L. M.; Paik, S.; Pegram, M. D.; Perez, E. A.; Press, M. F.; Rhodes, A.; Sturgeon, C.; Taube, S. E.; Tubbs, R.; Vance, G. H.; van de Vijver, M.; Wheeler, T. M.; Hayes, D. F. American Society of Clinical Oncology/College of American Pathologists Guideline Recommendations for Human Epidermal Growth Factor Receptor 2 Testing in Breast Cancer. *J. Clin. Oncol.* **2007**, *26* (1), 118–145. https://doi.org/10.1200/JCO.2006.09.2775.
(69) Wolff, A. C.; Hammond, M. E. H.; Allison, K. H.; Harvey, B. E.; Mangu, P. B.; Bartlett, J. M. S.; Bilous, M.; Ellis, I. O.; Fitzgibbons, P.; Hanna, W.; Jenkins, R. B.; Press, M. F.; Spears, P. A.; Vance, G. H.; Viale, G.; McShane, L. M.; Dowsett, M. Human Epidermal Growth Factor Receptor 2 Testing in Breast Cancer: American Society of Clinical Oncology/College of American Pathologists Clinical Practice Guideline Focused Update. *Arch. Pathol. Lab. Med.* **2018**, *142* (11), 1364–1382. https://doi.org/10.5858/arpa.2018-0902-SA.
(70) Liu, J.; Cui, D.; Jiang, Y.; Li, Y.; Liu, Z.; Tao, L.; Zhao, Q.; Diao, A. Selection and Characterization of a Novel Affibody Peptide and Its Application in a Two-Site ELISA for the Detection of Cancer Biomarker Alpha-Fetoprotein. *Int. J. Biol. Macromol.* **2021**, *166*, 884–892. https://doi.org/10.1016/j.ijbiomac.2020.10.245.

(71) Furuya, H.; Pagano, I.; Chee, K.; Kobayashi, T.; Wong, R. S.; Lee, R.; Rosser, C. J. Comparison of Commercial ELISA Kits, a Prototype Multiplex Electrochemoluminescent Assay, and a Multiplex Bead-Based Immunoassay for Detecting a Urine-Based Bladder-Cancer-Associated Diagnostic Signature. *Diagnostics* **2019**, *9* (4), 166. https://doi.org/10.3390/diagnostics9040166.

(72) Wang, L.; Skotland, T.; Berge, V.; Sandvig, K.; Llorente, A. Exosomal Proteins as Prostate Cancer Biomarkers in Urine: From Mass Spectrometry Discovery to Immunoassay-Based Validation. *Eur. J. Pharm. Sci.* **2017**, *98*, 80–85. https://doi.org/10.1016/j.ejps.2016.09.023.

(73) Aydin, S. A Short History, Principles, and Types of ELISA, and Our Laboratory Experience with Peptide/Protein Analyses Using ELISA. *Peptides* **2015**, *72*, 4–15. https://doi.org/10.1016/j.peptides.2015.04.012.

(74) Cinquanta, L.; Fontana, D. E.; Bizzaro, N. Chemiluminescent Immunoassay Technology: What Does It Change in Autoantibody Detection? *Autoimmun. Highlights* **2017**, *8* (1), 9. https://doi.org/10.1007/s13317-017-0097-2.

(75) Cui, C.; Shu, W.; Li, P. Fluorescence In Situ Hybridization: Cell-Based Genetic Diagnostic and Research Applications. *Front. Cell Dev. Biol.* **2016**, *4*. https://doi.org/10.3389/fcell.2016.00089.

(76) Goodwin, S.; McPherson, J. D.; McCombie, W. R. Coming of Age: Ten Years of next-Generation Sequencing Technologies. *Nat. Rev. Genet.* **2016**, *17* (6), 333–351. https://doi.org/10.1038/nrg.2016.49.

(77) Yohe, S.; Thyagarajan, B. Review of Clinical Next-Generation Sequencing. *Arch. Pathol. Lab. Med.* **2017**, *141* (11), 1544–1557. https://doi.org/10.5858/arpa.2016-0501-RA.

(78) Buermans, H. P. J.; den Dunnen, J. T. Next Generation Sequencing Technology: Advances and Applications. *Biochim. Biophys. Acta BBA - Mol. Basis Dis.* **2014**, *1842* (10), 1932–1941. https://doi.org/10.1016/j.bbadis.2014.06.015.

(79) Mantere, T.; Kersten, S.; Hoischen, A. Long-Read Sequencing Emerging in Medical Genetics. *Front. Genet.* **2019**, *10*, 426. https://doi.org/10.3389/fgene.2019.00426.

(80) Multi-Site Analytical Validation of TruSight® Tumor 15 (TST15), Determining Robustness and Concordance. 4.

(81) Cescon, D. W. Circulating Tumor DNA and Liquid Biopsy in Oncology. **2020**, *1*, 15.

(82) Fortuna, G. M. G.; Dvir, K. Circulating Tumor DNA: Where Are We Now? A Mini Review of the Literature. **2020**, *11* (9), 10.

(83) Grabuschnig, S.; Bronkhorst, A. J.; Holdenrieder, S.; Rodriguez, I. R.; Schliep, K. P.; Schwendenwein, D.; Ungerer, V.; Sensen, C. W. Putative Origins of Cell-Free DNA in Humans: A Review of Active and Passive Nucleic Acid Release Mechanisms. *Int J Mol Sci* **2020**, 24.

(84) Li, L.; Wei, Y.; To, C.; Zhu, C.-Q.; Tong, J.; Pham, N.-A.; Taylor, P.; Ignatchenko, V.; Ignatchenko, A.; Zhang, W.; Wang, D.; Yanagawa, N.; Li, M.; Pintilie, M.; Liu, G.; Muthuswamy, L.; Shepherd, F. A.; Tsao, M. S.; Kislinger, T.; Moran, M. F. Integrated Omic Analysis of Lung Cancer Reveals Metabolism Proteome Signatures with Prognostic Impact. *Nat. Commun.* **2014**, *5* (1), 5469. https://doi.org/10.1038/ncomms6469.

(85) Ruggles, K. V.; Tang, Z.; Wang, X.; Grover, H.; Askenazi, M.; Teubl, J.; Cao, S.; McLellan, M. D.; Clauser, K. R.; Tabb, D. L.; Mertins, P.; Slebos, R.; Erdmann-Gilmore, P.; Li, S.; Gunawardena, H. P.; Xie, L.; Liu, T.; Zhou, J.-Y.; Sun, S.; Hoadley, K. A.; Perou, C. M.; Chen, X.; Davies, S. R.; Maher, C. A.; Kinsinger, C. R.; Rodland, K. D.; Zhang, H.; Zhang, Z.; Ding, L.; Townsend, R. R.; Rodriguez, H.; Chan, D.; Smith, R. D.; Liebler, D. C.; Carr, S. A.; Payne, S.; Ellis, M. J.; Fenyő, D. An Analysis of the Sensitivity of Proteogenomic Mapping of Somatic Mutations and Novel Splicing Events in Cancer. *Mol. Cell. Proteomics* **2016**, *15* (3), 1060–1071. https://doi.org/10.1074/mcp.M115.056226.

(86) Lapek, J. D.; Greninger, P.; Morris, R.; Amzallag, A.; Pruteanu-Malinici, I.; Benes, C. H.; Haas, W. Detection of Dysregulated Protein-Association Networks by High-Throughput Proteomics Predicts Cancer Vulnerabilities. *Nat. Biotechnol.* **2017**, *35* (10), 983–989. https://doi.org/10.1038/nbt.3955.

(87) Faria, S. S.; Morris, C. F. M.; Silva, A. R.; Fonseca, M. P.; Forget, P.; Castro, M. S.; Fontes, W. A Timely Shift from Shotgun to Targeted Proteomics and How It Can Be Groundbreaking for Cancer Research. *Front. Oncol.* **2017**, *7*, 13. https://doi.org/10.3389/fonc.2017.00013.

(88) Clerico, A.; Belloni, L.; Carrozza, C.; Correale, M.; Dittadi, R.; Dotti, C.; Fortunato, A.; Vignati, G.; Zucchelli, G. C.; Migliardi, M. A Black Swan in Clinical Laboratory Practice: The Analytical Error Due to Interferences in Immunoassay Methods. *Clin. Chem. Lab. Med. CCLM* **2018**, *56* (3), 397–402. https://doi.org/10.1515/cclm-2017-0881.

(89) Zachary, A. A.; Vega, R. M.; Lucas, D. P.; Leffell, M. S. HLA Antibody Detection and Characterization by Solid Phase Immunoassays: Methods and Pitfalls. In *Immunogenetics*; Christiansen, F. T., Tait, B. D., Eds.; Methods in Molecular Biology™; Humana Press: Totowa, NJ, 2012; Vol. 882, pp 289–308. https://doi.org/10.1007/978-1-61779-842-9_17.

(90) Ellington, A. A.; Kullo, I. J.; Bailey, K. R.; Klee, G. G. Antibody-Based Protein Multiplex Platforms: Technical and Operational Challenges. *Clin. Chem.* **2010**, *56* (2), 186–193. https://doi.org/10.1373/clinchem.2009.127514.

(91) Tighe, P. J.; Ryder, R. R.; Todd, I.; Fairclough, L. C. ELISA in the Multiplex Era: Potentials and Pitfalls. *PROTEOMICS – Clin. Appl.* **2015**, *9* (3–4), 406–422. https://doi.org/10.1002/prca.201400130.

(92) El-Aneed, A.; Cohen, A.; Banoub, J. Mass Spectrometry, Review of the Basics: Electrospray, MALDI, and Commonly Used Mass Analyzers. *Appl. Spectrosc. Rev.* **2009**, *44* (3), 210–230. https://doi.org/10.1080/05704920902717872.

(93) Becker, R. Rays of Positive Electricity and Their Application to Chemical Analysis. By J.J. Thomson. VI Und 132 S. Mit 50 Abbildungen. Verlag von Longmans, Green & Co., London. 1913. Preis Geh. 5 s. *Z. Für Elektrochem. Angew. Phys. Chem.* **1914**, *20* (8), 259–260. https://doi.org/10.1002/bbpc.19140200812.

(94) Konermann, L.; Ahadi, E.; Rodriguez, A. D.; Vahidi, S. Unraveling the Mechanism of Electrospray Ionization. *Anal. Chem.* **2013**, *85* (1), 2–9. https://doi.org/10.1021/ac302789c.

(95) Nilsson, T.; Mann, M.; Aebersold, R.; Yates, J. R.; Bairoch, A.; Bergeron, J. J. M. Mass Spectrometry in High-Throughput Proteomics: Ready for the Big Time. *Nat. Methods* **2010**, *7* (9), 681–685. https://doi.org/10.1038/nmeth0910-681.

(96) Metwally, H.; Duez, Q.; Konermann, L. Chain Ejection Model for Electrospray Ionization of Unfolded Proteins: Evidence from Atomistic Simulations and Ion Mobility Spectrometry. *Anal. Chem.* **2018**, *90* (16), 10069–10077. https://doi.org/10.1021/acs.analchem.8b02926.

(97) Jaskolla, T. W.; Karas, M. Compelling Evidence for Lucky Survivor and Gas Phase Protonation: The Unified MALDI Analyte Protonation Mechanism. *J. Am. Soc. Mass Spectrom.* **2011**, *22* (6), 976–988. https://doi.org/10.1007/s13361-011-0093-0.

(98) Moyer, S. C.; Cotter, R. J. Peer Reviewed: Atmospheric Pressure MALDI. *Anal. Chem.* **2002**, *74* (17), 468 A-476 A. https://doi.org/10.1021/ac022091j.

(99) Keller, C.; Maeda, J.; Jayaraman, D.; Chakraborty, S.; Sussman, M. R.; Harris, J. M.; Ané, J.-M.; Li, L. Comparison of Vacuum MALDI and AP-MALDI Platforms for the Mass Spectrometry Imaging of Metabolites Involved in Salt Stress in Medicago Truncatula. *Front. Plant Sci.* **2018**, *9*, 1238. https://doi.org/10.3389/fpls.2018.01238.

(100) *Modern Proteomics – Sample Preparation, Analysis and Practical Applications*; Mirzaei, H., Carrasco, M., Eds.; Advances in Experimental Medicine and Biology; Springer International Publishing: Cham, 2016; Vol. 919. https://doi.org/10.1007/978-3-319-41448-5.

(101) Douglas, D. J.; Konenkov, N. V. Mass Resolution of Linear Quadrupole Ion Traps with Round Rods: Linear Quadrupole Ion Traps with Round Rods. *Rapid Commun. Mass Spectrom.* **2014**, *28* (21), 2252–2258. https://doi.org/10.1002/rcm.7018.

(102) Dupuis, N.; Chang, J.; Steers, M.; Weng, Z.; Gyuris, J.; Pestano, G. Abstract 2011: Feasibility of Serum Proteomic Companion Diagnostic (CDx) Test Development on the Microflex LT Platform. *Cancer Res.* **2015**, *75* (15 Supplement), 2011. https://doi.org/10.1158/1538-7445.AM2015-2011.

(103) microflex LRF https://www.bruker.com/en/products-and-solutions/mass-spectrometry/maldi-tof/microflex.html (accessed 2021 -08 -19).

(104) Leung, L. M.; Fondrie, W. E.; Doi, Y.; Johnson, J. K.; Strickland, D. K.; Ernst, R. K.; Goodlett, D. R. Identification of the ESKAPE Pathogens by Mass Spectrometric Analysis of Microbial Membrane Glycolipids. *Sci. Rep.* **2017**, *7* (1), 6403. https://doi.org/10.1038/s41598-017-04793-4.

(105) Sorensen, M.; Chandler, C. E.; Gardner, F. M.; Ramadan, S.; Khot, P. D.; Leung, L. M.; Farrance, C. E.; Goodlett, D. R.; Ernst, R. K.; Nilsson, E. Rapid Microbial Identification and Colistin Resistance Detection via MALDI-TOF MS Using a Novel on-Target Extraction of Membrane Lipids. *Sci. Rep.* **2020**, *10* (1), 21536. https://doi.org/10.1038/s41598-020-78401-3.

(106) Fenselau, C.; Demirev, P. A. Characterization of Intact Microorganisms by MALDI Mass Spectrometry. *Mass Spectrom. Rev.* **2001**, *20* (4), 157–171. https://doi.org/10.1002/mas.10004.

(107) Singhal, N.; Kumar, M.; Kanaujia, P. K.; Virdi, J. S. MALDI-TOF Mass Spectrometry: An Emerging Technology for Microbial Identification and Diagnosis. *Front. Microbiol.* **2015**, *6*. https://doi.org/10.3389/fmicb.2015.00791.

(108) Nolting, D.; Malek, R.; Makarov, A. Ion Traps in Modern Mass Spectrometry. *Mass Spectrom. Rev.* **2019**, *38* (2), 150–168. https://doi.org/10.1002/mas.21549.

(109) *Encyclopedia of Analytical Chemistry: Applications, Theory and Instrumentation*, 1st ed.; Meyers, R. A., Ed.; Wiley, 2006. https://doi.org/10.1002/9780470027318.
(110) Glish, G. L.; Burinsky, D. J. Hybrid Mass Spectrometers for Tandem Mass Spectrometry. *J. Am. Soc. Mass Spectrom.* **2008**, *19* (2), 161–172. https://doi.org/10.1016/j.jasms.2007.11.013.
(111) Rousu, T.; Herttuainen, J.; Tolonen, A. Comparison of Triple Quadrupole, Hybrid Linear Ion Trap Triple Quadrupole, Time-of-Flight and LTQ-Orbitrap Mass Spectrometers in Drug Discovery Phase Metabolite Screening and Identification *in Vitro* - Amitriptyline and Verapamil as Model Compounds: Comparison of MS Instruments in Metabolite Screening. *Rapid Commun. Mass Spectrom.* **2010**, *24* (7), 939–957. https://doi.org/10.1002/rcm.4465.
(112) Sobsey, C. A.; Ibrahim, S.; Richard, V. R.; Gaspar, V.; Mitsa, G.; Lacasse, V.; Zahedi, R. P.; Batist, G.; Borchers, C. H. Targeted and Untargeted Proteomics Approaches in Biomarker Development. *Proteomics* **2019**, *n/a* (n/a), 1900029. https://doi.org/10.1002/pmic.201900029.
(113) Pappireddi, N.; Martin, L.; Wühr, M. A Review on Quantitative Multiplexed Proteomics. *ChemBioChem* **2019**, *20* (10), 1210–1224. https://doi.org/10.1002/cbic.201800650.
(114) Griss, J.; Vinterhalter, G.; Schwämmle, V. IsoProt: A Complete and Reproducible Workflow To Analyze ITRAQ/TMT Experiments. *J. Proteome Res.* **2019**, *18* (4), 1751–1759. https://doi.org/10.1021/acs.jproteome.8b00968.
(115) *Shotgun Proteomics: Methods and Protocols*; Martins-de-Souza, D., Ed.; Methods in Molecular Biology; Springer New York: New York, NY, 2014; Vol. 1156. https://doi.org/10.1007/978-1-4939-0685-7.
(116) *Proteome Bioinformatics*; Keerthikumar, S., Mathivanan, S., Eds.; Methods in Molecular Biology; Springer New York: New York, NY, 2017; Vol. 1549. https://doi.org/10.1007/978-1-4939-6740-7.
(117) Shinoda, K.; Tomita, M.; Ishihama, Y. EmPAI Calc—for the Estimation of Protein Abundance from Large-Scale Identification Data by Liquid Chromatography-Tandem Mass Spectrometry. *Bioinformatics* **2010**, *26* (4), 576–577. https://doi.org/10.1093/bioinformatics/btp700.
(118) Schilling, B.; Gibson, B. W.; Hunter, C. L. Generation of High-Quality SWATH® Acquisition Data for Label-Free Quantitative Proteomics Studies Using TripleTOF® Mass Spectrometers. In *Proteomics*; Comai, L., Katz, J. E., Mallick, P., Eds.; Methods in Molecular Biology; Springer New York: New York, NY, 2017; Vol. 1550, pp 223–233. https://doi.org/10.1007/978-1-4939-6747-6_16.
(119) Goeminne, L. J. E.; Gevaert, K.; Clement, L. Experimental Design and Data-Analysis in Label-Free Quantitative LC/MS Proteomics: A Tutorial with MSqRob. *J. Proteomics* **2018**, *171*, 23–36. https://doi.org/10.1016/j.jprot.2017.04.004.
(120) Kennedy, J. J.; Whiteaker, J. R.; Schoenherr, R. M.; Yan, P.; Allison, K.; Shipley, M.; Lerch, M.; Hoofnagle, A. N.; Baird, G. S.; Paulovich, A. G. Optimized Protocol for Quantitative Multiple Reaction Monitoring-Based Proteomic Analysis of Formalin-Fixed, Paraffin-Embedded Tissues. *J. Proteome Res.* **2016**, *15* (8), 2717–2728. https://doi.org/10.1021/acs.jproteome.6b00245.
(121) Popp, R.; Li, H.; LeBlanc, A.; Mohammed, Y.; Aguilar-Mahecha, A.; Chambers, A. G.; Lan, C.; Poetz, O.; Basik, M.; Batist, G.; Borchers, C. H. Immuno-Matrix-

Assisted Laser Desorption/Ionization Assays for Quantifying AKT1 and AKT2 in Breast and Colorectal Cancer Cell Lines and Tumors. *Anal. Chem.* **2017**, *89* (19), 10592–10600. https://doi.org/10.1021/acs.analchem.7b02934.

(122) Baxevanos, P.; Mountzios, G. Novel Chemotherapy Regimens for Advanced Lung Cancer: Have We Reached a Plateau? *Ann. Transl. Med.* **2018**, *6* (8), 139–139. https://doi.org/10.21037/atm.2018.04.04.

(123) Michielin, O.; van Akkooi, A.; Lorigan, P.; Ascierto, P. A.; Dummer, R.; Robert, C.; Arance, A.; Blank, C. U.; Chiarion Sileni, V.; Donia, M.; Faries, M. B.; Gaudy-Marqueste, C.; Gogas, H.; Grob, J. J.; Guckenberger, M.; Haanen, J.; Hayes, A. J.; Hoeller, C.; Lebbé, C.; Lugowska, I.; Mandalà, M.; Márquez-Rodas, I.; Nathan, P.; Neyns, B.; Olofsson Bagge, R.; Puig, S.; Rutkowski, P.; Schilling, B.; Sondak, V. K.; Tawbi, H.; Testori, A.; Keilholz, U. ESMO Consensus Conference Recommendations on the Management of Locoregional Melanoma: Under the Auspices of the ESMO Guidelines Committee. *Ann. Oncol.* **2020**, *31* (11), 1449–1461. https://doi.org/10.1016/j.annonc.2020.07.005.

(124) 510(k) Substantial Equivalence Determination Decision Summary.

(125) Rocca, M. F.; Barrios, R.; Zintgraff, J.; Martínez, C.; Irazu, L.; Vay, C.; Prieto, M. Utility of Platforms Viteks MS and Microflex LT for the Identification of Complex Clinical Isolates That Require Molecular Methods for Their Taxonomic Classification. *PLOS ONE* **2019**, *14* (7), e0218077. https://doi.org/10.1371/journal.pone.0218077.

(126) Parker, L. A.; Chilet-Rosell, E.; Hernández-Aguado, I.; Pastor-Valero, M.; Gea, S.; Lumbreras, B. Diagnostic Biomarkers: Are We Moving from Discovery to Clinical Application? *Clin. Chem.* **2018**, *64* (11), 1657–1667. https://doi.org/10.1373/clinchem.2018.292854.

(127) Banerji, U.; Dean, E. J.; Pérez-Fidalgo, J. A.; Batist, G.; Bedard, P. L.; You, B.; Westin, S. N.; Kabos, P.; Garrett, M. D.; Tall, M.; Ambrose, H.; Barrett, J. C.; Carr, T. H.; Cheung, S. Y. A.; Corcoran, C.; Cullberg, M.; Davies, B. R.; de Bruin, E. C.; Elvin, P.; Foxley, A.; Lawrence, P.; Lindemann, J. P. O.; Maudsley, R.; Pass, M.; Rowlands, V.; Rugman, P.; Schiavon, G.; Yates, J.; Schellens, J. H. M. A Phase I Open-Label Study to Identify a Dosing Regimen of the Pan-AKT Inhibitor AZD5363 for Evaluation in Solid Tumors and in *PIK3CA* -Mutated Breast and Gynecologic Cancers. *Clin. Cancer Res.* **2018**, *24* (9), 2050–2059. https://doi.org/10.1158/1078-0432.CCR-17-2260.

(128) Brown, J. S.; Banerji, U. Maximising the Potential of AKT Inhibitors as Anti-Cancer Treatments. *Pharmacol. Ther.* **2017**, *172*, 101–115. https://doi.org/10.1016/j.pharmthera.2016.12.001.

(129) Juric, D.; Castel, P.; Griffith, M.; Griffith, O. L.; Won, H. H.; Ellis, H.; Ebbesen, S. H.; Ainscough, B. J.; Ramu, A.; Iyer, G.; Shah, R. H.; Huynh, T.; Mino-Kenudson, M.; Sgroi, D.; Isakoff, S.; Thabet, A.; Elamine, L.; Solit, D. B.; Lowe, S. W.; Quadt, C.; Peters, M.; Derti, A.; Schegel, R.; Huang, A.; Mardis, E. R.; Berger, M. F.; Baselga, J.; Scaltriti, M. Convergent Loss of PTEN Leads to Clinical Resistance to a PI(3)Kα Inhibitor. *Nature* **2015**, *518* (7538), 240–244. https://doi.org/10.1038/nature13948.

(130) Lin, P.-C.; Lin, J.-K.; Lin, H.-H.; Lan, Y.-T.; Lin, C.-C.; Yang, S.-H.; Chen, W.-S.; Liang, W.-Y.; Jiang, J.-K.; Chang, S.-C. A Comprehensive Analysis of

Phosphatase and Tensin Homolog Deleted on Chromosome 10 (PTEN) Loss in Colorectal Cancer. *World J. Surg. Oncol.* **2015**, *13* (1). https://doi.org/10.1186/s12957-015-0601-y.

(131) Li, S.; Shen, Y.; Wang, M.; Yang, J.; Lv, M.; Li, P.; Chen, Z.; Yang, J. Loss of PTEN Expression in Breast Cancer: Association with Clinicopathological Characteristics and Prognosis. *Oncotarget* **2017**, *8* (19), 32043–32054. https://doi.org/10.18632/oncotarget.16761.

(132) Lee, J. S.; Lee, H. W.; Lee, E. H.; Park, M.; Lee, J. S.; Kim, M.-S.; Kim, T. G.; Nam, H.-Y.; Hwang, S. W.; Park, J. H. Prognostic Significance of Phosphoinositide 3-Kinase P110α and P110β Isoforms in Non-Small Cell Lung Cancer. *Int J Clin Exp Pathol* **2018**, 1554–1561.

(133) Cross, T. G.; Hornshaw, M. P. Can LC and LC-MS Ever Replace Immunoassays? *J. Appl. Bioanal.* **2016**, *2* (4), 108–116. https://doi.org/10.17145/jab.16.015.

(134) de Gramont, A.; Watson, S.; Ellis, L. M.; Rodón, J.; Tabernero, J.; de Gramont, A.; Hamilton, S. R. Pragmatic Issues in Biomarker Evaluation for Targeted Therapies in Cancer. *Nat. Rev. Clin. Oncol.* **2015**, *12* (4), 197–212. https://doi.org/10.1038/nrclinonc.2014.202.

(135) De Matos, L. L.; Trufelli, D. C.; De Matos, M. G. L.; Da Silva Pinhal, M. A. Immunohistochemistry as an Important Tool in Biomarkers Detection and Clinical Practice. *Biomark. Insights* **2010**, *5*, 9–20. https://doi.org/10.4137/BMI.S2185.

(136) Hoofnagle, A. N.; Wener, M. H. The Fundamental Flaws of Immunoassays and Potential Solutions Using Tandem Mass Spectrometry. *J. Immunol. Methods* **2009**, *347* (1–2), 3–11. https://doi.org/10.1016/j.jim.2009.06.003.

(137) O'Hurley, G.; Sjöstedt, E.; Rahman, A.; Li, B.; Kampf, C.; Pontén, F.; Gallagher, W. M.; Lindskog, C. Garbage in, Garbage out: A Critical Evaluation of Strategies Used for Validation of Immunohistochemical Biomarkers. *Mol. Oncol.* **2014**, *8* (4), 783–798. https://doi.org/10.1016/j.molonc.2014.03.008.

(138) Meier, F.; Geyer, P. E.; Virreira Winter, S.; Cox, J.; Mann, M. BoxCar Acquisition Method Enables Single-Shot Proteomics at a Depth of 10,000 Proteins in 100 Minutes. *Nat. Methods* **2018**, *15* (6), 440–448. https://doi.org/10.1038/s41592-018-0003-5.

(139) Ludwig, C.; Gillet, L.; Rosenberger, G.; Amon, S.; Collins, B. C.; Aebersold, R. Data-independent Acquisition-based SWATH - MS for Quantitative Proteomics: A Tutorial. *Mol. Syst. Biol.* **2018**, *14* (8), e8126. https://doi.org/10.15252/msb.20178126.

(140) Pfammatter, S.; Bonneil, E.; McManus, F. P.; Prasad, S.; Bailey, D. J.; Belford, M.; Dunyach, J.-J.; Thibault, P. A Novel Differential Ion Mobility Device Expands the Depth of Proteome Coverage and the Sensitivity of Multiplex Proteomic Measurements*□S. *Mol. Cell. Proteomics* **2018**, *17* (10), 2051–2067.

(141) Parker, C. E.; Borchers, C. H. Mass Spectrometry Based Biomarker Discovery, Verification, and Validation - Quality Assurance and Control of Protein Biomarker Assays. *Mol. Oncol.* **2014**, *8* (4), 840–858. https://doi.org/10.1016/j.molonc.2014.03.006.

(142) Anderson, N. L.; Anderson, N. G.; Haines, L. R.; Hardie, D. B.; Olafson, R. W.; Pearson, T. W. Mass Spectrometric Quantitation of Peptides and Proteins Using

Stable Isotope Standards and Capture by Anti-Peptide Antibodies (SISCAPA). *J. Proteome Res.* **2004**, *3* (2), 235–244. https://doi.org/10.1021/pr034086h.

(143) Lévesque, S.; Dufresne, P. J.; Soualhine, H.; Domingo, M.-C.; Bekal, S.; Lefebvre, B.; Tremblay, C. A Side by Side Comparison of Bruker Biotyper and VITEK MS: Utility of MALDI-TOF MS Technology for Microorganism Identification in a Public Health Reference Laboratory. *Plos One* **2015**, *10* (12), e0144878. https://doi.org/10.1371/journal.pone.0144878.

(144) Patel, R. MALDI-TOF MS for the Diagnosis of Infectious Diseases. *Clin. Chem.* **2015**, *61* (1), 100–111. https://doi.org/10.1373/clinchem.2014.221770.

(145) Popp, R.; Basik, M.; Spatz, A.; Batist, G.; Zahedi, R. P.; Borchers, C. H. How IMALDI Can Improve Clinical Diagnostics. *The Analyst* **2018**, *143* (10), 2197–2203. https://doi.org/10.1039/C8AN00094H.

(146) Proc, J. L.; Kuzyk, M. A.; Hardie, D. B.; Yang, J.; Smith, D. S.; Jackson, A. M.; Parker, C. E.; Borchers, C. H. A Quantitative Study of the Effects of Chaotropic Agents, Surfactants, and Solvents on the Digestion Efficiency of Human Plasma Proteins by Trypsin. *J. Proteome Res.* **2010**, *9* (10), 5422–5437. https://doi.org/10.1021/pr100656u.

(147) Landry, J. P.; Ke, Y.; Yu, G.-L.; Zhu, X. D. Measuring Affinity Constants of 1450 Monoclonal Antibodies to Peptide Targets with a Microarray-Based Label-Free Assay Platform. *J. Immunol. Methods* **2015**, *417*, 86–96. https://doi.org/10.1016/j.jim.2014.12.011.

(148) Landry, J. P.; Fei, Y.; Zhu, X. Simultaneous Measurement of 10,000 Protein-Ligand Affinity Constants Using Microarray-Based Kinetic Constant Assays. *Assay Drug Dev. Technol.* **2012**, *10* (3), 250–259. https://doi.org/10.1089/adt.2011.0406.

(149) Neubert, H.; Shuford, C. M.; Olah, T. V.; Garofolo, F.; Schultz, G. A.; Jones, B. R.; Amaravadi, L.; Laterza, O. F.; Xu, K.; Ackermann, B. L. Protein Biomarker Quantification by Immunoaffinity Liquid Chromatography–Tandem Mass Spectrometry: Current State and Future Vision. *Clin. Chem.* **2020**, *66* (2), 282–301. https://doi.org/10.1093/clinchem/hvz022.

(150) Kuzyk, M. A.; Smith, D.; Yang, J.; Cross, T. J.; Jackson, A. M.; Hardie, D. B.; Anderson, N. L.; Borchers, C. H. Multiple Reaction Monitoring-Based, Multiplexed, Absolute Quantitation of 45 Proteins in Human Plasma*□S. *Mol. Cell. Proteomics* **2009**, *8* (8), 1860–1877.

(151) Hoeppe, S.; Schreiber, T. D.; Planatscher, H.; Zell, A.; Templin, M. F.; Stoll, D. Targeting Peptide Termini, a Novel Immunoaffinity Approach to Reduce Complexity in Mass Spectrometric Protein Identification□S. *Mol. Cell. Proteomics* **2010**, *10* (2), 11. https://doi.org/10.1074/mcp.M110.002857.

(152) Senko, M. W.; Beu, S. C.; McLaffertycor, F. W. Determination of Monoisotopic Masses and Ion Populations for Large Biomolecules from Resolved Isotopic Distributions. *J. Am. Soc. Mass Spectrom.* **1995**, *6* (4), 229–233. https://doi.org/10.1016/1044-0305(95)00017-8.

(153) R Core Team. *R: A Language and Environment for Statistical Computing*; R Foundation for Statistical Computing: Vienna, Austria, 2019.

(154) Mohammed, Y.; Domański, D.; Jackson, A. M.; Smith, D. S.; Deelder, A. M.; Palmblad, M.; Borchers, C. H. PeptidePicker: A Scientific Workflow with Web

Interface for Selecting Appropriate Peptides for Targeted Proteomics Experiments. *J. Proteomics* **2014**, *106*, 151–161. https://doi.org/10.1016/j.jprot.2014.04.018.

(155) Burkhart, J. M.; Schumbrutzki, C.; Wortelkamp, S.; Sickmann, A.; Zahedi, R. P. Systematic and Quantitative Comparison of Digest Efficiency and Specificity Reveals the Impact of Trypsin Quality on MS-Based Proteomics. *J. Proteomics* **2012**, *75* (4), 1454–1462. https://doi.org/10.1016/j.jprot.2011.11.016.

(156) Tu, T.; Gross, M. L. Miniaturizing Sample Spots for Matrix-Assisted Laser Desorption/Ionization Mass Spectrometry. *TrAC Trends Anal. Chem.* **2009**, *28* (7), 833–841. https://doi.org/10.1016/j.trac.2009.03.013.

(157) Blank-Landeshammer, B.; Richard, V. R.; Mitsa, G.; Marques, M.; LeBlanc, A.; Kollipara, L.; Feldmann, I.; Couetoux du Tertre, M.; Gambaro, K.; McNamara, S.; Spatz, A.; Zahedi, R. P.; Sickmann, A.; Batist, G.; Borchers, C. H. Proteogenomics of Colorectal Cancer Liver Metastases: Complementing Precision Oncology with Phenotypic Data. *Cancers* **2019**, *11* (12), 1907. https://doi.org/10.3390/cancers11121907.

(158) Dhingra, K. Oncology 2020: A Drug Development and Approval Paradigm. *Ann. Oncol.* **2015**, *26* (11), 2347–2350. https://doi.org/10.1093/annonc/mdv353.

(159) Sinicrope, F. A.; Okamoto, K.; Kasi, P. M.; Kawakami, H. Molecular Biomarkers in the Personalized Treatment of Colorectal Cancer. *Clin. Gastroenterol. Hepatol.* **2016**, *14* (5), 651–658. https://doi.org/10.1016/j.cgh.2016.02.008.

(160) Lièvre, A.; Bachet, J.-B.; Le Corre, D.; Boige, V.; Landi, B.; Emile, J.-F.; Côté, J.-F.; Tomasic, G.; Penna, C.; Ducreux, M.; Rougier, P.; Penault-Llorca, F.; Laurent-Puig, P. *KRAS* Mutation Status Is Predictive of Response to Cetuximab Therapy in Colorectal Cancer. *Cancer Res.* **2006**, *66* (8), 3992–3995. https://doi.org/10.1158/0008-5472.CAN-06-0191.

(161) Yu, H.; Boyle, T. A.; Zhou, C.; Rimm, D. L.; Hirsch, F. R. PD-L1 Expression in Lung Cancer. *J. Thorac. Oncol.* **2016**, *11* (7), 964–975. https://doi.org/10.1016/j.jtho.2016.04.014.

(162) Chen, M.; Manley, J. L. Mechanisms of Alternative Splicing Regulation: Insights from Molecular and Genomics Approaches. *Nat. Rev. Mol. Cell Biol.* **2009**, *10* (11), 741–754. https://doi.org/10.1038/nrm2777.

(163) Dawson, M. A.; Kouzarides, T. Cancer Epigenetics: From Mechanism to Therapy. *Cell* **2012**, *150* (1), 12–27. https://doi.org/10.1016/j.cell.2012.06.013.

(164) Wan, X.; Ding, X.; Chen, S.; Song, H.; Jiang, H.; Fang, Y.; Li, P.; Guo, J. The Functional Sites of MiRNAs and LncRNAs in Gastric Carcinogenesis. *Tumor Biol.* **2015**, *36* (2), 521–532. https://doi.org/10.1007/s13277-015-3136-5.

(165) Mateo, J.; Ganji, G.; Lemech, C.; Burris, H. A.; Han, S.-W.; Swales, K.; Decordova, S.; DeYoung, M. P.; Smith, D. A.; Kalyana-Sundaram, S.; Wu, J.; Motwani, M.; Kumar, R.; Tolson, J. M.; Rha, S. Y.; Chung, H. C.; Eder, J. P.; Sharma, S.; Bang, Y.-J.; Infante, J. R.; Yan, L.; de Bono, J. S.; Arkenau, H.-T. A First-Time-in-Human Study of GSK2636771, a Phosphoinositide 3 Kinase Beta-Selective Inhibitor, in Patients with Advanced Solid Tumors. *Clin. Cancer Res.* **2017**, *23* (19), 5981–5992. https://doi.org/10.1158/1078-0432.CCR-17-0725.

(166) Morales-Betanzos, C. A.; Lee, H.; Gonzalez Ericsson, P. I.; Balko, J. M.; Johnson, D. B.; Zimmerman, L. J.; Liebler, D. C. Quantitative Mass Spectrometry Analysis of PD-L1 Protein Expression, *N* -Glycosylation and Expression

Stoichiometry with PD-1 and PD-L2 in Human Melanoma. *Mol. Cell. Proteomics* **2017**, *16* (10), 1705–1717. https://doi.org/10.1074/mcp.RA117.000037.

(167) Baselga, J.; Campone, M.; Piccart, M.; Burris, H. A.; Rugo, H. S.; Sahmoud, T.; Noguchi, S.; Gnant, M.; Pritchard, K. I.; Lebrun, F.; Beck, J. T.; Ito, Y.; Yardley, D.; Deleu, I.; Perez, A.; Bachelot, T.; Vittori, L.; Xu, Z.; Mukhopadhyay, P.; Lebwohl, D.; Hortobagyi, G. N. Everolimus in Postmenopausal Hormone-Receptor–Positive Advanced Breast Cancer. *N. Engl. J. Med.* **2012**, *366* (6), 520–529. https://doi.org/10.1056/NEJMoa1109653.

(168) Furman, R. R.; Sharman, J. P.; Coutre, S. E.; Cheson, B. D.; Pagel, J. M.; Hillmen, P.; Barrientos, J. C.; Zelenetz, A. D.; Kipps, T. J.; Flinn, I.; Ghia, P.; Eradat, H.; Ervin, T.; Lamanna, N.; Coiffier, B.; Pettitt, A. R.; Ma, S.; Stilgenbauer, S.; Cramer, P.; Aiello, M.; Johnson, D. M.; Miller, L. L.; Li, D.; Jahn, T. M.; Dansey, R. D.; Hallek, M.; O'Brien, S. M. Idelalisib and Rituximab in Relapsed Chronic Lymphocytic Leukemia. *N. Engl. J. Med.* **2014**, *370* (11), 997–1007. https://doi.org/10.1056/NEJMoa1315226.

(169) Motzer, R. J.; Escudier, B.; Oudard, S.; Hutson, T. E.; Porta, C.; Bracarda, S.; Grünwald, V.; Thompson, J. A.; Figlin, R. A.; Hollaender, N.; Urbanowitz, G.; Berg, W. J.; Kay, A.; Lebwohl, D.; Ravaud, A. Efficacy of Everolimus in Advanced Renal Cell Carcinoma: A Double-Blind, Randomised, Placebo-Controlled Phase III Trial. **2008**, *372*, 8.

(170) Hudes, G.; Dutcher, J.; Staroslawska, E.; Bodrogi, I.; Schmidt-Wolf, I. G. H.; O'Toole, T.; Moore, L. Temsirolimus, Interferon Alfa, or Both for Advanced Renal-Cell Carcinoma. *N. Engl. J. Med.* **2007**, 11.

(171) Bachman, K. E.; Argani, P.; Samuels, Y.; Silliman, N.; Ptak, J.; Szabo, S.; Konishi, H.; Karakas, B.; Blair, B. G.; Lin, C.; Peters, B. A.; Velculescu, V. E.; Park, B. H. The PIK3CA Gene Is Mutated with High Frequency in Human Breast Cancers. *Cancer Biol. Ther.* **2004**, *3* (8), 772–775. https://doi.org/10.4161/cbt.3.8.994.

(172) Huang, J.; Zhang, L.; Greshock, J.; Colligon, T. A.; Wang, Y.; Ward, R.; Katsaros, D.; Lassus, H.; Butzow, R.; Godwin, A. K.; Testa, J. R.; Nathanson, K. L.; Gimotty, P. A.; Coukos, G.; Weber, B. L.; Degenhardt, Y. Frequent Genetic Abnormalities of the PI3K/AKT Pathway in Primary Ovarian Cancer Predict Patient Outcome. *Genes. Chromosomes Cancer* **2011**, *50* (8), 606–618. https://doi.org/10.1002/gcc.20883.

(173) Sartore-Bianchi, A.; Martini, M.; Molinari, F.; Veronese, S.; Nichelatti, M.; Artale, S.; Di Nicolantonio, F.; Saletti, P.; De Dosso, S.; Mazzucchelli, L.; Frattini, M.; Siena, S.; Bardelli, A. PIK3CA Mutations in Colorectal Cancer Are Associated with Clinical Resistance to EGFR-Targeted Monoclonal Antibodies. *Cancer Res.* **2009**, *69* (5), 1851–1857. https://doi.org/10.1158/0008-5472.CAN-08-2466.

(174) Stamatkin, C.; Ratermann, K. L.; Overley, C. W.; Black, E. P. Inhibition of Class IA PI3K Enzymes in Non-Small Cell Lung Cancer Cells Uncovers Functional Compensation among Isoforms. *Cancer Biol. Ther.* **2015**, *16* (9), 1341–1352. https://doi.org/10.1080/15384047.2015.1070986.

(175) Froehlich, B. C.; Popp, R.; Sobsey, C. A.; Ibrahim, S.; LeBlanc, A. M.; Mohammed, Y.; Aguilar-Mahecha, A.; Poetz, O.; Chen, M. X.; Spatz, A.; Basik, M.; Batist, G.; Zahedi, R. P.; Borchers, C. H. Systematic Optimization of the

IMALDI Workflow for the Robust and Straightforward Quantification of Signalling Proteins in Cancer Cells. *PROTEOMICS – Clin. Appl.* **2020**, 2000034. https://doi.org/10.1002/prca.202000034.

(176) Grant, R. P.; Hoofnagle, A. N. From Lost in Translation to Paradise Found: Enabling Protein Biomarker Method Transfer by Mass Spectrometry. *Clin. Chem.* **2014**, *60* (7), 941–944. https://doi.org/10.1373/clinchem.2014.224840.

(177) Gu, H.; Liu, G.; Wang, J.; Aubry, A.-F.; Arnold, M. E. Selecting the Correct Weighting Factors for Linear and Quadratic Calibration Curves with Least-Squares Regression Algorithm in Bioanalytical LC-MS/MS Assays and Impacts of Using Incorrect Weighting Factors on Curve Stability, Data Quality, and Assay Performance. *Anal. Chem.* **2014**, *86* (18), 8959–8966. https://doi.org/10.1021/ac5018265.

(178) Ibrahim, S.; Froehlich, B. C.; Aguilar-Mahecha, A.; Aloyz, R.; Poetz, O.; Basik, M.; Batist, G.; Zahedi, R. P.; Borchers, C. H. Using Two Peptide Isotopologues as Internal Standards for the Streamlined Quantification of Low-Abundance Proteins by Immuno-MRM and Immuno-MALDI. *Anal. Chem.* **2020**, *92* (18), 12407–12414. https://doi.org/10.1021/acs.analchem.0c02157.

(179) Aguilar-Mahecha, A.; Joseph, S.; Cavallone, L.; Buchanan, M.; Krzemien, U.; Batist, G.; Basik, M. Precision Medicine Tools to Guide Therapy and Monitor Response to Treatment in a HER-2+ Gastric Cancer Patient: Case Report. *Front. Oncol.* **2019**, *9*, 698. https://doi.org/10.3389/fonc.2019.00698.

(180) Berns, K.; Horlings, H. M.; Hennessy, B. T.; Madiredjo, M.; Hijmans, E. M.; Beelen, K.; Linn, S. C.; Gonzalez-Angulo, A. M.; Stemke-Hale, K.; Hauptmann, M.; Beijersbergen, R. L.; Mills, G. B.; van de Vijver, M. J.; Bernards, R. A Functional Genetic Approach Identifies the PI3K Pathway as a Major Determinant of Trastuzumab Resistance in Breast Cancer. *Cancer Cell* **2007**, *12* (4), 395–402. https://doi.org/10.1016/j.ccr.2007.08.030.

(181) Eisenhauer, E. A.; Therasse, P.; Bogaerts, J.; Schwartz, L. H.; Sargent, D.; Ford, R.; Dancey, J.; Arbuck, S.; Gwyther, S.; Mooney, M.; Rubinstein, L.; Shankar, L.; Dodd, L.; Kaplan, R.; Lacombe, D.; Verweij, J. New Response Evaluation Criteria in Solid Tumours: Revised RECIST Guideline (Version 1.1). *Eur. J. Cancer* **2009**, *45* (2), 228–247. https://doi.org/10.1016/j.ejca.2008.10.026.

(182) Xiang, X.; Zhuang, L.; Chen, H.; Yang, X.; Li, H.; Li, G.; Yu, J. Everolimus Inhibits the Proliferation and Migration of Epidermal Growth Factor Receptor-resistant Lung Cancer Cells A549 via Regulating the MicroRNA-4328/Phosphatase and Tensin Homolog Signaling Pathway. *Oncol. Lett.* **2019**, *18* (5), 5269–5276. https://doi.org/10.3892/ol.2019.10887.

(183) Du, L.; Li, X.; Zhen, L.; Chen, W.; Mu, L.; Zhang, Y.; Song, A. Everolimus Inhibits Breast Cancer Cell Growth through PI3K/AKT/MTOR Signaling Pathway. *Mol. Med. Rep.* **2018**, *17* (5), 7163–7169. https://doi.org/10.3892/mmr.2018.8769.

(184) Uhlen, M.; Zhang, C.; Lee, S.; Sjöstedt, E.; Fagerberg, L.; Bidkhori, G.; Benfeitas, R.; Arif, M.; Liu, Z.; Edfors, F.; Sanli, K.; von Feilitzen, K.; Oksvold, P.; Lundberg, E.; Hober, S.; Nilsson, P.; Mattsson, J.; Schwenk, J. M.; Brunnström, H.; Glimelius, B.; Sjöblom, T.; Edqvist, P.-H.; Djureinovic, D.; Micke, P.; Lindskog, C.; Mardinoglu, A.; Ponten, F. A Pathology Atlas of the Human Cancer

Transcriptome. *Science* **2017**, *357* (6352), eaan2507. https://doi.org/10.1126/science.aan2507.

(185) Expression of PIK3CA in cancer - Summary - The Human Protein Atlas https://www.proteinatlas.org/ENSG00000121879-PIK3CA/pathology (accessed 2020 -07 -20).

(186) Expression of PTEN in cancer - Summary - The Human Protein Atlas https://www.proteinatlas.org/ENSG00000171862-PTEN/pathology (accessed 2020 -07 -20).

(187) Distler, U.; Kuharev, J.; Navarro, P.; Tenzer, S. Label-Free Quantification in Ion Mobility–Enhanced Data-Independent Acquisition Proteomics. *Nat. Protoc.* **2016**, *11* (4), 795–812. https://doi.org/10.1038/nprot.2016.042.

(188) Mertins, P.; Tang, L. C.; Krug, K.; Clark, D. J.; Gritsenko, M. A.; Chen, L.; Clauser, K. R.; Clauss, T. R.; Shah, P.; Gillette, M. A.; Petyuk, V. A.; Thomas, S. N.; Mani, D. R.; Mundt, F.; Moore, R. J.; Hu, Y.; Zhao, R.; Schnaubelt, M.; Keshishian, H.; Monroe, M. E.; Zhang, Z.; Udeshi, N. D.; Mani, D.; Davies, S. R.; Townsend, R. R.; Chan, D. W.; Smith, R. D.; Zhang, H.; Liu, T.; Carr, S. A. Reproducible Workflow for Multiplexed Deep-Scale Proteome and Phosphoproteome Analysis of Tumor Tissues by Liquid Chromatography–Mass Spectrometry. *Nat. Protoc.* **2018**, *13* (7), 1632–1661. https://doi.org/10.1038/s41596-018-0006-9.

(189) Percy, A. J.; Michaud, S. A.; Jardim, A.; Sinclair, N. J.; Zhang, S.; Mohammed, Y.; Palmer, A. L.; Hardie, D. B.; Yang, J.; LeBlanc, A. M.; Borchers, C. H. Multiplexed MRM-Based Assays for the Quantitation of Proteins in Mouse Plasma and Heart Tissue. *PROTEOMICS* **2017**, *17* (7), 1600097. https://doi.org/10.1002/pmic.201600097.

(190) Mnatsakanyan, R.; Shema, G.; Basik, M.; Batist, G.; Borchers, C. H.; Sickmann, A.; Zahedi, R. P. Detecting Post-Translational Modification Signatures as Potential Biomarkers in Clinical Mass Spectrometry. *Expert Rev. Proteomics* **2018**, *15* (6), 515–535. https://doi.org/10.1080/14789450.2018.1483340.

(191) Luongo, F.; Colonna, F.; Calapà, F.; Vitale, S.; Fiori, M. E.; De Maria, R. PTEN Tumor-Suppressor: The Dam of Stemness in Cancer. *Cancers* **2019**, *11* (8), 1076. https://doi.org/10.3390/cancers11081076.

(192) Berger, A. H.; Knudson, A. G.; Pandolfi, P. P. A Continuum Model for Tumour Suppression. *Nature* **2011**, *476* (7359), 163–169. https://doi.org/10.1038/nature10275.

(193) Rosenberger, G.; Bludau, I.; Schmitt, U.; Heusel, M.; Hunter, C. L.; Liu, Y.; MacCoss, M. J.; MacLean, B. X.; Nesvizhskii, A. I.; Pedrioli, P. G. A.; Reiter, L.; Röst, H. L.; Tate, S.; Ting, Y. S.; Collins, B. C.; Aebersold, R. Statistical Control of Peptide and Protein Error Rates in Large-Scale Targeted Data-Independent Acquisition Analyses. *Nat. Methods* **2017**, *14* (9), 921–927. https://doi.org/10.1038/nmeth.4398.

(194) Pfammatter, S.; Bonneil, E.; McManus, F. P.; Thibault, P. Accurate Quantitative Proteomic Analyses Using Metabolic Labeling and High Field Asymmetric Waveform Ion Mobility Spectrometry (FAIMS). *J. Proteome Res.* **2019**, *18* (5), 2129–2138. https://doi.org/10.1021/acs.jproteome.9b00021.

(195) Jannetto, P. J.; Fitzgerald, R. L. Effective Use of Mass Spectrometry in the Clinical Laboratory. *Clin. Chem.* **2016**, *62* (1), 92–98. https://doi.org/10.1373/clinchem.2015.248146.

(196) Heaney, L. M.; Jones, D. J.; Suzuki, T. Mass Spectrometry in Medicine: A Technology for the Future? *Future Sci. OA* **2017**, *3* (3), FSO213. https://doi.org/10.4155/fsoa-2017-0053.

(197) Dou, M.; Clair, G.; Tsai, C.-F.; Xu, K.; Chrisler, W. B.; Sontag, R. L.; Zhao, R.; Moore, R. J.; Liu, T.; Pasa-Tolic, L.; Smith, R. D.; Shi, T.; Adkins, J. N.; Qian, W.-J.; Kelly, R. T.; Ansong, C.; Zhu, Y. High-Throughput Single Cell Proteomics Enabled by Multiplex Isobaric Labeling in a Nanodroplet Sample Preparation Platform. *Anal. Chem.* **2019**, *91* (20), 13119–13127. https://doi.org/10.1021/acs.analchem.9b03349.

(198) Solari, F. A.; Dell'Aica, M.; Sickmann, A.; Zahedi, R. P. Why Phosphoproteomics Is Still a Challenge. *Mol. Biosyst.* **2015**, *11* (6), 1487–1493. https://doi.org/10.1039/C5MB00024F.

(199) Venne, A. S.; Kollipara, L.; Zahedi, R. P. The next Level of Complexity: Crosstalk of Posttranslational Modifications. *PROTEOMICS* **2014**, *14* (4–5), 513–524. https://doi.org/10.1002/pmic.201300344.

(200) Hoofnagle, A. N.; Whiteaker, J. R.; Carr, S. A.; Kuhn, E.; Liu, T.; Massoni, S. A.; Thomas, S. N.; Townsend, R. R.; Zimmerman, L. J.; Boja, E.; Chen, J.; Crimmins, D. L.; Davies, S. R.; Gao, Y.; Hiltke, T. R.; Ketchum, K. A.; Kinsinger, C. R.; Mesri, M.; Meyer, M. R.; Qian, W.-J.; Schoenherr, R. M.; Scott, M. G.; Shi, T.; Whiteley, G. R.; Wrobel, J. A.; Wu, C.; Ackermann, B. L.; Aebersold, R.; Barnidge, D. R.; Bunk, D. M.; Clarke, N.; Fishman, J. B.; Grant, R. P.; Kusebauch, U.; Kushnir, M. M.; Lowenthal, M. S.; Moritz, R. L.; Neubert, H.; Patterson, S. D.; Rockwood, A. L.; Rogers, J.; Singh, R. J.; Van Eyk, J. E.; Wong, S. H.; Zhang, S.; Chan, D. W.; Chen, X.; Ellis, M. J.; Liebler, D. C.; Rodland, K. D.; Rodriguez, H.; Smith, R. D.; Zhang, Z.; Zhang, H.; Paulovich, A. G. Recommendations for the Generation, Quantification, Storage, and Handling of Peptides Used for Mass Spectrometry–Based Assays. *Clin. Chem.* **2016**, *62* (1), 48–69. https://doi.org/10.1373/clinchem.2015.250563.

(201) Honour, J. W. Development and Validation of a Quantitative Assay Based on Tandem Mass Spectrometry. *Ann. Clin. Biochem.* **2011**, *48* (2), 97–111. https://doi.org/10.1258/acb.2010.010176.

(202) Villanueva, J.; Carrascal, M.; Abian, J. Isotope Dilution Mass Spectrometry for Absolute Quantification in Proteomics: Concepts and Strategies. *J. Proteomics* **2014**, *96*, 184–199. https://doi.org/10.1016/j.jprot.2013.11.004.

(203) Buhrman, D. L.; Price, P. I.; Rudewicz, P. J. Quantitation of SR 27417 in Human Plasma Using Electrospray Liquid Chromatography-Tandem Mass Spectrometry: A Study of Ion Suppression. *J. Am. Soc. Mass Spectrom.* **1996**, *7* (11), 1099–1105. https://doi.org/10.1016/S1044-0305(96)00072-4.

(204) Ciccimaro, E.; Blair, I. A. Stable-Isotope Dilution LC–MS for Quantitative Biomarker Analysis. *Bioanalysis* **2010**, *2* (2), 311–341. https://doi.org/10.4155/bio.09.185.

(205) LeBlanc, A.; Michaud, S. A.; Percy, A. J.; Hardie, D. B.; Yang, J.; Sinclair, N. J.; Proudfoot, J. I.; Pistawka, A.; Smith, D. S.; Borchers, C. H. Multiplexed MRM-

Based Protein Quantitation Using Two Different Stable Isotope-Labeled Peptide Isotopologues for Calibration. *J. Proteome Res.* **2017**, *16* (7), 2527–2536. https://doi.org/10.1021/acs.jproteome.7b00094.

(206) Chiva, C.; Pastor, O.; Trilla-Fuertes, L.; Gámez-Pozo, A.; Fresno Vara, J. Á.; Sabidó, E. Isotopologue Multipoint Calibration for Proteomics Biomarker Quantification in Clinical Practice. *Anal. Chem.* **2019**, *91* (8), 4934–4938. https://doi.org/10.1021/acs.analchem.8b05802.

(207) Rule, G. S.; Rockwood, A. L. Improving Quantitative Precision and Throughput by Reducing Calibrator Use in Liquid Chromatography-Tandem Mass Spectrometry. *Anal. Chim. Acta* **2016**, *919*, 55–61. https://doi.org/10.1016/j.aca.2016.03.020.

(208) Hoffman, M. A.; Schmeling, M.; Dahlin, J. L.; Bevins, N. J.; Cooper, D. P.; Jarolim, P.; Fitzgerald, R. L.; Hoofnagle, A. N. Calibrating from Within: Multipoint Internal Calibration of a Quantitative Mass Spectrometric Assay of Serum Methotrexate. *Clin. Chem.* **2020**, *66* (3), 474–482. https://doi.org/10.1093/clinchem/hvaa003.

(209) Grant, R. P. The March of the Masses. *Clin. Chem.* **2013**, *59* (6), 871–873. https://doi.org/10.1373/clinchem.2013.205435.

(210) Kuzyk, M. A.; Parker, C. E.; Domanski, D.; Borchers, C. H. Development of MRM-Based Assays for the Absolute Quantitation of Plasma Proteins. *Methods Mol. Biol. Clifton NJ* **2013**, *1023*, 53–82. https://doi.org/10.1007/978-1-4614-7209-4_4.

(211) Percy, A. J.; Chambers, A. G.; Parker, C. E.; Borchers, C. H. Absolute Quantitation of Proteins in Human Blood by Multiplexed Multiple Reaction Monitoring Mass Spectrometry. *Methods Mol. Biol. Clifton NJ* **2013**, *1000*, 167–189. https://doi.org/10.1007/978-1-62703-405-0_13.

(212) Kollipara, L.; Zahedi, R. P. Protein Carbamylation: In Vivo Modification or in Vitro Artefact? *PROTEOMICS* **2013**, *13* (6), 941–944. https://doi.org/10.1002/pmic.201200452.

(213) Manza, L. L.; Stamer, S. L.; Ham, A.-J. L.; Codreanu, S. G.; Liebler, D. C. Sample Preparation and Digestion for Proteomic Analyses Using Spin Filters. *PROTEOMICS* **2005**, *5* (7), 1742–1745. https://doi.org/10.1002/pmic.200401063.

(214) Wiśniewski, J. R.; Zougman, A.; Nagaraj, N.; Mann, M. Universal Sample Preparation Method for Proteome Analysis. *Nat. Methods* **2009**, *6* (5), 359–362. https://doi.org/10.1038/nmeth.1322.

(215) Skyline-daily https://proteome.gs.washington.edu/software/test/brendanx/Skyline-test/ (accessed 2021 -03 -08).

(216) R Core Team. *R: A Language and Environment for Statistical Computing*; R Foundation for Statistical Computing: Vienna, Austria, 2020.

(217) Mani, D. R.; Abbatiello, S. E.; Carr, S. A. Statistical Characterization of Multiple-Reaction Monitoring Mass Spectrometry (MRM-MS) Assays for Quantitative Proteomics. *BMC Bioinformatics* **2012**, *13* (S16), S9. https://doi.org/10.1186/1471-2105-13-S16-S9.

(218) Cuadros-Rodríguez, L.; Bagur-González, M. G.; Sánchez-Viñas, M.; González-Casado, A.; Gómez-Sáez, A. M. Principles of Analytical Calibration/Quantification

for the Separation Sciences. *J. Chromatogr. A* **2007**, *1158* (1–2), 33–46. https://doi.org/10.1016/j.chroma.2007.03.030.

(219) Taylor, P. J.; Hogan, N. S.; Lynch, S. V.; Johnson, A. G.; Pond, S. M. Improved Therapeutic Drug Monitoring of Tacrolimus (FK506) by Tandem Mass Spectrometry. *Clin. Chem.* **1997**, *43* (11), 2189–2190.

(220) Clinical Laboratory Improvement Amendments (CLIA) | CMS https://www.cms.gov/Regulations-and-Guidance/Legislation/CLIA?redirect=/clia (accessed 2019 -08 -27).

(221) Mao, M.; Tian, F.; Mariadason, J. M.; Tsao, C. C.; Lemos, R.; Dayyani, F.; Gopal, Y. N. V.; Jiang, Z.-Q.; Wistuba, I. I.; Tang, X. M.; Bornman, W. G.; Bollag, G.; Mills, G. B.; Powis, G.; Desai, J.; Gallick, G. E.; Davies, M. A.; Kopetz, S. Resistance to BRAF Inhibition in BRAF-Mutant Colon Cancer Can Be Overcome with PI3K Inhibition or Demethylating Agents. *Clin. Cancer Res.* **2013**, *19* (3), 657–667. https://doi.org/10.1158/1078-0432.CCR-11-1446.

(222) Medico, E.; Russo, M.; Picco, G.; Cancelliere, C.; Valtorta, E.; Corti, G.; Buscarino, M.; Isella, C.; Lamba, S.; Martinoglio, B.; Veronese, S.; Siena, S.; Sartore-Bianchi, A.; Beccuti, M.; Mottolese, M.; Linnebacher, M.; Cordero, F.; Di Nicolantonio, F.; Bardelli, A. The Molecular Landscape of Colorectal Cancer Cell Lines Unveils Clinically Actionable Kinase Targets. *Nat. Commun.* **2015**, *6* (1), 7002. https://doi.org/10.1038/ncomms8002.

(223) Addona, T. A.; Abbatiello, S. E.; Schilling, B.; Skates, S. J.; Mani, D. R.; Bunk, D. M.; Spiegelman, C. H.; Zimmerman, L. J.; Ham, A.-J. L.; Keshishian, H.; Hall, S. C.; Allen, S.; Blackman, R. K.; Borchers, C. H.; Buck, C.; Cardasis, H. L.; Cusack, M. P.; Dodder, N. G.; Gibson, B. W.; Held, J. M.; Hiltke, T.; Jackson, A.; Johansen, E. B.; Kinsinger, C. R.; Li, J.; Mesri, M.; Neubert, T. A.; Niles, R. K.; Pulsipher, T. C.; Ransohoff, D.; Rodriguez, H.; Rudnick, P. A.; Smith, D.; Tabb, D. L.; Tegeler, T. J.; Variyath, A. M.; Vega-Montoto, L. J.; Wahlander, Å.; Waldemarson, S.; Wang, M.; Whiteaker, J. R.; Zhao, L.; Anderson, N. L.; Fisher, S. J.; Liebler, D. C.; Paulovich, A. G.; Regnier, F. E.; Tempst, P.; Carr, S. A. Multi-Site Assessment of the Precision and Reproducibility of Multiple Reaction Monitoring–Based Measurements of Proteins in Plasma. *Nat. Biotechnol.* **2009**, *27* (7), 633–641. https://doi.org/10.1038/nbt.1546.

(224) Prakash, A.; Rezai, T.; Krastins, B.; Sarracino, D.; Athanas, M.; Russo, P.; Ross, M. M.; Zhang, H.; Tian, Y.; Kulasingam, V.; Drabovich, A. P.; Smith, C.; Batruch, I.; Liotta, L.; Petricoin, E.; Diamandis, E. P.; Chan, D. W.; Lopez, M. F. Platform for Establishing Interlaboratory Reproducibility of Selected Reaction Monitoring-Based Mass Spectrometry Peptide Assays. *J. Proteome Res.* **2010**, *9* (12), 6678–6688. https://doi.org/10.1021/pr100821m.

(225) Kuhn, E.; Whiteaker, J. R.; Mani, D. R.; Jackson, A. M.; Zhao, L.; Pope, M. E.; Smith, D.; Rivera, K. D.; Anderson, N. L.; Skates, S. J.; Pearson, T. W.; Paulovich, A. G.; Carr, S. A. Interlaboratory Evaluation of Automated, Multiplexed Peptide Immunoaffinity Enrichment Coupled to Multiple Reaction Monitoring Mass Spectrometry for Quantifying Proteins in Plasma. *Mol. Cell. Proteomics* **2012**, *11* (6), M111.013854. https://doi.org/10.1074/mcp.M111.013854.

(226) Abbatiello, S. E.; Schilling, B.; Mani, D. R.; Zimmerman, L. J.; Hall, S. C.; MacLean, B.; Albertolle, M.; Allen, S.; Burgess, M.; Cusack, M. P.; Gosh, M.;

Hedrick, V.; Held, J. M.; Inerowicz, H. D.; Jackson, A.; Keshishian, H.; Kinsinger, C. R.; Lyssand, J.; Makowski, L.; Mesri, M.; Rodriguez, H.; Rudnick, P.; Sadowski, P.; Sedransk, N.; Shaddox, K.; Skates, S. J.; Kuhn, E.; Smith, D.; Whiteaker, J. R.; Whitwell, C.; Zhang, S.; Borchers, C. H.; Fisher, S. J.; Gibson, B. W.; Liebler, D. C.; MacCoss, M. J.; Neubert, T. A.; Paulovich, A. G.; Regnier, F. E.; Tempst, P.; Carr, S. A. Large-Scale Interlaboratory Study to Develop, Analytically Validate and Apply Highly Multiplexed, Quantitative Peptide Assays to Measure Cancer-Relevant Proteins in Plasma. *Mol. Cell. Proteomics* **2015**, *14* (9), 2357–2374. https://doi.org/10.1074/mcp.M114.047050.

(227) De Luca, A.; Maiello, M. R.; D'Alessio, A.; Pergameno, M.; Normanno, N. The RAS/RAF/MEK/ERK and the PI3K/AKT Signalling Pathways: Role in Cancer Pathogenesis and Implications for Therapeutic Approaches. *Expert Opin. Ther. Targets* **2012**, *16* (sup2), S17–S27. https://doi.org/10.1517/14728222.2011.639361.

(228) Nitulescu, G. M.; Margina, D.; Juzenas, P.; Peng, Q.; Olaru, O. T.; Saloustros, E.; Fenga, C.; Spandidos, D. A.; Libra, M.; Tsatsakis, A. M. Akt Inhibitors in Cancer Treatment: The Long Journey from Drug Discovery to Clinical Use (Review). *Int. J. Oncol.* **2016**, *48* (3), 869–885. https://doi.org/10.3892/ijo.2015.3306.

(229) Sobsey, C. A.; Froehlich, B. C.; Batist, G.; Borchers, C. Immuno-MALDI-MS for Accurate Quantitation of Targeted Peptides from Volume-Restricted Samples. In *Neuronal Cell Death*; Methods in Molecular Biology; Humana Press: New York, NY, 2021.

(230) Melville, J. *Uwot: The Uniform Manifold Approximation and Projection (UMAP) Method for Dimensionality Reduction*; 2020.

(231) Pang, Z.; Chong, J.; Li, S.; Xia, J. MetaboAnalystR 3.0: Toward an Optimized Workflow for Global Metabolomics. *Metabolites* **2020**, *10* (5), 186. https://doi.org/10.3390/metabo10050186.

(232) F, R.; B, G.; A, S.; K-A, L. C. MixOmics: An R Package for 'omics Feature Selection and Multiple Data Integration. *PLoS Comput. Biol.* **2017**, *13* (11), e1005752.

(233) Aggarwal, C. C.; Hinneburg, A.; Keim, D. A. On the Surprising Behavior of Distance Metrics in High Dimensional Space. In *Database Theory — ICDT 2001*; Van den Bussche, J., Vianu, V., Eds.; Goos, G., Hartmanis, J., van Leeuwen, J., Series Eds.; Lecture Notes in Computer Science; Springer Berlin Heidelberg: Berlin, Heidelberg, 2001; Vol. 1973, pp 420–434. https://doi.org/10.1007/3-540-44503-X_27.

(234) Hahsler, M.; Piekenbrock, M.; Doran, D. Dbscan: Fast Density-Based Clustering with R. *J. Stat. Softw.* **2019**, *91* (1), 1–30. https://doi.org/10.18637/jss.v091.i01.

(235) Pouliquen, D.; Boissard, A.; Coqueret, O.; Guette, C. Biomarkers of Tumor Invasiveness in Proteomics (Review). *Int. J. Oncol.* **2020**, *57* (2), 409–432. https://doi.org/10.3892/ijo.2020.5075.

(236) Li, H.; Popp, R.; Frohlich, B.; Chen, M. X.; Borchers, C. H. Peptide and Protein Quantification Using Automated Immuno-MALDI (IMALDI). *JoVE J. Vis. Exp.* **2017**, No. 126, e55933–e55933. https://doi.org/10.3791/55933.

(237) Froehlich, B. C. *R-Scripts-for-Plotting-and-Analyzing-MALDI-Data*; GitHub, 2021.

(238) Rudd, M. L.; Price, J. C.; Fogoros, S.; Godwin, A. K.; Sgroi, D. C.; Merino, M. J.; Bell, D. W. A Unique Spectrum of Somatic *PIK3CA* (P110α) Mutations Within Primary Endometrial Carcinomas. *Clin. Cancer Res.* **2011**, *17* (6), 1331–1340. https://doi.org/10.1158/1078-0432.CCR-10-0540.

(239) Martínez-Sáez, O.; Chic, N.; Pascual, T.; Adamo, B.; Vidal, M.; González-Farré, B.; Sanfeliu, E.; Schettini, F.; Conte, B.; Brasó-Maristany, F.; Rodríguez, A.; Martínez, D.; Galván, P.; Rodríguez, A. B.; Martinez, A.; Muñoz, M.; Prat, A. Frequency and Spectrum of PIK3CA Somatic Mutations in Breast Cancer. *Breast Cancer Res.* **2020**, *22* (1), 45. https://doi.org/10.1186/s13058-020-01284-9.

(240) Carbognin, L.; Miglietta, F.; Paris, I.; Dieci, M. V. Prognostic and Predictive Implications of PTEN in Breast Cancer: Unfulfilled Promises but Intriguing Perspectives. *Cancers* **2019**, *11* (9), 1401. https://doi.org/10.3390/cancers11091401.

Appendix 1

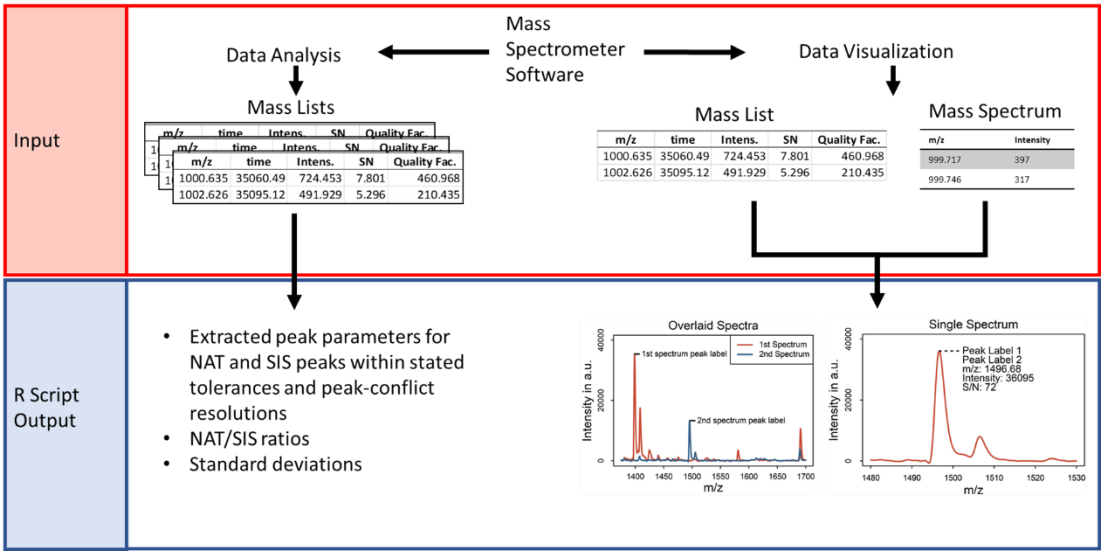

Supporting Figure S 1. Data analysis and visualization pipeline using custom R scirpts. Mass lists and mass spectra are exported as *.xlsx and *.txt files, respectively. Data analysis: From the mass lists, the peak parameters (intensity, S/N ratio and peak area) of the NAT, END and SIS peaks are extracted. NAT/SIS ratios as well as CVs are calculated. Data visualization: Mass spectra are imported from the *.txt file and visualizaed using custom graphic parameters. Peak labeling is performed by extracting the peak parameters for the selected peaks from the corresponding mass lists and displaying them, together with custom labels, according to the user's settings.

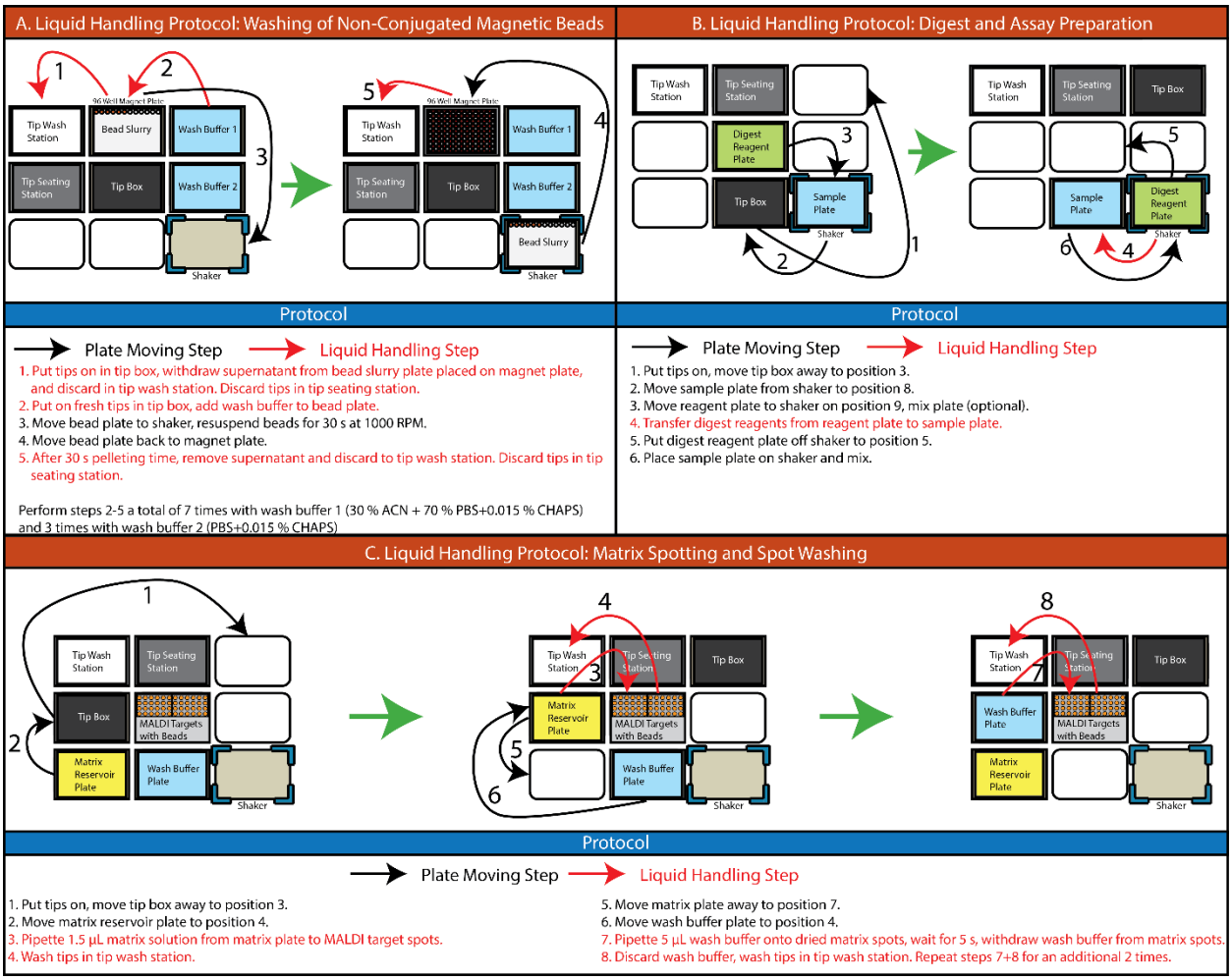

Supporting Figure S 2. Automated liquid handling protocols utilizing a Bravo 96 LT liquid handling robot. (A) Washing non-conjugated magnetic beads to remove detergents present in the bead stock solution prior to antibody coupling. (B) Adding tryptic digestion reagents to cell lysate samples, as well as adding internal standard and antibody-coupled beads prior to antibody enrichment. (C) Adding MALDI matrix on top of dried antigen-antibody-bead MALDI target spots and washing the dried matrix spot with wash buffer.

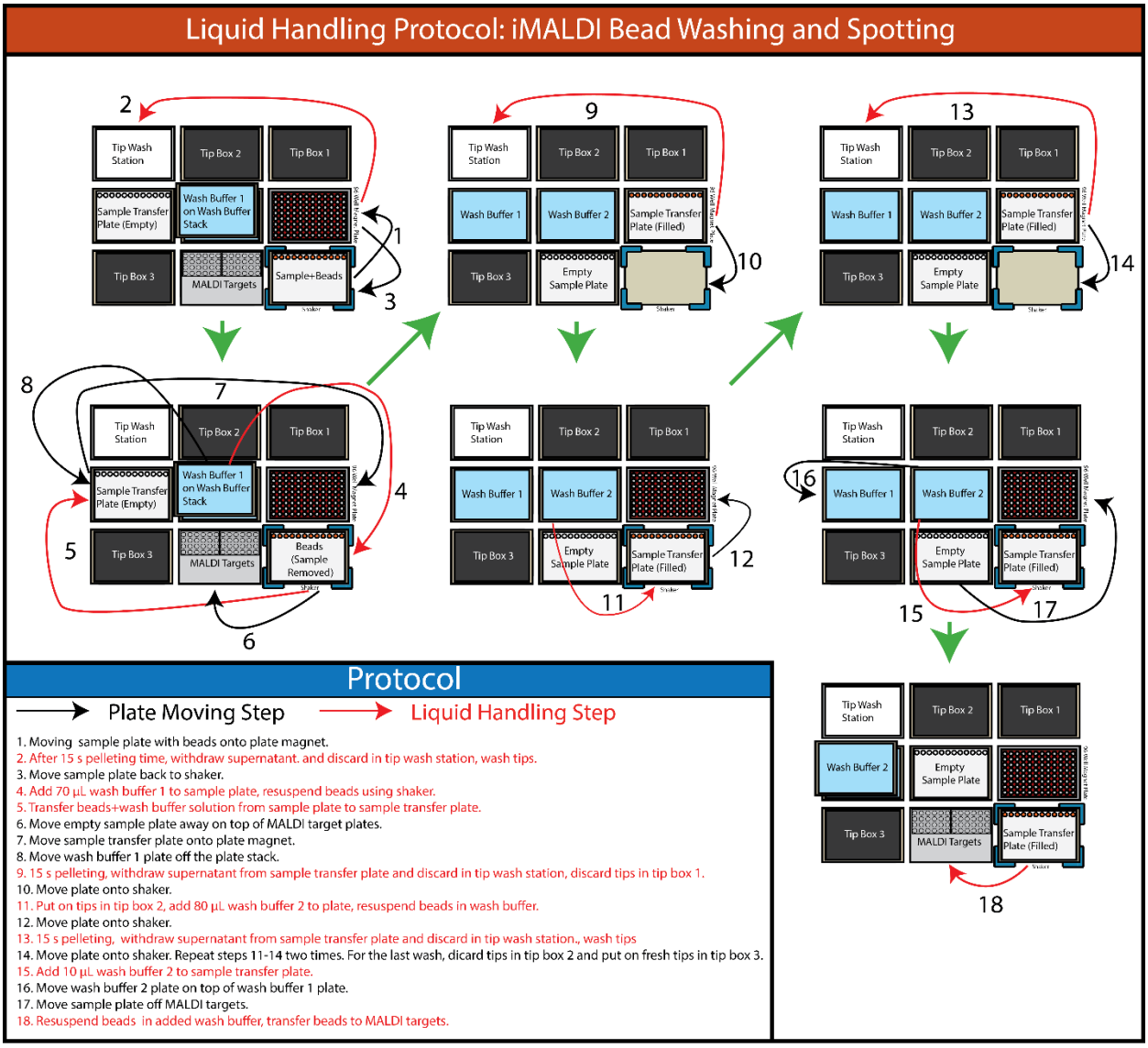

Supporting Figure S 3 Liquid handling protocol for washing antigen-antibody-bead complex and spotting the loaded beads onto a MALDI Plate using a Bravo 96 LT liquid handling robot (Agilent Technologies).

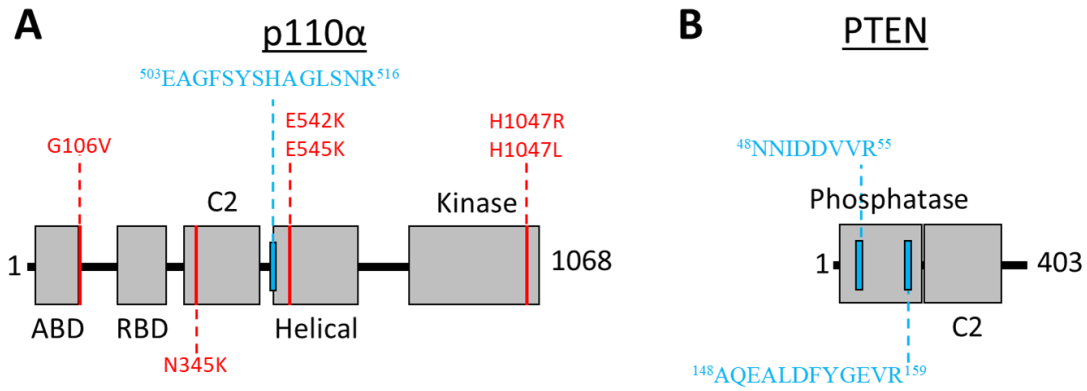

Supporting Figure S 4 Overview of PI3K p110α and PTEN protein sequences. A: Overview of p110α sequence, showing functional domains, examples of common 'hot spot' mutations frequently found in various cancers[238,239], as well as the location of the proteotypic peptide used for iMALDI assay development. ABD= Adapter-binding domain, RBD= Ras-binding domain, C2= C2-domain, Helical= Helical domain, Kinase= Lipid kinase domain. B: Overview of PTEN sequence, showing functional domains, as well as the location of the proteotypic peptides used for iMALDI and iMRM assay development. Unlike for p110α, frequent 'hot spot' mutations are less common, with most PTEN mutations consisting of deletions and frame-shift mutations[240] [ref]. Phosphatase= Phosphatase domain, C2= C2 domain.

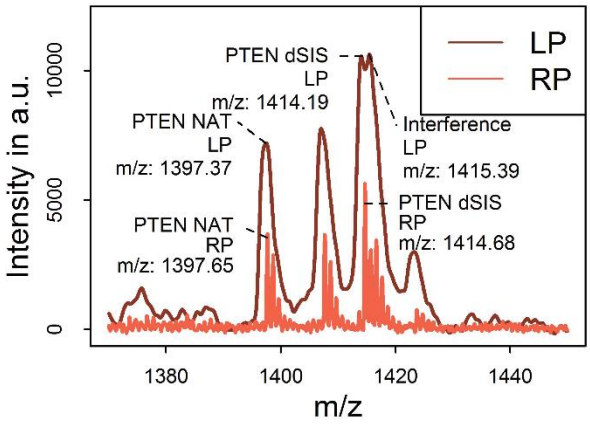

Supporting Figure S 5. Overlaid mass spectra of 2.5 fmol NAT calibration standard prepared in E.coli digest recorded in both linear (LP, dark red) and reflectron (RP, light red) mode, showing a background peak overlapping with the SIS peak in the linear mode. This interference affects PTEN quantification.

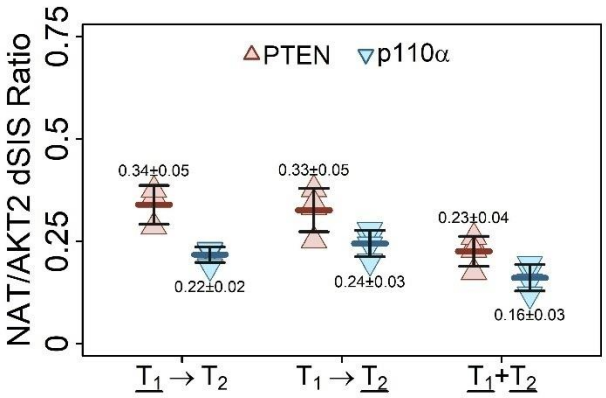

Supporting Figure S 6 Comparison of sequential ($\underline{T_1}\rightarrow T_2$ or $T_1\rightarrow\underline{T_2}$) and simultaneous enrichment of PTEN and p110α NAT peptides ($\underline{T_1}+\underline{T_2}$). Peptide intensities were normalized using 1 fmol AKT2 dSIS which was spiked into the MALDI matrix. A slightly lower recovery was detected for simultaneous enrichment, but was not significant ($p>0.01$).

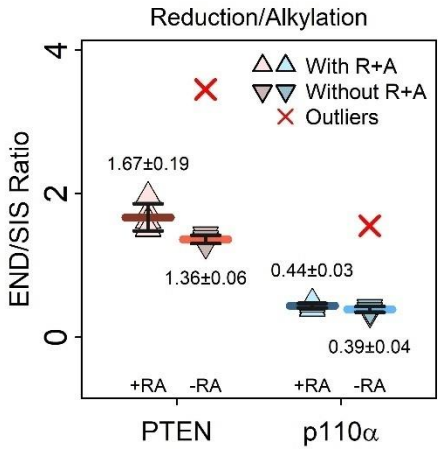

Supporting Figure S 7 Reduction and alkylation (+RA) of disulfide bonds prior to tryptic digest does not significantly alter PTEN and p110α recovery. Ten µg MDA-MB-231 lysate (total protein) with (+RA) and without reduction and alkylation (-RA) were analyzed by multiplexed iMALDI (n=5). Error bars represent absolute standard deviation; horizontal bars represent the mean. * An outlier (END/SIS Ratio > 3rd quartile+3x Interquartile Range) was excluded due to a potential contamination observed in the MALDI-TOF spectrum.

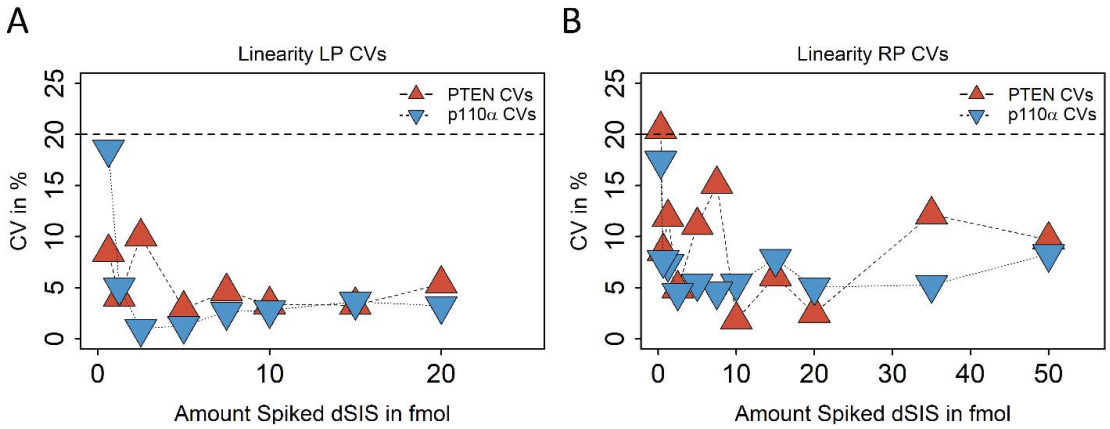

Supporting Figure S 8 CVs of calibration curves presented in figure 2B and Supplementary Figure S1A, and which were used to assess linearity. Ten µg of MDA-MB 231 digest per replicate were spiked with 0-50 fmol PTEN+p110α dSIS peptides and 2.5 fmol PTEN and p110α SIS. The CVs of the normalized signals for each tested standard is shown. N=3 per concentration. Data recorded in (A) linear and (B) reflectron mode, showing that CVs were consistently below 20%.

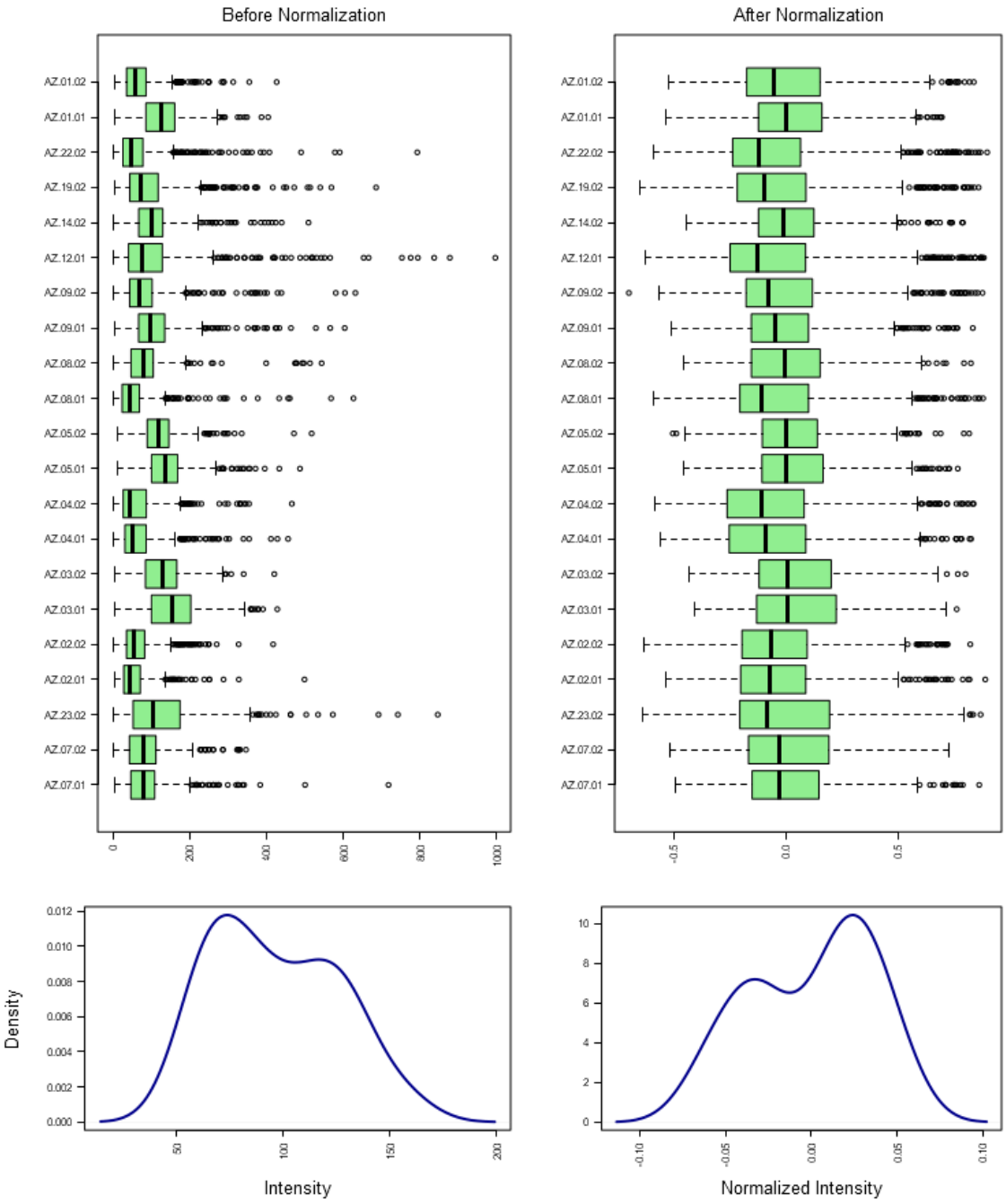

Supporting Figure S 9. Normalization of untargeted proteomics data. Data nomalization, scaling and visualization was done using Metaboanalyst.

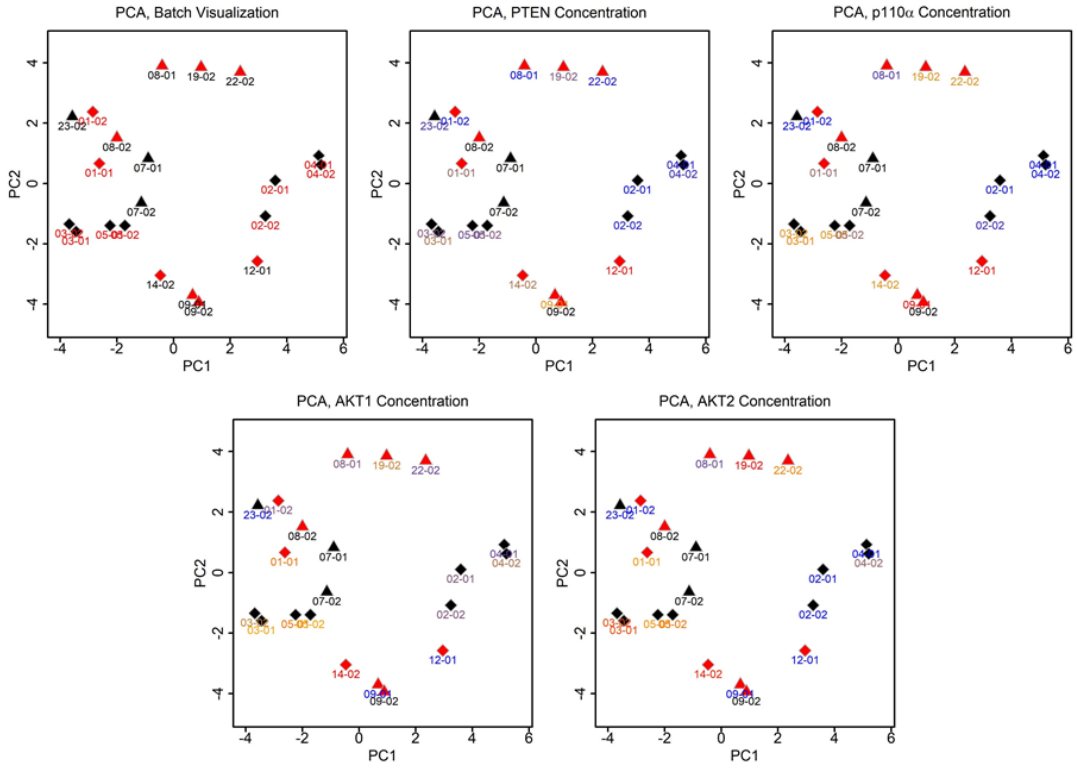

Supporting Figure S 10. Principle component analysis of untargeted proteomics data from FFPE tissue samples from patients treated with AZD5363. Samples are represented as colored shapes representing their tissue type. Triangles represent breast cancer tissue, rhombuses represent gynecological cancer tissue. Red filling represents responders, black filling represents non-responders. Patient ID's below the data points are colored based on which batch the sample was analysed in (1 or 2), or their PTEN/p110α/AKT1+2 concentration as determined by iMALDI (blue=lowest, red= highest, black= no data).

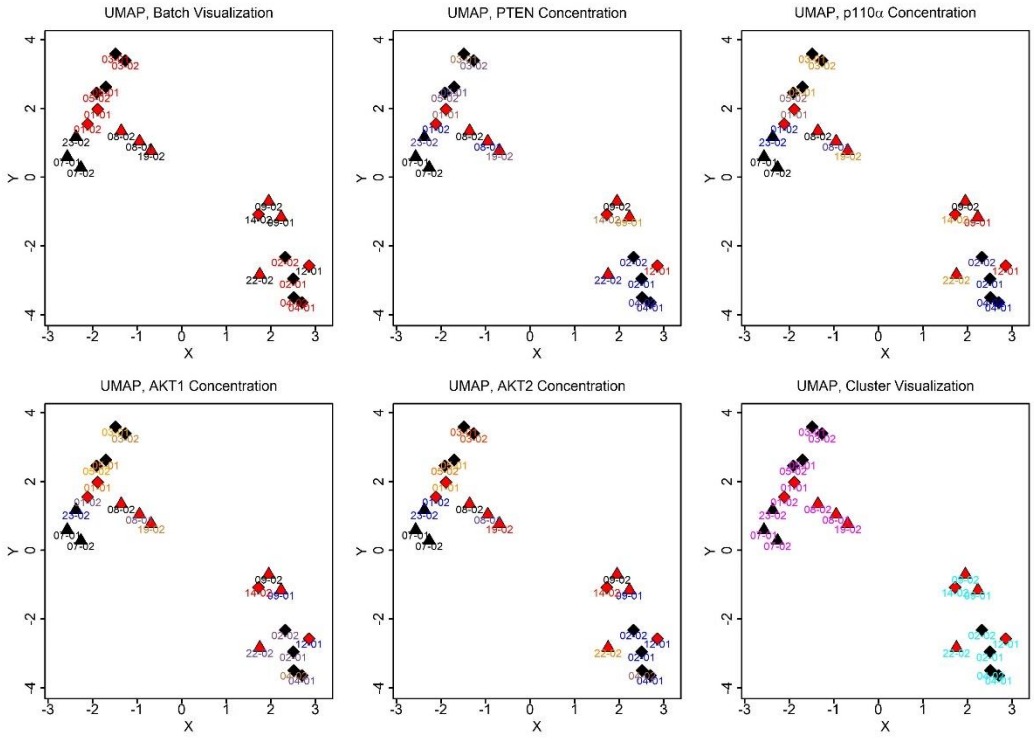

Supporting Figure S 11. Uniform Manifold Approximation and Projection of untargeted proteomics data from FFPE tissue samples from patients treated with AZD5363. Samples are represented as colored shapes representing their tissue type. Triangles represent breast cancer tissue, rhombuses represent gynecological cancer tissue. Red filling represents responders, black filling represents non-responders. Patient ID's below the data points are colored based on which batch the sample was analysed in (1 or 2), their PTEN/p110α/AKT1+2 concentration as determined by iMALDI (blue=lowest, red= highest, black= no data), or based on clustering results by HDBSCAN.

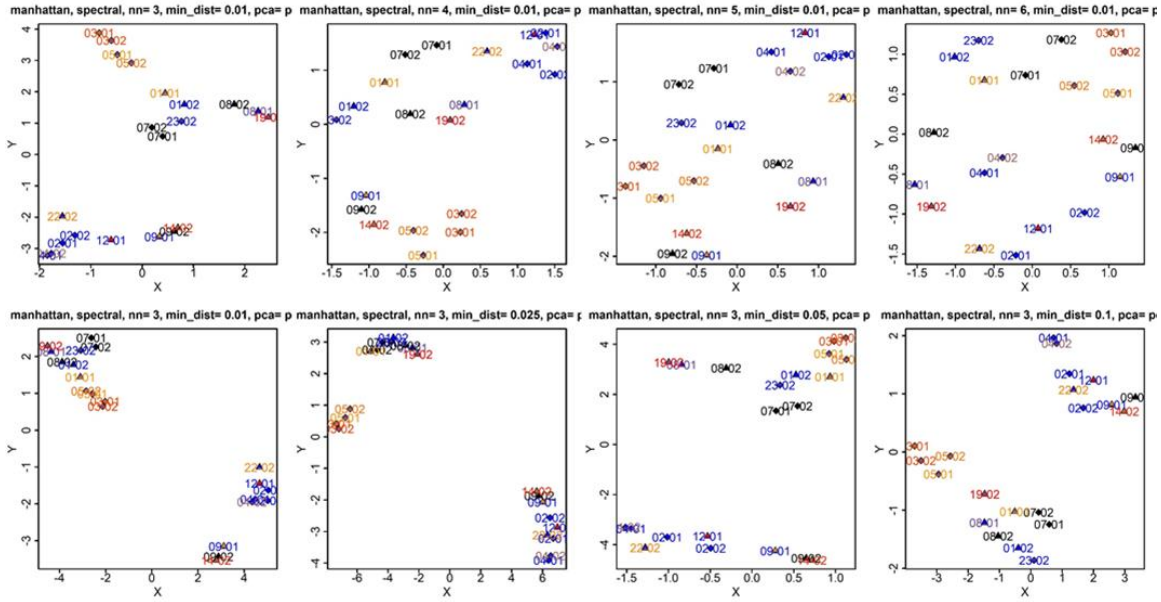

Supporting Figure S 12. Optimization of Uniform Manifold Approximation and Projection of untargeted proteomics data from FFPE tissue samples from patients treated with AZD5363. Samples are labeled based on their sample ID and colored according to their respective AKT1 concentration as determined by iMALDI (blue=lowest, red= highest, black= no data)

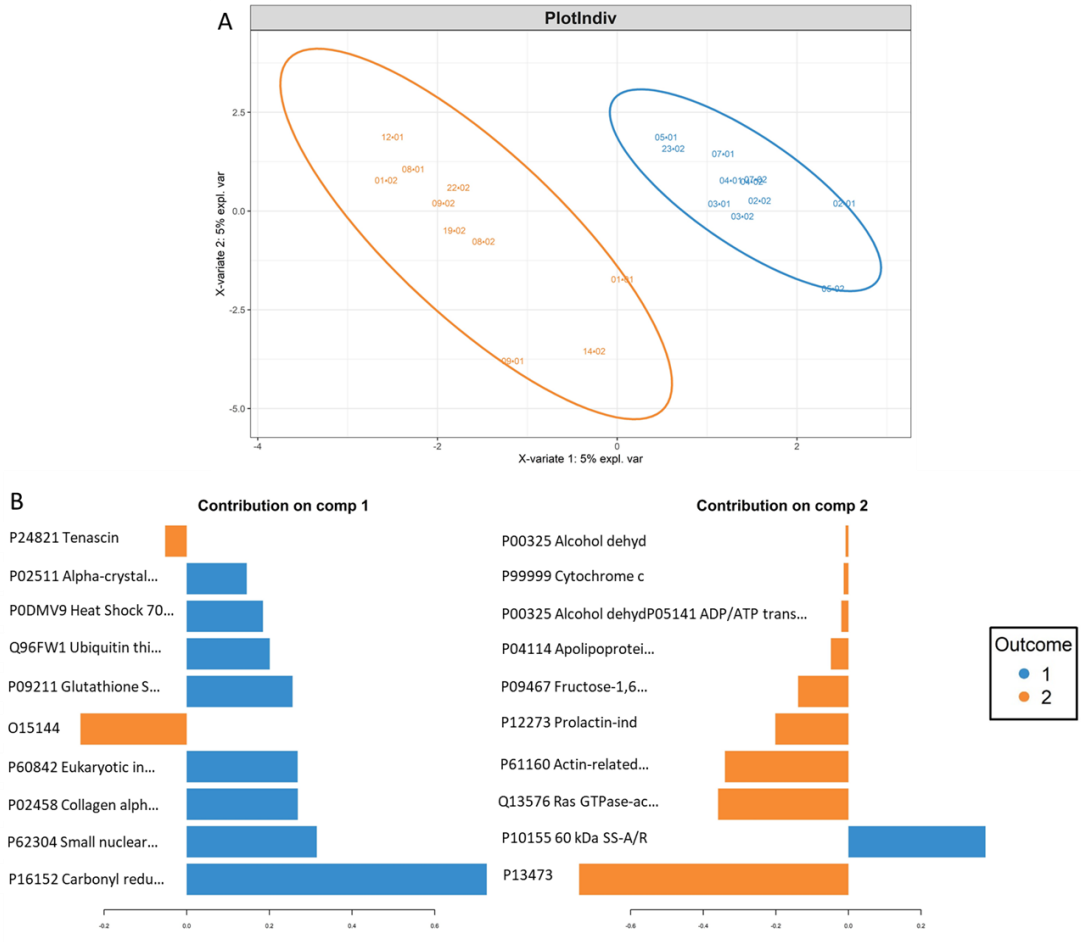

Supporting Figure S 13. sPLSDA of untargeted proteomics data from FFPE tissue samples from patients treated with AZD5363 comparing responders and non-responders. Data analysis and visualtion was done using Metaboanalyst.

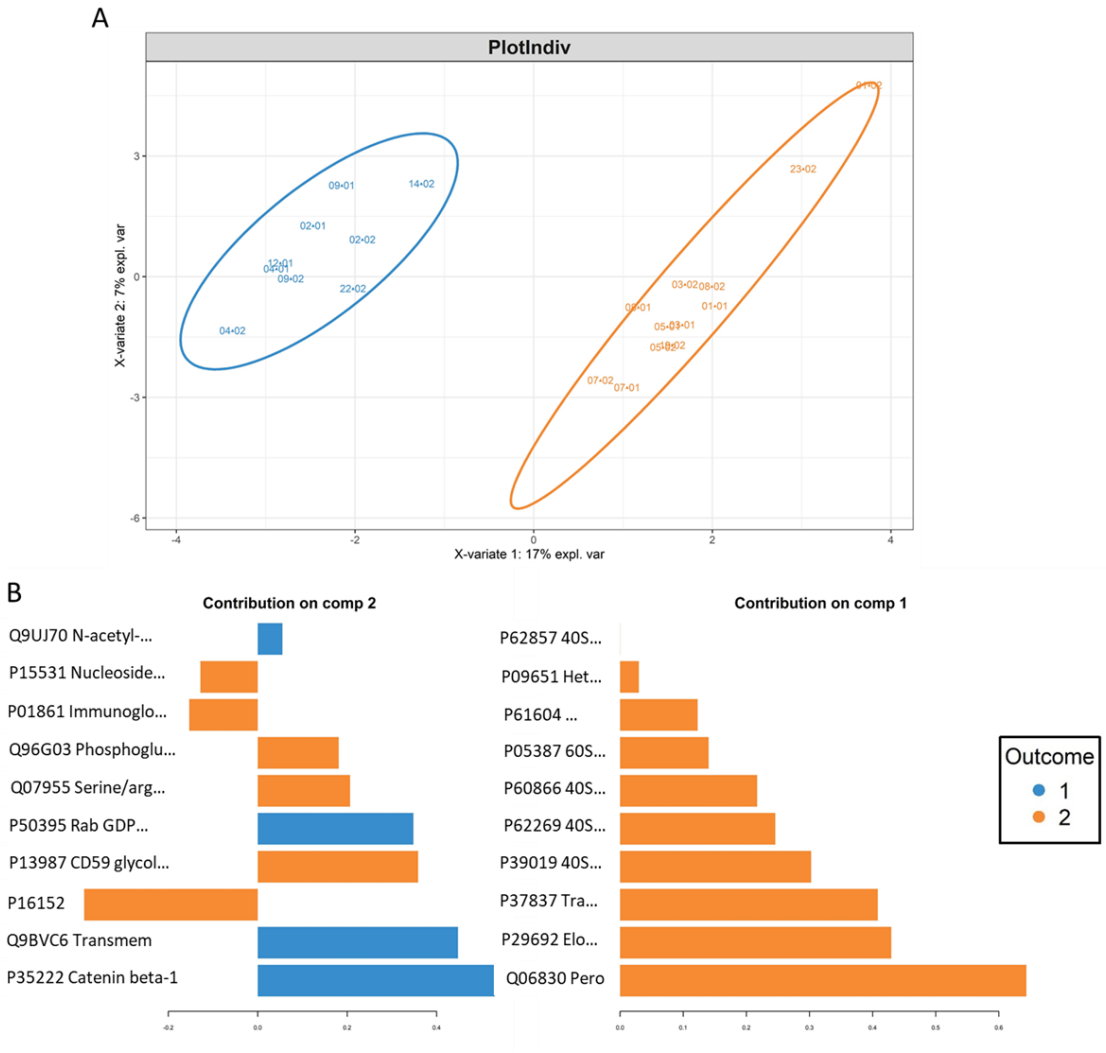

Supporting Figure S 14. sPLSDA of untargeted proteomics data from FFPE tissue samples from patients treated with AZD5363 comparing clusters identified by UMAP analysis. Data analysis and visualtion was done using Metaboanalyst.

Appendix 2

Supporting Table S 1. Comparison of generated polyclonal antibodies (pAb), showing peak intensities (*) for endogenous PTEN+p110α target peptide (END) and the internal standard (dSIS), as well as their peak ratios (#).

				Replicate					
	Experiment	**Peptide**	**pAb #**	**1**	**2**	**3**	**4**	**Mean**	**CV in %**
1	PTEN pAb	NAT*	1	469	704	1085	696	738	35
2	PTEN pAb	AKT 2 dSIS*	1	208	424	635	263	382	50
3	PTEN pAb	NAT/dSIS#	1	2.25	1.66	1.71	2.65	2.07	23
4	PTEN pAb	NAT*	2	322	477	653	442	473	29
5	PTEN pAb	AKT 2 dSIS*	2	218	240	469	303	307	37
6	PTEN pAb	NAT/dSIS #	2	1.48	1.99	1.39	1.46	1.58	17
7	p110α pAb	NAT*	1	555	913	875	871	803	21
8	p110α pAb	AKT 2 dSIS*	1	198	457	501	475	408	35
9	p110α pAb	NAT/dSIS#	1	2.80	2.00	1.74	1.83	2.10	23
10	p110α pAb	NAT*	2	654	854	842	707	764	13
11	p110α pAb	AKT 2 dSIS*	2	323	396	454	417	397	14
12	p110α pAb	NAT/dSIS #	2	2.02	2.16	1.86	1.69	1.93	10

Supporting Table S 2. Comparison of automated versus manual washing of antigen-antibody-bead complex, showing peak intensities (*) for PTEN+p110α dSIS and AKT2 dSIS (internal standard), as well as their peak ratios (#).(#).

				Replicate						
	Wash	**Protein**	**Peptide**	**1**	**2**	**3**	**4**	**5**	**Mean**	**CV in %**
1	Manual	PTEN	dSIS*	2336	2100	2628	2618	2014	2339	12
2	Manual	PTEN	AKT2 dSIS*	2187	1769	1929	2128	1436	1890	16
3	Manual	PTEN	dSIS/AKT2 dSIS#	1.07	1.19	1.36	1.23	1.40	1.25	11
4	Manual	p110α	dSIS*	1203	1214	1649	1499	1087	1330	18
5	Manual	p110α	AKT2 dSIS*	2187	1769	1929	2128	1436	1890	16
6	Manual	p110α	dSIS/AKT2 dSIS#	0.55	0.69	0.85	0.70	0.76	0.71	15
7	Automated	PTEN	dSIS*	2797	2097	3252	1913	2671	2546	21
8	Automated	PTEN	AKT2 dSIS*	2416	1510	2655	1766	2043	2078	22
9	Automated	PTEN	dSIS/AKT2 dSIS#	1.16	1.39	1.22	1.08	1.31	1.23	10
10	Automated	p110α	dSIS*	1478	956	1557	888	1082	1192	26
11	Automated	p110α	AKT2 dSIS*	2416	1510	2655	1766	2043	2078	22
12	Automated	p110α	dSIS/AKT2 dSIS#	0.61	0.63	0.59	0.50	0.53	0.57	9

Supporting Table S 3. Optimization of tryptic digestion using MDA-MB 231 cell lysate, showing peak intensities (*) for endogenous PTEN+p110α target peptide (END) and the internal standard (dSIS), as well as their peak ratios (#), for different incubation times (IT) and protein:trypsin ratios (P:T). (#).(#).

					Replicate					
	IT in h	**P:T**	**Protein**	**Peptide**	**1**	**2**	**3**	**4**	**Mean**	**CV in %**
1	0.5	10:1	PTEN	END*	3376	3579	5666	7120	4935	36
2	0.5	10:1	PTEN	dSIS*	3017	3617	5334	6435	4601	34
3	0.5	10:1	PTEN	END/dSIS#	1.12	0.99	1.06	1.11	1.07	5
4	1	10:1	PTEN	END*	4600	4974	6175	6618	5592	17
5	1	10:1	PTEN	dSIS*	3944	4885	6016	6387	5308	21
6	1	10:1	PTEN	END/dSIS#	1.17	1.02	1.03	1.04	1.06	7
7	2	10:1	PTEN	END*	4758	3064	6413	6013	5062	30
8	2	10:1	PTEN	dSIS*	3916	2913	5859	5611	4575	31
9	2	10:1	PTEN	END/dSIS#	1.22	1.05	1.09	1.07	1.11	7
10	4	10:1	PTEN	END*	3432	4737	6411	6844	5356	29
11	4	10:1	PTEN	dSIS*	2874	4003	5632	6036	4636	32
12	4	10:1	PTEN	END/dSIS#	1.19	1.18	1.14	1.13	1.16	3
13	0.5	1:2	PTEN	END*	3441	3771	5264	3642	4029	21
14	0.5	1:2	PTEN	dSIS*	2625	2480	3768	3426	3075	20
15	0.5	1:2	PTEN	END/dSIS#	1.31	1.52	1.40	1.06	1.32	15
16	1	1:2	PTEN	END*	3752	2895	6018	5385	4513	32
17	1	1:2	PTEN	dSIS*	2679	2049	4170	3803	3175	31
18	1	1:2	PTEN	END/dSIS#	1.40	1.41	1.44	1.42	1.42	1
19	2	1:2	PTEN	END*	6111	3520	5551	7841	5756	31
20	2	1:2	PTEN	dSIS*	4349	2587	4025	5249	4053	27
21	2	1:2	PTEN	END/dSIS#	1.40	1.36	1.38	1.49	1.41	4
22	4	1:2	PTEN	END*	4654	3202	5476	4458	4447	21
23	4	1:2	PTEN	dSIS*	3185	2140	3638	2798	2940	22
24	4	1:2	PTEN	END/dSIS#	1.46	1.50	1.51	1.59	1.51	4
25	0.5	10:1	p110α	END*	803	1035	1575	1884	1324	37
26	0.5	10:1	p110α	dSIS*	2444	3108	4213	5626	3848	36
27	0.5	10:1	p110α	END/dSIS#	0.33	0.33	0.37	0.33	0.34	6
28	1	10:1	p110α	END*	1656	1133	2308	1477	1644	30
29	1	10:1	p110α	dSIS*	4884	3590	6225	4695	4848	22
30	1	10:1	p110α	END/dSIS#	0.34	0.32	0.37	0.31	0.34	8
31	2	10:1	p110α	END*	1902	1555	2209	1904	1893	14
32	2	10:1	p110α	dSIS*	5089	4571	6029	5352	5260	12
33	2	10:1	p110α	END/dSIS#	0.37	0.34	0.37	0.36	0.36	4
34	4	10:1	p110α	END*	1336	1690	2266	1875	1792	22
35	4	10:1	p110α	dSIS*	3843	5116	6654	4792	5101	23
36	4	10:1	p110α	END/dSIS#	0.35	0.33	0.34	0.39	0.35	8
37	0.5	1:2	p110α	END*	691	802	801	835	782	8

38	0.5	1:2	p110α	dSIS*	1738	2697	2464	2162	2265	18
39	0.5	1:2	p110α	END/dSIS[#]	0.40	0.30	0.33	0.39	0.35	14
40	1	1:2	p110α	END*	1261	2026	1876	1289	1613	25
41	1	1:2	p110α	dSIS*	2694	4241	4607	3210	3688	24
42	1	1:2	p110α	END/dSIS[#]	0.47	0.48	0.41	0.40	0.44	9
43	2	1:2	p110α	END*	2734	1163	2197	2038	2033	32
44	2	1:2	p110α	dSIS*	5524	2489	5564	4114	4423	33
45	2	1:2	p110α	END/dSIS[#]	0.50	0.47	0.39	0.50	0.46	10
46	4	1:2	p110α	END*	1171	2041	2132	2542	1971	29
47	4	1:2	p110α	dSIS*	2322	4094	4667	5012	4024	30
48	4	1:2	p110α	END/dSIS[#]	0.50	0.50	0.46	0.51	0.49	5

Supporting Table S 4. Testing different calibration strategies, showing endogenous PTEN and p110α enriched from in MDA-MB 231 lysate. Peak intensities (*) for endogenous PTEN+p110α target peptide (END) and dSIS (internal standard) as well as their peak ratios (#) are shown.

					Replicate					
	Protein	**MS Mode**	**Peptide**	**Peak Parameter**	**1**	**2**	**3**	**4**	**Mean**	**CV in %**
1	PTEN	Linear	END*	Intensity	7574	4083	4259	4565	5120	32
2	PTEN	Linear	END*	S/N Ratio	15.00	10.47	9.58	13.32	12.09	21
3	PTEN	Linear	END*	Area	23948	11443	12170	12767	15082	39
4	PTEN	Linear	dSIS*	Intensity	5611	3469	3569	3585	4058	26
5	PTEN	Linear	dSIS*	S/N Ratio	11.11	8.89	8.02	10.46	9.62	15
6	PTEN	Linear	dSIS*	Area	17814	9402	10101	10388	11926	33
7	PTEN	Linear	END/dSIS#	Intensity	1.35	1.18	1.19	1.27	1.25	6
8	PTEN	Linear	END/dSIS#	S/N Ratio	1.35	1.18	1.19	1.27	1.25	6
9	PTEN	Linear	END/dSIS#	Area	1.34	1.22	1.20	1.23	1.25	5
10	PTEN	Reflectron	END*	Intensity	8107	4916	3106	2656	4696	53
11	PTEN	Reflectron	END*	S/N Ratio	47.65	33.42	26.15	24.81	33.01	32
12	PTEN	Reflectron	END*	Area	6943	3781	2778	2037	3885	56
13	PTEN	Reflectron	dSIS*	Intensity	4744	3239	1921	1794	2924	47
14	PTEN	Reflectron	dSIS*	S/N Ratio	28.08	22.23	16.26	16.82	20.85	27
15	PTEN	Reflectron	dSIS*	Area	4002	2430	1640	1322	2349	51
16	PTEN	Reflectron	END/dSIS#	Intensity	1.71	1.52	1.62	1.48	1.58	7
17	PTEN	Reflectron	END/dSIS#	S/N Ratio	1.70	1.50	1.61	1.48	1.57	6
18	PTEN	Reflectron	END/dSIS#	Area	1.73	1.56	1.69	1.54	1.63	6
19	p110α	Linear	END*	Intensity	4529	2344	2528	2465	2966	35
20	p110α	Linear	END*	S/N Ratio	9.26	6.03	5.74	7.36	7.10	23
21	p110α	Linear	END*	Area	16745	7629	8445	7826	10161	43
22	p110α	Linear	dSIS*	Intensity	9682	4819	6150	5823	6618	32
23	p110α	Linear	dSIS*	S/N Ratio	20.57	12.56	13.77	17.85	16.18	23
24	p110α	Linear	dSIS*	Area	41746	17445	20189	18605	24496	47
25	p110α	Linear	END/dSIS#	Intensity	0.47	0.49	0.41	0.42	0.45	8
26	p110α	Linear	END/dSIS#	S/N Ratio	0.45	0.48	0.42	0.41	0.44	7
27	p110α	Linear	END/dSIS#	Area	0.40	0.44	0.42	0.42	0.42	4
28	p110α	Reflectron	END*	Intensity	3759	2018	1461	839	2019	62
29	p110α	Reflectron	END*	S/N Ratio	23.35	14.11	12.70	8.23	14.60	44
30	p110α	Reflectron	END*	Area	5395	2783	2498	1304	2995	58
31	p110α	Reflectron	dSIS*	Intensity	7812	4357	2661	1980	4202	62
32	p110α	Reflectron	dSIS*	S/N Ratio	48.81	30.56	23.33	19.58	30.57	42
33	p110α	Reflectron	dSIS*	Area	7368	3568	2637	1502	3769	68
34	p110α	Reflectron	END/dSIS#	Intensity	0.48	0.46	0.55	0.42	0.48	11
35	p110α	Reflectron	END/dSIS#	S/N Ratio	0.48	0.46	0.54	0.42	0.48	11
36	p110α	Reflectron	END/dSIS#	Area	0.73	0.78	0.95	0.87	0.83	11

Supporting Table S 5. Testing different calibration strategies, showing quantified endogenous PTEN and p110a amounts (in µg) in 10 µg MDA-MB 231 lysate using calibrations prepared in different calibration matrices and using different peak parameters.

					Replicate					
	Cal. Matrix	**Peak Parameter**	**Protein**	**MS Mode**	**1**	**2**	**3**	**4**	**Mean**	**CV in %**
1	PBSC	S/N Ratio	PTEN	Linear	4.4	3.8	3.9	4.2	4.1	7
2	PBSC	Intensity	PTEN	Linear	4.4	3.8	3.9	4.2	4.1	7
3	PBSC	Area	PTEN	Linear	4.6	4.2	4.1	4.2	4.3	5
4	BSA	S/N Ratio	PTEN	Linear	4.7	4.1	4.2	4.4	4.3	6
5	BSA	Intensity	PTEN	Linear	4.7	4.1	4.2	4.4	4.3	6
6	BSA	Area	PTEN	Linear	4.7	4.3	4.2	4.3	4.4	5
7	E.coli digest	S/N Ratio	PTEN	Linear	6.2	5.4	5.5	5.8	5.7	6
8	E.coli digest	Intensity	PTEN	Linear	6.2	5.4	5.5	5.8	5.7	6
9	E.coli digest	Area	PTEN	Linear	6.7	6.1	6.1	6.2	6.3	5
10	PBSC	S/N Ratio	PTEN	Reflectron	3.9	3.5	3.7	3.4	3.6	6
11	PBSC	Intensity	PTEN	Reflectron	3.9	3.5	3.7	3.4	3.6	6
12	PBSC	Area	PTEN	Reflectron	3.5	3.2	3.4	3.2	3.3	5
13	BSA	S/N Ratio	PTEN	Reflectron	3.9	3.5	3.7	3.4	3.6	6
14	BSA	Intensity	PTEN	Reflectron	3.9	3.5	3.7	3.4	3.6	6
15	BSA	Area	PTEN	Reflectron	3.5	3.2	3.4	3.2	3.3	5
16	E.coli digest	S/N Ratio	PTEN	Reflectron	4	3.6	3.8	3.6	3.8	5
17	E.coli digest	Intensity	PTEN	Reflectron	4	3.6	3.8	3.6	3.8	5
18	E.coli digest	Area	PTEN	Reflectron	4	3.6	3.9	3.6	3.8	6
19	PBSC	S/N Ratio	p110α	Linear	1.3	1.4	1.2	1.2	1.3	8
20	PBSC	Intensity	p110α	Linear	1.3	1.4	1.2	1.2	1.3	8
21	PBSC	Area	p110α	Linear	1.1	1.2	1.2	1.2	1.2	4
22	BSA	S/N Ratio	p110α	Linear	1.3	1.3	1.2	1.2	1.2	5
23	BSA	Intensity	p110α	Linear	1.3	1.3	1.1	1.2	1.2	8
24	BSA	Area	p110α	Linear	1.1	1.2	1.1	1.1	1.1	4
25	E.coli digest	S/N Ratio	p110α	Linear	1.2	1.3	1.2	1.1	1.2	7
26	E.coli digest	Intensity	p110α	Linear	1.3	1.3	1.1	1.2	1.2	8
27	E.coli digest	Area	p110α	Linear	1.1	1.2	1.1	1.1	1.1	4
28	PBSC	S/N Ratio	p110α	Reflectron	1.1	1	1.2	1	1.1	9
29	PBSC	Intensity	p110α	Reflectron	1.1	1	1.2	1	1.1	9
30	PBSC	Area	p110α	Reflectron	2.8	2.5	2.7	2.5	2.6	6
31	BSA	S/N Ratio	p110α	Reflectron	1.2	1.1	1.3	1.1	1.2	8
32	BSA	Intensity	p110α	Reflectron	1.2	1.1	1.3	1.1	1.2	8
33	BSA	Area	p110α	Reflectron	1.4	1.5	1.7	1.6	1.6	8
34	E.coli digest	S/N Ratio	p110α	Reflectron	1.1	1.1	1.2	1.1	1.1	4
35	E.coli digest	Intensity	p110α	Reflectron	1.1	1.1	1.2	1.1	1.1	4
36	E.coli digest	Area	p110α	Reflectron	1.4	1.4	1.7	1.6	1.5	10

Supporting Table S 6. Testing different calibration strategies, showing the linear regressions calculated from calibrations prepared in different calibration matrices and using different peak parameters.

				Linear Mode			Reflectron Mode		
	Protein	**Calibration Matrix**	**Peak Parameter**	**Intercept**	**Slope**	**R^2**	**Intercept**	**Slope**	**R^2**
1	PTEN	E.coli digest	Intensity	-0.22	0.58	0.87	-0.69	1.24	0.97
2	PTEN	E.coli digest	S/N	-0.21	0.58	0.87	-0.69	1.23	0.97
3	PTEN	E.coli digest	Area	-0.18	0.53	0.86	-0.69	1.27	0.98
4	PTEN	BSA digest	Intensity	-0.06	0.73	0.99	-0.83	1.33	0.98
5	PTEN	BSA digest	S/N	-0.06	0.73	0.99	-0.83	1.32	0.98
6	PTEN	BSA digest	Area	-0.02	0.71	0.99	-1.06	1.54	0.97
7	PTEN	PBSC	Intensity	0.17	0.72	0.95	-0.6	1.26	1
8	PTEN	PBSC	S/N	0.17	0.72	0.95	-0.59	1.24	0.99
9	PTEN	PBSC	Area	0.31	0.66	0.94	-0.81	1.47	0.99
10	p110a	E.coli digest	Intensity	-0.1	0.99	0.99	-0.8	1.76	0.98
11	p110a	E.coli digest	S/N	-0.1	0.99	0.99	-0.8	1.75	0.98
12	p110a	E.coli digest	Area	-0.04	0.95	0.98	-0.92	1.98	0.99
13	p110a	BSA digest	Intensity	-0.04	0.94	0.99	-0.79	1.72	0.99
14	p110a	BSA digest	S/N	-0.05	0.92	0.99	-0.78	1.71	0.99
15	p110a	BSA digest	Area	0.02	0.93	1	-1.14	2.07	0.98
16	p110a	PBSC	Intensity	-0.02	0.9	0.98	-0.37	1.47	0.99
17	p110a	PBSC	S/N	0	0.89	0.98	-0.36	1.46	0.99
18	p110a	PBSC	Area	0.06	0.85	0.96	-0.75	1.85	1

Supporting Table S 7. Comparison of different bead types for iMALDI, showing peak S/N ratios for PTEN+p110α dSIS. For calculating the mean and CV, not detected (n.d.) peaks were treated as 0.

				Replicates					
	MALDI Target Size	**Bead Type**	**Protein**	**1**	**2**	**3**	**4**	**Mean**	**CV in %**
1	2600 µm	Protein G Dynabeads	PTEN	24	16	19	19	20	17
2	2600 µm	Protein G Dynabeads	p110α	24	13	14	15	17	30
3	2600 µm	M280 Tosylactivated	PTEN	6	n.d.	n.d.	4	2.5	119
4	2600 µm	M280 Tosylactivated	p110α	6	n.d.	3	4	3	76
5	2600 µm	MagReSyn Protein G	PTEN	13	10	8	9	10	22
6	2600 µm	MagReSyn Protein G	p110α	20	20	19	16	19	10
7	700 µm	Protein G Dynabeads	PTEN	n.d.	4	4	n.d.	2	115
8	700 µm	Protein G Dynabeads	p110α	3	n.d.	3	n.d.	2	116
9	700 µm	M280 Tosylactivated	PTEN	n.d.	n.d.	n.d.	n.d.	n.d.	n.d.
10	700 µm	M280 Tosylactivated	p110α	n.d.	n.d.	n.d.	n.d.	n.d.	n.d.
11	700 µm	MagReSyn Protein G	PTEN	13	10	23	11	14	43
12	700 µm	MagReSyn Protein G	p110α	7	6	13	8	8	34

Supporting Table S 8. Comparison of direct and indirect immuno-enrichment, showing peak intensities (*) for PTEN NAT and AKT2 dSIS (internal standard), as well as their peak ratios (#). Replicate #2 for direct immuno-enrichment (labeled in red) was excluded for calculating mean and CV values.

			Replicates							
	Enrichment	**Peptide**	**1**	**2**	**3**	**4**	**5**	**6**	**Mean**	**CV in %**
1	Direct	NAT*	863	1119	911	893	1179	926	954	13
2	Direct	AKT2 dSIS*	1973	1751	2473	2190	2956	2443	2407	15
3	Direct	NAT/AKT2 dSIS#	0.44	0.64	0.37	0.41	0.40	0.38	0.40	7
4	Indirect	NAT*	1307	1598	1274	1573	1086	1466	1384	14
5	Indirect	AKT2 dSIS*	4114	5277	4572	5483	4051	6132	4938	17
6	Indirect	NAT/AKT2 dSIS#	0.32	0.3	0.28	0.29	0.27	0.24	0.28	10

Supporting Table S 9. Testing different incubation times, temperatures and mixing conditions, showing peak intensities (*) for PTEN+p110α NAT and AKT2 dSIS (internal standard), as well as their peak ratios (#). Inc. Cond.= Incubation Condition, Prot.= Protein, Rot=rotating, RT= room temperature.

				Replicates											
	Inc. Cond.	**Prot.**	**Peptide**	**1**	**2**	**3**	**4**	**5**	**6**	**7**	**8**	**9**	**10**	**Mean**	**CV in %**
1	1 h rot	PTEN	NAT*	984	1537	1504	1562	2448	1109	1497	1520	2449	2316	1693	31
2	1 h rot	PTEN	AKT2 dSIS*	1550	2610	2516	2455	3791	1974	2090	2400	4274	3738	2740	33
3	1 h rot	PTEN	NAT/AKT2 dSIS#	0.63	0.59	0.60	0.64	0.65	0.56	0.72	0.63	0.57	0.62	0.62	7
4	1 h shake	PTEN	NAT*	1280	1721	1996	1620	1721	1880					1703	14
5	1 h shake	PTEN	AKT2 dSIS*	1831	2734	3303	3096	2490	2841					2716	19
6	1 h shake	PTEN	NAT/AKT2 dSIS#	0.70	0.63	0.60	0.52	0.69	0.66					0.63	10
7	22 h 4° C	PTEN	NAT*	1952	1244	1819	2598	2781	2186	2455	1328	2086	2164	2061	24
8	22 h 4° C	PTEN	AKT2 dSIS*	2382	1573	2307	2966	3253	2814	2966	1912	2839	2515	2553	20
9	22 h 4° C	PTEN	NAT/AKT2 dSIS#	0.82	0.79	0.79	0.88	0.86	0.78	0.83	0.69	0.73	0.86	0.80	7
10	22 h RT	PTEN	NAT*	1759	2108	2001	1802	1972	2247	2148	1984	2228	2430	2068	10
11	22 h RT	PTEN	AKT2 dSIS*	1942	2460	2097	1967	2275	2411	2203	1975	2445	2611	2239	11
12	22 h RT	PTEN	NAT/AKT2 dSIS#	0.91	0.86	0.95	0.92	0.87	0.93	0.98	1.00	0.91	0.93	0.93	5
13	1 h rot	p110α	NAT*	903	1601	1451	1524	2211	1062	1288	1338	2599	2392	1637	35
14	1 h rot	p110α	AKT2 dSIS*	1550	2610	2516	2455	3791	1974	2090	2400	4274	3738	2740	33
15	1 h rot	p110α	NAT/AKT2 dSIS#	0.58	0.61	0.58	0.62	0.58	0.54	0.62	0.56	0.61	0.64	0.59	5
16	1 h shake	p110α	NAT*	1356	1824	2218	2125	1904	2093					1920	16
17	1 h shake	p110α	AKT2 dSIS*	1831	2734	3303	3096	2490	2841					2716	19
18	1 h shake	p110α	NAT/AKT2 dSIS#	0.74	0.67	0.67	0.69	0.76	0.74					0.71	6
19	22 h 4° C	p110α	NAT*	2526	1175	1995	2625	3578	2597	3074	1618	2714	2581	2448	28
20	22 h 4° C	p110α	AKT2 dSIS*	2382	1573	2307	2966	3253	2814	2966	1912	2839	2515	2553	20
21	22 h 4° C	p110α	NAT/AKT2 dSIS#	1.06	0.75	0.86	0.88	1.10	0.92	1.04	0.85	0.96	1.03	0.94	12
22	22 h RT	p110α	NAT*	1892	2146	1730	1961	1780	1999	2179	1902	2089	2295	1997	9
23	22 h RT	p110α	AKT2 dSIS*	1942	2460	2097	1967	2275	2411	2203	1975	2445	2611	2239	11
24	22 h RT	p110α	NAT/AKT2 dSIS#	0.97	0.87	0.82	1.00	0.78	0.83	0.99	0.96	0.85	0.88	0.90	9

Supporting Table S 10.NAT/SIS peptide intensity ratios of the multiplexing experiments presented in Figure 9 are shown. E.coli lysate digest (10 µg per replicate) was spiked with 1 fmol ('low') or 10 fmol ('high') PTEN+p110α NAT. Peptides were enriched using either singleplex, sequential (i.e. PTEN-p110α or p110α-PTEN, referred to as $T_1 \rightarrow T_2$ or $T_1 \rightarrow T_2$), or simultaneous enrichment (T_1+T_2). Mean NAT/SIS ratios and corresponding standard deviations in fmol are displayed, as well as the corresponding CVs in %. Additionally, the ratio of the mean NAT/SIS ratios using multiplexed assays and the corresponding mean NAT/SIS ratio of the singleplex assay are displayed (e.g. mean NAT/SIS $PTEN_{T1 \rightarrow T2\ High}$ divided by mean NAT/SIS $PTEN_{Singleplex\ High}$). Data was recorded in the linear mode. Both multiplexing methods showed similar performance.

	Peptide	Singleplex High	Singleplex Low	$T_1 \rightarrow T_2$ High	$T_1 \rightarrow T_2$ Low	$T_1 \rightarrow T_2$ High	$T_1 \rightarrow T_2$ Low	$T_1 \rightarrow T_2$ High	$T_1 \rightarrow T_2$ Low
NAT in fmol	-	**10**	**1**	**10**	**1**	**10**	**1**	**10**	**1**
1	PTEN	2	0.3	2.1	-	1.9	0.3	1.9	0.3
2	PTEN	1.5	0.3	1.9	0.3	1.8	0.3	1.8	0.2
3	PTEN	1.9	0.3	2	0.3	2	0.3	1.9	0.3
4	PTEN	1.8	0.3	2	0.3	2	0.2	1.8	0.2
Mean	PTEN	1.8	0.3	2	0.3	1.9	0.3	1.9	0.3
Abs. SD	PTEN	0.2	0.02	0.1	0.01	0.1	0.02	0.1	0.01
CV	PTEN	11.4	8.1	3.5	1.8	4	8.8	3.1	4.4
$\frac{NAT}{SIS}_{Multiplex} / \frac{NAT}{SIS}_{Singleplex}$	PTEN	-	-	1.09	1.07	1.05	1.04	1.02	0.93
1	p110α	4.3	0.5	4.4	0.4	4.5	0.4	4.5	0.4
2	p110α	4.4	0.4	4.1	0.4	5.1	0.4	4.2	0.4
3	p110α	4.5	0.4	4.2	0.4	4.8	0.4	4.4	0.4
4	p110α	4.6	0.4	4.2	0.4	4.8	0.4	4.4	0.4
Mean	p110α	4.5	0.4	4.2	0.4	4.8	0.4	4.4	0.4
Abs. SD	p110α	0.1	0.1	0.2	0.02	0.2	0.03	0.1	0.02
CV	p110α	3	12.9	3.6	5.7	4.9	8	2.7	4.1
$\frac{NAT}{SIS}_{Multiplex} / \frac{NAT}{SIS}_{Singleplex}$	p110α	-	-	0.95	0.93	1.08	0.95	0.99	0.88

Supporting Table S 11 NAT/AKT dSIS peptide intensity ratios of the multiplexing experiments presented in Supporting Figure S 6are displayed. E.coli lysate digest (10 µg per replicate) were spiked with 1 fmol ('low') or 10 fmol ('high') PTEN+p110α NAT. Peptides were enriched using either sequential enrichment (PTEN→p110α or p110α→PTEN, referred to as $\underline{T_1}\rightarrow T_2$ or $T_1\rightarrow\underline{T_2}$) or simultaneous enrichment ($\underline{T_1}+\underline{T_2}$). A constant amount of AKT2 dSIS was spiked into the MALDI matrix (1 fmol per spot). Data was recorded in the linear ion mode. Both multiplexing methods showed similar performance.

	Peptide	$\underline{T_1}\rightarrow T_2$ High	$\underline{T_1}\rightarrow T_2$ Low	$T_1\rightarrow\underline{T_2}$ High	$T_1\rightarrow\underline{T_2}$ Low	$\underline{T_1}+\underline{T_2}$ High	$\underline{T_1}+\underline{T_2}$ Low
NAT in fmol	-	10	1	10	1	10	1
1	PTEN	2.8		3.3	0.3	2.1	0.2
2	PTEN	3.1	0.4	3.5	0.4	2.4	0.3
3	PTEN	3.3	0.4	4.2	0.3	3	0.2
4	PTEN	2.5	0.3	3.5	0.3	2.2	0.2
Mean	PTEN	2.9	0.3	3.6	0.3	2.4	0.2
Abs. SD	PTEN	0.4	0.05	0.4	0.05	0.4	0.04
CV	PTEN	12	14	11	16	16	16
1	p110α	2.9		3.1	0.3	2	0.2
2	P110α	2.9	0.2	3.4	0.3	2.3	0.2
3	p110α	2.8	0.2	3.5	0.2	2.5	0.2
4	p110α	2.7	0.2	3.3	0.2	1.9	0.1
Mean	p110α	2.8	0.2	3.3	0.2	2.2	0.2
Abs. SD	p110α	0.1	0.03	0.1	0.03	0.3	0.03
CV	p110α	4	11	4	13	12	20

Supporting Table S 12. END/SIS peptide intensity ratios of the reduction and alkylation experiments shown in Supporting Figure S 7 are shown. MDA-MB 231 cell lysate (10 µg total protein per replicate) with or without reduction and alkylation prior to digestion was analysed. PTEN+p110α SIS peptides (2.5 fmol per replicate) were added to each sample. Data was recorded in the linear mode. No significant difference ($p<0.01$) was found between samples with or without reduction and alkylation prior to digestion.

		Replicate							
Protein	**Reduced+ Alkylated**	**1**	**2**	**3**	**4**	**5**	**Mean**	**Abs. SD**	**CV**
PTEN	+	1.74	1.96	1.51	1.62	1.52	1.67	0.19	11
PTEN	-	1.35	1.43	1.38	1.29	3.45	1.36	0.06	4
p110α	+	0.42	0.45	0.4	0.45	0.48	0.44	0.03	7
p110α	-	0.42	0.42	0.34	0.38	1.55	0.39	0.04	10

Supporting Table S 13. Linearity values of the calibration curves presented in Figure 13 1A are displayed. MDA-MB 231 lysate digest (10 µg per replicate) was spiked with varying amounts of PTEN+p110α dSIS and constant amounts of corresponding SIS standards (2.5 fmol). dSIS/SIS ratios (normalized by multiplying dSIS/SIS ratios by the amount of spiked-in SIS) are displayed for each replicate. Corresponding means, standard deviation, and relative standard deviation (Abs. SD, CV) are shown for each tested dSIS amount. Data presented were collected in the linear mode. The linear range of the calibration curve is from 0.6 to 20 fmol. N.d.=Not detectable.

	PTEN				p110α			
Spiked dSIS in fmol	dSIS/SIS (normalized)	Mean	Abs. SD	CV	dSIS/SIS (normalized)	Mean	Abs. SD	CV
50	46.9				33.5			
50	43.9	47.4	3.8	8	29.2	32.3	2.7	8
50	51.5				34.2			
35	35.2				23.1			
35	35.4	36.1	1.4	4	25.0	24.7	1.4	6
35	37.7				26.0			
20	25.7				17.0			
20	23.2	24.2	1.3	5	16.0	16.7	0.5	3
20	23.6				17.0			
15	19.1				13.3			
15	20.0	19.8	0.7	3	13.5	13.1	0.5	4
15	20.3				12.6			
10	13.6				8.7			
10	14.4	14.1	0.5	3	9.2	9.0	0.3	3
10	14.3				9.1			
7.5	10.9				6.7			
7.5	10.4	10.9	0.5	5	6.9	6.9	0.2	3
7.5	11.5				7.1			
5	6.5				4.7			
5	6.1	6.4	0.2	3	4.6	4.7	0.1	1
5	6.4				4.7			
2.5	2.8				2.3			
2.5	3.3	3.1	0.3	10	2.4	2.4	0.0	1
2.5	3.2				2.4			
1.25	1.6				1.4			
1.25	1.5	1.6	0.1	4	1.3	1.3	0.1	5
1.25	1.7				1.3			
0.62	0.9				1.0			
0.62	0.9	0.9	0.1	8	0.7	0.8	0.2	19
0.62	0.8				0.7			
0.31	n.d.	-	-	-	0.6	0.5	0.1	9

0.31	n.d.	0.5
0.31	n.d.	0.5

Supporting Table S 14. Linearity values of the calibration curves presented in Figure 13 2A are displayed. MDA-MB 231 lysate digest (10 µg per replicate) were spiked with varying amounts of PTEN+p110α dSIS and constant amounts of corresponding SIS standards (2.5 fmol). dSIS/SIS ratios (normalized by multiplying dSIS/SIS ratios by the amount of spiked-in SIS) are shown for each replicate. Corresponding means, standard deviation and relative standard deviation (Abs. SD, CV) are shown for each tested dSIS amount. Data presented were collected in the reflectron mode. The linear range of the calibration curve was from 0.6 to 20 fmol. *N.d.*=Not detectable.

	PTEN				p110α			
Spiked dSIS in fmol	**dSIS/SIS (normalized)**	**Mean**	**Abs. SD**	**CV**	**dSIS/SIS (normalized)**	**Mean**	**Abs. SD**	**CV**
50	141.4				66.9			
50	121.4	127.2	12.3	10	57.1	61.2	5.1	8
50	118.8				59.7			
35	68.8				38.1			
35	82.0	79.5	9.7	12	34.6	36.0	1.9	5
35	87.7				35.2			
20	46.4				24.0			
20	47.9	46.6	1.2	3	23.9	23.3	1.2	5
20	45.6				21.9			
15	35.3				18.1			
15	31.6	33.0	2.0	6	20.1	18.5	1.5	8
15	32.1				17.3			
10	21.1				10.6			
10	20.5	20.9	0.4	2	11.6	11.3	0.6	5
10	21.2				11.6			
7.5	16.1				8.2			
7.5	12.3	14.9	2.3	15	7.6	8.0	0.4	5
7.5	16.3				8.2			
5	9.7				4.7			
5	9.0	8.8	1.0	11	5.2	5.0	0.3	5
5	7.8				5.2			
2.5	3.5				2.1			
2.5	3.4	3.4	0.2	5	2.0	2.1	0.1	5
2.5	3.2				2.1			
1.25	1.2				0.9			
1.25	1.5	1.4	0.2	12	1.0	0.9	0.1	7
1.25	1.6				0.8			
0.62	1.1				0.4			
0.62	1.0	1.1	0.1	9	0.3	0.4	0.0	8
0.62	1.2				0.3			
0.31	n.d.	-	-	-	0.3	0.2	0.0	17

0.31	n.d.	0.2
0.31	n.d.	0.3

Supporting Table S 15. Accuracy results shown in Figure 13 1C are displayed. MDA-MB 231 cell lysate (10 µg total protein per replicate) was spiked with 2, 10 or 18 fmol PTEN+p110α dSIS peptides. PTEN+p110α SIS peptides (2.5 fmol per replicate) were added to each sample as internal standard. Recovered dSIS peptide amounts and accuracy (recovered amount/theoretical spike-in amount) were calculated. Data was recorded in linear mode. High accuracies were found across the working range of the assay.

		Absolute Peptide Amounts Quantified in fmol			Accuracy in %		
	Peptide	2 fmol spike-in	10 fmol spike-in	18 fmol spike-in	2 fmol spike-in	10 fmol spike-in	18 fmol spike-in
Replicate 1	PTEN	2.1	10.9	15.6	104	109	87
Replicate 2	PTEN	2	9.5	17	101	95	95
Replicate 3	PTEN	2	9.9	16.9	100	99	94
Replicate 4	PTEN	2.1	9.7	15.2	104	97	84
Mean	PTEN	2	10	16.2	102	100	90
Abs. SD	PTEN	0	0.6	0.9	2	6	5
CV (%)	PTEN	2	6	6	2	6	6
Replicate 1	p110α	2.2	11	17.2	111	110	95
Replicate 2	p110α	2.2	10.3	17.8	110	104	99
Replicate 3	p110α	2.3	10.2	17.9	114	102	99
Replicate 4	p110α	2.2	10.2	16.6	112	102	92
Mean	p110α	2.2	10.5	17.4	112	105	97
Abs. SD	p110α	0	0.4	0.6	2	4	3
CV (%)	p110α	2	4	4	2	4	4

Supporting Table S 16. Accuracy results shown in Figure 13 2C are shown. MDA-MB 231 cell lysate (10 µg total protein per replicate) was spiked with 2, 10, or 18 fmol PTEN+p110α dSIS peptides. PTEN+p110α SIS peptides (2.5 fmol per replicate) were added to each sample as internal standard. Recovered dSIS peptide amounts and accuracy (recovered amount/theoretical spike-in amount) were calculated. Data was recorded in the reflectron mode. High accuracies were found across the working range of the assay.

		Absolute Peptide Amounts Quantified in fmol			Accuracy in %		
	Peptide	2 fmol spike-in	10 fmol spike-in	18 fmol spike-in	2 fmol spike-in	10 fmol spike-in	18 fmol spike-in
Replicate 1	PTEN	2	11	19.6	101	110	109
Replicate 2	PTEN	2.1	10.5	21	107	105	117
Replicate 3	PTEN	1.8	11.1	19.2	90	111	107
Replicate 4	PTEN	1.9	10.9	20.7	96	109	115
Mean	PTEN	2	10.9	20.1	99	109	112
Abs. SD	PTEN	0.1	0.3	0.8	7	3	5
CV (%)	PTEN	7	2	4	7	2	4
Replicate 1	p110α	2	11.5	19.9	101	115	110
Replicate 2	p110α	2.1	11.1	19.6	105	111	109
Replicate 3	p110α	2.1	10.2	18.7	106	102	104
Replicate 4	p110α	2.1	10.1	19.9	106	101	111
Mean	p110α	2.1	10.7	19.5	105	107	109
Abs. SD	p110α	0	0.7	0.5	3	7	3
CV (%)	p110α	2	6	3	2	6	3

Supporting Table S 17. Interference results shown in Figure 13 1D are given here. MDA-MB 231 cell lysate (10 µg total protein per replicate) was spiked with recombinant PTEN and p110α/p85α protein (approximately 15 fmol per replicate). Samples were serially diluted by a factor of 2, 4, and 8 using PBSC. PTEN+p110α dSIS peptides (2.5 fmol per replicate) were added to each sample as internal standard. Endogenous PTEN and p110α amounts (in fmol) were calculated for each sample. Data was recorded in the linear mode. Dilutional linearity was demonstrated.

		Dilution			
	Protein	**No dilution**	**2x**	**4x**	**8x**
Replicate 1	PTEN	13.4	6.8	3.4	1.9
Replicate 2	PTEN	14.4	7.5	3	1.8
Replicate 3	PTEN	14.1	6.9	3.4	1.7
Replicate 4	PTEN	13.8	7.2	3.5	1.8
Mean	PTEN	13.9	7.1	3.3	1.8
Abs. SD.	PTEN	0.4	0.3	0.2	0.1
CV (%)	PTEN	3	5	7	6
Replicate 1	p110α	10.8	5.6	3.2	1.4
Replicate 2	p110α	11.8	5.5	2.7	1.3
Replicate 3	p110α	11.2	5.5	2.9	1.3
Replicate 4	p110α	12.0	5.8	2.8	1.3
Mean	p110α	11.4	5.6	2.9	1.3
Abs. SD.	p110α	0.5	0.1	0.2	0
CV (%)	p110α	5	2	7	4

Supporting Table S 18 Interference results shown in Figure 13 2D are given here. MDA-MB 231 cell lysate (10 µg total protein per replicate) was spiked with recombinant PTEN and p110α/p85α protein (approximately 15 fmol per replicate). Samples were serially diluted by a factor of 2, 4, and 8 using PBSC. PTEN+p110α dSIS peptides (2.5 fmol per replicate) were added to each sample as internal standard. Endogenous PTEN and p110α amounts (in fmol) were calculated for each sample. Data was recorded in the reflectron mode. Dilutional linearity was demonstrated.

		Dilution			
	Protein	**No dilution**	**2x**	**4x**	**8x**
Replicate 1	PTEN	13.4	5.8	2.9	1.3
Replicate 2	PTEN	13.8	6.1	2.6	1.4
Replicate 3	PTEN	15.6	6.7	2.5	1.4
Replicate 4	PTEN	15.4	6.6	2.8	1.5
Mean	PTEN	14.5	6.3	2.7	1.4
Abs. SD.	PTEN	1.1	0.4	0.2	0.1
CV (%)	PTEN	8	7	7	5
Replicate 1	p110α	10.5	5.0	3	1.3
Replicate 2	p110α	10.2	5.0	2.6	1.3
Replicate 3	p110α	12.3	5.5	2.5	1.2
Replicate 4	p110α	13.8	5.5	2.3	1.1
Mean	p110α	11.7	5.2	2.6	1.2
Abs. SD.	p110α	1.7	0.3	0.3	0.1
CV (%)	p110α	14	5	11	5

Supporting Table S 19. 5-day precision results for PTEN in LP shown in Figure 14 1A are given here. Three pools of MDA-MD 231 lysate were spiked with 2, 10, and 18 fmol PTEN+p110α dSIS (per 10 µg total lysate protein). Each pool (10 µg total protein per replicate) was analysed each day in triplicate. Quantified amounts of PTEN dSIS per replicate (in fmol) are shown. *An outlier (amount quantified > 3rd quartile$_{\text{5-day 'low' results}}$+3x Interquartile Range$_{\text{5-day 'low' results}}$) was excluded from the 'low' sample on Day 4.

	2 fmol spike-in					10 fmol spike-in					18 fmol spike-in				
Day	**1**	**2**	**3**	**4**	**5**	**1**	**2**	**3**	**4**	**5**	**1**	**2**	**3**	**4**	**5**
Rep. 1	2.1	2.0	2.1	2.4	2.4	9.1	9.3	9.5	12.2	10.5	14.5	14.4	15.3	15.6	15.0
Rep. 2	2.1	2.2	2.2	3.7*	2.4	9.4	9.1	10.3	11.4	10.4	14.4	14.3	16.7	14.3	18.7
Rep. 3	2.1	2.1	2.3	2.2	2.4	9.1	9.2	9.3	9.5	11.3	14.8	14.6	15.1	15.7	18.6
Mean	2.1	2.1	2.2	2.3	2.4	9.2	9.2	9.7	11.0	10.7	14.6	14.5	15.7	15.2	17.4
Abs. SD.	0.0	0.1	0.1	0.1	0.0	0.2	0.1	0.5	1.4	0.5	0.2	0.2	0.8	0.8	2.1
CV (%)	1	3	5	6	0	2	1	6	13	5	1	1	5	5	12
Spike	2	2	2	2	2	10	10	10	10	10	18	18	18	18	18
Acc. (%)	106	105	110	113	120	92	92	97	110	107	81	80	87	84	97
Mean$_{\text{5 Day}}$	2.2	2.2	2.2	2.2	2.2	10.0	10.0	10.0	10.0	10.0	15.5	15.5	15.5	15.5	15.5
Abs. SD.$_{\text{5 Day}}$	0.1	0.1	0.1	0.1	0.1	1.0	1.0	1.0	1.0	1.0	1.4	1.4	1.4	1.4	1.4
CV$_{\text{5 Day}}$ (%)	6	6	6	6	6	10	10	10	10	10	9	9	9	9	9
Acc.$_{\text{5 Day}}$ (%)	111	111	111	111	111	100	100	100	100	100	86	86	86	86	86
CV$_{\text{Total}}$ (%)	7	7	7	7	7	11	11	11	11	11	10	10	10	10	10

Supporting Table S 20. Five-day precision results for p110α in LP shown in Figure 14 1C are given here. Three pools of MDA-MD 231 lysate were spiked with 2, 10, and 18 fmol PTEN+p110α dSIS (per 10 µg total lysate protein). Each pool (10 µg total protein per replicate) was analysed each day in triplicate. Quantified amounts of p110α dSIS per replicate (in fmol) are shown. *An outlier (amount quantified > 3rd quartile$_{\text{5-day 'low' results}}$+3x Interquartile Range$_{\text{5-day 'low' results}}$) was excluded from the 'low' sample on Day 4.

	2 fmol spike-in					10 fmol spike-in					18 fmol spike-in				
Day	**1**	**2**	**3**	**4**	**5**	**1**	**2**	**3**	**4**	**5**	**1**	**2**	**3**	**4**	**5**
Rep. 1	2.3	2.2	2.5	2.5	2.3	10.2	10.0	10.8	13.5	11.1	16.6	16.6	17.1	16.8	16.8
Rep. 2	2.6	2.3	2.3	4.1*	2.4	10.5	9.9	10.9	12.3	10.7	16.1	16.9	17.4	16.3	20.1
Rep. 3	2.5	2.3	2.4	2.4	2.4	10.2	10.0	9.8	10.2	12.5	16.0	16.3	16.0	17.6	18.7
Mean	2.5	2.3	2.4	2.4	2.4	10.3	10.0	10.5	12.0	11.4	16.2	16.6	16.8	16.9	18.5
Abs. SD.	0.2	0.1	0.1	0.1	0.0	0.2	0.1	0.6	1.7	1.0	0.3	0.3	0.8	0.7	1.7
CV (%)	6	2	5	4	1	2	1	6	14	8	2	2	5	4	9
Spike	2.0	2.0	2.0	2.0	2.0	10.0	10.0	10.0	10.0	10.0	18.0	18.0	18.0	18.0	18.0
Acc. (%)	123	114	121	122	118	103	100	105	120	114	90	92	93	94	103
Mean$_{\text{5 Day}}$	2.4	2.4	2.4	2.4	2.4	10.8	10.8	10.8	10.8	10.8	17.0	17.0	17.0	17.0	17.0
Abs. SD.$_{\text{5 Day}}$	0.1	0.1	0.1	0.1	0.1	1.1	1.1	1.1	1.1	1.1	1.1	1.1	1.1	1.1	1.1
CV$_{\text{5 Day}}$ (%)	4	4	4	4	4	10	10	10	10	10	7	7	7	7	7
Acc.$_{\text{5 Day}}$ (%)	119	119	119	119	119	108	108	108	108	108	94	94	94	94	94
CV$_{\text{Total}}$ (%)	6	6	6	6	6	12	12	12	12	12	8	8	8	8	8

Supporting Table S 21. Five-day precision results for PTEN in RP shown in Figure 14 2A are given here. Three pools of MDA-MD 231 lysate were spiked with 2, 10, and 18 fmol PTEN+p110α dSIS (per 10 µg total lysate protein). Each pool (10 µg total protein per replicate) was analyzed each day in triplicate. Quantified amounts of PTEN dSIS per replicate (in fmol) are shown.

	2 fmol spike-in					10 fmol spike-in					18 fmol spike-in				
Day	**1**	**2**	**3**	**4**	**5**	**1**	**2**	**3**	**4**	**5**	**1**	**2**	**3**	**4**	**5**
Rep. 1	2.0	1.8	1.9	2.2	2.0	10.5	10.2	10.0	16.9	10.7	20.2	17.0	19.2	20.0	17.1
Rep. 2	1.9	2.0	1.9	3.7	2.0	11.0	9.3	10.1	15.4	12.3	17.8	19.0	18.0	20.9	23.8
Rep. 3	2.0	2.0	2.0	2.0	2.1	10.5	9.7	9.9	9.9	11.0	17.2	19.6	18.9	20.1	26.9
Mean	2.0	1.9	1.9	2.1	2.0	10.7	9.7	10.0	14.1	11.3	18.4	18.6	18.7	20.3	22.6
Abs. SD.	0.1	0.1	0.1	0.2	0.1	0.3	0.4	0.1	3.7	0.8	1.6	1.4	0.6	0.5	5.0
CV (%)	4	5	3	8	3	3	5	1	26	7	9	7	3	3	22
Spike	2.0	2.0	2.0	2.0	2.0	10.0	10.0	10.0	10.0	10.0	18.0	18.0	18.0	18.0	18.0
Acc. (%)	99	96	96	106	100	107	97	100	141	113	102	103	104	113	126
$Mean_{5\ Day}$	2.0	2.0	2.0	2.0	2.0	11.2	11.2	11.2	11.2	11.2	19.7	19.7	19.7	19.7	19.7
$Abs.\ SD._{5\ Day}$	0.1	0.1	0.1	0.1	0.1	2.2	2.2	2.2	2.2	2.2	2.7	2.7	2.7	2.7	2.7
$CV_{5\ Day}$ (%)	5	5	5	5	5	19	19	19	19	19	14	14	14	14	14
$Acc._{5\ Day}$ (%)	99	99	99	99	99	111	111	111	111	111	109	109	109	109	109
CV_{Total} (%)	7	7	7	7	7	21	21	21	21	21	16	16	16	16	16

Supporting Table S 22. Five -day precision results for p110α in RP shown in Figure 14 2A are displayed. Three pools of MDA-MD 231 lysate were spiked with 2, 10, and 18 fmol PTEN+p110α dSIS (per 10 µg total lysate protein). Each pool (10 µg total protein per replicate) was analyzed each day in triplicate. Quantified amounts of p110α dSIS per replicate (in fmol) are shown.

	2 fmol spike-in					10 fmol spike-in					18 fmol spike-in				
Day	**1**	**2**	**3**	**4**	**5**	**1**	**2**	**3**	**4**	**5**	**1**	**2**	**3**	**4**	**5**
Rep. 1	2.1	1.9	2.2	2.3	2.1	11.0	10.6	9.9	17.6	10.6	20.2	18.4	21.3	20.0	17.6
Rep. 2	2.0	2.1	2.0	4.2	2.0	12.5	10.1	11.4	13.7	11.5	20.1	19.1	19.6	22.9	23.1
Rep. 3	2.0	2.1	2.1	2.1	1.9	11.9	10.5	10.3	10.5	12.3	18.9	21.2	20.9	21.5	21.7
Mean	2.0	2.0	2.1	2.2	2.0	11.8	10.4	10.6	13.9	11.5	19.7	19.6	20.6	21.5	20.8
Abs. SD.	0.1	0.1	0.1	0.2	0.1	0.8	0.3	0.8	3.6	0.8	0.7	1.4	0.9	1.4	2.9
CV (%)	3	4	5	7	4	6	3	7	25	7	4	7	4	7	14
Spike	2.0	2.0	2.0	2.0	2.0	10.0	10.0	10.0	10.0	10.0	18.0	18.0	18.0	18.0	18.0
Acc. (%)	100	102	105	111	101	118	104	106	139	115	110	109	115	119	115
$Mean_{5\ Day}$	2.1	2.1	2.1	2.1	2.1	11.6	11.6	11.6	11.6	11.6	20.4	20.4	20.4	20.4	20.4
$Abs.\ SD._{5\ Day}$	0.1	0.1	0.1	0.1	0.1	2.0	2.0	2.0	2.0	2.0	1.6	1.6	1.6	1.6	1.6
$CV_{5\ Day}$ (%)	5	5	5	5	5	17	17	17	17	17	8	8	8	8	8
$Acc._{5\ Day}$ (%)	103	103	103	103	103	116	116	116	116	116	113	113	113	113	113
CV_{Total} (%)	7	7	7	7	7	19	19	19	19	19	11	11	11	11	

Supporting Table S 23. Endogenous PTEN and p110α amounts quantified in various FF tissue samples shown in Figure 15 C are given here. Biological replicates were analyzed in duplicate (10 µg total protein per replicate). Quantified amounts of PTEN and p110α per replicate (in fmol) are shown. Data was recorded in the linear mode. Not detectable (n.d.) was treated as 0 for calculating means and standard deviation. *Replicates excluded due to contamination.

		Vehicle		Trastuzumab		Everolimus		Trastuzumab + Everolimus	
Biological Replicate	Technical Replicate	PTEN	p110α	PTEN	p110α	PTEN	p110α	PTEN	p110α
Bio. Rep. #1	1	4.1	1.0	3.6	0.8	5.3	1.1	4.8	0.8
Bio. Rep. #1	2	4.3	0.9	4.0	0.8	5.4	1.2	4.7	0.9
Bio. Rep. #2	1	0.8	0.4	3.2	0.6	5.0	0.8	3.5	0.6
Bio. Rep. #2	2	0.9	n.d.	2.9	0.8	5.2	0.8	3.9	0.8
Bio. Rep. #3	1	9.2*	2.1*	8.6*	2.0*	3.2	0.8	4.1	1.0
Bio. Rep. #3	2	n.d.	n.d.	4.2	1.1	3.3	0.9	4.3	1.1
Mean		2.0	0.4	3.6	0.8	4.6	0.9	4.2	0.9
Abs.SD		2.0	0.5	0.5	0.2	1.0	0.2	0.5	0.2
CV		99.6	105.5	14.9	24.1	22.3	17.7	11.4	17.6

Supporting Table S 24. Endogenous PTEN and p110α amounts quantified in various FF tissue samples shown in Figure 15 A are given here. Colorectal cancer liver metastases (mCRC) and breast FF tissue samples (10 µg total protein per replicate) were analysed in triplicate. Quantified amounts of PTEN and p110α per replicate (in fmol) are shown.

		mCRC Tissues				Breast Tissue				
	Protein	**L #1**	**L #2**	**L #3**	**L #4**	**B #1**	**B #2**	**B #3**	**B #4**	**B #5**
Rep. 1	PTEN	1.0	1.9	1.6	3.9	2.6	3.3	1.3	2.2	1.1
Rep. 2	PTEN	0.9	2.1	1.5	3.9	2.1	3.1	1.5	1.7	0.0
Rep. 3	PTEN	0.0	1.7	1.3	3.7	2.3	3.5	1.4	2.7	1.2
Mean	PTEN	0.7	1.9	1.5	3.8	2.3	3.3	1.4	2.2	0.8
Abs. SD.	PTEN	0.6	0.2	0.2	0.1	0.2	0.2	0.1	0.5	0.7
CV (%)	PTEN	87	11	10	3	9	7	6	22	87
Rep. 1	p110α	0.6	0.7	1.0	1.2	0.8	1.4	0.6	0.6	1.1
Rep. 2	p110α	0.6	0.8	1.1	1.1	0.9	1.3	0.6	0.5	0.0
Rep. 3	p110α	0.6	0.7	0.9	1.2	1.0	1.2	0.6	0.8	0.9
Mean	p110α	0.6	0.7	1.0	1.2	0.9	1.3	0.6	0.6	0.7
Abs. SD.	p110α	0.0	0.1	0.1	0.1	0.1	0.1	0.0	0.1	0.6
CV (%)	p110α	7.2	7.6	6.7	7.6	12.8	6.5	7.5	17.5	87.7

Supporting Table S 25. Summary of experimental conditions for PTEN iMRM and iMALDI assays using 2-PIC.

PARAMETER		IMRM	IMALDI
SAMPLE PREPARATION		manual	automated on Agilent Bravo 96LT
		denaturation, reduction and alkylation	denaturation
DIGESTION		FASP	in-solution
		Trypsin/LysC	TPCK-treated trypsin
		1:20 protein:enzyme (w:w) overnight at 37°C	1:2 protein:enzyme (w:w) for 1 h at 37°C.
HIGH POINT INTERNAL STANDARD SIS1 SPIKE-IN		NNIDDV**V**R+6 Da	AQEALDFYGEV**R**+10 Da
		40 fmol	17.5 fmol
LOW POINT INTERNAL STANDARD SIS2 SPIKE-IN		NNIDDVV**R**+10 Da	AQEA**L**DFYGEV**R**+17 Da
		2 fmol	1.75 fmol
IMMUNO-ENRICHMENT	Antibody used (rabbit polyclonal)	anti-NNIDDVVR	anti-AQEALDFYGEVR
	Antibody (Ab)-beads complex	0.5 µg Ab per 30 µg Protein A Dynabeads beads per sample (up to 30 µg of total protein)	0.2 µg Ab per 30 µg Protein G Dynabeads per sample (up to 30 µg of total protein)
	Ab incubation with beads	overnight at 4°C, slow shaking	at room temperature for 1 h
	Samples	three samples prepared as one replicate: 10, 15 and 30 µg	three samples prepared in duplicate: 10, 15 and 30 µg
	Ab-beads complex incubation with samples	overnight at 4°C, slow shaking	1 h at room temperature, slow shaking
	Wash protocol	PBSC buffer (1x PBS + 0.003 % CHAPS	PBSC2 buffer (25:75 ACN:1x PBS+0.015 % CHAPS)
		200 µL of PBSC, 200 µL of 0.1x PBSC, 200 µL of H_2O	70 µL PBSC2, 3x 80 µL 5 mM AmBic
	Peptide elution	20 µL of 3% ACN, 5% acetic acid, 50 mM citrate for 2 min	no elution, direct application on MALDI plate

SAMPLE PREPARATION	---	addition of Matrix solution (3 mg/mL HCCA, 7 mM AmCit in 70% ACN, 0.1% TFA) followed by washing the dried spots with 3x5 uL 7 mM ammonium citrate (5 s incubation time before withdrawing the wash solution)
MS INSTRUMENTATION	Agilent 6495 QQQ online-coupled to Agilent 1290 Infinity UHPLC. Agilent RRHD Eclipse Plus C18 column (2.1 mm inner diameter × 150 mm length, 1.8 µm particle size). 11-min binary gradient.	MALDI Bruker Microflex LRF (Reflectron positive ion mode)
DATA ANALYSIS SOFTWARE	Skyline-Daily 19.1	FlexAnalysis (v3.4, Build 70).
2-PIC REGRESSION	$1/x^2$ weighted linear regression (WLS) through the origin	ordinary least squares (OLS)

Supporting Table S 26. Descriptive statistics for samples from AstraZeneca.

	Responders (n= 8)	**Non-Responders (n=7)**
Cancer type	Breast = 3 Gyne = 5	Breast = 4 Gyne = 3
Patient Weight (kg)	66.75 +/- 19.75	61.14 +/- 9.34
Age (years)	60.00 +/- 10.86	61.57 +/- 7.84
Sex	F = 8, M=0	F=7, M=0
WHO PS	PS 0 = 3, Ps 1 = 5	PS 0 = 4, PS1 = 3
ER/PR	+ = 4, unknown = 4	+ = 5, unknown = 2
Her2	+ = 2, - = 1, unknown = 5	+ = 0, unknown = 3
# of Met Sites	2.88 +/- 1.05	3.43 +/- 1.76
Lines of treatment	1^{st} = 1 , 3^{rd} = 1, >3^{rd} = 4, unknown = 2	1^{st} = 1 , 2^{nd} = 2, 3^{rd} = 2, >3^{rd} = 1, unknown = 1
PFS (adjusted, days)	182.25 +/- 134.01	47.57 +/- 17.97
Sample site	Metastatic = 5, Primary = 3	Metastatic=1, Primary=6
Age	7.30 +/- 0.78 (4 unknown)	7.62 +/- 1.36 (2 unknown)
Size	355.75 mm2 +/- 171.41	334.17 mm2 +/- 52.08
Cellularity	67.88 +/- 13.66 (necrosis 4.5 +/- 2.8)	62.14 +/- 23.28 (necrosis 4.43 +/- 3.37)

Supporting Table S 27. Amount of AKT1, AKT2, PTEN and p110α quantified using iMALDI in FFPE tissue samples from patients treated with AZD5363. Underlined values represent protein amounts which were detected, but below the LLOQ.

Sample ID	Cancer Type	Response	Group #	LC-MS Batch	Quantity analyzed (total µg/replicate)	AKT1/ µg	AKT2/ µg	PTEN CV	PTEN/ ug	p110α CV	p110a/ ug
01-01	BREAST	SD	2	2	10.0	0.26	0.11	5	0.13	147	0.03
01-02	BREAST	SD	2	2	10.0	0.11	0.00	NA	NA	NA	NA
02-01	BREAST	PD	1	2	10.0	0.11	0.12	NA	NA	NA	NA
02-02	BREAST	PD	1	2	10.0	0.10	0.08	148	0.03	0	0.01
03-01	BREAST	PD	1	2	10.0	0.21	0.16	12	0.16	68	0.06
03-02	BREAST	PD	1	2	10.0	0.17	0.16	1	0.11	68	0.05
04-01	BREAST	PD	1	2	10.0	0.09	0.05	0	0.04	#DIV/0!	0.00
04-02	BREAST	PD	1	2	10.0	0.14	0.07	5	0.04	#DIV/0!	0.00
05-01	BREAST	PD	1	2	10.0	0.26	0.11	28	0.11	42	0.05
05-02	BREAST	PD	1	2	10.0	0.21	0.13	6	0.12	2	0.03
07-01	GYNE	PD	1	1	7.4	NA	NA	NA	NA	NA	NA
07-02	GYNE	PD	1	1	8.2	NA	NA	NA	NA	NA	NA
08-01	GYNE	SD	2	1	10.0	0.10	0.04	NA	n.d.	241	0.02
08-02	GYNE	SD	2	1	10.0	NA	NA	NA	NA	NA	NA
09-01	GYNE	SD	2	1	9.6	NA	NA	0	0.21	0	0.11
09-02	GYNE	SD	2	1	8.9	NA	NA	NA	NA	NA	NA
12-01	BREAST	SD	2	1	9.7	NA	NA	0	0.45	0	0.11
12-02	BREAST			NA		NA	NA	NA	NA	NA	NA
14-01	BREAST	SD	2	1	6.8	0.41	0.18	10	0.16	57	0.05
14-02	BREAST		2	1	10.0	NA	NA	NA	NA	NA	NA
16-01	GYNE	PD	1	NA	10.0	0.38	0.18	2	0.26	18	0.06
16-02	GYNE	PD	1	NA	6.8	NA	NA	4	0.36	17	0.03
17-01	GYNE	PR	2	NA	6.6	0.34	0.15	10	0.05	87	0.05

19-01	GYNE	SD	2	1	10.0	0.17	0.21	29	0.11	38	0.05
19-02	GYNE	SD	2	1	10.0	NA	NA	NA	NA	NA	NA
21-01	BREAST			NA	10.0	NA	NA	16	0.21	28	0.08
21-02	BREAST			NA		NA	NA	NA	NA	NA	NA
22-01	GYNE	SD	2	1	10.0	0.09	0.12	0	0.03	0	0.05
23-01	GYNE	PD	1	1	10.0	0.34	0.12	NA	n.d.	NA	NA
23-02	GYNE	PD	1	1	10.0	NA	NA	0	0.08	n.d.	n.d.